NASA
SPACE VEHICLE
DESIGN CRITERIA
(CHEMICAL PROPULSION)

SOLID ROCKET

THRUST VECTOR CONTROL

NASA

NATIONAL AERONAUTICS AND SPACE ADMINISTRATION

FOREWORD

NASA experience has indicated a need for uniform criteria for the design of space vehicles. Accordingly, criteria are being developed in the following areas of technology:

> Environment
> Structures
> Guidance and Control
> Chemical Propulsion

Individual components of this work will be issued as separate monographs as soon as they are completed. This document, part of the series on Chemical Propulsion, is one such monograph. A list of all monographs issued prior to this one can be found on the final pages of this document.

These monographs are to be regarded as guides to design and not as NASA requirements, except as may be specified in formal project specifications. It is expected, however, that these documents, revised as experience may indicate to be desirable, eventually will provide uniform design practices for NASA space vehicles.

This monograph, "Solid Rocket Thrust Vector Control," was prepared under the direction of Howard W. Douglass, Chief, Design Criteria Office, Lewis Research Center; project management was by M. Murray Bailey. The monograph was written by Robert F. H. Woodberry and Richard J. Zeamer of Hercules, Inc., and was edited by Russell B. Keller, Jr. of Lewis. To assure technical accuracy of this document, scientists and engineers throughout the technical community participated in interviews, consultations, and critical review of the text. In particular, Thomas S. Clark of United Technology Center, Division of United Aircraft Corporation; Lionel H. Erickson of Thiokol Chemical Corporation; Myron Morgan of Aerojet Solid Propulsion Company; and James J. Pelouch, Jr. of the Lewis Research Center reviewed the monograph in detail.

Comments concerning the technical content of this monograph will be welcomed by the National Aeronautics and Space Administration, Lewis Research Center (Design Criteria Office), Cleveland, Ohio 44135.

December 1974

GUIDE TO THE USE OF THIS MONOGRAPH

The purpose of this monograph is to organize and present, for effective use in design, the significant experience and knowledge accumulated in development and operational programs to date. It reviews and assesses current design practices, and from them establishes firm guidance for achieving greater consistency in design, increased reliability in the end product, and greater efficiency in the design effort. The monograph is organized into two major sections that are preceded by a brief introduction and complemented by a set of references.

The State of the Art, section 2, reviews and discusses the total design problem, and identifies which design elements are involved in successful design. It describes succinctly the current technology pertaining to these elements. When detailed information is required, the best available references are cited. This section serves as a survey of the subject that provides background material and prepares a proper technological base for the *Design Criteria* and Recommended Practices.

The Design Criteria, shown in italics in section 3, state clearly and briefly what rule, guide, limitation, or standard must be imposed on each essential design element to assure successful design. The *Design Criteria* can serve effectively as a checklist of rules for the project manager to use in guiding a design or in assessing its adequacy.

The Recommended Practices, also in section 3, state how to satisfy each of the criteria. Whenever possible, the best procedure is described; when this cannot be done concisely, appropriate references are provided. The Recommended Practices, in conjunction with the *Design Criteria,* provide positive guidance to the practicing designer on how to achieve successful design.

Both sections have been organized into decimally numbered subsections so that the subjects within similarly numbered subsections correspond from section to section. The format for the Contents displays this continuity of subject in such a way that a particular aspect of design can be followed through both sections as a discrete subject.

The design criteria monograph is not intended to be a design handbook, a set of specifications, or a design manual. It is a summary and a systematic ordering of the large and loosely organized body of existing successful design techniques and practices. Its value and its merit should be judged on how effectively it makes that material available to and useful to the designer.

CONTENTS

LIST OF FIGURES

LIST OF TABLES

xiii

SOLID ROCKET
THRUST VECTOR CONTROL

1. INTRODUCTION

Most vehicles used for launching spacecraft require some guidance or steering to ensure that the required flight trajectory will be achieved. In addition, steering is needed to compensate for flight disturbances (e.g., winds) and for vehicle imperfections (e.g., misalignment of thrust and center of gravity). To provide this steering, solid propellant rocket vehicles are equipped with a thrust vector control system. Both mechanical and aerodynamic techniques have been used to redirect the motor thrust and provide the required steering forces. This monograph is limited to treatment of thrust vector control systems that superimpose a side force on the motor thrust, steering being achieved by the side force causing a moment about the vehicle center of gravity. A brief review of thrust vector control systems is presented, and two systems, flexible joint and liquid injection, are treated in detail. These two systems were selected because they are in use on a number of operational vehicles and they are most likely to be used in future aerospace vehicles. The choice between these two systems depends upon the particular vehicle performance requirements, system weights, cost, reliability, development risk, and envelope constraints. However, it is possible that a control system different from the selected systems could result in an optimum vehicle performance within the restrictions imposed for particular types of missions. Sufficient references are presented to allow investigation in detail of control systems other than the two selected.

Treatment of the flexible-joint thrust vector control system is limited to the design of the flexible joint and its insulation against hot motor gases; no evaluation is presented of the movable nozzle, the actuation system, or the means for attachment of the flexible joint to the movable nozzle and the fixed structure. Treatment of the liquid-injection thrust vector control system is limited to discussion of the injectant, valves, piping, storage tanks, and pressurization system; no evaluation is presented of the nozzle except for (1) the effect of the injectant and erosion at the injection port and (2) the effect of injection on pressure distribution within the nozzle.

The design technology for the two selected systems has progressed to the point where the basic problems have been overcome and efficient and reliable systems can be designed for any required use. Design problems with flexible joints have been associated with difficulty in establishing the envelope for the movable nozzle; definition of the actuator power

requirements to vector the movable nozzle; definition of allowable properties for the elastomer and the reinforcement; adhesive bonding of the elastomer to the reinforcements; test methods that adequately simulate the motor operating conditions; and quality control inspection of the molded joint. Design problems in liquid injection systems have been associated with definition of the maximum steering-force duty cycle; determination of the optimum location and geometry of the injector valves; and incompatibility of the injectant with many of the materials used for the nozzle walls, seals, and injectant pressurization system. Emphasis in the monograph is placed on those areas where specific technical approaches have solved design and development problems.

The material herein is organized around the major tasks in thrust vector control: configuration as related to motor requirements; design parameters controlling the response of the mechanism; material selection; system design; structural and thermal analysis; manufacturing; testing, both nondestructive and destructive; and inspection. These tasks are considered in the order and manner in which the designer must handle them. Within these task areas, the critical aspects of the performance, structural, thermal, and physical boundary requirements that the thrust vector control system must satisfy are presented.

2. STATE OF THE ART

The vehicle flight-control system must perform two functions: fly the vehicle along a commanded trajectory, and maintain vehicle flight stability in the atmosphere. Vehicles without aerodynamic stabilizing fins normally are unstable, and those with fins may be only marginally stable. Disturbances that effect vehicle attitude and stability include atmospheric winds; motor thrust misalignments due to fabrication tolerances and thrust-vector-control-system offsets such as those that occur with flexible joints; shifts of vehicle center of gravity; and unbalanced forces during launch and staging. It is desirable that these disturbances be corrected with proper timing and amplitude so that control energy requirements, structural loads, and aerodynamic heating are minimized. Control requirements are a function of interrrelated effects of disturbances, the trajectory required, and the vehicle aerodynamic and structural dynamics. The determination of flight-control requirements and the design of the control system are two of the most complex problems in the development of a space vehicle system.

The control system causes a side force to be applied to the vehicle at some distance from the vehicle center of gravity, resulting in a control moment and a change in the vehicle attiude. A number of force-producing mechanisms have been employed or considered as means to provide attitude and trajectory control of aerospace vehicles. The available systems considered in this monograph are divided into two main groups: movable-nozzle systems, and fixed-nozzle systems. A classification of the different force-producing systems associated with movable and fixed nozzles is shown in figure 1. Other sytems have been used, and still others have been evaluated to determine feasibility. Systems that have been used include jet reaction (refs. 1 to 6), movable external rocket motors (refs. 7 to 9), and aerodynamic fins (refs. 10 and 11). Preliminary evaluations have been conducted on movable pintles (refs. 1, 12, 13, and 14), movable plug (ref. 2), electro gas dynamic (ref. 15), and electric arc discharge (ref. 16).

The correct definition and design of the flight-control system is a complex problem requiring tradeoff analyses between control requirements and the penalties of the control system as they relate to vehicle performance. Factors affecting the selection of a thrust vector control system are the control moment required, the characteristics of vehicle response, the stability requirements during flight, reliability requirements, cost restrictions, and the behavior of the candidate systems. Movable-nozzle systems are linear response systems; i.e., the turning moment is almost directly proportional to the amount of nozzle vectoring, although the power required to cause that amount of nozzle vectoring may not be directly proportional. Fixed-nozzle systems generally are nonlinear systems; i.e., twice the rate of injectant flow in a liquid injection system does not cause twice the turning moment.

3
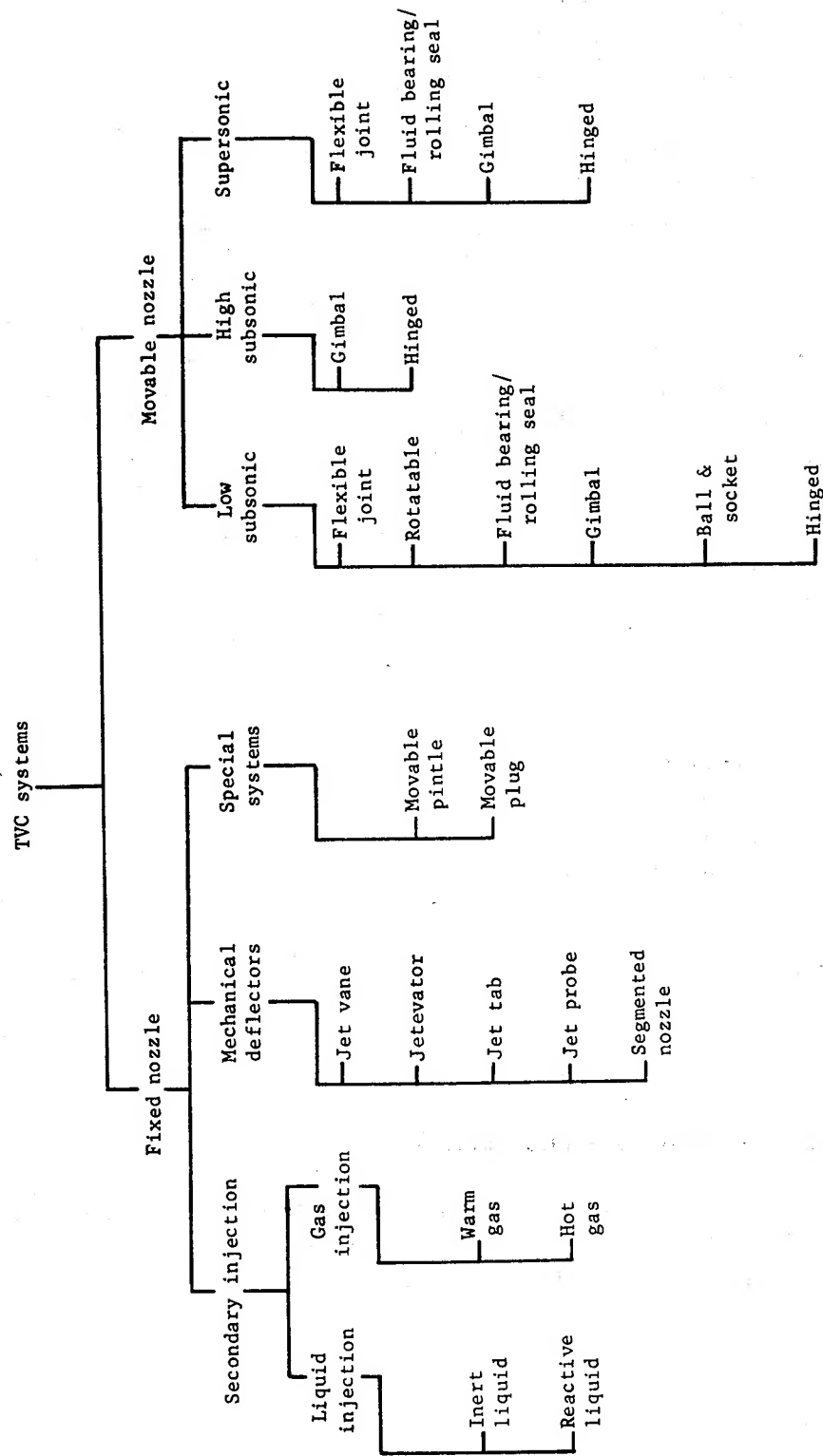
Figure 1. - Classification of thrust vector control systems.

4

Thrust vector control mechanisms have been undergoinging continual change. Concepts used in the past have been outmoded by increased severity of operational requirements and by development of lighter, more reliable systems. The general characteristics and technology status of the systems listed in figure 1 are presented in tables I through IV; basic design features of major systems are shown in figures 2 through 11. The systems summarized in tables I to IV can be divided into three categories: (1) systems that are operational, (2) systems that have been tested in static firings, and (3) experimental systems that either have been abandoned or require significant development.

Movable nozzles. — The movable-nozzle systems (table I) either are operational (e.g., rotatable nozzle and flexible joint) or have been static fired (e.g., gimbal/swivel subsonic splitline, gimbal/integral low-subsonic splitline, supersonic splitline, and ball and socket). All of the systems have demonstrated problems or limitations. All movable nozzle systems require that the actuation hardware for the staging maneuvers be carried throughout the remainder of the flight. The rotatable nozzle is limited to multinozzle motors because movement of only one nozzle would cause pitch, yaw, and roll forces to be applied to the vehicle; effective maneuvering of the vehicle requires movement of at least two nozzles. The supersonic splitline and ball-and-socket type are not developed systems, and it is unlikely that further development will be conducted since the other movable nozzle systems have demonstrated all the advantages of these nozzles but with fewer operational and design problems.

The fluid bearing/rolling seal (designated as TECHROLL[®]) is a constant-volume, fluid-filled bearing configured with a pair of rolling convolutes that permit omniaxis deflection of the rocket motor nozzle. The bearing is shown in figure 8 in the neutral and deflected positions. The fluid-filled bearing is pressurized by nozzle ejection loads and serves as both the movable nozzle bearing and nozzle seal. The seal is fabricated from a fabric-reinforced elastomeric composite material that does not require complex manufacturing processes or tight tolerances. The most significant advantage of this bearing is that the actuation torques are lower than those of any other thrust vector control system. The most significant disadvantages of the bearing are that it has a low rotational stiffness about the nozzle axis in the unpressurized condition, the pivot-point location is limited, and the low lateral stiffness results in larger offset torques than those occurring with a flexible joint. The rotational stiffness is important for upper stages only when vibrational problems could occur during lower-stage motor operation. To overcome the limits on pivot-point location, it has been proposed that the rolling convolutes be oriented on a cone; however, this design will increase the actuation torque. The larger offset torque must be allowed for when defining nozzle vectoring angle requirements. A 24-in. (60.96 cm)[*]diameter bearing has been bench tested and static fired in a large rocket motor that normally uses a flexible joint (ref. 35), thus allowing a direct performance comparison of the two systems. The

---

[®]Trademark of United Technologies (formerly United Aircraft Corporation).

[*] Parenthetical units here and elsewhere in the monograph are in the International System of Units (SI units). A table of conversion factors appears in Appendix A. For simplicity and brevity, SI units are not presented in the tables in the monograph.

TABLE I. – Advantages, Disadvantages, and Current Status of Movable Nozzle Systems

System	Advantages	Disadvantages	Status of Technology
Flexible joint (refs. 17-30) (fig. 7)	State of the art Flexible duty cycle No splitlines Large deflection capability Flexible pivot point location Negligible thrust loss Minimum seal problem Can be used for deeply submerged nozzle Fast response capability Lightweight	Joint requires thermal protection Joint requires protection of elastomer during storage Only small tension loads can be applied to joint Joint pivot point is floating, dependent on motor pressure and vector angle Nozzle aligned only at one design pressure and misaligned at all other pressures	Operational system for Poseidon C3 first and second stage. Twelve successful flight tests on Army Re-entry Measurements Program – Phase B; throat diameter approximately 2.8 in., ±8° deflection. System static fired to 15° vector angle at 355 deg/sec and 300 psi. One static firing, 13-in. and 34-in. throat, submerged nozzles. Three static firings, 2.3-in., 2.6-in., and 8 in. throat. System bench tested to 15° vector angle at 428 deg/sec and 300 psi.
Rotatable nozzle (refs. 31 and 32) (fig. 6)	State of the art Flexible duty cycle Low bearing loadings	Limited to multiport motors Large bearing required Movement of a nozzle results in pitch, yaw, and roll forces Nozzle rotation angle much larger than jet deflection angle	Operational system for Polaris A2 second stage and Polaris A3 first stage.
Fluid bearing/ rolling seal (refs. 33-36) (fig. 8)	State of the art Flexible duty cycle No splitlines Large deflection capability Negligible thrust loss Minimum seal problem Can be used for deeply submerged or supersonic splitline nozzles Fast response capability Lightweight Minimum envelope required Low spring torque	Bearing requires thermal protection Low rotational stiffness about nozzle axis in unpressurized condition Bearing pivot point is floating, dependent on motor pressure and vector angle Nozzle aligned only at one design pressure and misaligned at all other pressures	Flightweight systems for Trident I (C4) first-, second-, and third-stage motors demonstrated in static firings. Static firings, 4-in. and 10-in. throat, submerged nozzles. Two static firings, 2.4-in. and 8.5-in. throat.

6

TABLE I. – Advantages, Disadvantages, and Current Status of Movable Nozzle Systems (concluded)

System	Advantages	Disadvantages	Status of Technology
Gimbal/swivel subsonic splitline (refs. 37 and 38) (fig. 2)	State of the art Flexible duty cycle Negligible thrust loss Large deflection capability Low-to-medium blowout load Low entry erosion	Excessive envelope required for submerged nozzle High erosion and heat flux in splitline Limited operation time Inflexible pivot-point locations	Operational system for Minuteman I and II first and third stages and Minuteman III first stage. One fullscale firing, 38-in. throat, single external-gimbal nozzle. Two subsonic firings, 15-in. throat, single external-gimbal nozzle. One firing, 4.71-in. throat, single external-gimbal nozzle.
Gimbal/integral low subsonic splitline (refs. 37-40) (fig. 3)	State of the art Minimum splitline erosion and heat flux Minimum seal problem Continuity of entry, throat, and exit cone Flexible duty cycle Negligible thrust loss Large deflection capability Long burn time durability	High blowout load High actuation torque Large volume required within chamber Medium entry erosion Inflexible pivot-point location Potentially large vectoring envelopes	One firing, 24-in. throat, single submerged nozzle. Two firings, 15-in. throat, single submerged nozzle. One firing, 9.2-in. throat, single submerged nozzle. One firing, 3.9-in. throat, single submerged nozzle. Two firings, 1.75-in. throat, single submerged nozzle: $\pm14°$, 235 sec operation, 163 sec actual firing, 20 pulses, 72 sec coast time.
Supersonic splitline (refs. 41 - 44) (fig. 4)	Attractive for submerged nozzle Low entry erosion Lightweight potential Fast response capability Low blowout load Small deflection envelope	Sealing and erosion problems at splitline High actuation torque Limited to small vector angles	Two firings of Minuteman motor, first-stage size: one successful, one failure, single nozzle one-plane motion. Several firings, 4.9-in. throat
Ball and socket (ref. 45) (fig. 5)	Potentially lightweight Small envelope requirement Large deflection capability Flexible pivot-point location Deflection of the seal region is minimized and seal gap is maintained by uniformly distributed load	High coulomb torque Unpredictable friction torque Sealing problem Antirotation device required High axial thrust loss	One firing, 9.6-in. throat, single submerged nozzle. Development discontinued in favor of flexible joint.

Notes: Throat dimension in column 4 is throat diameter.
Factors for converting U.S. customary units to SI units are presented in Appendix A.

7

TABLE II. – Advantages, Disadvantages, and Current Status of Secondary Injection Systems

System	Advantages	Disadvantages	Status of Technology
Liquid injection (refs. 46-51) (fig. 9)	State of the art Liquid injection thrust adds to motor thrust Little prelaunch checkout required Fast response capability	Limited thrust deflection System weight is high Careful attention must be given to selection of liquid and bladder material for long-term storage A long hold period after the system is energized requires replenishment of the liquid and pressurization devices Lack of flexibility for accommodation of changes in control requirements Must be designed for worst-on-worst requirements	Operational system for Polaris A3 second stage; Minuteman III second and third stages; 120-in. motor for Titan IIIC and IIID; Sprint first- and second-stage motors; Hibex motor; and Lance motor. Development static firings on 120-in. Titan IIIM motor, 156-in. motor, and 260-in. motor.
Gaseous injection (refs. 52-62) (fig. 10)	Little prelaunch check out required Fast response capability Lighter in weight than liquid injection systems	Should be limited to applications with required thrust deflection angles less than 7° Cannot be used where precise velocity control is required Hot-gas valve is subjected to severe thermal environment Warm-gas valve requires large and heavy gas generators Additional propellant necessary to recover thrust losses	Demonstration static firing on 156-in. motor. Demonstration static firing on 120-in. motor. Demonstration static firings of Minuteman motor, first-stage size. Problems concerning durability of materials for valves and pintles need to be solved.

Note: Dimension given in column 4 is motor diameter.

8

TABLE III. – Advantages, Disadvantages, and Current Status of Mechanical Deflector Systems

System	Advantages	Disadvantages	Status of Technology
Jet vane (refs. 10, 63, and 64)	Actuation torques are low Small installation envelope around nozzle Power requirements are low, and thus actuator weights are low Fast response capability	High thrust losses Restricted to motors with low-temperature propellant or short burn time Large vane rotation angle required for small jet thrust deflection	Operational system for Sergeant, Talos, and Pershing and for Algo II and III motors. No current development.
Jetevator (refs. 65-69)	Side force is linear with jetevator deflection angle	Jetevator envelopes nozzle exit, restricting maximum available nozzle exit diameter Restricted to motors with low-temperature propellant or short burn time Heat shields required to protect afterdome, nozzle exterior, and actuation system significantly increase total system envelope Large thrust loss (half of generated side force) Torque varies with time System is relatively heavy Limited to multiport systems for omniaxis vectoring.	Operational system for Polaris A1 first and second stages and Polaris A2 first stage. Operational system for BOMARC and SUBROC. No current development.
Jet tab (refs. 70-74) (fig. 11)	Side force is directly proportional to ratio of tab area to nozzle area	Restricted to motors with low-temperature propellant or short burn time. Caused significant local erosion in the nozzle Large thrust loss (equal to generated side force) Jet tabs at the exit plane increase envelope requirements	Limited to development static firings. Test results indicate significant design and material problems. No current development.
Segmented nozzle (refs. 12 and 58)	Major portion of nozzle is fixed to motor Thrust losses at small deflection angles are negligible.	(Testing to date insufficient to determine disadvantages of system)	Limited to experimental static firings. No current development.

9

Table IV. — Advantages, Disadvantages, and Current Status of Special Systems

System	Advantages	Disadvantages	Status of Technology
Movable pintle (refs. 1 and 12-14)	Can be used as a throttling device	Side force is nonlinear with pintle cant angle Small pintle cant angles produce negative side forces Pintle subjected to severe thermal environment	Analytical and experimental development only. No current development.
Movable plug (ref. 2)	Omniaxial movement is possible	Plug subjected to severe thermal environment	Limited to cold-flow air tests. No current development.

10

Fixed structure

Subsonic splitline

Movable nozzle
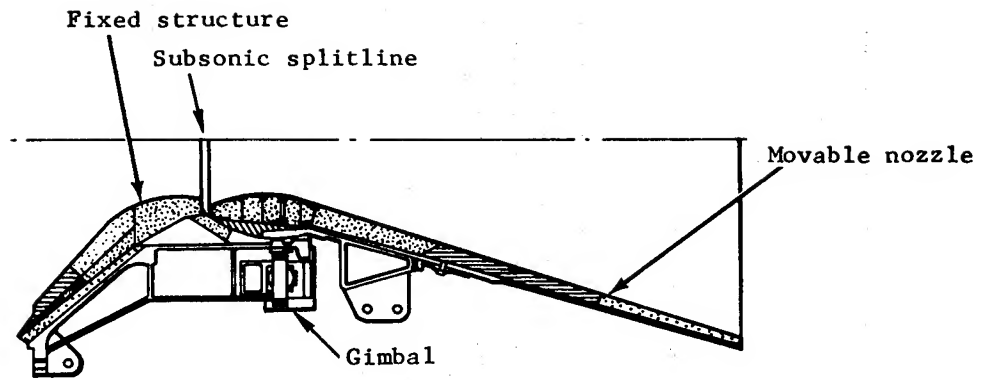
Gimbal

Figure 2. - Gimbal/swivel subsonic-splitline nozzle.

Low subsonic splitline

Movable nozzle

Fixed structure
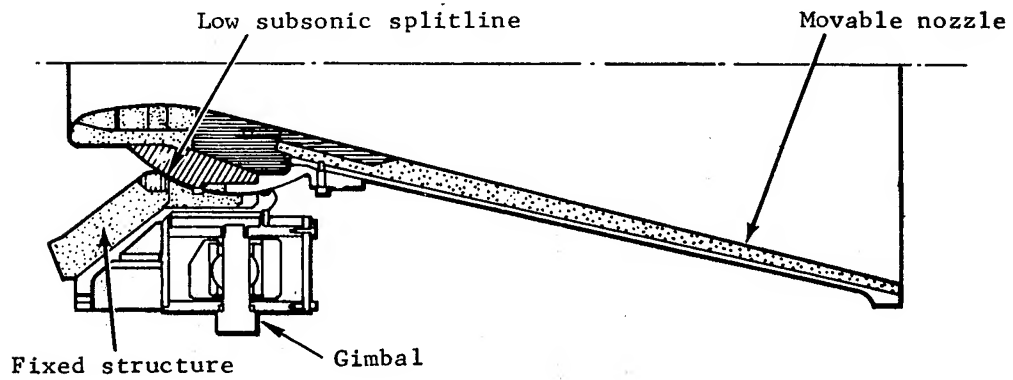
Gimbal

Figure 3. - Gimbal/integral low-subsonic-splitline nozzle.

Fixed structure

Supersonic splitline

Movable nozzle

Gimbal
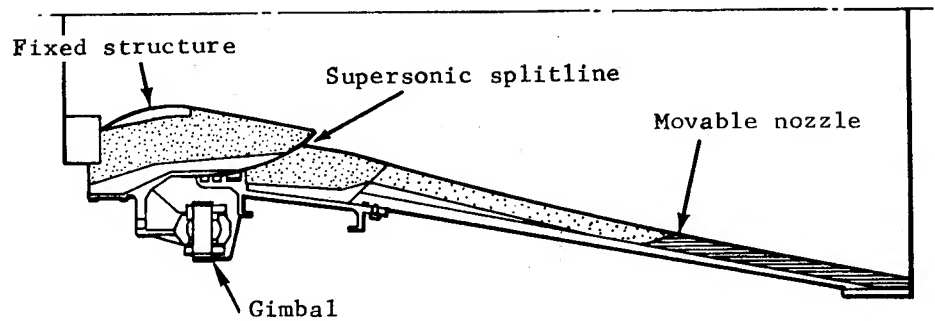
Figure 4. - Supersonic-splitline nozzle.

11
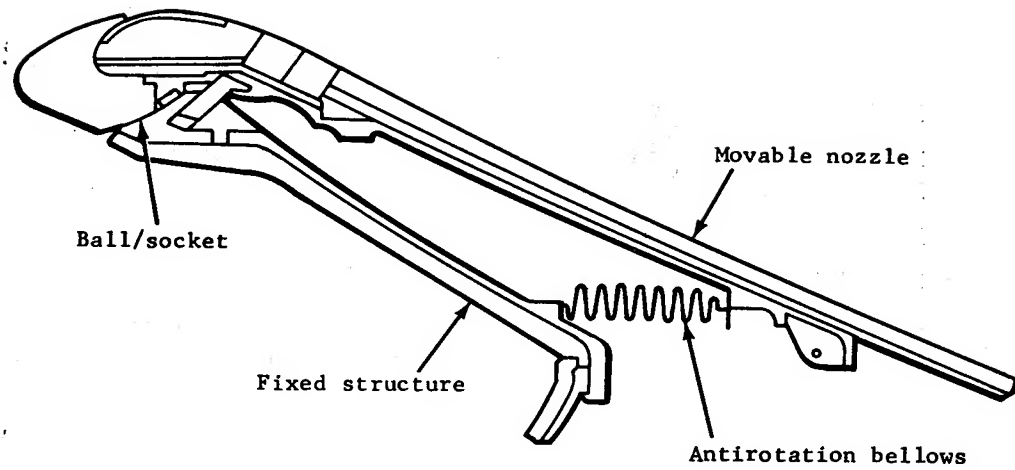
Figure 5. - Ball-and-socket nozzle.
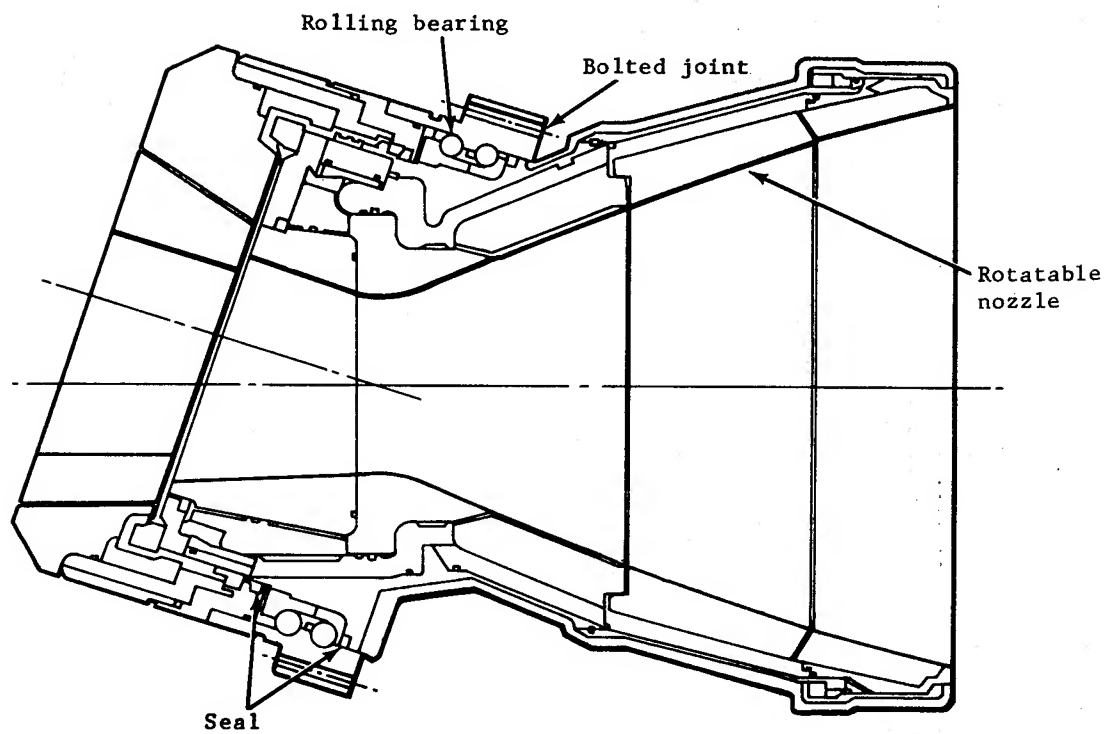
Figure 6. - Rotatable canted nozzle.
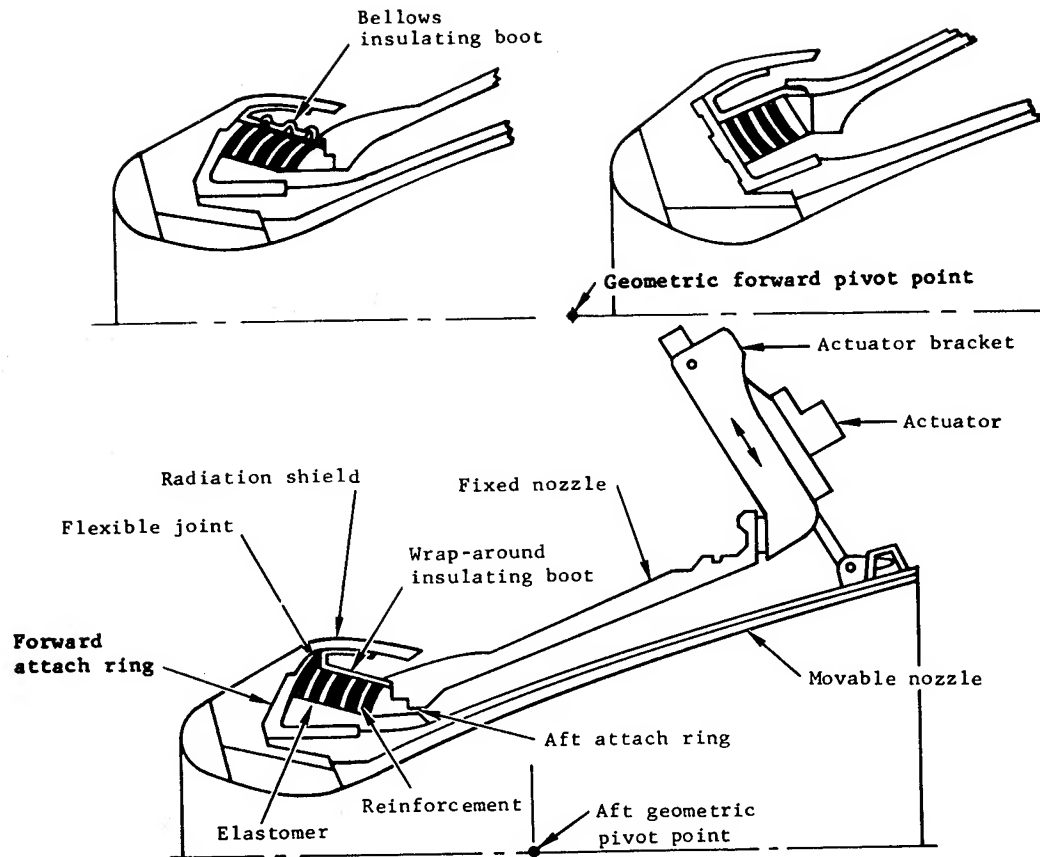
(a) Flexible joints with insulating boot
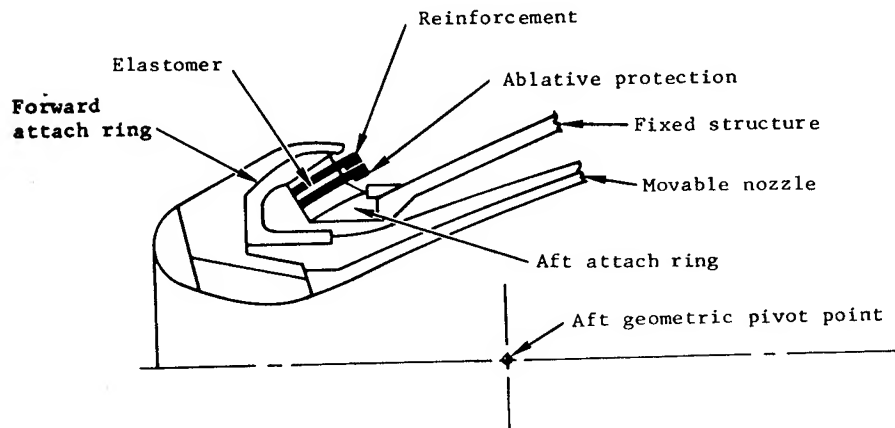
(b) Flexible joint with sacrificial ablative protector.

Figure 7. - Flexible-joint nozzle.

13

(a) Neutral position

(b) Vectored position
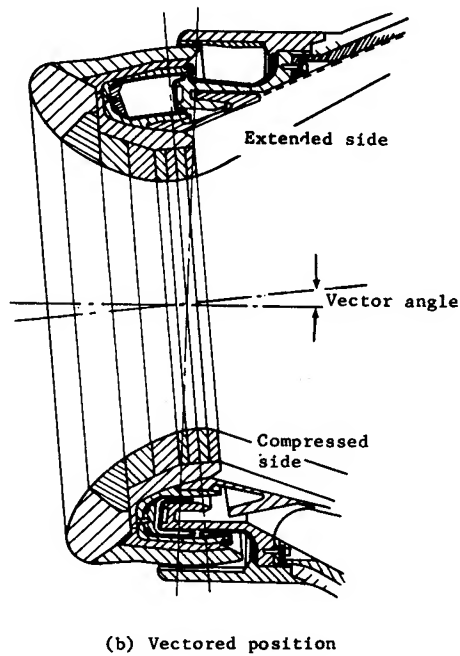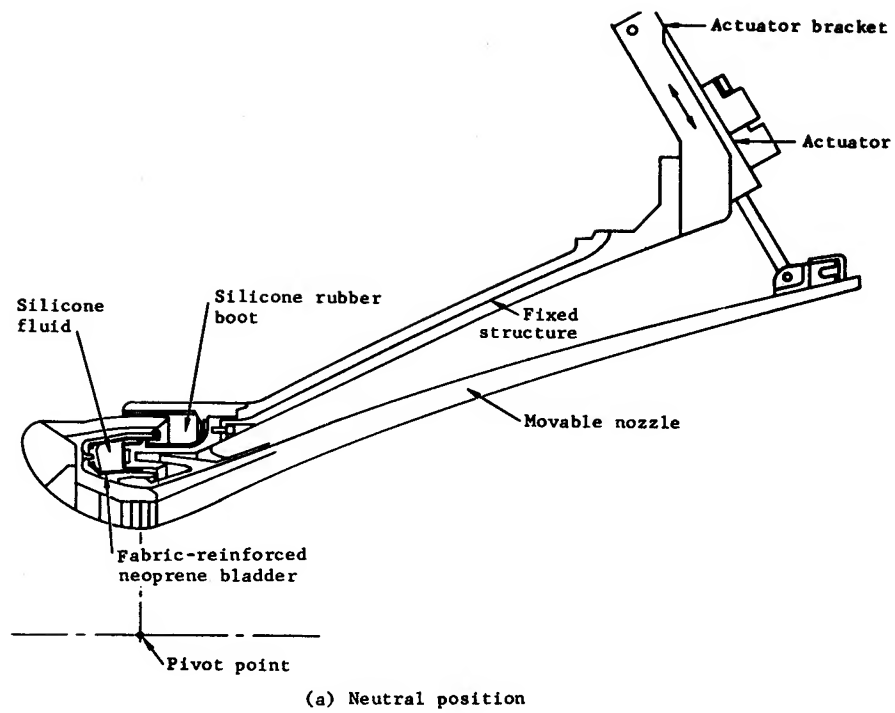
Figure 8. - Fluid-bearing/rolling-seal nozzle.

14
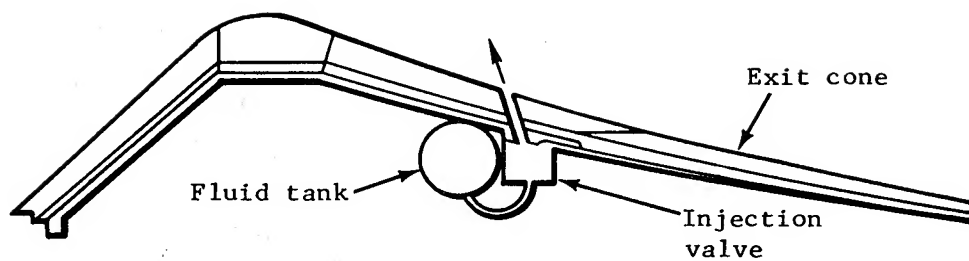
(a) External nozzle
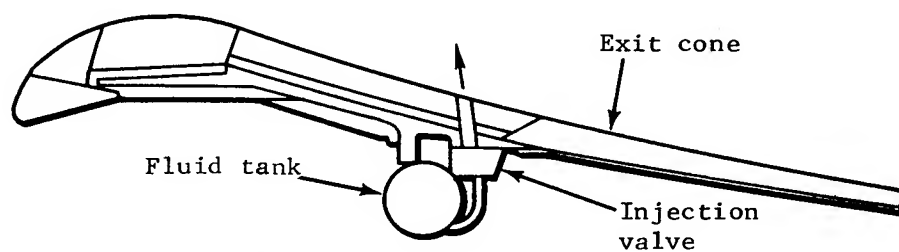
(b) Submerged nozzle

Figure 9. - Liquid injection TVC system.
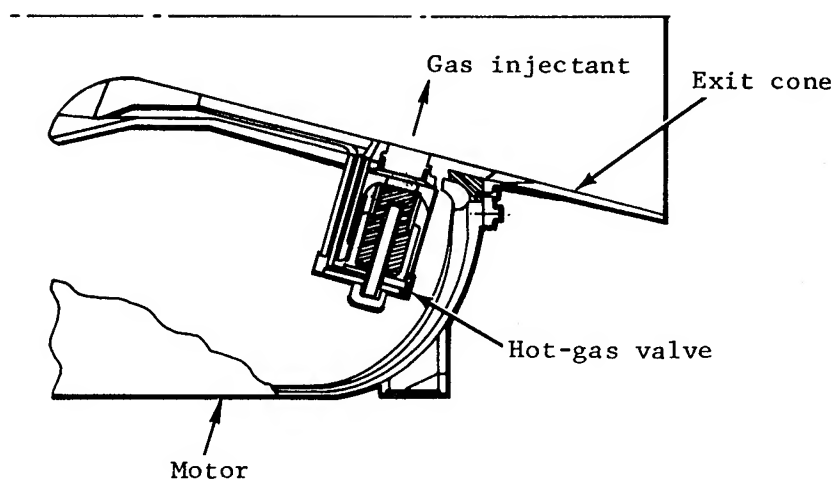
Figure 10. - Hot-gas TVC system, leg mounted.

Exit cone

Jet tab

(a) External nozzle

Exit cone

Jet tab

(b) Submerged nozzle
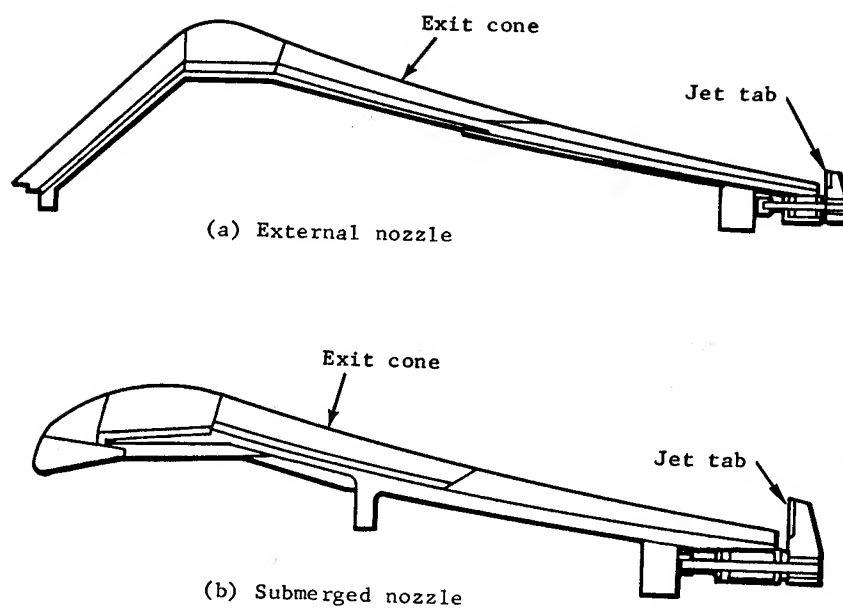
Figure 11. - Jet tab TVC systems.

comparison showed that the actuation torque for the fluid bearing/rolling seal was 30 percent of the actuation torque for the flexible joint. Fluid bearing/rolling seals up to 24-in. (60.96 cm) diameter have been tested in static firings up to vector angles of ± 6.5°, at vectoring rates up to 40 deg/sec, and motor pressures up to 1000 psig (6.89 MN/m²) (refs. 35 and 36). An 8-in. (20.32 cm)-diameter bearing has been tested in static firings up to vector angles of ± 12° at vectoring rates up to 140 deg/sec and motor pressures up to 2700 psia (18.6 MN/m²) for firing times of 20 seconds (ref. 35). This bearing has also been tested at vector angles of ± 15°, vectoring rate of 762 deg/sec, and motor pressure of 2100 psia (14.5 MN/m²) for a firing time of 5.5 seconds (ref. 35). The fluid bearing/rolling seal has been selected for use in a large high-performance motor, but as yet has not been demonstrated or accepted for an operational flight motor and therefore will not be evaluated further in this monograph.

The flexible joint has demonstrated the capabilities of the gimbal splitline but with fewer development problems, has been demonstrated in a number of flight motors, and is operational in the first- and second-stage motors for Poseidon C3; therefore, this joint is treated in detail in this monograph (secs. 2.1 and 3.1).

Liquid injection. — A large amount of experience on secondary-injection TVC systems (table II) has been accumulated. The liquid-injection system is a state-of-the-art system that is operational on several vehicles. This system has the advantage over the movable-nozzle system in that most of the excess liquid can be dumped after staging and recovery of flight attitude, the vehicle thereby having less inert weight during the remainder of the flight than the vehicle that must continue to carry nozzle actuation hardware. Hot-gas injection systems are promising, but valve and piping problems due to the severe thermal environment need to be solved. Warm-gas injection systems reduce the thermal environment problem but require large and heavy gas generators. The liquid-injection system therefore is treated in detail in this monograph (secs. 2.2 and 3.2).

Mechanical systems. — The mechanical deflector systems listed on table III either were operational (e.g., jet vane and jetevator) but have now been replaced by other systems, or were limited to development static firings (e.g., jet tab and segmented nozzle) and in general are no longer being considered in the industry. These techniques generally suffer from high weights and material problems due to exposure to hot exhaust gases. The movable pintle and plug (table IV) have not advanced beyond limited experimental evaluation and are not now under development.

2.1 FLEXIBLE JOINT

The flexible joint is a nonrigid pressure-tight connection between the rocket motor and a movable nozzle that allows the nozzle to be deflected by as much as 15° in a given direction*. The deflection of the nozzle deflects the motor thrust vector and generates a moment about the vehicle center of gravity, thereby altering the course of the vehicle.

Two kinds of flexible joints are shown in figure 7. The flexible joint is shown in a neutral position in figure 12 and in a vectored position in figure 13. These figures also show the descriptive terms used throughout this monograph. A complete list of symbols and definitions appears in Appendix B.

2.1.1 Configuration

The flexible joint consists of rings of an elastomeric material alternating with rings of metallic or composite material. These rings are usually spherical sections with a common center of radius referred to as the geometric pivot point. A joint wherein the rings were identically shaped conical sections has been designed and successfully tested (ref. 22). This design had the advantage of requiring a single set of tooling for all the rings rather than tooling for each ring as is necessary with spherical rings. Since each ring had the same shape, the joint was limited to a cylindrical envelope.

One end of the flexible joint is connected to a fixed structure, and the other is connected to a movable nozzle. Since the joint is symmetrical about its centerline, the nozzle can vector in any direction. When the nozzle is acted upon by an external actuator force, the elastomeric components are strained in shear, each reinforcement ring rotates a proportional part of the total vector angle, and the nozzle rotates about the effective pivot point (fig. 13). Usually the effective pivot point does not coincide with the geometric pivot point because of different amounts of distortion in each reinforcement. Omniaxis movement of the nozzle is obtained by using two actuators 90° apart. In addition to providing a means for thrust vectoring, the joint also acts as a pressure seal. Flexible joints are designed so that the axial compressive pressure imposed on the elastomer is higher than the chamber pressure.

An important property of the elastomer in the operation of a joint is that the bulk compressive modulus is approximately 15 000 times the shear modulus. This relation means

---

* This amount of motion has been demonstrated, but an upper limit to deflection angle has not been established.

18
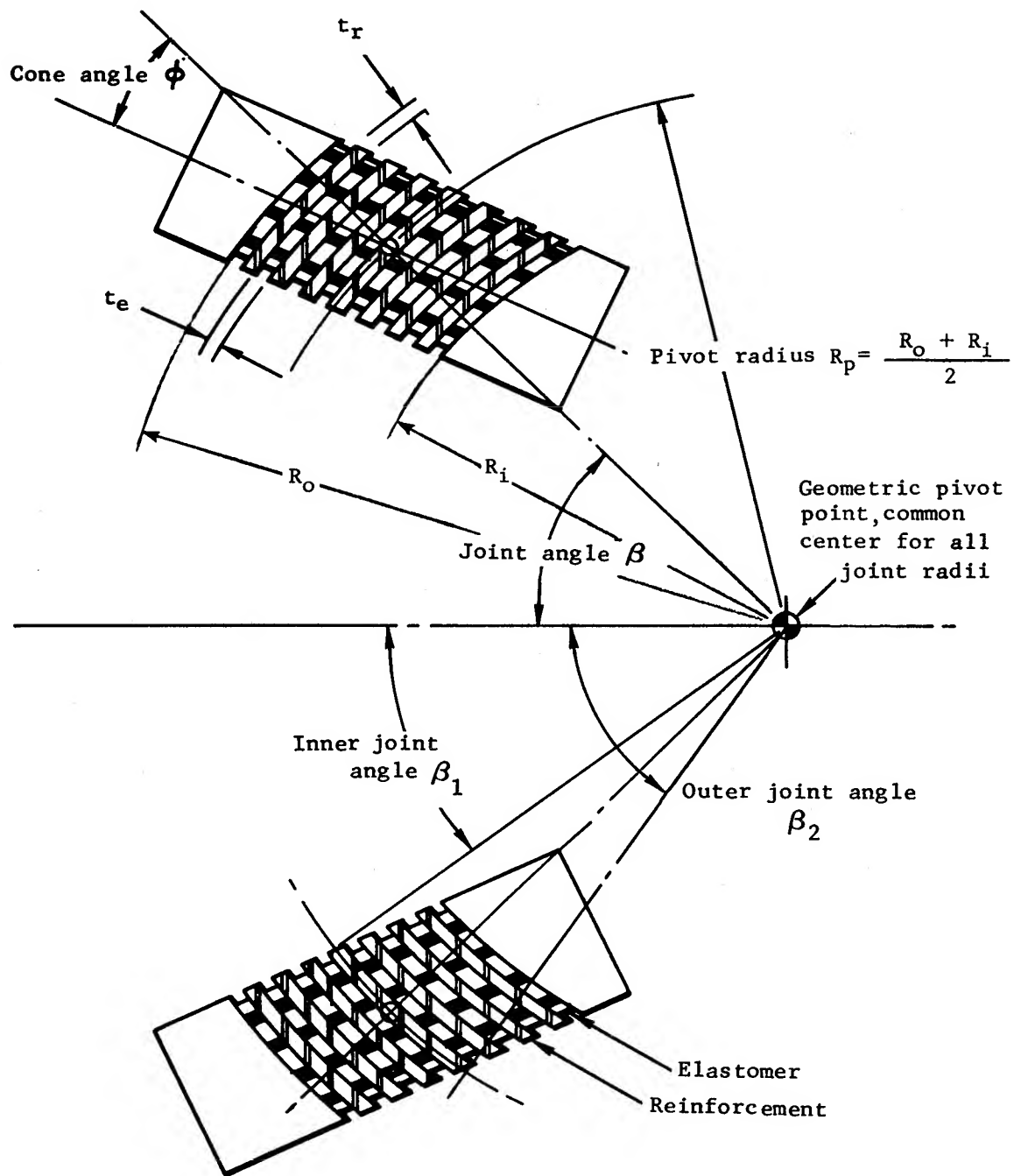
Figure 12. - Flexible joint in neutral position.

19

Deflected joint

Original joint envelope

Geometric pivot point

Vector angle θ

Effective pivot point

Joint $\mathcal{C}_L$

Deflected joint

Actuator force

Rotation occurs
about effective pivot point
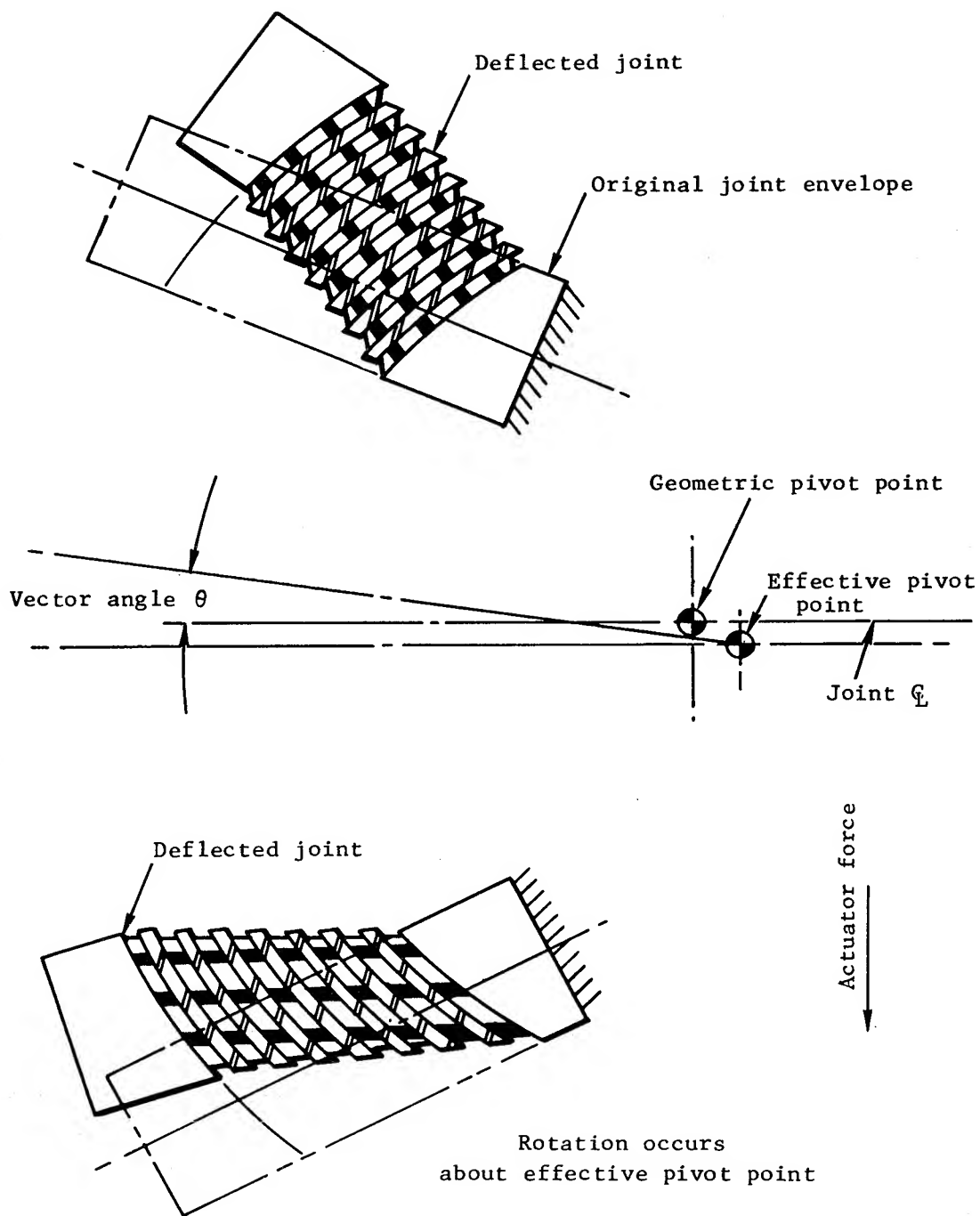
Figure 13. - Flexible joint in vectored position.

that a joint can transmit high axial compressive loads with low resulting axial deflections, but permits high shear deflections at low applied torques.

The reinforcements provide rigidity to the joint against motor pressure and axial loads due to motor pressure and constrain the joint to vector instead of deflecting sideways as would an all-elastomer cylinder when an actuator load was applied.

The movable nozzle with a flexible joint consists of four main subsystems: the movable-nozzle section, the attachment to the fixed structure, the actuation system, and the flexible joint. The movable-nozzle section and the attachment of the flexible joint to the fixed structure are treated in reference 75, and actuation systems are treated in reference 76. The effect of the actuation system on the flexible joint when the joint and actuator characteristics interact is discussed in this monograph.

2.1.1.1 DESIGN OPTIMIZATION

Flexible-joint design consists of the determination of the joint configuration, the number of reinforcement rings, the material for the reinforcement rings and elastomeric layers, and the materials for environmental protection. These elements must be selected and combined to provide the required spring stiffness, performance, and reliability at minimum weight and within cost and envelope limitations. Joint design is affected also by the attachment to the fixed structure and the movable nozzle. In some programs, the basic joint design requirements including motor pressure, vector angle, and envelope constraints are specified. In other programs, these design requirements must be determined in studies to define the optimum tradeoff relationship between the joint design requirements and the stage and vehicle design requirements (ref. 77).

The joint design is dependent on many geometric variables, and no general solution for joint design exists. Preliminary design is based on empirical relationships (refs. 17, 23, 78, and 79). A selected design is analyzed by finite-element techniques (refs. 80, 81, and 82), and the design is modified according to the analytical results. Analysis of a flexible joint is complicated by nonlinearity of material properties, large deflections and strains, nonsymmetric loading systems, and nonsymmetric geometries during vectoring. However, reasonable correlation between joint test results and calculated results has been obtained by use of an incremental procedure (ref. 80). The load is applied incrementally, and a finite-element analysis is conducted, using material properties associated with the stress at the previous increment and a geometry determined from the previous increment. When the applied load is axisymmetric, the deflected geometry will be axisymmetric. When the applied load is asymmetric (e.g., an actuation load applied by one actuator), the deflected geometry will not be axisymmetric. The deflected geometries at two cross sections 180° apart in the plane of actuation have been analyzed by finite-element methods that assume each cross section is axisymmetric (refs. 22 and 78). Methods of mathematical analyses

21

other than the finite element have been employed to consider finite joint deformations and material anisotropy (refs. 83 and 84).

2.1.1.2 ENVELOPE LIMITATIONS

The joint envelope is defined by the pivot radius R_p, the inner and outer joint angles β_1 and β_2, and the cone angle ϕ (fig. 12). The pivot radius is determined primarily by the nozzle throat diameter, but the inner and outer joint angles and cone angle are selected by the designer. All joints that have been successfully tested to date have had angle β_1 ranging from 40° to 45°, angle β_2 ranging from 45° to 55°, and angle ϕ that was not greater than the joint angle β (fig. 12) nor less than 0°. It has been demonstrated by analysis that joints with an angle β_2 up to 70° are feasible; these results suggest that the largest demonstrated value for $\beta_2-55°-$ may not be the limit.

The difference between the inner and outer joint angles $(\beta_2 - \beta_1)$ is maintained at the minimum value possible without exceeding the allowable elastomer stresses, so that the joint spring torque is kept to a minimum. It has been shown analytically (ref. 17) that the cone angle significantly affects the joint axial deflection and the elastomer and reinforcement stresses. As the cone angle increases, these values increase, and the effective pivot point moves farther from the geometric pivot point (fig. 13). However, decreasing the cone angle has resulted in nozzles with large re-entry sections that increase the weight of the movable section of the nozzle and require larger clearance envelopes in the motor, thereby reducing the amount of propellant.

Cost also has been a factor in determining the joint envelope. A large flexible joint (ref. 22) with conical-shaped reinforcements was manufactured. The joint was designed with a cylindrical envelope ($\phi = \beta$ as shown on fig. 13), and each reinforcement had the same cross section, thus reducing tooling and fabrication costs.

2.1.2 Design Requirements

The requirements affecting the design of a flexible joint are nozzle actuation torque, vector angle, axial deflection, frequency response, motor pressure, environmental effects, pressure sealing, cost, and weight.

The actuation torque (sec. 2.1.2.1), is made up of many contributing torques, each of which must be estimated for preliminary design and subsequently checked in static firings. The vector angle (sec. 2.1.2.2) required to produce sufficient maneuvering force on the vehicle is dependent on the position of the pivot point (fig. 13) and the vehicle performance requirements. Axial deflection (sec. 2.1.2.3) affects the clearance envelope required between

the fixed and movable portions of the nozzle; in addition, the axial deflection controls the axial spring stiffness of the flexible joint between the fixed and movable nozzle sections. The natural frequency and frequency response of the movable section (sec. 2.1.2.4) depend upon the axial stiffness and the mass properties of the movable section. The frequency response affects design of the actuator and guidance control system; sufficient stiffness must be designed into the movable nozzle to avoid dynamic coupling of various forcing functions. The motor pressure influences the selection of the joint materials and dimensions and affects the joint response to all of the aforementioned design requirements. The joint needs to be protected against a high-temperature environment on the motor side and the atmospheric environment on the outside (sec. 2.1.2.5). In addition, the joint must be a pressure seal between the motor and the atmosphere (sec. 2.1.2.6).

Flexible joints with elastomeric rings formulated from natural rubber have been operated at elastomer temperatures ranging from 65° F (291 K) to 85° F (302 K), and have been vectored in motors operating up to 600 000 feet (182 900 m) altitude with the elastomer at not less than 65° F (291 K). A joint with neoprene*/polybutadiene has demonstrated acceptable results in bench tests at temperatures from -40° F (233 K) to 165° F (347 K) (ref. 85).

2.1.2.1 ACTUATION TORQUE

In order to define the requirements of the control system and to actuate the nozzle in accordance with the motor or vehicle requirements, the designer must know the total actuation torque required. The actuation torque usually is defined about the geometric pivot point. The total torque is the summation of a number of contributing torques, including torques due to internal and external aerodynamics. The total torque is made up of the following component torques:

- Joint spring torque

- Frictional torque

- Offset torque

- Inertial torque

- Gravitational torque

---

* Materials are identified in Appendix B.

- Insulating boot torque

- Internal aerodynamic torque

- External aerodynamic torque

The total actuation torque varies from motor to motor and from cycle to cycle during continuous sinusoidal cycling on the nozzle. The total variability including both items has been determined to be ± 20% (refs. 86 and 87). The variability of a new design must be determined, since prior results may be based on joints that are not identical to the new design.

2.1.2.1.1 Joint Spring Torque

The flexible-joint spring torque (resistance of the joint to movement) usually is the maximum torque contributing to the actuation torque. It is dependent on a number of factors: total thickness of elastomer, pivot radius, joint angles, and motor pressure; it is also affected by environmental effects on the elastomer mechanical characteristics (sec. 2.1.2.5.2). The resistance of the joint to movement is overcome by the actuator; for convenience of analysis, the necessary torque is calculated as the moment arm from the geometric pivot point to the line of action of the actuator.

The spring torque is dependent on the combined thickness of all the elastomer rings and not on the thickness of each ring (ref. 17). The spring torque is roughly proportional to the cube of the pivot radius (i.e., $T_q \approx R_p{}^3$). Therefore, to ensure that the spring torque and envelope are a minimum, the joint diameter is minimized by placing the joint as close to the throat plane as possible; the pivot radius is then made as small as possible, but not so small as to increase the stresses in the joint above the allowable values. The inner and outer joint angles β_1 and β_2 (fig. 12) control the joint thickness. As noted, the difference between these angles is kept to a minimum consistent with the elastomer allowable stresses. The joint spring torque reduces as the motor pressure increases (refs. 13, 22, 86, and 87). This phenomenon is attributed to the effect of compression on the elastomer shear modulus properties, the configuration of the joint, and the change in shape of the joint (refs. 83 and 84). If sufficient pressure is applied, the spring torque can become zero. Little data are available on the variation in spring torque. Tests conducted on joints for two different motors that used a natural-rubber formulation show a variation of ± 20% at zero pressure. This torque variation in absolute units remained approximately constant and independent of motor pressure (refs. 86 and 87). The variation was correlated with lot-to-lot variation in the shear modulus of the elastomer (sec. 2.1.3.1).

For rapid calculation of the spring torque for joints with spherical reinforcement rings, a number of equations have been developed (refs. 17, 21, 23, and 78). Of these, the best correlation with test results for many different joints is the expression (adptd. from ref. 78)

$$\frac{T_q}{\theta} = \frac{12G_o r_o{}^3 r_i{}^3}{r_o{}^3 - r_i{}^3} \left[I(\beta_2) - I(\beta_1) \right] \qquad (1)$$

where

T_q = joint spring torque, in. - lbf (m-N)

θ = vector angle, radians

G_o = elastomer secant shear modulus at 50 psi (0.345 MN/m^2) shear stress (sec. 2.1.7.1), with no externally imposed pressure, at the elastomer temperatures expected in operation, psi (N/m^2)

r_o = $R_p + nt_e/2$, in. (cm)

r_i = $R_p - nt_e/2$, in. (cm)

R_p = pivot radius in. (cm)

t_e = thickness of individual elastomer layer, in. (cm)

n = number of elastomer rings

β_1 , β_2 = inner and outer joint angles, deg

$I(\beta)$ = integral values listed in table V (ref. 78)

TABLE V. — Integral Values I(β) for β = 15° to β = 60° (ref. 78)

β, deg	$I(\beta)$	β, deg	$I(\beta)$	β, deg	$I(\beta)$	β, deg	$I(\beta)$
15	0.0518	27	0.1601	39	0.3110	51	0.4849
16	.0588	28	.1713	40	.3249	52	.4999
17	.0661	29	.1828	41	.3389	53	.5148
18	.0739	30	.1946	42	.3531	54	.5298
19	.0820	31	.2067	43	.3674	55	.5448
20	.0906	32	.2189	44	.3818	56	.5599
21	.0995	33	.2315	45	.3963	57	.5749
22	.1088	34	.2442	46	.4109	58	.5899
23	.1184	35	.2572	47	.4256	59	.6048
24	.1283	36	.2704	48	.4403	60	.6198
25	.1386	37	.2838	49	.4551		
26	.1492	38	.2973	50	.4700		

From test data, the following empirical relationship for calculating the spring torque at pressure has been developed for joints with steel reinforcements and natural-rubber-formulation elastomers (adptd. from ref. 78):

$$\frac{T_q}{\theta} = \frac{0.156\, G r_o^3\, r_i^3\, (\beta_2 - \beta_1)}{r_o^3 - r_i^3} \tag{2}$$

where

G = effective elastomer shear modulus when subjected to external pressure, psi (N/m^2)

$$= G_o + A\sigma^2 \tag{3}$$

A = constant depending upon reinforcement material

$= -0.2595 \times 10^{-6}$ for steel

$$\sigma^2 = \frac{P_c \sin^2 \beta_2}{(\sin^2 \beta_2 - \sin^2 \beta_1)\, \cos^2 \phi} \tag{4}$$

P_c = motor pressure, psi (N/m^2)

ϕ = cone angle, deg

For joints with cone angles varying from 15° to 50°, at high pressure, torques calculated from equation (2) have agreed within ± 8% with torques measured in bench tests.

2.1.2.1.2 Friction Torque

Friction torque in a conventional movable nozzle arises from sliding surfaces such as bearings and O-rings. Since there are no sliding surfaces in a flexible-joint nozzle, coulomb friction theoretically does not exist. Elimination of the joint friction eliminates problems from three major sources:

(1) Friction varies significantly from unit to unit and cannot be predicted with accuracy.

(2) Friction is the major source of steady-state error in the servo actuator system.

(3) The change from static to sliding friction causes a breakaway peak in actuation.

Although there is no sliding friction in a flexible joint, the joint does respond to actuation in a manner similar to that of a spring-mass system with both viscous friction and coulomb friction. The viscous friction probably is associated with the viscoelastic behavior of soft elastomeric materials. Viscous damping is an important consideration in determining the stability characteristics of the thrust vector control system. No methods are available to calculate either coulomb friction or viscous friction. Attempts to calculate the damping coefficient from the decaying actuator force transient occurring at the end of a step vector-angle function applied to a nozzle have been unsuccessful because no correlation could be obtained with the friction coefficient calculated from actuation data. For sinusoidal actuation of the nozzle, the viscous torque component does not contribute to the maximum actuation torque, since the viscous friction torque is a maximum when the nozzle is at zero position and zero when the nozzle is fully vectored.

The coulomb friction and viscous friction are determined experimentally. A nozzle is vectored at different frequencies but constant amplitude, and the actuator force is measured. A typical actuator force response is shown on figure 14(a); the actuator force at zero vector angle is the total friction. When the variation in total friction force with vectoring rate is plotted as shown in figure 14(b), the two friction components can be determined.

Experimental data have shown that for joints fabricated by the same manufacturer the variation in viscous friction is ± 30% and for coulomb friction is ± 15% (ref. 88). Joints fabricated by different manufacturers to the same specifications have demonstrated significantly different friction torque results, although the variability was approximately the same. Test results have indicated that the viscous friction is dependent on vectoring amplitude in addition to vectoring rate. The coulomb friction has been shown to be dependent on vectoring amplitude and pressure. The phenomenon of friction is little understood, and the elastomer properties and dimensions influencing friction have not been identified.

2.1.2.1.3 Offset Torque

Offset torque is the torque resulting from asymmetry in the nozzle due to misalignment and manufacturing tolerances. Consequently, offset torque can occur in bench tests as well as during motor firings. The offset torque during a motor firing is an aerodynamic torque additive to that due to nozzle vectoring. The amount of alignment offset is dependent on
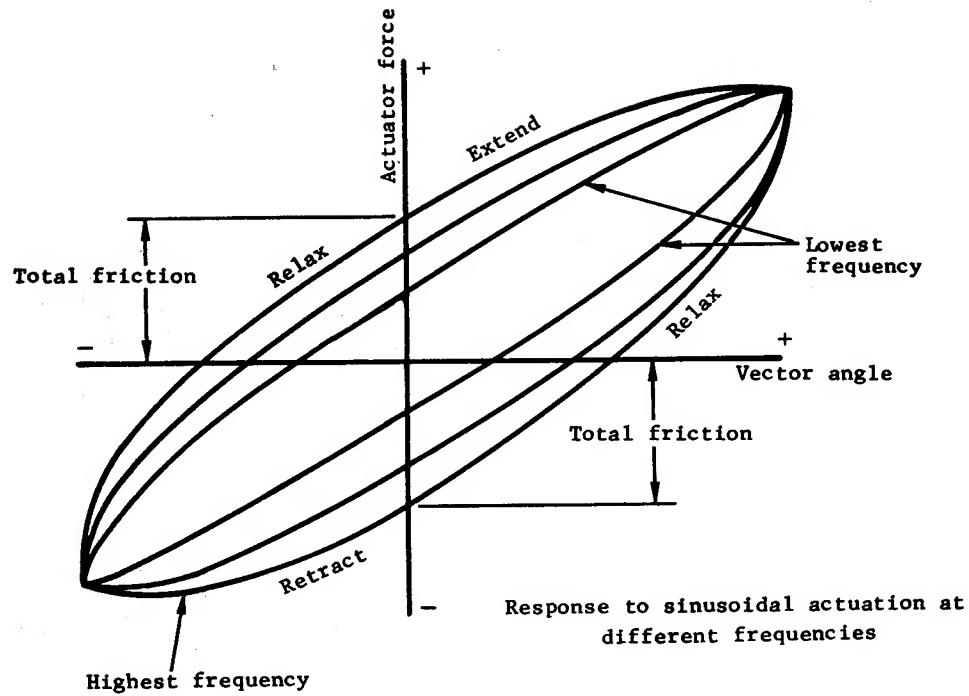
(a) Variation in vector angle with sinusoidal actuation force
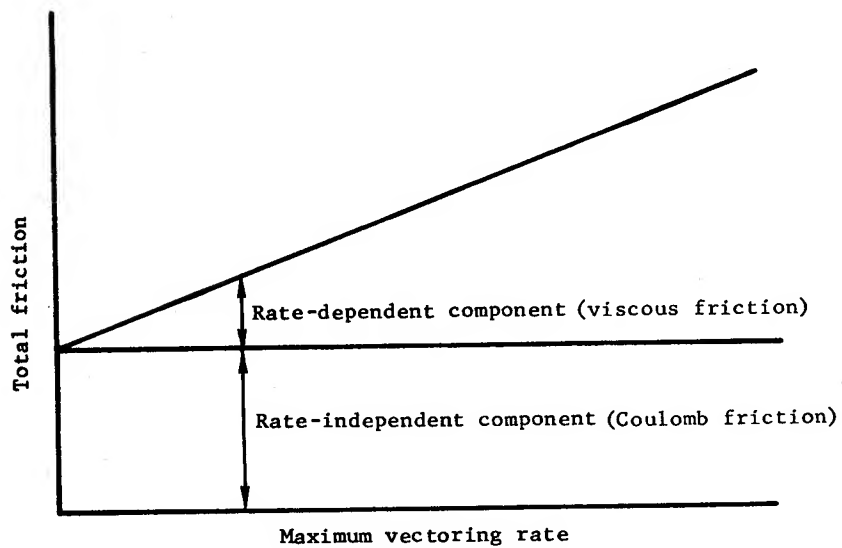
(b) Variation in total friction with maximum sinusoidal vectoring rate

Figure 14. - Graphical presentation of the effects of friction in a flexible-joint nozzle.

axial deflection characteristics of the joint and the motor pressure at which the nozzle must be at zero vector angle (sec. 2.1.2.3). The offset torque for joints up to 22-in. (55.88 cm) diameter has been small in comparison with the spring torque, and it is ignored in determining the actuation torque. However, it is possible that for larger joints the offset torque could be a significant contribution to the actuation torque.

2.1.2.1.4 Inertial Torque

The inertial torque is the torque about the pivot point resulting from accelerations produced on the nozzle by the actuator and is dependent on the vectoring acceleration. The inertial torque is determined by assuming that the mass of the nozzle acts at the center of gravity of the movable section of the nozzle and that the movable section vectors about the geometric pivot point. One end of the joint is connected to a fixed structure, and in the determination of section mass and center of gravity of the movable nozzle it is usually assumed that half the mass of the joint acts with the movable section. For joints designed to demonstrate maximum vector angles at zero motor pressure, the inertial torque usually is small compared with the spring torque even at high vectoring rates up to 500 deg/sec for sinusoidal actuation cycles, and is much less than the variability in actuation torque from motor to motor.

2.1.2.1.5 Gravitational Torque

The gravitational torque is the torque produced about the geometric pivot point by the movable nozzle mass as a result of accelerations imposed by the vehicle. As the vehicle maneuvers, pitch, yaw, and axial and lateral accelerations occur at the vehicle center of gravity, causing axial and lateral accelerations at the center of gravity of the movable nozzle. As before in the determination of net mass and center of gravity, half of the joint mass is assumed to act with the movable section. For large booster vehicles, the gravitational torque usually is small compared with the spring torque.

2.1.2.1.6 Insulating-Boot Torque

A flexible joint often is protected against hot motor gases by use of an insulating boot (fig. 7). Either this insulating boot is wrapped directly around the joint, or a dead air space separates the joint and the boot.

The wrap-around boot adds significantly to the nozzle vectoring torque. For example, use of a wrap-around boot fabricated of silica-filled butadiene acrylonitrile rubber (GTR V-45) on a 13-in. (33 cm)-diameter joint increased the actuation torque from 1000 in.-lbf/deg (113 m–N/deg) to 2100 in.-lbf/deg (237 m-N/deg) (ref. 13). When the design of the boot was changed to a bellows type (fig. 7), the actuation torque increased from 1000 in.-lbf/deg to 1600 in.-lbf/deg (180 m-N/deg) (ref. 14). A wrap-around boot design (fig. 7(a)) incorporating DC 1255 silicone rubber resulted in a 20% increase in actuation torque for a

joint 22 in. (55.88 cm) in diameter. This increase was not uniform from joint to joint and was found to be dependent on whether the boot was bonded to the reinforcements: the increase was greater when the boot was bonded to the reinforcements. In general, as the ratio of joint diameter to insulating boot thickness increases, the proportionate increase in actuation torque due to the boot will be less. For example, the increase in torque attributable to the insulating boot for a joint 112 in. (2.84 m) in diameter was 11 to 15 percent.

2.1.2.1.7 Internal Aerodynamic Torque

The internal aerodynamic torque acting on a submerged nozzle is the result of unsymmetric flow between the propellant grain and the movable nozzle. Pressure variations that occur around the vectored nozzle cause side forces and a resultant torque.

If the pivot point is forward of the nozzle throat, the aerodynamic torque is a restoring torque and hence is an increment to the actuation torque and needs to be calculated. If the pivot point is aft of the nozzle throat, the aerodynamic torque is sustaining and reduces the actuation torque (ref. 23). For an aft pivot point, the aerodynamic torque usually is ignored in calculating the actuation torque, thus ensuring a conservative estimate for actuation torque. However, if a system were designed to be vectored only at pressures that result in a low spring torque, the aerodynamic torque with an aft pivot point could overcome the spring torque and produce a negative actuation torque. A negative actuation torque can be tolerated in a closed-loop system.

The aerodynamic torque is calculated by summing the moments about the geometric pivot point produced by the pressure forces acting on the nozzle wall. This procedure requires a knowledge of the wall static pressure and the pressure differentials existing in the nozzle. Two procedures are available for developing the internal wall pressure in a vectored nozzle: airflow simulation tests (ref. 89), and a two-dimensional method-of-characteristics solution (ref. 90). When the aerodynamic torque is calculated from the results of airflow simulation tests, the calculated value generally is within ± 20% of the measured value. When the aerodynamic torque is calculated from the results of a two-dimensional method-of-characteristics analysis, the result generally is within ± 50% of measured value.

As the grain burns and the clearances between the nozzle and the grain increase, the pressure distribution becomes more symmetrical, so that the aerodynamic torque becomes of little significance near the end of propellant burn.

2.1.2.1.8 External Aerodynamic Torque

During flight, the external air stream impinges on the nozzle exit cone and creates a torque component, especially in the high dynamic pressure region when large vector angles are required. In specific cases, this effect perhaps could be utilized to increase the

maneuverability of the vehicle in this flight region or to provide vehicle control after motor burnout. The external aerodynamic torque could be calculated from the pressure acting on the nozzle exterior surface in the same manner as the internal aerodynamic torque is calculated (sec. 2.1.2.1.2). However, in most booster applications, the exit cone is shrouded by a motor case skirt that prevents significant air impingement that would cause an external aerodynamic torque.

2.1.2.2 NOZZLE VECTOR ANGLE AND PIVOT POINT

The amount of nozzle vector angle is determined by the vehicle control requirements. When the nozzle is vectored, the resultant side force acts approximately through the pivot point. The pivot point can be forward or aft of the nozzle throat (fig. 15). The position of the
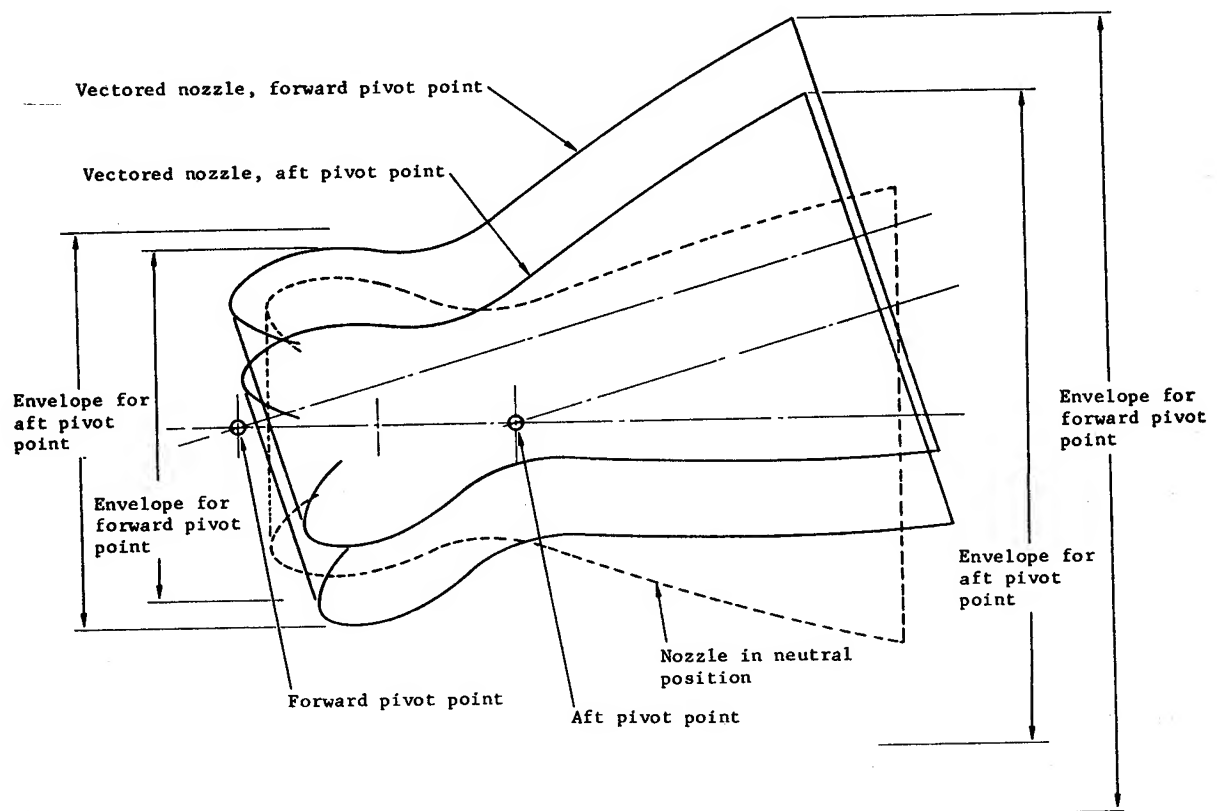
Figure 15. - Effect of pivot-point position on required envelope.

geometric pivot point is selected from a tradeoff study that considers the effect of position on the exterior clearance envelope between the fixed and movable parts, the actuator force and stroke to fulfill vehicle guidance requirements, and the spatial envelope available for the movable nozzle A summary of the comparative effects of a forward or aft pivot point is presented in table VI.

TABLE VI. — Comparative Effects of Forward and Aft Geometric Pivot Point

Item	Comparative effect	
	Forward pivot	Aft pivot
Clearance envelope in nose cone region	Reduced	Increased
Clearance envelope for exit cone	Increased	Reduced
Actuator stroke to produce a particular vector angle	Increased	Reduced
Actuator force to produce a particular vector angle	Reduced	Increased
Vector angle to produce a particular vehicle movement	Increased	Reduced

As shown, a forward pivot point will reduce the moment arm to the vehicle center of gravity and thus require a large vectoring angle to generate the necessary turning moment. Similarly, an aft pivot point will reduce the required vectoring angle. A forward pivot point will require less envelope for movement of the nozzle nose cap region but more envelope for the exit cone (fig. 15). The moment arm from the pivot point to the actuator is greater with a forward pivot point, and therefore less actuator force is required; however, because the exit cone movement is increased, the actuator stroke is increased.

Because of the reduced nose-cap movement, forward pivot points generally are used for nozzles having little or no submergence into the motor chamber. Aft pivot points generally are used for nozzles having deep submergence, because the envelope for exit cone movement is critical. However, the increased nose-cap movement reduces the envelope available for propellant (fig. 15). Regardless of whether a forward or aft pivot is selected, the joint angle β on joints tested to date has been between 45° and 50°.

The position of the effective pivot point is dependent upon the applied loads and joint configuration. The actuator force, in addition to vectoring the joint, causes a movement of the joint in the radial and axial direction, so that the effective pivot point is offset from the geometric pivot point (fig. 13). Vectoring of the joint causes each reinforcement to deflect differently, strongly influencing the position of the effective pivot point. At zero motor pressure, only the actuator force causes pivot point movement. At motor pressure, an axial compressive load is applied to the joint and causes additional pivot point movement. Figure 16 shows the measured pivot point movement for three different joints varying from 21 inches (53.3 cm) diameter to 112 inches (2.84 m) diameter, vectored at zero motor pressure and at maximum expected operating pressure. The pivot point movement can be decreased by decreasing the cone angle. Analytical studies (ref. 17) have indicated that the reinforcement stresses decrease as the cone angle decreases (sec. 2.1.5.3), because the reinforcement deflection decreases. Reduced reinforcement deflection results in reduced pivot point movement. As shown in figure 16, pressure acting on the joint also reduces the lateral movement of the pivot point due to vectoring.

A knowledge of the effective-pivot-point location is important in establishing the clearance envelope between the fixed and movable nozzle components. In one flexible-joint program, the effective pivot point was assumed to have moved an amount equal to the axial deflection, and a clearance envelope was set up accordingly. It was subsequently determined that the effective pivot point had moved approximately 1.5 in. (3.81 cm) while joint axial deflection was 0.4 in. (1.02 cm). The allowed clearance envelope was too small and had to be increased by removing part of the joint. No method has been developed that accurately predicts the lateral movement of the pivot point. An approximate method to determine the pivot-point position due to axial load is presented in the following section.

2.1.2.3 AXIAL DEFLECTION

Although the flexible joint is relatively stiff in compression in comparison with its vectoring stiffness, a measurable amount of axial compression occurs when the motor is pressurized. It is necessary to know the axial compression to determine nozzle envelope requirements, the axial compressive spring stiffness, and the nozzle misalignment requirements. The axial compression acts to reduce some clearances between the fixed and movable nozzle components, increases the vectoring clearance around the exit cone, and influences the position of the pivot point. The spring stiffness is required in the design of the guidance control system. The fixed-length actuator causes vectoring of the nozzle by motor pressure, and the nozzle is misaligned at zero pressure so that it is aligned at some required pressure.

The axial compression is dependent on the elastomer stiffness, the reinforcement stiffness, and the cone angle. The axial compression involves an interaction among elastomer properties in compression, deformation of the elastomer, reinforcement stiffness, joint envelope, and the ratio of the dimensions of the elastomer rings to the reinforcement rings.

Joint description	Force system at geometric pivot point	Position of effective pivot with respect to geometric pivot point
Mean joint diameter = 112 in. (2.84 m) Pivot radius = 73 in. (1.85 m) Cone angle = 50° Vector angle = 2°	(a) Zero motor pressure 53 000 lbf(2.358 x 10⁵ N) Aft → 5.1 x 10⁶ in.-lbf (5.76 x 10⁵ m-N)	Geometric pivot point Aft → 6 in. (15.24 cm) Axial position is reference plane Effective pivot point
	(b) At motor pressure 49 000 lbf (2.180 x 10⁵ N) 1.15 x 10⁶ lbf (5.115 x 10⁶ N) 4.8 x 10⁶ in.-lbf (5.42 x 10⁵ m-N)	5-1/2 in. (13.97 cm) Geometric pivot point 1-1/2 in. (3.81 cm) Effective pivot point Aft → Joint axial deflection at pressure = 0.24 in. (6.10 mm)
Mean joint diameter = 21 in. (53.3 cm) Pivot radius = 13.90 in. (35.3 cm) Cone angle = 50° Vector angle = 5°	(a) Zero motor pressure 1770 lbf (7873 N) Aft → 1480 lbf (6583 N) 56 000 in.-lbf (6327 m-N)	Geometric pivot point 1 in. (2.54 cm) 0.5 in. (1.27 cm) Effective pivot point Aft →
	(b) At motor pressure 1000 lbf (4448 N) Aft → 210 000 lbf (9.341 x 10⁵ N) 835 lbf (3714 N) 32 000 in.-lbf (3615 m-N)	2-1/4 in. (5.71 cm) Aft → Geometric pivot point 0.02 in. (0.5 mm) Effective pivot point Joint axial deflection at pressure = 0.4 in. (1.02 cm)
Mean joint diameter = 21.14 in. (53.7 cm) Pivot radius = 13.70 in. (34.80 cm) Cone angle = 50.5° Vector angle = 5°	(a) Zero motor pressure 1130 lbf (5026 N) 3100 lbf (13789 N) 46 000 in.-lbf (5197 m-N)	Effective pivot point Aft → 0.14 in. (3.6 mm) Geometric pivot point
	(b) At motor pressure 785 lbf (3491 N) 110 000 lbf (4.893 x 10⁵ N) 2160 lbf (9608 N) 32 000 in.-lbf (3615 m-N)	Effective pivot point 2 in. (5.08 cm) 0.02 in. (0.5 mm) Geometric pivot point Aft → Joint axial deflection at pressure = 0.3 in. (7.6 mm)

Figure 16. - Movement of pivot point for three different flexible-joint nozzles.

34

Test results have shown that these interactions result in a nonlinear response to applied axial compressive loads (refs. 22, 86, and 87).

The loading conditions for a flexible joint consist of an external radial pressure and an axial compression load due to the motor pressure acting on the movable section of the nozzle. The axial compression load due to motor pressure is calculated by integrating the pressures acting on the movable section. Solutions in the form of equations to predict axial compression have not been satisfactory. Measured deflections have been as much as four times the calculated deflection. Most success in predicting axial compression has been obtained with computerized finite-element methods of analysis (refs. 78, 81, and 82). Reasonable correlations between calculated and measured axial deflections have been made with the use of a sequential-loading finite-element method. The geometry of the joint for each loading increment is changed to the deflected geometry due to previous loading increments. For each loading increment, the elastomer shear modulus is assumed constant at the secant shear modulus at 50 psi (0.345 MN/m^2) shear stress (sec. 2.1.7.1), and all other elastomer properties are determined assuming isotropy and incompressibility (i.e., Poisson's ratio = 0.5).

An approximate estimate of the position of the effective pivot point when the joint is loaded by motor pressure is made by considering the movement of the geometric pivot point for each reinforcement. When loaded by motor pressure, each reinforcement rotates but undergoes negligible change in cross-sectional shape. Consequently, the geometric pivot point for each reinforcement can be defined. Each reinforcement rotates a different amount, and the effective pivot point is approximately at a mean of all the geometric pivot points.

2.1.2.3.1 Nozzle Misalignment

Axial deflection causes a vectoring misalignment of the nozzle. When the actuator attachment points are a fixed distance apart, as in the case just after booster launch before the guidance system begins to control the vehicle, the nozzle is not free to translate aft as the motor pressure increases. An actuator length that holds the movable components aligned to the fixed components at zero motor pressure would be too short at operating pressure. The nozzle at pressure would vector as though the actuators were retracted (fig. 17). Since alignment of the exit cone to the fixed components is less important in an unpressurized condition than in the pressurized condition, the actuator length at zero pressure is set to minimize the angle between the movable and the fixed components at some nominally pressurized condition. At zero pressure, this actuator length is too great, and the nozzle is vectored as though the actuators were extended. As the motor pressure increases, the misalignment decreases.
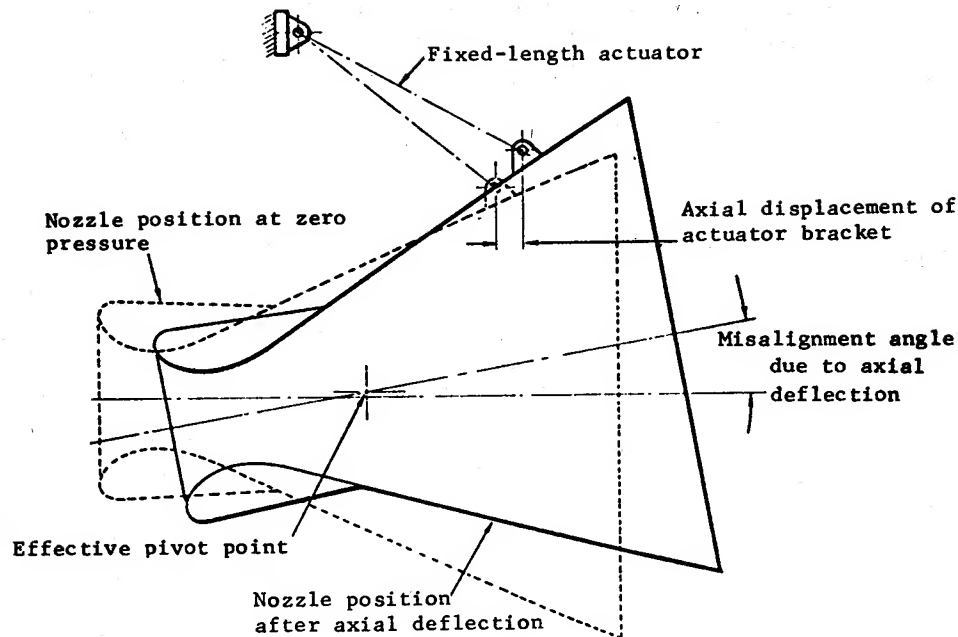
Figure 17. - Effect of axial deflection (due to motor pressure) on nozzle alignment.

The actuator bracket (fig. 7(a)) usually is connected to the motor case; hence the actuator bracket deflects as the motor is pressurized. The effect of actuator-bracket deflection has to be included in determining misalignment. If the actuator bracket is connected to the aft adapter of a glass-filament-wound motor case, the misalignment due to actuator bracket deflection is much larger than that due to axial deflection of the joint. This difference arises because the rotation of the aft adapter can be as much as 3° at maximum expected operating pressure MEOP.

2.1.2.4 FREQUENCY RESPONSE

The movable nozzle section and the flexible joint form a spring-mass system. The fixed structure forms an additional spring in the guidance control system. If a strong natural frequency of the control system applied through the actuators is near the frequency of a natural mode of nozzle oscillation, the nozzle oscillations will be reinforced. An instance has occurred where the hydraulic actuator stiffness was low enough to be the primary stiffness

36

determining the nozzle natural frequency. All of the nozzle subsystems are designed to have enough stiffness so that their individual natural frequencies are high when compared with the driving frequencies transmitted through the control system. Preliminary estimates of the stiffness of each subsystem can be made, but mathematical models of the nozzle and actuation system are difficult to build without test data. Consequently, tests to determine frequency response, closed-loop damping, and open-loop damping are conducted early in a development program.

2.1.2.5 ENVIRONMENTAL PROTECTION

Flexible joints are protected against exposure to hot motor gases, warm atmospheres, and atmospheres that could cause rapid aging of the elastomer. The effect of temperature has been demonstrated on a natural-rubber formulation (ref. 91), the results showing that increasing temperature decreases the shear modulus, the allowable stresses and strains, and the strength of the bonds to the reinforcement. Atmospheric aging of specimens of natural-rubber formulations show increased shear modulus and reduced allowable stresses and strains (ref. 92). Other studies have shown that silicone rubber is much less sensitive to aging (refs. 93 and 94).

Limited studies (ref. 85) with laboratory specimens have been conducted on formulations of (1) neoprene, (2) neoprene/polybutadiene, (3) ethylene propylene terpolymer (EPDM), (4) butyl, and (5) silicone, for use in joints over a temperature range from -40° F (233 K) to 165° F (347 K). The results showed that for all formulations (1) tensile strength is little affected from -40° F (233 K) to 70° F (294 K) and decreases up to 165° F (347 K), and (2) tensile elongation is a maximum at 70° F (294 K). Shear studies of the neoprene/polybutadiene and silicone formulations showed that (1) the shear strength increases with decreasing temperature, and (2) shear elongation is a maximum at 70° F (294 K). The secant shear modulus at 50 psi (0.345 MN/m^2) shear stress for neoprene/polybutadiene is little affected from 70° F (294 K) to 165° F (347 K) but increases significantly at -40° F (233 K), whereas the silicone formulation is little affected from -40° F (233 K) to 165° F (347 K). The neoprene/polybutadiene formulation was bench tested in a joint at -40° F (233 K), 70° F (294 K), and 165° F (347 K); the results showed that (1) axial compression increased with increasing temperature, (2) the actuation torque did not change from 20° F (266 K) to 120° F (322 K), and (3) with the value at 70° F (294 K) as a reference, the actuation torque increased 18 percent at -40° F (233 K) and decreased 18 percent at 165° F (347 K).

2.1.2.5.1 Thermal Protection

In most cases, the flexible joint is protected against exposure to warm or cold atmospheres by controlling the atmosphere surrounding the joint prior to firing. Most joint testing is conducted with the joint at temperatures from 65° F (291 K) to 85° F (302 K). Limited

bench testing has been conducted on joints at conditions from -40° F (233 K) to 165° F (347 K) (ref. 85).

The joint is protected from hot motor gases either by use of an insulating boot (fig. 7(a)), or by use of sacrificial ablative protectors (fig. 7(b)). As noted earlier, either the insulating boot has been wrapped directly around the joint or a dead air space has separated the joint and the boot. The wrap-around boot provides less heat-transfer barrier for the same thickness, because there is no dead air space to act as an additional insulation between the boot and the joint. For the bellows-type designs, pressure relief holes through the boot are required to balance the pressure across the boot. The vent holes need to be sufficient to allow the gas pressure to equalize during high rates of change of pressure occurring at ignition, so that tearing of the boot is prevented. This design requires more envelope than the wrap-around design.

The design of the insulating boot requires decisions whether to use a wrap-around or a bellows design, and whether to expose the boot to the chamber environment of radiant heat transfer from the high-temperature motor gas stream or to minimize this heating by providing a radiation shield mounted on either the fixed or movable nozzle components. Both the exposed boot (refs. 13, 14, and 23) and the protected boot (refs. 95 and 96) have been used. Motor designs using an exposed boot require an ablative plastic material for the boot,making it necessary to know the char and erosion behavior as a function of strain in addition to gas composition, pressure, temperature, and velocity. When a radiation shield is provided, the boot material is a silicone rubber. The boot and radiation shield are designed so that the gap between the movable and fixed sections (fig. 7(a)) occurs in a stagnant region. Even when the joint is actuated and the shape of the annular cavity around the circumference is altered, there is little circumferential flow in the annulus. One such design, 22 in. (55.88 cm) in diameter and using a silicone rubber boot, showed only slight charring with no erosion. Consequently, the boot needed to be thick enough to withstand only the radiant heating through the gap between the boot and the protection shield. For the exposed boot, the required insulating material is stiffer, and thus the increase in actuation torque is greater than that of the protected boot. However, the protected boot requires more envelope.

The sacrificial ablative protectors extend outboard of the elastomer rings a distance sufficient to provide a heat-transfer barrier between the hot motor gases and the elastomer. To minimize heating in the cavity between protectors, the protectors are cross sectioned so that the gap between protectors is less than the elastomer thickness (fig. 7(b)). The gap between protectors must be wide enough to prevent contact during vectoring or motor pressurization. Because there is a possible path from the hot motor gases to the elastomer, it is necessary to determine the environment in the region of the protectors and to relate this environment to the char and erosion characteristics of the protector material. Slag accumulation in the gaps after static firing has been noted, but this buildup did not cause anomalies in the vectoring response of the nozzle during firing. This result was attributed to

the lack of adherence between the slag and the carbon-fiber/phenolic--resin composite used for the protectors. The sacrificial ablative protector does not cause an increase in actuation torque and requires less envelope than the insulating boot with a radiation shield.

All thermal protection designs have been tested successfully: the exposed insulating boot with and without bellows (refs. 13 and 14), the protected insulating boot with and without bellows (refs. 23, 95, and 96), and the sacrificial ablative protectors (ref. 25). Selection of a design is made from a study evaluating such factors as gas characteristics (temperature, composition), gas flow (velocity, stagnation regions, pressure), envelope requirements, actuation power source, and overall system weight (actuation system, joint, insulating system) in relation to performance factors (e.g., range, payload, and reliability) and cost.

2.1.2.5.2 Aging Protection

Tests of flexible joints using a natural-rubber formulation (GTR 44125) with the rubber surfaces protected from the environment have demonstrated that, with aging, performance changes, axial compression is reduced, and spring torque is increased. The performance change has been attributed to continued reaction of the components of the elastomer. The spring torque increased by approximately six percent per year for 3½ years (ref. 97) and remained constant thereafter (ref. 26). The joints in this program were stored in an atmosphere at 80° F (300 K) and approximately 50% humidity. This is the only program where joints have been stored for a sufficiently long period and in sufficient quantity for data to be available. Similar results have been obtained in quadruple-lap shear and uniaxial tensile testing of specimens of the same rubber formulation; however, accelerated aging at 110° F (317 K) and 90% relative humidity for 9 months resulted in an increase in shear modulus from 24 psi (0.165 MN/m²) to 30 psi (0.207 MN/m²) (ref. 22).

The decrease in axial deflection that accompanies increased spring torque due to aging affects the nozzle misalignment (sec. 2.1.2.3), since it will change the zero alignment at the nominally selected operating pressure to some misalignment at that pressure. Currently, changes in joint performance are monitored, and projections of future performance are made. The future performance is compared with the motor requirements to evaluate probable joint life (ref. 26).

Elastomers less susceptible to aging are under development, but the rigorous requirements of shear modulus and shear strength make it difficult to develop a satisfactory elastomer. Further, the long time periods necessary to evaluate an elastomer make it difficult to assess property degradation with age for a new elastomer formulation. Accelerated aging tests at high relative humidity have indicated possible degrees of aging that have subsequently been found to be more severe than aging under normal service conditions (ref. 22). Silicone-rubber formulations are less susceptible to aging but have a shear modulus approximately 50% greater than that of natural-rubber formulations and a shear stress at failure approximately 50% less than natural-rubber formulations; in addition, silicones are more difficult to bond to metals.

A possible additional problem that has been considered is oxidation of the elastomer at its surface by either ozone or oxygen. Such oxidation has been prevented by ensuring that all possible exposed elastomer surfaces are coated with an impervious material such as chlorobutyl rubber or Hypalon rubber.

The elastomer in the uncured condition is susceptible to aging. A natural-rubber formulation showed a decrease in the shear modulus of cured rubber of 1 psi (6895 N/m^2) for each month of age of the uncured rubber stored at 40° F (278 K). The elastomer in this formulation was manufactured to as high a shear modulus as the specification allows so that if the shear modulus of the cured rubber decreased because of aging of the stored uncured rubber the formulation would remain within specification. The uncured rubber was stored for six months at 40° F (278 K) and if after storage the shear modulus of the cured rubber was within specification the rubber was used, but if outside of specification limits the rubber was rejected.

2.1.2.6 PRESSURE SEALING

If the axial compressive force due to motor pressure is sufficiently high, the geometry of a flexible joint assures that the joint will seal against leakage without the need for any special precautions. The dimensions of the movable nozzle and joint are such that a compressive axial load is applied to the joint, the result being a compressive stress in the flexible joint that is greater than the motor pressure. Consequently, small unbonded spots and voids are tolerated. When joints are manufactured by injection molding or compression molding (sec. 2.1.6.3), unbonding can be controlled only on a sample basis, because unbonded areas cannot be detected. For joints that are manufactured by secondary bonding (sec. 2.1.6.3), each bond line can be inspected for unbonding by ultrasonic techniques as the joint is being assembled. Regardless of the manufacturing method, there is no quantitative definition of the amount of unbonding that will result in a leak.

2.1.3 Material Selection

For fabrication of a flexible joint and its environmental protection, materials need to be selected for the elastomer, reinforcement, bonding system between the reinforcement and elastomer, insulating boot, and protection from the external atmosphere. The choice of material for a given use depends on the motor operating requirements (e.g., motor pressure, vector angle), the environmental operating conditions (e.g., propellant gas temperature, propellant gas velocity, atmospheric ozone content), and the envelope available. Each of these variables in turn is evaluated in a tradeoff study involving range, payload, reliability, and cost that seeks to optimize vehicle and motor performance.

2.1.3.1 ELASTOMERS

The important properties in the elastomer selection are the shear modulus, shear stress, reproducibility of these properties from lot to lot, and the ease of bonding the elastomer to the selected reinforcement material. Since it has been demonstrated that the joint spring torque could become zero because of axial compression, efforts are being made to determine shear properties with superimposed compression (ref. 78).

The joint spring torque is directly proportional to the elastomer shear modulus (sec. 2.1.2.1.1). In the selection of an elastomeric material, the aim is to use an elastomer with as low a shear modulus as possible and with a minimum of continued reaction of the components (sec. 2.1.2.5.2), which will increase shear modulus. Natural-rubber formulations have been developed with secant shear moduli (sec. 2.1.7.1) ranging from 20 psi (0.138 MN/m^2) to 35 psi (0.241 MN/m^2) at 50 psi (0.345 MN/m^2) shear stress. The low required shear modulus has presented difficulties to the elastomer formulators in preparing formulations that fulfilled the chemical stability requirement.

The shear stress in the elastomer is caused by vectoring and motor pressure. Of these, motor pressure usually is the more significant. Successful joints using elastomers having a minimum specified quadruple-lap shear stress (sec. 2.1.7.1) of 500 psi (3.45 MN/m^2) have been designed, manufactured, and tested, and all failures were cohesive.

To meet the requirements of shear modulus and shear stress, most joints have been fabricated of natural rubber or polyisoprene formulations. The joints of both stages of the Poseidon motors are natural-rubber formulations, either GTR 44125 or TR 3005 (refs. 98 and 99). The joint for the 260-in. (6.604 m) motor (ref. 22) and a joint designed to operate at 3000 psi (20.7 MN/m^2) to ± 15° at 300 deg/sec (ref. 14) used GTR 44125 elastomer. Required properties for these elastomers are minimum shear stress of 500 psi (3.45 MN/m^2) and secant shear modulus (at 50 psi (0.345 MN/m^2) shear stress) of 22 psi (0.152 MN/m^2) to 26 psi (0.179 MN/m^2) for GTR 44125 and 18.5 psi (0.128 MN/m^2) to 24 psi (0.166 MN/m^2) for TR 3005. Actual shear strengths for these elastomers are greater than 1000 psi (6.9 MN/m^2) (ref. 100) for GTR 44125 and 660 psi (4.55 MN/m^2) for TR 3005, all failures being cohesive. Polyisoprene elastomers have been used for the joints of the 156-in. (3.962 m) motor (ref. 23), the 100-in. (2.54 m) motor (ref. 19), and an advanced dual-chamber motor (ref. 18). The polyisoprene elastomers demonstrate shear properties that are equal to those of the natural-rubber formulations but the shear modulus is greater, being approximately 27 psi (0.186 MN/m^2) minimum. Natural-rubber formulations have been used for joints when the minimum expected operating temperature was not less than 50° F (283 K). Because of the difficulty in making an elastomer with a low shear modulus, close process controls are maintained to ensure a lot-to-lot variation in shear modulus not greater than 10 psi (0.070 MN/m^2).

A neoprene/polybutadiene formulation has been bench tested in a joint designed to operate between -40° F (233 K) and 165° F (347 K) at an equivalent motor pressure of 2550 psi

(17.6 MN/m²) to ± 17.5° at 360 deg/sec (ref. 85). Required properties of the rubber were a secant shear modulus (at 50 psi (0.345 MN/m²) shear stress) of not more than 50 psi (0.345 MN/m²) when the shear strength was greater than 600 psi (4.14 MN/m²), and a secant shear modulus that could decrease linearly to 25 psi (0.172 MN/m²) at 300 psi (2.07 MN/m²) shear stress; these values apply over the required temperature range. The required values were achieved over most of the temperature range except at -40° F (233 K), where the secant shear modulus was 72 psi (0.496 MN/m²).

Silicone elastomer formulations that are satisfactory for use in flexible joints from -40° F (233 K) to 165° F (347 K) have been developed (ref. 85), but these elastomers are difficult to bond to metals. The best bonds have been achieved with steel, but even these bonds demonstrated adhesive failures. The failure adhesive shear strength for silicone elastomers varied from 250 psi (1.72 MN/m²) to 560 psi (3.86 MN/m²); the shear modulus varied from 25 psi (0.172 MN/m²) to 40 psi (0.276 MN/m²), the higher modulus generally being associated with the higher strength. These elastomers have been used for low-temperature applications (dimethyl silicone formulations have a glass transition temperature at -85° F (208 K), and methyl-phenol silicone formulations, at -160° F (166 K). The induced shear stress due to motor pressure is directly dependent upon elastomer ring thickness, and because the allowable shear strengths are less for silicone formulations, joints using these formulations require thinner elastomer layers. The shear stress is minimized by designing the joint to have an envelope with a cone angle of approximately zero degrees (ref. 17).

2.1.3.2 REINFORCEMENTS

Joints have been fabricated with steel reinforcements and with composite reinforcements. The composite reinforcements have been formed with S-glass filaments and epoxy resin (refs. 27, 28, and 29) and S-glass filaments and phenolic resin (refs. 24 and 25).

The important properties in the selection of the reinforcement material are compressive yield stress, ultimate and yield tensile stress, modulus of elasticity, ease of fabrication, ease with which elastomers can be bonded to the material, and cost of the material. For composite reinforcements, the interlaminar shear stress is also an important property. In addition the selection of material depends on the joint envelope. For joints with a large cone angle, the mechanical properties have been the dominant factor in selecting materials. For conical envelope joints, the reinforcement stresses are relatively low (ref. 17), and factors such as ease of fabrication and cost became important.

The stresses in a reinforcement are a tensile hoop stress on the outer radius and a compressive hoop stress on the inner radius (sec. 2.1.5.2) due to motor pressure and vectoring. Failures in the reinforcements have always occurred at the inner radius, where the stress is compressive. For joints with steel reinforcements, the failure appears as a local wrinkling with unbonding between the elastomer and the reinforcement, so that the joint is

no longer a pressure seal. The wrinkling proceeds circumferentially around the reinforcement in a high-frequency wave pattern. For joints with composite reinforcements, the failure has appeared as rupture across a reinforcement thickness (ref. 27), interlaminar shear failure between different types of lamina in the laminate (ref. 28), or compressive failure (ref. 25).

Correlation of test data for metal reinforcements with calculated results (ref. 17, pp. 14-48, and sec. 2.1.5.2) indicates that the stress at failure is the compressive yield stress. However, buckling as a possible failure mode cannot be discounted. The failure buckling stress is dependent on the reinforcement dimensions, compressive yield stress, and the modulus of elasticity (sec. 2.1.5.2).

The reinforcement material selected affects the bond to the elastomer. Elastomers that have failed cohesively when bonded to steel have failed adhesively at lower stresses when bonded to aluminum. Although it has been shown analytically that aluminum could be used as a reinforcement material, it has not been used in any joints. Joints that were fabricated with natural-rubber elastomers and either epoxy-resin composites or phenolic-resin composites have never shown failure at the bond between the reinforcement and elastomer during bench testing.

The joints of the motors on both stages of Poseidon contain 4130 steel heat treated to 180 000 psi (1241 MN/m^2) ultimate tensile stress, and the 260-in. motor (6.6 m) (ref. 22) incorporates 4130 normalized steel. The joints of the 100-in. (2.54 m) motor (ref. 19) and 156-in. (3.96 m) motor (ref. 23) used 304 Condition-A stainless steel, and the joint for the advanced dual-chamber motor (ref. 18) used 17-7PH annealed stainless steel. All of these joints have been bench tested successfully to pressures in excess of ultimate design requirements.

The first joints with composite reinforcements used continuous hoop-wound S-glass filaments with ERL 2256/Tonox 6040 epoxy resin to provide hoop strength and stiffness (ref. 27). During bench testing, these reinforcements failed transverse to the windings, thus showing a need for transverse strength. The transverse strength was provided by S-glass filament mats laid up between the continuously wound S-glass filaments (ref. 34), the mat filaments being oriented at an angle across the hoop windings (refs. 27, 28, and 29). Joints with these configurations exhibited a change in the reinforcement failure mode and an improvement in joint strength when bench tested. To reduce the fabrication costs of composite reinforcements and to improve process control, joints were fabricated with closed-die compression-molded reinforcements consisting of FM 4030-190 (phenolic-preimpregnated S-glass roving) chopped into one-inch lengths (ref. 24). These joints were bench tested and static fired. Early joints for all three stages of the Trident I (C4) engineering development motors were fabricated with reinforcements of S-glass cloth preimpregnated with phenolic resin (ref. 25). These joints were successfully bench tested, and static firings with vectored nozzles were conducted successfully on second- and

third-stage motors. However, in the motor development program structural problems occurred in the reinforcements in flightweight joints. The resin system was changed from phenolic to an epoxy resin, and no further problems occurred. Fundamental strength and stiffness data have not been generated for the composite materials used in reinforcements.

2.1.3.3 ADHESIVE BOND SYSTEM

For test joints with either steel or composite reinforcement and a natural-rubber formulation intended for operation between 65° F (291 K) and 85° F (303 K), fabricated by injection molding or compression molding, the adhesive system has consisted of Chemlok 205 primer and Chemlok 220 adhesive. The bond failed at low strength levels in steel test specimens even though the surfaces of the steel were carefully prepared. This problem was overcome by ensuring that the material lots were of sufficient quality and that the adhesive layer thickness was controlled (sec. 2.1.6.2). Applying the same controls to composite reinforcements resulted in joints in which failures always occurred in the reinforcement.

The adhesive system for the joint with secondary bonding consisted of a primer system for the reinforcements, FMC 47 epoxy resin, and Chemlok 305 adhesive (ref. 22). The primer system is a high-temperature system. After the primer was applied to the reinforcements, the reinforcements were cured at 300° F (422 K). The adhesive, an ambient-cure adhesive, was cured during joint molding.

The adhesive system for test specimens with steel plates and neoprene/polybutadiene-rubber formulation for operation between -40° F (233 K) and 165° F (347 K), fabricated by compression molding, was Chemlok 205 primer and Chemlok 231 adhesive. Shear failures with this system were cohesive (ref. 85). The adhesive system for test specimens with a silicone rubber formulation for the same environment was 75 percent Chemlok 608 dissolved in methanol. Shear failures with this system were adhesive at 165° F (347 K) and cohesive at 70° F (294 K) and -40° F (233 K).

2.1.3.4 JOINT THERMAL PROTECTION

The joint thermal protection has been effected either by insulating boots or by sacrificial thermal protectors (sec. 2.1.2.5.1). The important properties for the joint thermal-protection materials are a low thermal diffusivity, high heat of ablation under strain levels anticipated in service, and mechanical flexibility with minimum char fracture at temperatures expected in service.

The choice of insulating boot material depends on whether the boot is protected by a radiation shield (fig. 7(a)). For insulating boots protected by a radiation shield, K1255 silicone rubber has been used. For joints with exposed insulating boots, materials have been

DC 1255 reinforced with chopped asbestos filler to reinforce the char layer (ref. 18) and silica-filled butadiene acrylonitrile rubber (refs. 13, 14, 19, and 20). All of these materials have performed successfully, but they have increased the joint spring torque (sec. 2.1.2.5.1).

The sacrificial thermal protector materials have been either S-glass/phenolic-resin or carbon-cloth/phenolic-resin composites. The molded S-glass/phenolic- or epoxy-resin reinforcements (sec. 2.1.3.2) included the protectors in the molding (ref. 24). The carbon-cloth/phenolic-resin protectors were fabricated as an integral part of S-glass/phenolic- or epoxy-resin composite reinforcements (ref. 25). Both of these materials have performed successfully in static firings (refs. 24 and 25) without causing an increase in joint spring torque.

2.1.4 Mechanical Design

2.1.4.1 GENERAL CONSIDERATIONS

A flexible-joint configuration has been flown on an operational vehicle, and approximately a dozen other joint configurations have been either bench tested or demonstrated in static firings (refs. 13, 14, 17 through 20, 22 through 29, 95, and 96). However, no general mathematical equations have been developed that correlate with test results for all configurations. The design of a flexible joint is developed from simple empirical relationships, derived from limited data, to establish preliminary dimensions and joint performance. These relationships are presented in this monograph as follows:

Torsional stiffness at zero pressure	- Section 2.1.2.1.1
Effect of pressure on torsional stiffness	- Section 2.1.2.1.1
Elastomer layer thickness	- Section 2.1.5.1
Reinforcement thickness	- Section 2.1.5.2

For joints with steel reinforcements, the initial component dimensions are established from the preliminary-analysis relationships. An improved analysis is then conducted with finite-element methods of analyses (refs. 17, 79 through 82, and sec. 2.1.5.3), and the joint design modified according to the results of the finite-element analysis. If necessary, the modified joint is analyzed again.

To establish a joint design with composite reinforcements, a different method has been used because the properties of the composite were unknown. A joint is designed and fabricated at the expected joint dimensions. The elastomer layer thickness and number of elastomer

layers are calculated according to procedures in section 2.1.5.1. The reinforcements are designed according to procedures in section 2.1.5.2, maximum strength at failure being assumed to be 60 000 psi (414 MN/m²). To establish the allowable composite strength, the joint is pressure tested to failure without vectoring and the results correlated with the preliminary analysis of section 2.1.5.2 and a detailed finite-element analysis of the joint. The allowable composite strength is defined as the calculated reinforcement stress at failure regardless of the joint mode of failure. The joint design is modified in accordance with this allowable composite strength at ultimate load conditions and analyzed by finite-element methods.

2.1.4.1.1 Design Definitions

The design of a flexible joint usually is established and then defined on the basis of the relationship between the loading conditions that will be imposed on the joint and the capacity of the joint to withstand these loads. Limit load, design factor of safety, design load, allowable load, and margin of safety are joint design terms that are used with respect to this relationship between joint loading and joint loading capacity. These terms, as they are used in this monograph, are defined in the following paragraphs.

Limit load. — The limit load is the maximum specified or calculated value of a service load or service pressure that can be expected to occur under (1) the maximum 3-standard-deviation operating limits of the motor or vehicle including all environmental and physical variables that influence loads, (2) the specified maximum operating limits of the motor or vehicle, or (3) the maximum motor or vehicle operating limits defined by a combination of 3-standard-deviation limits and specified operating limits.

Design safety factor. — The design safety factor is an arbitrary multiplier greater than 1 applied in design to account for design contingencies (e.g., variations in material properties, fabrication quality, and load distributions within the structure).

Design load (or pressure). — The design load (or pressure) is the product of the limit load (or pressure) and the design factor of safety.

Design stress. — The design stress is the stress, in any structural element, resulting from the application of the design load or combination of design loads, whichever condition results in the highest stress.

Allowable load (or stress). — The allowable load (or stress) is the load that, if exceeded in the slightest, produces joint failure. Joint failure may be defined as yielding or ultimate failure, whichever condition prevents the joint from performing its intended function. Allowable load is sometimes referred to as criterion load or stress.

Margin of safety. — The margin of safety (MS) is the fraction by which the allowable load or stress exceeds the design load or stress. The margin of safety is defined as

$$MS = \frac{1}{R} - 1 \qquad\qquad (5)$$

where R is the ratio of the design load or stress to the allowable load or stress.

2.1.4.2 DESIGN SAFETY FACTOR

Ideally, the design safety factor would be calculated from a knowledge of the randomness of the design variables and the required reliability and confidence levels. Unfortunately, there is insufficient understanding of the relationship of the assumed failure criteria to the complex stress distributions in a joint, and the methods of analysis are not sufficiently accurate. At present, a safety factor is established largely on the basis of engineering judgement combined with experience. As an example, if the motor specification requires an overall safety factor of 1.25, the joint is designed to a safety factor of 1.5.

2.1.4.3 FLEXIBLE-JOINT LOADS

All flexible-joint loads used in the flexible-joint structural analysis (sec. 2.1.5) are design loads as defined above. The loads on the flexible joint are those that result from

- Motor pressure

- Vectoring

- Vehicle accelerations during flight

- Handling and storage conditions

The motor pressure acts as a crushing pressure and also causes an axial compression on the joint. Significant tensile and compressive hoop stresses are developed in the reinforcement rings. In general, the compressive hoop stress in the reinforcements is more critical than the tensile stresses.

Vectoring of the joint increases the reinforcement hoop stresses on one side of the joint and reduces these stresses on the other. Shear stresses induced in the elastomer rings increase with motor pressure. Vectoring rate affects the elastomer shear stresses since the shear modulus is dependent on strain rate.

As a result of vehicle accelerations during launch, flight, or staging, the mass of the movable section of the nozzle imposes loads on the joint. These loads can cause all the stresses

47

induced by motor pressure or vectoring and, in addition, can cause an axial tensile load on the joint. Usually the stresses due to vehicle accelerations are not critical conditions.

Handling and storage conditions cause all the stresses induced by the previous conditions. During handling and storage care is taken that no axial tensile loads are imposed on the joint, since such loads can cause debonding of the elastomer from the reinforcement.

2.1.5 Structural Analysis

The structural analysis consists of the determination of the elastomer thickness, the reinforcement thickness, and the finite-element analysis. All structural analyses consist of two parts: a stress analysis to determine internal stresses, and a strength analysis comparing internal stresses to allowable stresses.

2.1.5.1 ELASTOMER THICKNESS

The stresses in the elastomer are caused by vectoring and motor pressure. The shear stress due to vectoring is approximately constant in the elastomer and depends on the total thickness of elastomer (i.e., number of elastomer rings x thickness of each layer) and not the thickness of each ring. The induced stress due to vectoring is dependent on the joint spring torque, decreasing as the joint spring torque is reduced. The shear stress due to vectoring is given by the expression (ref. 23)

$$\tau_v = \frac{0.01745 G_o\, R_p\, \theta}{n t_e} \tag{6}$$

where

$$\tau_v = \text{shear stress due to vectoring, psi (N/m}^2\text{)}$$

and, as before (eq.(1)),

$$G_o = \text{secant shear modulus at 50 psi (0.345MN/m}^2\text{) shear stress (sec. 2.1.7.1),}$$
$$\text{psi (N/m}^2\text{), at the elastomer temperatures expected in operation.}$$

$$R_p = \text{pivot radius, in. (cm)}$$

$$\theta = \text{vector angle, deg}^*$$

$$n = \text{number of elastomer layers}$$

$$t_e = \text{thickness of individual elastomer layer, in. (cm)}$$

---

[*] Angle θ is expressed numerically in degrees, not radians, in this empirical expression.

The shear stress due to pressure is dependent upon the thickness of each elastomer layer and is given by the expression (ref. 79)

$$\tau_P = \frac{t_e P_c K_e R_p^2}{17.5} \tag{7}$$

where

τ_P = shear stress due to pressure, psi (N/m^2)

P_c = motor pressure, psi (N/m^2)

K_e = correction factor for elastomer stress, depending upon cone angle.

Calculated results have shown that the shear stress increases as the cone angle increases (ref. 17). The correction factor K_e has been derived from the results of reference 17 and is shown in figure 18.
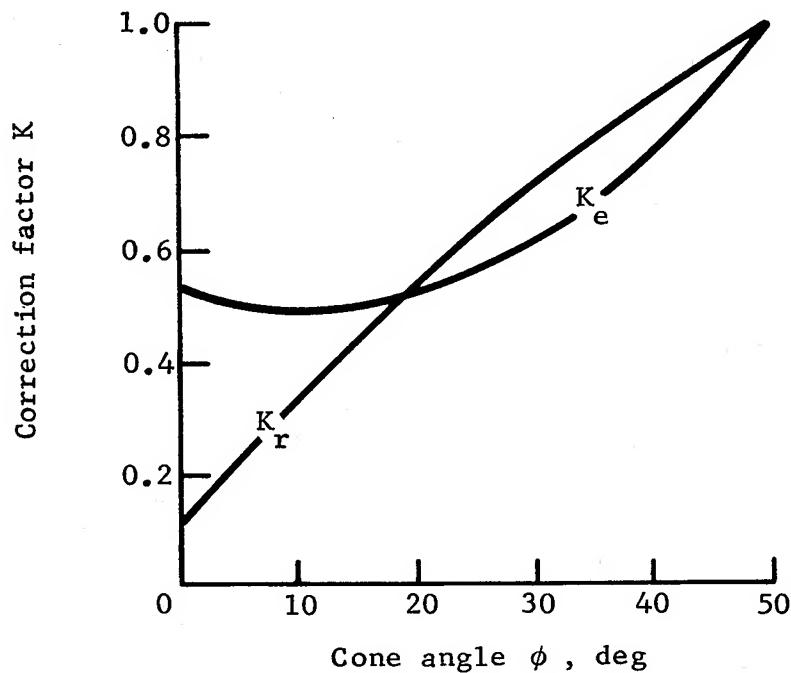
Figure 18. - Shear-stress correction factors related to cone angle (ref. 17).

49

The resultant shear stress τ_r in the elastomer is the sum of the stresses due to vectoring and pressure, i.e.,

$$\tau_r = \tau_v + \tau_P \tag{8}$$

The resultant stress is compared with the allowable shear stress.

The allowable shear stress has been considered to be the minimum measured shear stress from a quadruple-lap shear specimen (sec. 2.1.7.1). All successful joints designed to date have ignored the increase in failure shear stress due to superimposed pressure. The state of stress in an elastomer is a complex three-dimensional field, and the associated failure criterion is not known. Until the failure criterion is known, it is not known whether ignoring the increase in failure shear stress due to pressure is conservative.

The following procedure is used to determine the elastomer thickness:

(1) Calculate the net radial thickness of elastomer required for spring torque (sec. 2.1.2.1.1).

(2) Calculate the shear stress due to vectoring τ_v.

(3) Calculate the shear stress due to the maximum expected operating pressure τ_P for various elastomer layer thicknesses.

(4) Calculate the net shear stress τ_r at various elastomer layer thicknesses.

(5) Determine the design ultimate shear stress: $\tau_{ult} = \tau_r \times$ design safety factor

(6) Plot the design ultimate shear stress as a function of elastomer layer thickness and compare it with the allowable shear stress to determine the maximum allowable elastomer layer thickness.

If axial compression is a design parameter, the axial deflection is calculated by finite-element methods, using the calculated thickness, and compared with the requirements. The elastomer thickness may be reduced if the axial compression exceeds requirements, but the net radial thickness is maintained in order to satisfy spring torque requirements. The effect of reducing the thickness is to reduce the net shear stress and the axial deflection, increase the number of elastomer layers, and affect the compressive failure mode of the reinforcements.

2.1.5.2 REINFORCEMENT THICKNESS

The stresses in the reinforcements are caused by motor pressure and vectoring. For both of these loading conditions, each reinforcement cross section rotates but does not significantly

change shape. Such rotation causes a bending stress distribution radially across the reinforcement with tension at the outer radius and compression on the inner radius. The compressive stress on the inner radius has always been greater than the tensile stress on the outer surface, so that it is only necessary to determine the compressive stress (refs. 17, 22, 13, 14, 24, 27 to 29, 101, and 102). For motors that will be operated a number of times, fatigue characteristics and fracture mechanics are considerations that make the tensile stresses of equal concern.

The compressive hoop stress due to pressure depends on the number and dimensions of the reinforcements (ref. 79):

$$\sigma_P = \frac{4087\,P_c}{n-1}\,K_r\,\Omega \tag{9}$$

where

σ_P = compressive hoop stress due to pressure, psi (N/m^2)

K_r = correction factor for reinforcement stress, the value depending on the cone angle (ref. 17). The correction factor K_r has been derived from the results of reference 17 and is shown in figure 18.

n = number of elastomer layers determined as described in section 2.1.5.1.

$$\Omega = \frac{R_p^{2.4}\cos\beta}{3283\,t_r^3 + t_r\cos^2\beta\left\{R_p^2\,(\beta_2-\beta_1)^2 - 3283\,t_r^2\right\}}$$

t_r = thickness of reinforcement in joint, in. (cm)

β, β_1, β_2 = joint angles (fig. 12), deg[*]

The compressive hoop stress due to vectoring σ_v is given by (ref. 79)

$$\sigma_v = \frac{43950\,\theta}{n-1}\,K_r\,\Omega \tag{10}$$

Equations (9) and (10) are empirical relationships derived from results of tests of joints that varied in diameter from 8 in. (20.3 cm) to 22 in. (55.9 cm). Corresponding empirical relationships have not been developed for tensile stresses. When the cone angle is large, the

---

[*]β, β_1, and β_2 are expressed numerically in degrees, not radians, in equation (9) and (10).

tensile stresses are only slightly less than the compressive stresses, but as the cone angle becomes smaller, the tensile stress diminishes until the reinforcement is in a completely compressive state (ref. 17).

The resultant hoop compressive stress σ_r in the reinforcement is the sum of the compressive stresses due to vectoring and pressure, i.e.,

$$\sigma_r = \sigma_v + \sigma_p \tag{11}$$

The net stress σ_r is compared with the allowable compressive stress.

Failure modes for steel reinforcements are buckling in high-frequency circumferential waves and bulk compression. The failure mode for composite reinforcements fabricated with hoop windings only is rupture across the reinforcement thickness. The failure modes for reinforcements fabricated with mats and continuous windings are interlaminar shear and bulk compression.

The allowable compressive stress for metal reinforcements depends upon the failure mode (buckling or bulk compression) and consequently is a function of the reinforcement material modulus of elasticity, reinforcement dimensions, and the thickness of the elastomer layers. The buckling stress for metal reinforcements has been established from a test program conducted on specimens representing the inside surface of a joint. The reinforcements were slightly curved across the width, and the column was long enough so that edge effects were negligible. The ratio of reinforcement thickness to elastomer thickness was varied, and different reinforcement materials were used: 301 CRES half-hard stainless steel, 304 CRES annealed stainless steel, 17-7PH CRES annealed stainless steel, 6061-T6 aluminum, and 7075-T6 aluminum. Results of the tests correlated with reinforcement material properties and dimensions are shown in figure 19. The bulk compression stress has been established as the compressive yield stress (ref. 17). Tests were conducted on two joints with stainless steel reinforcements; the joints were identical except that the steel was heat treated to different yield compression stress levels. The failure pressures for the joints were different, and the stress in the failed reinforcement of each joint, calculated by finite-element methods, was approximately equal to the compressive yield stresses for the reinforcement materials.

The allowable compressive stress for composite reinforcements is often established from test joints with composite reinforcements that approximate the desired joint design.

The following procedure is used to determine the reinforcement thickness:

(1) Determine the number of elastomer layers (sec. 2.1.5.1).

(2) Calculate the compressive hoop stress due to pressure (σ_P) for various reinforcement thicknesses (eq. (9)).
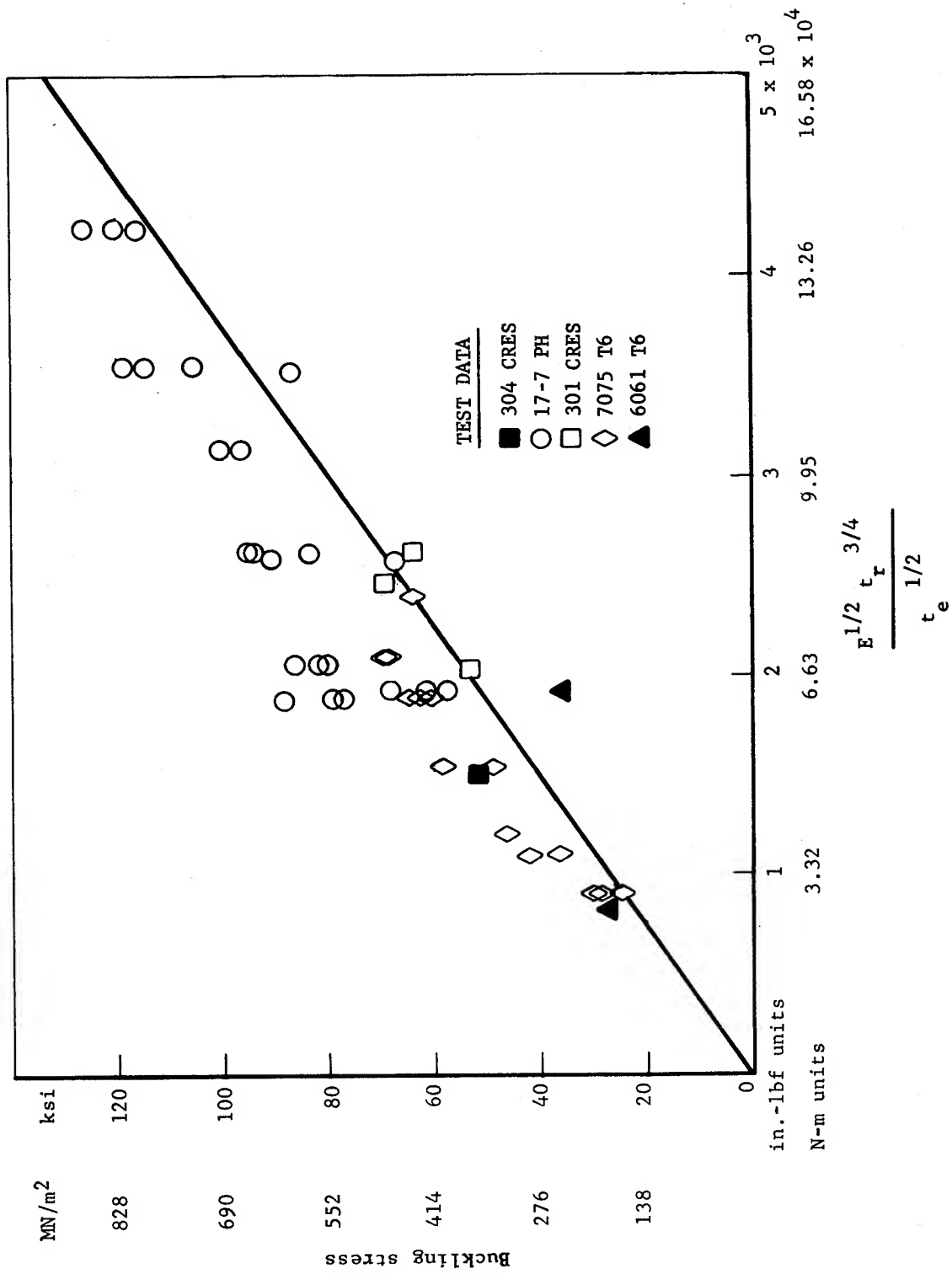
Figure 19. - Buckling stress for metal reinforcements as a function of the properties and dimensions of the reinforcement.

(3) Calculate the compressive hoop stress due to vectoring (σ_v) for various reinforcement thicknesses (eq. (10)).

(4) Calculate the net compressive hoop stress (σ_r) for various reinforcement thicknesses (eq. (11)).

(5) Determine the design ultimate compressive hoop stress for various reinforcement thicknesses: σ_{ult} = σ_r X design safety factor

(6) Determine the buckling compressive stress for various reinforcement thicknesses up to the reinforcement material compressive yield stress.

(7) Plot the design ultimate compressive hoop stress and the buckling stress as a function of reinforcement thickness. The intersection of these plots is the minimum allowable reinforcement thickness.

It has been the practice to make the reinforcements thick enough to ensure that the failure mode will be bulk compression. However, this approach probably results in over-strength reinforcements.

2.1.5.3 ADVANCED ANALYSIS

Analysis by finite-element methods (refs. 80 to 82) allows structures to be analyzed as an assembly, whereas the method employed in sections 2.1.5.1 and 2.1.5.2 analyzes the structural elements forming the assembly. Results from the finite-element method present a complete description of the stress, strain, and deformation distribution in an assembly. Within the limitations of the assumptions in the method, calculated results have shown good agreement with test results.

The limitations of the finite-element method are that (1) it is basically small-deflection theory modified to account for large-deformation effects; (2) material properties are elastic properties, although refinements have been introduced (ref. 103) to include nonlinear properties; and (3) for continuum structures such as a flexible joint, the structure must be axisymmetric during loading. Each of these limitations affect the analysis of a flexible joint. The strains in the elastomer are large strains; the elastomer material properties are not elastic but depend upon the local stresses in the elastomer; and, although motor pressure imposes an axisymmetric loading condition, vectoring is an asymmetric condition.

For the motor pressure condition, good correlation with axial deflection and reinforcement hoop strains has been obtained with the use of an incremental loading and deformation technique (ref. 80). A load is applied to the initial geometry; the stress and strain

distribution for that load are determined, and the shape for the next increment is established by algebraically adding the deflections to, the initial geometry. The final deflected shape is determined when the last load increment is applied; the final stress and strain distributions are obtained by summing the stresses and strains for each load increment. In general in this analysis four load increments give a reasonable correlation with test results. Although the shear modulus of the elastomer is dependent upon the local stresses, a constant secant shear modulus at 50 psi (0.345 MN/m^2) shear stress (sec. 2.1.7.1) is used for all loading increments. Other required properties are calculated on the assumption that the material is isotropic and has a value for Poisson's ratio as close to 0.5 as the computer can accept. Efforts to use an effective shear modulus (sec. 2.1.5.1) have been unsuccessful.

For the vectoring condition, the joint cross section changes, extending on one side and compressing on the other. An analysis technique similar to that for the motor pressure is used. Components of the actuator load are applied to the moving surface of the joint as a uniformly distributed axial loading, sinusoidally distributed shear loading, and a linearly varying bending distribution across the joint diameter. An increment of loading is applied as before to determine the geometry for the next increment. The stresses on one side will add to the stresses due to motor pressure and subtract on the other. Only the geometry for that side where the vectoring stresses add is used in the next increment. The geometry for that side is assumed to be axisymmetric, and the loads are applied incrementally. Final geometry and stress distribution are determined as described in the preceding paragraph; material properties as previously described are used.

Net stresses due to motor pressure and vectoring are obtained by algebraically adding the stresses due to each load condition. The strength analysis for the elastomer is conducted by comparing the maximum principal shear stress to the minimum measured shear stress measured from a quadruple-lap shear (QLS) specimen (sec. 2.1.7.1). The strength analysis for the reinforcements compares the maximum compressive hoop stress on the inner radius to the allowable compressive stress (sec. 2.1.5.2).

2.1.6 Manufacture

The sequence of steps for fabrication of a flexible joint involves manufacture of the reinforcements, development of the adhesive system between the reinforcement and the elastomer, and molding of the joint.

2.1.6.1 REINFORCEMENTS

The joint reinforcements have been fabricated by a number of methods; dimensional details, reinforcement material, and fabrication method are summarized in table VII.

TABLE VII. – Details of Reinforcements Used in Flexible Joints on Operational and Development Motors

Motor	Average spherical radius R_p, in.	Thickness t_r, in.	Material	Fabrication method	Ref.
100-Inch	14.6	0.038	304	Hydroformed	19
156-Inch	36.8	0.040	304	Spun	23
260-Inch	Conical: 58 outer radius, 54 inner radius	0.700	4130 normalized	Machined from roll ring forging	22
Poseidon C3 first stage	13.85	0.183	4130, 180 ksi	Stamped and machined	95
Poseidon C3 Second stage	13.69	0.108	4130, 180 ksi	Stamped and machined	96
Dual chamber	5.75	0.060	17-7PH annealed	Explosive formed	18
NAVORD TMC/TVC	7.18	0.110	4130, 180 ksi	Machined from plate	14
Poseidon C3 modified second-stage	13.69	0.108	Hoop-wound S-glass core overlaid with S-glass cloth and epoxy resin	Compression molded	27
Trident I (C4) second-stage	10.34	0.050	S-glass and carbon cloth pre-impregnated with phenolic resin	Matched-metal compression molded	25
NAVORD IRR	3.69	0.140	Chopped S-glass/phenolic resin	Closed-die compression molded	24

Notes: 1 in. = 2.54 cm

TMC/TVC = thrust magnitude control/thrust vector control

IRR = integral rocket ramjet

Steel reinforcements. — Hydroformed reinforcements for the 100-in. (2.54 m) motor have been formed by mounting an annealed circular plate in a pressurizing fixture (ref. 17). When pressure was applied to the plate, it expanded into an ellipsoidal shape. The reinforcement was then machined from the expanded plate and heat treated to the required properties. The spherical radius for each reinforcement in a joint was controlled by varying the height to which the plate was expanded.

The reinforcements for the 156-in. (3.96 m) motor (ref. 23) were formed by spinning. To reduce costs, all the reinforcements were spun from a standard conical preform, welded from three standard patterns that were cut from only one standard template. After welding, the conical preforms were stress relieved and pressed onto a mandrel in a horizontal shear spinning machine. Spinning was conducted in each direction from the center. The center of the reinforcement received the least amount of cold working and remained the thickest section. After spinning was completed, the reinforcement inner and outer diameters were finish machined. Reinforcement thickness was controlled by measuring the thickness of the conical preform prior to installation on the mandrel, and estimating the amount of thinning required. Thinning was accomplished by belt sanding for a predetermined time after the reinforcement was formed. This method assured that each reinforcement received the same amount of cold working by shear spinning and resulted in a uniform strength level for each reinforcement.

In the 260-in. (6.6 m) motor (ref. 22), although the reinforcements were 0.7 in. (17.8 mm) thick, the large diameter resulted in flexible sections. The reinforcements were not spherical sections as in all previous joints but were conical sections. Since the joint envelope was cylindrical, each reinforcement was identical and only a single set of tooling was required for all reinforcements. This design resulted in cost savings in comparison with a joint with spherical reinforcements of progressively increasing radii. The reinforcements were machined from roll ring forgings. Any distortion occurring in the finished reinforcements either due to machining or handling was easily corrected in the joint mold as a result of the flexibility of the large-diameter reinforcements.

Reinforcements for the Poseidon motors were fabricated by stamping washer-shaped disks into the required section; this process required a die for each reinforcement. At stamping, the steel was in a normalized condition. After stamping, the reinforcements were rough machined, heat treated to the required properties, and then final machined. This method results in distortion of the reinforcements, but this distortion has little effect on joint performance if each individual reinforcement is aligned in the joint molding fixture (sec. 2.1.6.3). The thinner reinforcements formed by hydroforming, spinning, or explosive forming have not exhibited this distortion.

The reinforcements for the dual-chamber motor were explosively formed from a circular blank of material. The blank was clamped over a die that had the required contour of the reinforcement, making it necessary to have a die for each reinforcement in the joint. Due to

forming, the thickness of the reinforcement was 4 percent to 5 percent less than the blank thickness. The reinforcement was final machined from the formed section.

The reinforcements for the NAVORD TMC/TVC joint (refs. 13 and 14) were machined from plate material. Only a few joints were to be fabricated, and this method eliminated the need for expensive tooling. The plate material was in a normalized condition and the reinforcements were rough machined. After machining, the reinforcements were heat treated and finish machined.

Composite reinforcements. — Early composite reinforcements were fabricated with S-901 12-end roving glass filaments with an epoxy resin (ref. 28). The reinforcement cross section was formed by hoop winding between two plates. This system resulted in insufficient transverse strength and was modified by overlaying the hoop-wound core with S34/901 glass cloth. A better method of forming these reinforcements was to "B-stage" (partially polymerize) the hoop-wound core, lay up the cloth on the faces of the core, replace in a mold, and cure under pressure (ref. 28). In this procedure, the ERR-4205 resin system was used because this sytem could be hardened, reliquified, and final cured. The same technique and materials were used to fabricate composite reinforcements for an experimental second-stage Poseidon C3 joint (ref. 27).

In the engineering development program, for the second stage of Trident I (C4) the joint reinforcements were fabricated from S-904 glass-fiber broadgoods and carbon-fiber broadgoods, each preimpregnated with phenolic resin (ref. 25). In the motor development program, however, to overcome structural problems, the S-904 glass-fiber broadgoods were preimpregnated with epoxy resin. The two types of broadgoods were sewn together, cut into specific patterns, assembled in a matched metal mold, and cured at 325° F (436 K). The glass broadgoods formed the reinforcement, and the carbon broadgoods formed the joint thermal protection. Each reinforcement had a different spherical radius, requiring a different mold for each reinforcement.

To reduce the cost and complexity of composite reinforcement fabrication, reinforcements for the NAVORD IRR joint were made from chopped S-glass/phenolic-resin compound molded in closed-die compression molds (ref. 24). The reinforcement molding integrally included the joint thermal protection. These reinforcements demonstrated the feasilibity of this method of fabrication.

2.1.6.2 JOINT ADHESIVE SYSTEM

The joint adhesive system may be formed during the molding process for joints fabricated by compression or injection molding, or it may be obtained by secondary bonding, as in the 260-in. (6.6 m) motor joint (ref. 22).

Rubber-to-metal adhesive bonds are sensitive to small process changes. In a flexible joint, high stresses are imposed on these bonds, and the bulk of the fabrication problems involve the adhesive system. To ensure increased reliability, the adhesive system is required to develop a bond strength greater than the elastomer strength, so that failures are cohesive failures. Systems designed to satisfy this requirement have consisted of a primer and an adhesive (sec. 2.1.3.3).

The strength of the bonds in this kind of system has been affected by bond layer thickness. When the bond layer was too thick and an injection molding process was used to fabricate the joint, the flowing rubber wiped the adhesive system off the reinforcement, the result being unacceptable unbonded conditions. When a compression molding process was used, the unbonding problem was not as acute but unbonding did occur. When the bond layer was too thin, the resulting bond strength was below acceptable levels, and adhesive failures occurred. During bench testing of joints (sec. 2.1.7.2), failures that were attributed to too thin a bond layer have occurred.

Failures have also occurred in the adhesive bond when the adhesive layer thickness was as required. These failures resulted from lot-to-lot variations in the adhesive system materials. For example, peel test specimens failed at values varying from 3 lbf per linear inch (5.25 N/cm) to 35 lbf per linear inch (61.25 N/cm).

A satisfactory adhesive system has been obtained by controlling the thickness of the adhesive layer, requiring acceptance tests of each lot of material to be used in joint fabrication, and maintaining close liaison with the adhesive suppliers. Thickness control has been obtained by monitoring the viscosity of the primer and adhesive, the rate at which these materials are sprayed on the reinforcements, and the time for spraying. The material lots to be used have been selected by conducting quadruple-lap shear tests (sec. 2.1.7.1) and peel tests, all lots that do not have sufficient strength being rejected.

2.1.6.3 FLEXIBLE JOINT

Flexible joints have been fabricated by three different methods: compression or layup molding (refs. 17, 23, 25, and 27), injection or transfer molding (refs. 13, 14, 24, 28, and 29), or secondary bonding of precured elastomer (ref. 22). A summary of the advantages and disadvantages of these methods is presented in table VIII.

The compression technique involves physically placing strips of partially cured elastomer between the reinforcements as the joint is assembled in the mold. The resulting assembly of parts is then compressed by closing the mold and providing molding pressure. During compression, the thickness of the elastomer layers has been controlled by inserting steel balls between the reinforcements. In early joints, the balls were positioned at the center of the reinforcements. As the joint was vectored, the balls gouged the reinforcement and cut

TABLE VIII. – Advantages and Disadvantages of Joint Fabrication Processes

Process	Advantages	Disadvantages
Injection molding	Demonstrated production technique used to fabricate joints for nozzles on Poseidon first- and second-stage motors.	Comparatively expensive process because of the complicated method of setup and fabrication. The tooling costs are much higher than those for compression-molded joints.
	Has the potential of giving uniform rubber-pad thicknesses. (However, in actual production of joints for Poseidon this method resulted in nonuniform pad thicknesses on many joints. The lack of uniformity seems to be associated with tool design and wear.)	Has inherent bonding problems. The elastomer must flow considerable distances over the reinforcements and end rings, and the flow of hot rubber tends to remove the primer or adhesive. This problem does not occur with silicone elastomer, because the primer/adhesive system can be precured on the components.
		Sometimes yields joints in which the rubber is not fully compacted in all areas. This condition results in joints that leak during the proof test and are therefore rejected.
Compression molding	Demonstrated production technique used to fabricate joints for nozzles on Poseidon first-stage and second-stage motors.	Spacers are required. The spacers sometimes move as a result of rubber flow, and uneven rubber-pad thicknesses can result. Furthermore, small local defects in the rubber-pad layers are created when spacers are removed.
	Low-cost manufacturing process and simple low-cost tooling. Joints produced by this method are approximately 30 percent lower in cost than those produced by the injection process.	Some difficulty with bonding and porosity attributable to the tolerance variation on calendered rubber.
	When natural rubber or polyisoprene rubbers are used, excellent bonding between the rubber and the reinforcements and between the rubber and end rings in achieved.	Some difficulty in bonding silicone elastomer.
Secondary bonding	Produces joints with very uniform pad thicknesses.	Process has inherent bonding problems.
	The rubber pads have good compaction and can be inspected prior to assembly.	Production experience limited. To date only a few joints have been fabricated by this process.
	Tooling costs are low.	

holes in the elastomer. In later joints where the width of the reinforcements was greater than that of the elastomer, the balls were positioned at the inner and outer edges of the joint and were removed after molding.

The injection molding technique consists simply of stacking the reinforcements in a mold that holds them in position and then injecting rubber from a reservoir into the gaps between the reinforcements.

The molding method selected depends on the preference of the fabricator; both techniques have been used for the same joint design and produced similar results. Major problems that occurred have been common to compression molding and injection molding. The three major problems have been porosity in the elastomer, variation in the thickness of each elastomer ring, and variation in the thickness between elastomer rings. Porosity in the elastomer occurred because the elastomer could flow easily out of the mold or into large voids in the mold. This problem was eliminated by designing a mold without voids and minimizing clearances between metal parts to avoid elastomer expansion out of the mold. Variation in the thickness of elastomer rings has been due to a number of causes. Excessive clearances in the mold to accommodate parts with excessive tolerances has caused thickness variations. Thickness variations have also occurred because of movement and deflection of the joint under the high pressures of molding. Tolerance problems are avoided if the pad thickness is controlled directly by the two metal surfaces involved; this procedure minimizes the number of tolerances involved in a worst-on-worst situation. The deflection of parts can be reduced only by stiffening the parts, but stiffening may be impossible because of design specifications. In such a situation, the deflection must be tolerated and allowed for. Movement of the parts in the mold, however, has been controlled by indexing parts from surfaces that are self-centering, i.e., conical or spherical surfaces. To avoid thickness variations in an elastomer layer for a joint with thick reinforcements, the reinforcements are inspected for flatness and spherical radius variations and are aligned in the mold to give uniform elastomer layer thickness.

The secondary bonding technique has had limited application. It was used on a large joint because of a lack of sufficiently large facilities to cure at high temperature and because it was cheaper (ref. 22). As each reinforcement was laid in the mold, the elastomer was bonded to the reinforcement. Care was taken during the layup of the reinforcements to ensure correct alignment. An ambient cure adhesive was used (sec. 2.1.3.3) and the joint was loaded at 5 psi (0.0345 MN/m^2) axial pressure by mechanical actuators during cure. The axial pressure was used to ensure good adherence between the elastomer and metal components.

Two important diagnostic aids exist in joint manufacture. These aids have assisted in the discovery of manufacturing problems and the determination of the effectiveness of corrective actions. The first diagnostic aid is molding of a joint without applying the adhesive system to the metal parts; with this exception, the molding process is carried out

normally. After molding, the rubber is easily removed from between the metal parts and examined for thickness and porosity. The second aid is simply the dissection of a normal, production joint by cutting through the rubber between metal parts; the resulting pieces reveal any areas where the rubber-to-metal bond was unsatisfactory. This technique also shows porosity and general condition of the rubber.

2.1.7 Testing

The flexible-joint test program is conducted to determine elastomer material characteristics, joint spring stiffnesses, nozzle operating characteristics, and nozzle failure strengths so that compliance with motor requirements is demonstrated. If new elastomeric materials are to be considered, a material characterization program is conducted (sec. 2.1.3). The test program consists of subscale testing, joint bench testing, nozzle actuation testing, static firing testing, joint aging testing, frequency-response testing, and destructive testing.

2.1.7.1 SUBSCALE TEST PROGRAM

The subscale test program is conducted to measure mechanical properties of the elastomer and of the bond between elastomer and reinforcement and to evaluate aging characteristics of the elastomer. In the preparation of test specimens, the surfaces of the test plates must be prepared in the same manner as the surfaces of the reinforcements in the joint; if possible, the test specimen is fabricated in the manner used for manufacture of the joint.

The most important properties of the elastomer used in the flexible joint are the shear modulus, the shear stress at failure, and the bond strength of the elastomer to the metal reinforcements. These properties are measured over the range of temperature in the elastomer expected during operation, with the quadruple-lap shear (QLS) specimen (fig. 20). The properties are defined in terms of the test as follows:

$$\text{Shear modulus } G_o = \frac{50 \text{ psi } (0.345 \text{ MN/m}^2) \text{ shear stress}}{\text{shear strain at } 50 \text{ psi } (0.345 \text{ MN/m}^2) \text{ shear stress}}$$

$$\text{Shear stress } \tau = \frac{\text{applied load}}{2 \times \text{length} \times \text{width of pad}}$$

$$\text{Shear strain } \gamma = \frac{\text{increase in crosshead separation}}{2 \times \text{thickness of pad}}$$
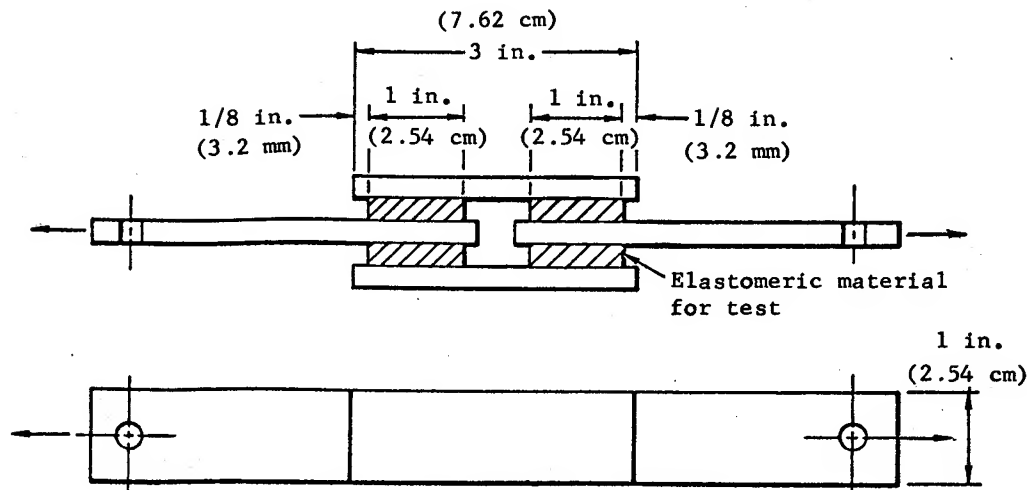
Figure 20. - Quadruple-lap shear test specimen.

Even though the elastomer in a joint is subjected to compression and shear if vectored at sufficient motor pressure, and to tension and shear if vectored at zero motor pressure, the properties have been determined only for applied shear loads. To improve the understanding of the physical characteristics of flexible joints (the reduction in actuation torque with pressure, overall joint instability, and nonlinearity of axial compression), limited efforts to determine elastomer shear properties when subjected to superimposed compression and tension have been conducted (refs. 22 and 78).

The shear modulus controls the joint spring torque, axial deflection, and pivot-point movement. The stress-strain response is nonlinear, but most analyses assume linearity at a reference secant shear modulus at 50 psi (0.345 MN/m^2) shear stress; this value is also used for quality control. The elastomer varies from lot to lot, and close quality control is necessary to ensure a modulus acceptance range of 10 psi (0.069 MN/m^2). In a production program, the testing of each lot can indicate a relaxation of manufacturing quality control or a change in the manufacturing process. The QLS is used as a quality control tool as well as a means to qualify new elastomers and new adhesive systems.

If the aging characteristics of the elastomer are not known, a subscale test program is initiated early in the program. This program includes testing not only the aging characteristics of the cured elastomer but also the effect of aging of the uncured elastomer on the resulting cured elastomer. When such effects are not determined and controlled early in a program, the results of joint tests are subject to misinterpretation.

63

In evaluating the aging of uncured elastomer, the uncured elastomer is stored in the usual material storage environment and, at intervals, test specimens are prepared and cured. Tests are conducted, and the shelf life of the uncured elastomer is determined from the results. The selected shelf life is the time during which no change occurs in the secant shear modulus of the cured elastomer.

To evaluate aging characteristics of cured material, cured elastomer from several lots is stored in the motor environment and, at intervals, a subscale test program conducted. The elastomer properties are plotted against time, and the results are extrapolated to predict service life of the elastomer. Properties obtained at zero time provide a basis for comparison. Service life testing is conducted at monthly intervals up to 6 months and annually thereafter. Results have shown that natural-rubber formulations increase in secant shear modulus up to 3½ years and then remain constant.

When a joint is injection molded, the test specimen cannot be fabricated in similar fashion; therefore the measured elastomer aging characteristics may differ from those of the elastomer in the full-scale joint. The aging characteristics of injection-molded joints usually are assessed by testing full-scale joints.

2.1.7.2 BENCH TEST PROGRAM

The joint bench test program is conducted to determine axial compression due to pressure, spring torque, offset torque, sealing capability of the joint, and the location of the effective pivot point; to verify calculations; and to demonstrate structural integrity of the joint. Thus data must be obtained as early as possible in a program to confirm clearance envelopes in the nozzle design. When a program is in the production phase, the bench test program is continued for quality control.

The axial compression is required to determine the axial spring stiffness and to check clearance envelopes. The bench testing is conducted at the same pressure and axial load as the joint is expected to transmit during actual motor operation. This condition requires a special test fixture, as shown in figure 21, that contains provisions for adjusting the axial load on the joint. An unloading piston is used for this purpose. The unloading piston is sized such that the net axial load on the joint at pressure while undergoing test is equal to the load that will be imposed on the joint during actual motor operation. The net gas-pressure load acting on the joint during motor operation is calculated as described in section 2.1.2.3. During the development tests, hoop strains at the edges of the reinforcements as well as the axial compression are measured. These data are of value in checking the validity of the analyses.

The quality of joints in a production program varies considerably from joint to joint. In one program, to eliminate possible low-quality joints and ensure the reliability of the motor, a
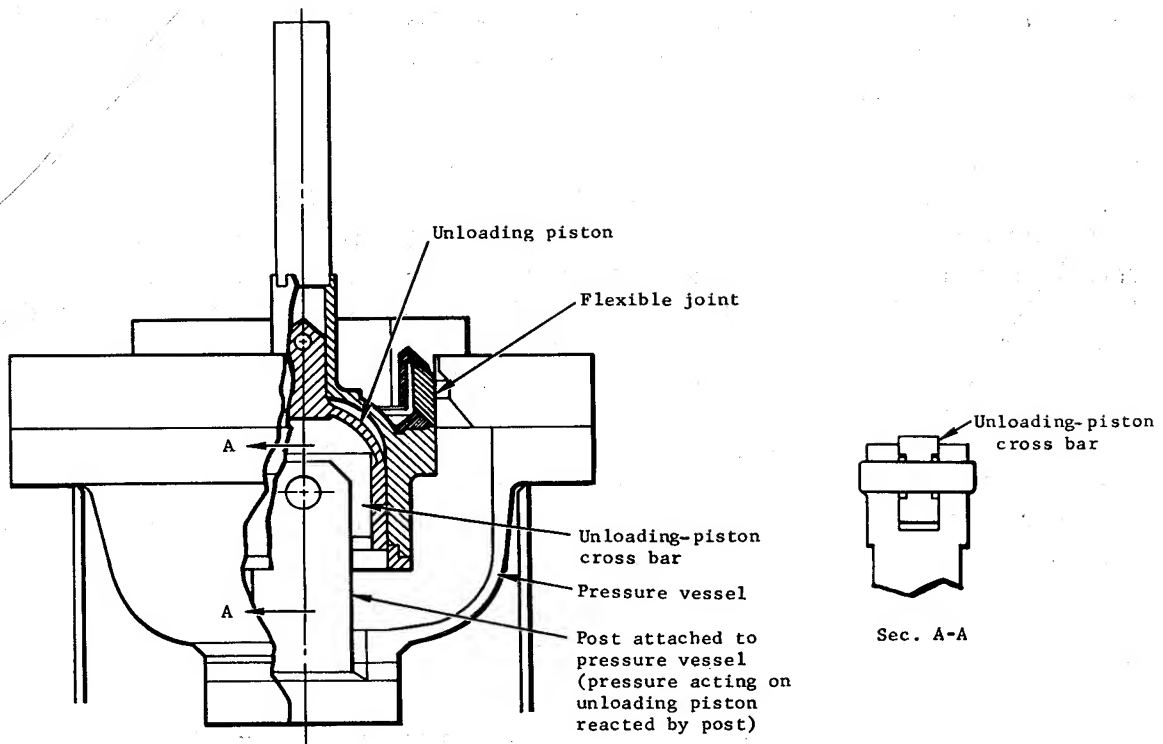
Figure 21. - Special fixture for testing joint axial deflection.

stringent tensile-pressure leak test was imposed. This test was an axial tensile test conducted after the axial compression and vectoring tests. The joint was sealed with end plates and pressurized internally, the pressure causing axial extension. The test fixture limited the extension of the joint, but pressure was still applied at maximum extension to check for any leakage. In the motor program, leaky joints were rejected after this test but, for those joints successfully passing this test, no failures attributed to joint failure occurred in the motors tested.

A typical joint test arrangement is shown in figure 22. One end of the joint is sealed into the test bucket and the other end is sealed into a flat-plate closure that is connected to an actuator arm. In this type of test, however, at test pressure more axial load is applied to the joint than occurs in a motor. Therefore, joints are tested only up to a pressure simulating the maximum axial load that will be applied to a joint in the motor. Consequently, the test pressure is less than the motor pressure. The reduced pressure affects the position of the effective pivot point. Attempts to design an unloading-piston test arrangement that vectors
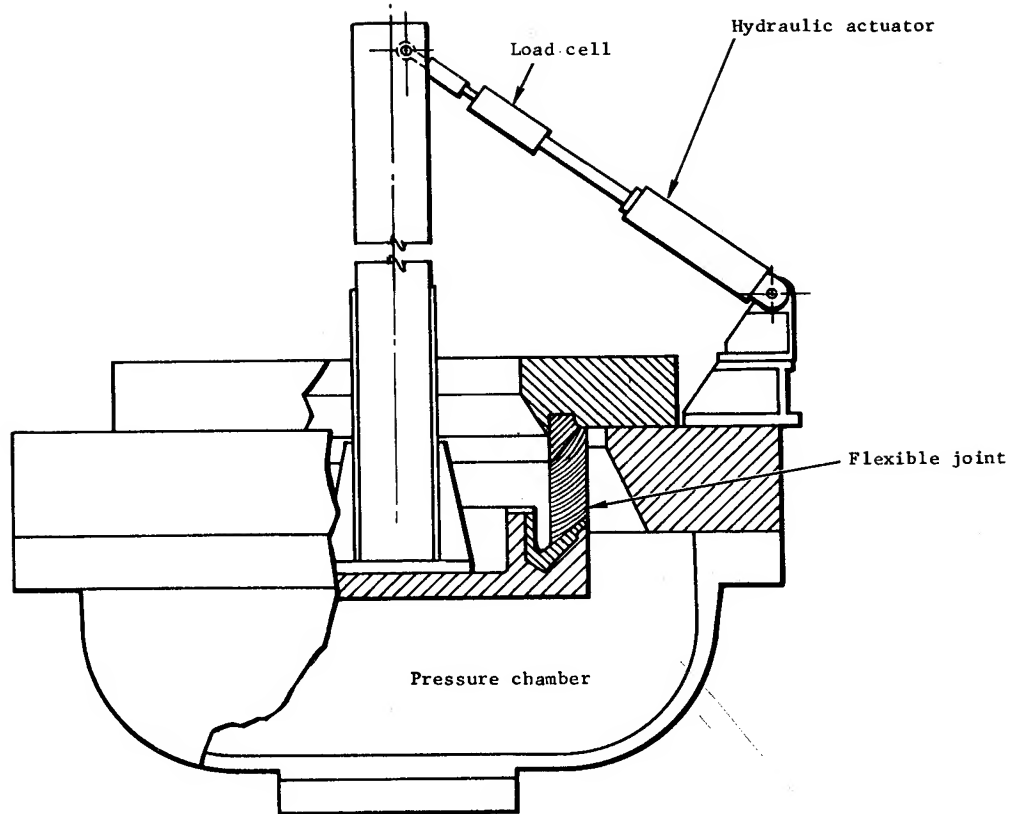
Figure 22. - Fixture for testing joint actuation under pressure.

with the joint have been unsuccessful, because the test arrangement must not control the pivot point but must allow the joint to vector freely about its effective pivot point.

Proper location of the test actuator is important. It should be positioned in the test with respect to the joint as it will in the motor. Although joint spring torque is used as a design concept, the joint is not in fact subjected to pure torque. It has been shown that when the actuator was not oriented correctly to the joint, the vectoring response in the test was different from that in the motor.

A flexible joint deflects linearly in addition to rotating; thus, it is difficult to locate the effective pivot point. Attempts have been made to locate the pivot point by digitally tracking one or two points on the joint or joint test fixture and using a rotational mathematical model to determine the instantaneous pivot point. Because the mathematical model does not include linear motion, the results are inaccurate to some unknown degree

that depends on the joint design. A more direct photographic method of measurement has been developed (ref. 91). This method shows the position of the effective pivot point directly on a photograph, thus eliminating the need to calculate the position from deflection measurements and avoiding the dependence of each calculated position on previous instantaneous positions.

Most bench tests of joints are conducted at approximately 75° F (297 K), because the environmental temperature requirements usually are limited to the range 60° F (289 K) to 85° F (303 K). The test temperature is recorded, and joint response at the temperature extremes is predicted from the elastomeric-material characterization described in section 2.1.7.1.

2.1.7.3 STATIC FIRING PROGRAM

During the static firing tests, measurements are taken to check the overall design and to obtain data needed to design other components that interact with the nozzle design. Measurements taken include axial compression, vectoring capability, nozzle misalignment requirements, friction characteristics, natural frequency, and damping coefficient.

The axial compression is required to check the envelope requirements when the motor must interact with another stage or equipment. During a firing, the nozzle is vectored to various angles up to the maximum required angle in order to check clearances between the fixed and movable portions and to check the movable nozzle envelope requirements. During this vectoring, actuator force is measured. For comparison of static firing and bench testing results, the nozzles are vectored at the same frequency.

Sizing of the correct actuator length for nozzle misalignment (sec. 2.1.2.3.1) is determined from the static firing. During a firing, at several times selected to give as wide a pressure range as possible, the actuators are held at the trial length for at least one-half second. Prior to the firing, the nozzle is actuated in the motor, sufficient measurements being made to enable calculation of the vector angle per inch of actuator stroke. From a comparison of firing and pre-firing data, the amount of zero-pressure misalignment is calculated and the actuator length for null nozzle position at pressure is determined.

The friction characteristics of the nozzle (i.e., the flexible joint) are required for the design of the guidance control system. As noted earlier, friction consists of viscous friction due to the viscoelastic characteristics of the elastomer (a rate-dependent component) and coulomb friction (a rate-independent component). During static firing tests, a nozzle is vectored at different rates but at constant amplitude, and the actuator force is measured. The data are plotted as shown in figure 14. Both total friction and the two components are thus determined.

Frequency-response tests are made during a static firing by imparting to the nozzle a duty cycle that consists of a succession of sinusoidal actuations, each of short duration and low amplitude. These actuations are made at different frequencies established from considerations of the control system response. Attempts have been made to calculate the damping coefficient from the decaying force transient that occurs at the end of a step function applied to a nozzle; however, the attempts were without success, since the damping coefficient could not be correlated with the viscous friction coefficient calculated from actuation data.

2.1.7.4 DESTRUCTIVE TESTING

The failure strength of a flexible joint is determined by destructive testing. Joint failure occurs as a result of motor pressure and vectoring. Currently, failure strength of a joint for combined conditions cannot be defined. A test is conducted in which pressure is increased incrementally, the joint being actuated to the maximum applied vector angle during motor operation at each pressure until failure of a component occurs. If the joint has not failed at the design ultimate pressure, and sufficient clearance envelope remains, the vector angle is increased until failure occurs. The failure test is conducted as an adjunct to the bench testing program.

2.1.7.5 AGING PROGRAM

In addition to the subscale aging program described in section 2.1.7.1, an aging program for the joints is conducted. Joints are stored in the service environment; at intervals, joint spring torque and axial deflection (sec. 2.1.7.2) are measured. These tests are conducted at zero time (for reference), at 3 months, 6 months, 1 year, and annually thereafter. Most changes occur in the first year. The measured values for spring torque and axial deflection are plotted against time; the results are extrapolated to determine joint life. This extrapolated life is compared with required motor life to demonstrate probability of satisfactory service life.

2.1.8 Inspection

The inspection of a flexible joint fabricated by injection or compression molding is difficult. No techniques have been successful in evaluating the quality of the elastomer or the quality of the adhesive bonds between the reinforcements and the elastomer in a molded joint. Assurance of joint quality is obtained by control of the quality of all materials used, dimensional control of the reinforcements, process control during mold setup and molding, and adherence to acceptance bench tests.

For joints fabricated by secondary bonding, it is possible to check the pre-molded elastomeric pads for internal defects such as voids, inclusions and delaminations, and the bond between the reinforcement and elastomer by C-scan ultrasonic techniques (ref. 22). In addition, joint quality is assured by control of the quality of all materials used, dimensional control of the reinforcements, and alignment of the reinforcements during joint layup.

2.1.8.1 INSPECTION PLAN

To ensure reliability of the joint, a detailed and comprehensive program of material and fabrication process control in conjunction with a nondestructive and destructive test program is conducted. This program permits detection of potential causes of failure and the timely repair and correction of these areas. Proper inspection processes are the key factors resulting in satisfactory joints. Development of a successful inspection plan involves the following steps:

(1) Determination of the types of defects that require detection.

(2) Evaluation of existing inspection techniques for sufficient sensitivity and accuracy and development of new acceptable or adequate techniques when necessary.

(3) Verification that the inspection techniques obtain a valid indication or description of the actual defects.

(4) Establishment of accept-reject standards for each type of defect and each inspection technique.

(5) Elimination of any redundant inspection, modification of existing inspections, and introduction of new inspections as knowledge and experience are gained during both development and production.

2.1.8.2 INSPECTION PROCESSES

Current practice is to inspect the joint dimensions and performance. The dimensions inspected are those that affect joint molding, joint performance, and joint assembly in the nozzle. In performance inspection, the operational integrity of the joint is demonstrated.

Reinforcement dimensions such as inner and outer diameter and flatness affect the joint molding. The spherical radius, thickness, and concentricity affect the joint performance. The elastomer thickness and porosity can be inspected only by molding a joint without adhesive on the reinforcement surfaces. After molding, the joint is disassembled to check elastomer thickness and porosity. The frequency of this inspection depends upon the

variation that is noted in the thickness. Radiographic inspection has been tried, but the large amount of metal in the joint prevents definition of the bond line or elastomer thickness being defined to the required accuracy.

After molding, the joint is dimensionally inspected for overall length, concentricity between the end attachment rings, and end-ring to end-ring reference plane parallelism. These dimensions affect the overall position of the nozzle with respect to the motor.

The operational integrity of the joint is demonstrated by bench testing (sec. 2.1.7.2). The significance of these tests is based on the premise that joints successfully passing these tests are suitable for assembly in a nozzle.

2.2 LIQUID INJECTION THRUST VECTOR CONTROL

Thrust vectoring by LITVC is accomplished by injecting a liquid into the supersonic exhaust of a rocket motor through holes in the wall of the nozzle exit cone. The injection produces side thrust by a combination of effects that include the thrust of the injectant jet itself, pressures on the nozzle wall from shock waves, and pressures on the nozzle wall resulting from addition of mass and energy to the exhaust flow. These effects are illustrated in figures 23, 24, and 25.

Liquid injection TVC has provided thrust vector deflections as large as 10°, equivalent to side forces of 17.6 percent of axial force (ref. 46). However, efficiency as measured by injectant specific impulse drops to about 30% of maximum at the high flowrates required for such large deflections. The low efficiency at high flowrates is due largely to the spreading of the LITVC pressures around the nozzle circumference, where local LITVC forces act in directions different from that of the desired thrust deflection. Serious losses in efficiency can occur if the higher pressures induced by LITVC reach the opposite side of the nozzle. This condition can be caused by very high injectant flowrates, by the injector being located too near the nozzle throat, or by a combination of both. Inefficiency due to incomplete mixing and reacting of the injectant with the gas may result from injecting too close to the nozzle exit or from using large concentrated injectant streams that do not disperse and mix easily (refs. 105, 106, and 107).

As the injectant flow is increased, the side force increases and usually reaches a maximum. Then as the flowrate is increased further, the side force decreases. This decrease occurs because the added flow is creating forces on the opposite side of the nozzle that cancel out the gain in side force on the injector side. Thus, maximum side force can be obtained at less-than-maximum flowrates (ref. 108).

The maximum practical thrust deflection angle is limited to about 6° because of the efficiency penalties that must be accepted if the system is designed to produce larger
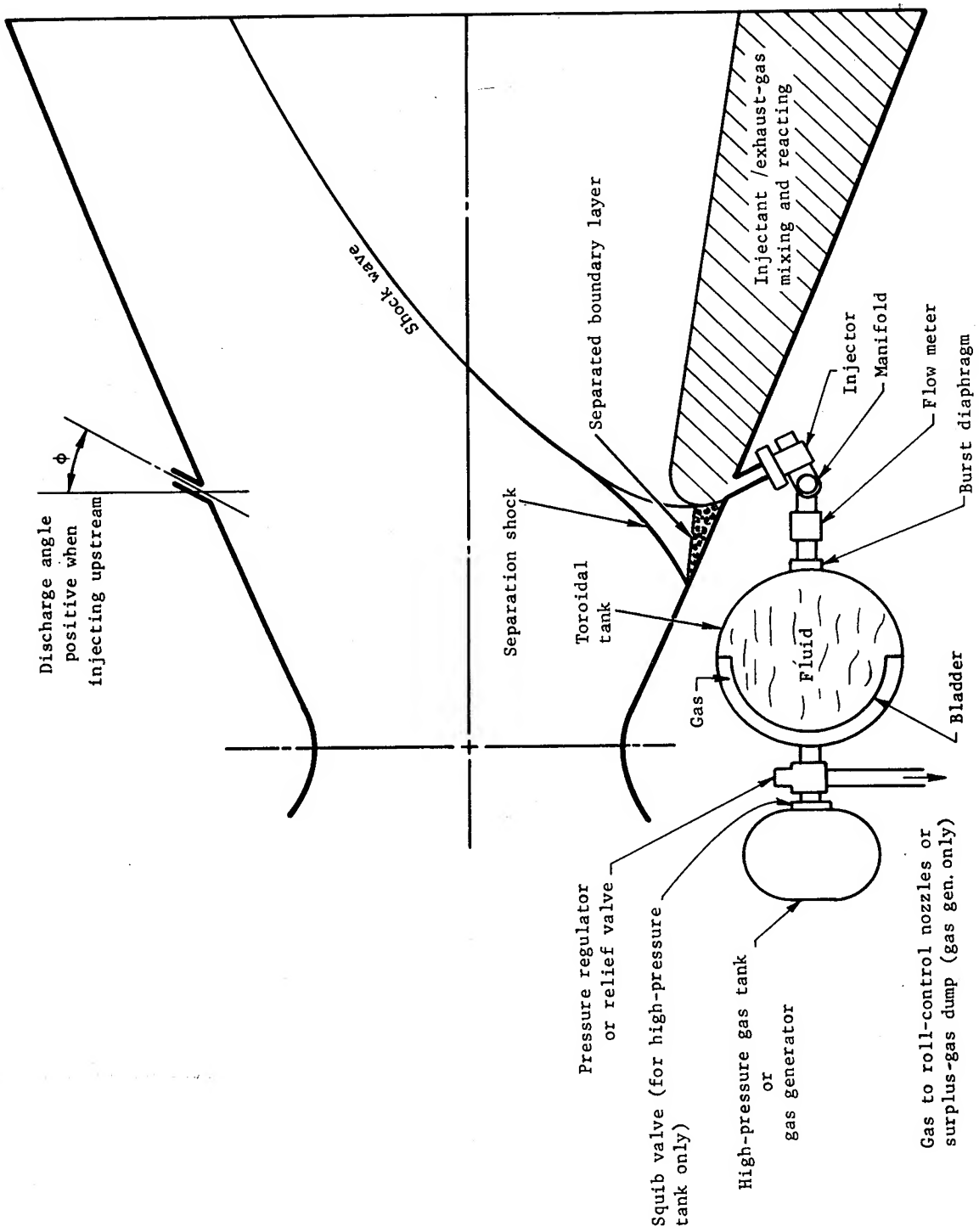
Figure 23. - Schematic of typical liquid injection TVC system and side force phenomena.

71
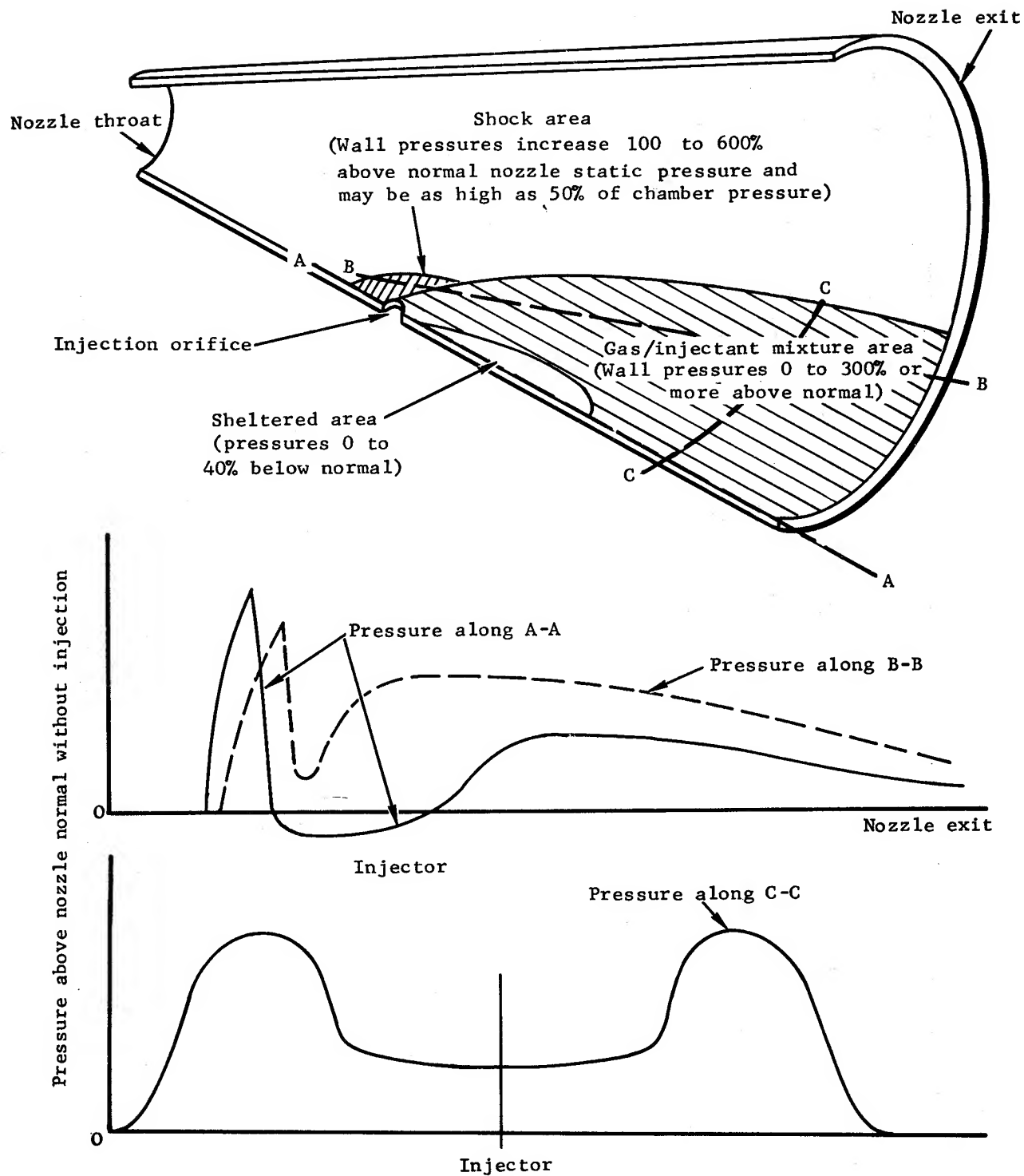
Figure 24. - Nozzle pressure distribution due to injection of inert injectant (ref. 104).

72
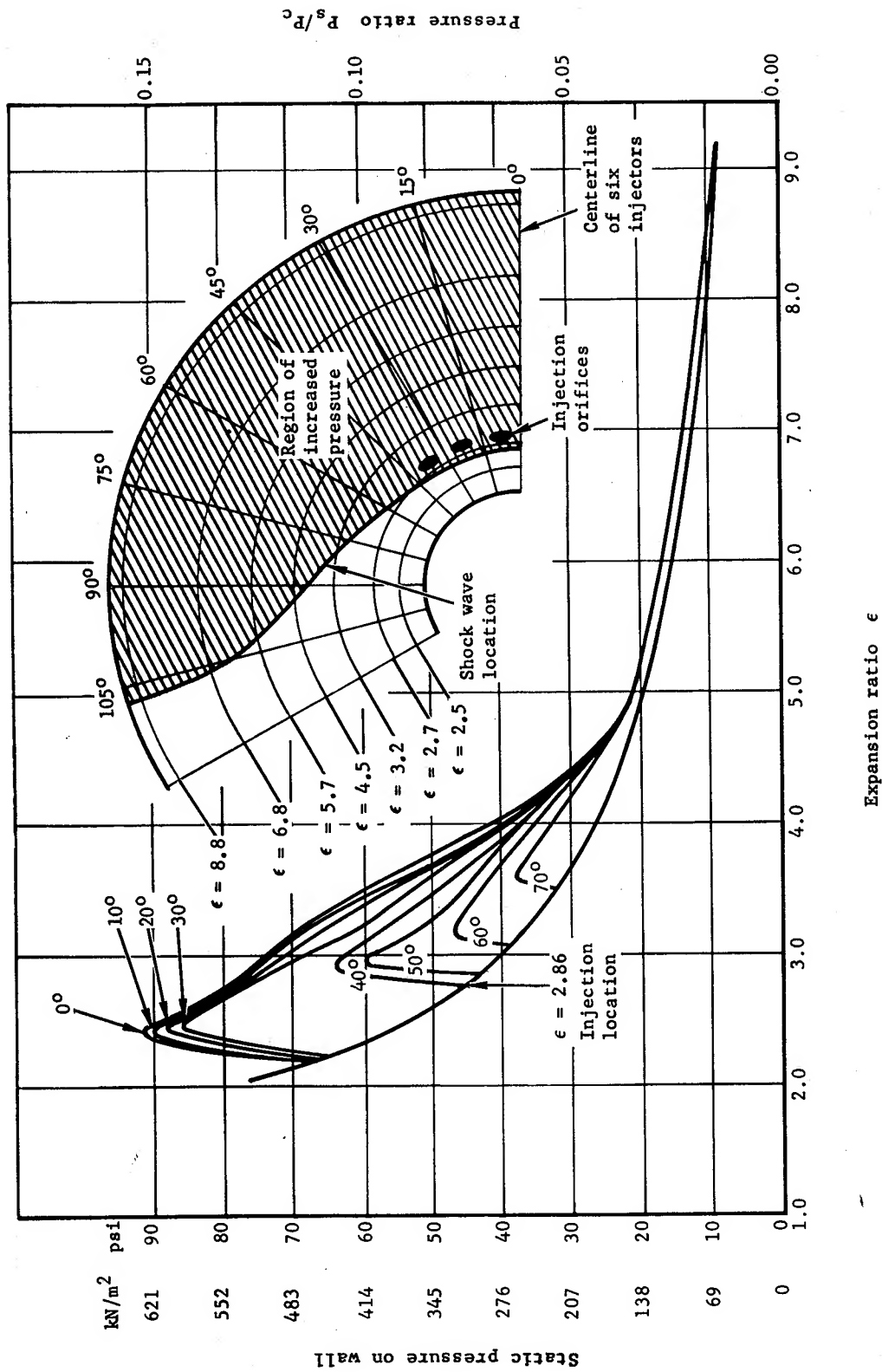
Figure 25. - Nozzle pressure distribution due to injection of reactive injectant.

73

deflections. To obtain higher deflections, larger injectors must be used, and these must be located nearer the exit to reduce the side-force limiting effects mentioned above. Thus, the efficiency of the system at all flowrates is compromised. Effects for various orifice sizes and injection locations are presented in references 46, 108, and 109.

Liquid injection has a number of desirable features, some of which are unique, as follows:

- During vectoring, the main motor thrust is increased by the axial component of the increased pressures on the nozzle wall. This axial component makes it doubly advantageous to lighten the LITVC system during flight by jettisoning surplus fluid through the injectors; as weight is removed from the vehicle, extra thrust is also obtained.

- Liquid injection TVC is inherently very rapid and can produce a signal-to-force time less than 20 msec without difficulty. This speed is the result of the fact that all moving parts – the valve pintle and drive parts, the liquid injectant, and the tank bladder – have low inertia and move with little friction, and the reaction of the fluid with the exhaust gas is almost instantaneous.

- Long-term storage of LITVC systems in a state of instant readiness has been demonstrated. These systems have contained sealed supplies of injectants including Freon 114-B2 and aqueous solutions of strontium perchlorate. Nitrogen tetroxide, one of the most highly reactive injectants, has been stored as long as 75 days in the Titan III system (ref. 47). Dry N_2O_4 probably can be stored indefinitely in clean aluminum tanks.

2.2.1 System Design

A typical LITVC system consists of a tank of injectant, a source of compressed gas, tubing, and injector valves. The liquid injectant, under pressure from the gas, flows through tubing to the injectors. The valves controlling flow operate on receipt of electric signals from the vehicle flight-control subsystem. Basic design features are illustrated in figure 26. Two different LITVC systems are shown in figures 27 and 28.

The objectives of an LITVC system-design effort are to establish the number and type of injectors, type of injectant, injector location and injection angle, the type and shape of the liquid injectant storage tank, and the method of pressurizing the liquid injectant. These parameters are established in the system-design analyses such that required vectoring performance is achieved at minimum weight without violating imposed constraints (e.g.,
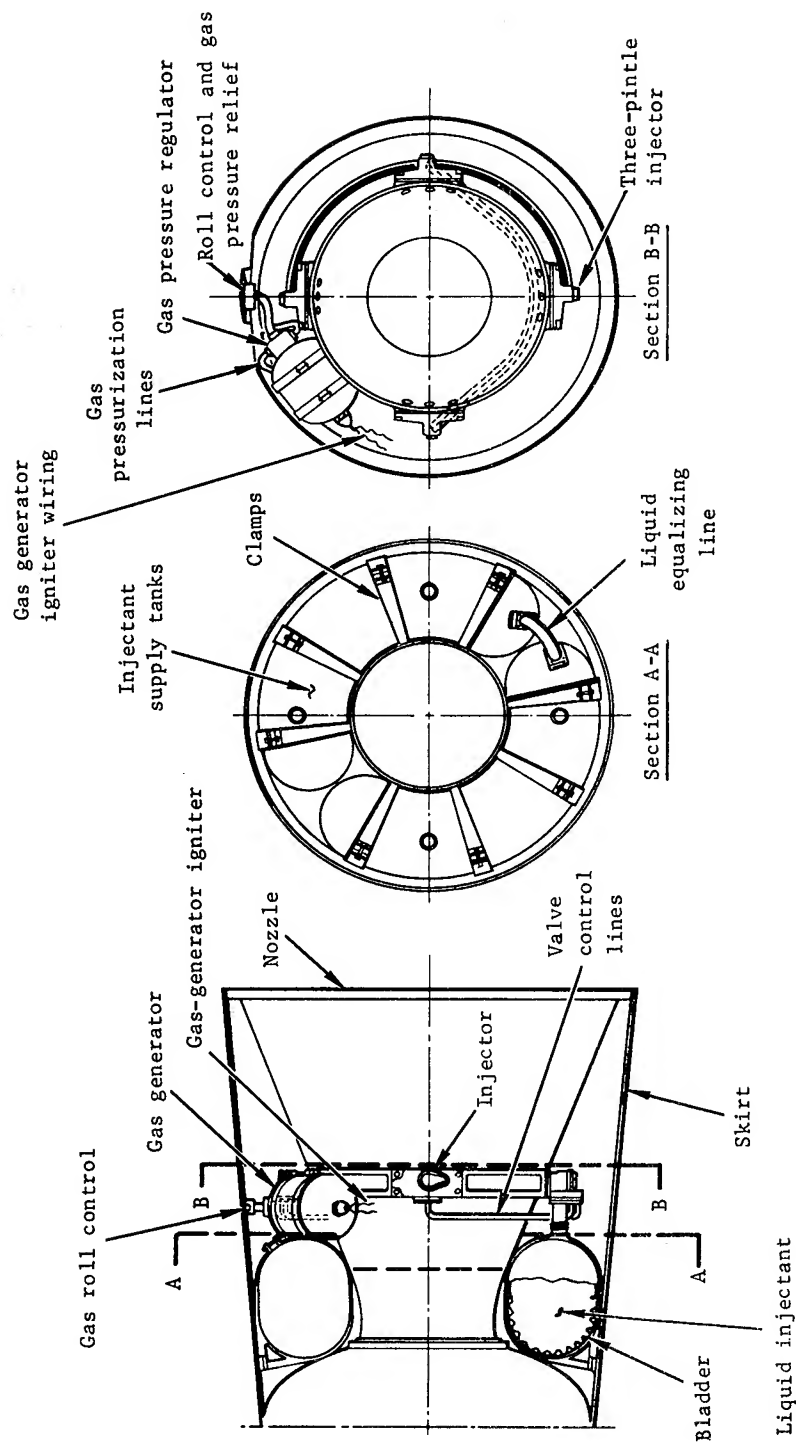
Figure 26. - Basic design features in a LITVC system.

Gas generator igniter wiring

Gas pressurization lines

Roll control and gas pressure relief

Gas pressure regulator

Three-pintle injector

Section B-B

Injectant supply tanks

Clamps

Liquid equalizing line

Section A-A

Nozzle

Gas-generator igniter

Gas generator

Gas roll control

Injector

Valve control lines

Skirt

Bladder

Liquid injectant

75

Nitrogen gas fill and vent valve

Common injectant and gas tank

Compressed nitrogen

Injectant

Injectant transfer tube

TVC electrical distribution box

TVC battery

TVC electrical power transfer switch

Injectant manifold

Nozzle

Manifold drain

Electromechanical injector valve

Pyroseal

Figure 27. - Schematic of Titan III ullage-blowdown LITVC system.
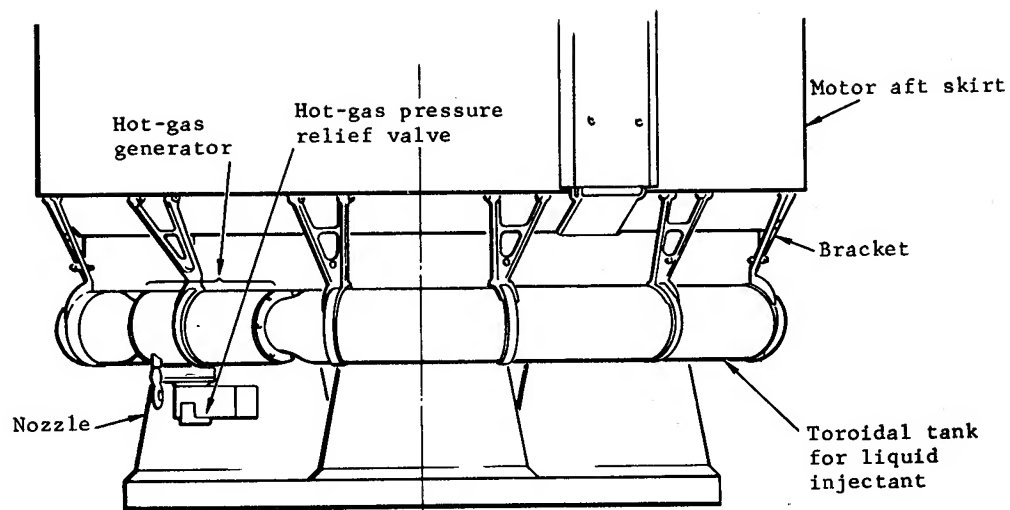
(a) Side view
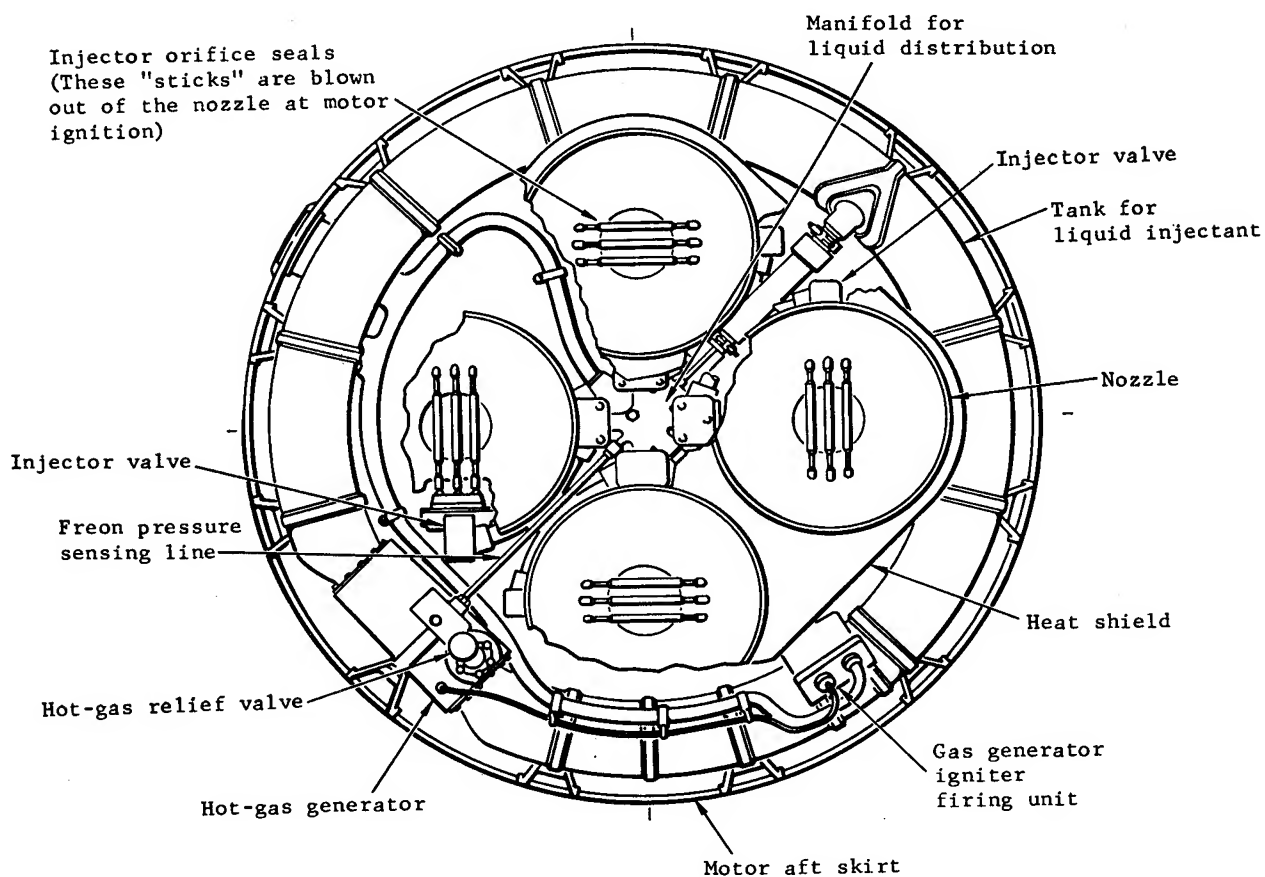
(b) End view

Figure 28. - LITVC system for Polaris A3 second stage.

77

envelope, response). The system-design analyses consist of an optimization study and an evaluation of the performance of injectants, injectors, and related parameters such as injection pressure and location in the nozzle.

2.2.1.1 SYSTEM OPTIMIZATION

To optimize an LITVC system for a particular design, the usual procedure is to compile weight, bulk, and performance data from known LITVC components and from selected designs provided by manufacturers. These data then are generalized in empirical equations or curves. Schematic designs representing the design alternates (e.g., type of fluid, number of injectors, and injection location) then are prepared to serve as a basis for optimization calculations. These alternates are evaluated for performance, weight, and compliance to the vehicle space envelope. For each design concept, an overall vehicle performance parameter is calculated for use in numerical evaluation; this parameter depends on the vehicle mission and typically has been either the payload or the vehicle final velocity at the end of motor burn. The results of the early optimization give preliminary determinations of the injectant choice, injectant amount, number of injectors, approximate system pressure, and so forth. This initial optimization reduces significantly the number of design possibilities to be considered and simplifies the detailed studies for injection pressure, orifice size and spacing, injector location and discharge angle, amount of injectant, and the system pressurization gas required. As the detailed studies of these items proceed, the empirical equations and curves are improved and the optimization is repeated as necessary to improve the preliminary results.

A limitation of LITVC that is important in the development period is lack of flexibility in changing the design to accommodate changes in maximum required side force or other design requirements. If the system being designed is very similar to an earlier design, the performance of which is known, then the new system can be designed close to the requirements. Usually, however, the new design is significantly different from any previous design, and data scaling has to be applied with the attendant uncertainties and the likelihood of overdesign. Also, systems usually are sized to meet the initial estimate of the worst-case trajectory requirements. Later these initial estimates are revised downwards. For these reasons, most systems in use are oversized.

Minor corrections, in particular redesign of pintle shape to provide better linearity and jet formation at lower flowrates and to reduce the amount of injectant carried in the tank, are changes that often are made late in the development period because they do not necessitate major redesign and additional tests. However, the items that most influence system weight and operating efficiency (sizes of tanks, brackets, tubing, injector valves, and the location and angle of the injector valves on the nozzle wall) are difficult and expensive to redesign after the initial design phase and therefore usually are left unchanged.

Oversizing is minimized by repeating the optimization procedure as late as possible before the system design concept is frozen. Corrected design and performance data are used, and the flight-control vectoring requirement is revised downward, if possible, usually by better definition of trajectory events. Thus, the more realistic the inputs in the optimization procedure, the more nearly correct and usually lighter weight is the final system design.

2.2.1.2 SELECTION OF INJECTANT

The chief factors considered in the selection of the liquid injectant are its side specific impulse, density, storability, and toxicity. Prime candidates for the injectant are nitrogen tetroxide and an aqueous solution of strontium perchlorate; other candidates are hydrazine, Freon 114-B2, and hydrogen peroxide. The basic properties and characteristics of major operational injectants are presented in table IX and discussed below.

Side specific impulse. – Side specific impulse is a measure of the vectoring power of the injectant and is defined as the side force, lbf (N), divided by the injectant flow rate, lbm/sec (kg/s). Reactive injectants have larger side specific impulses than inert injectants. Inert injectants such as Freon 114-B2 deliver side specific impulses of 70 to 160 lbf-sec/lbm (686 to 1569 N-sec/kg), while chemically reactive injectants such as strontium perchlorate solution or nitrogen tetroxide (N_2O_4) are significantly more effective, delivering side specific impulses of 180 to 300 lbf-sec/lbm (1765 to 2942 N-sec/kg) or more. At TVC angles less than 0.5° in Titan III configurations, side specific impulse values for N_2O_4 greater than 400 lbf-sec/lbm (3923 N-sec/kg) have been recorded. The actual delivered specific impulse depends on how well the design is optimized with respect to the injector location, size and spacing of injector orifices, injection angle, injection pressure, and injectant-stream characteristics.

Density. - Injectant density is a major influence on the volume and weight of tanks, piping, and injectors required. Storage space on some vehicles has been sufficiently limited to preclude use of a low-density injectant. Even when storage space was available, the required larger tanks, piping, and injectors imposed a weight penalty that eliminated low-density injectants from optimization studies. For this reason, the densities of injectants used usually have been approximately twice that of water. The high density has made it possible to store the injectant in compact tanks and permitted use of relatively small tubing, valves, and injectors. Thus, both weight and space on board the vehicle have been saved.

Storability. - Storability of a liquid depends both on the stability of the fluid under expected storage temperatures and pressures and on its compatibility with the tank materials it contacts. It is the measure of the capability of an injectant to be stored in the LITVC system in a state of readiness over long periods of time. This condition usually is achieved by controlling the purity of the injectant and by providing a tank material that will not react with the injectant and that contains no trace elements that could catalyze reactions.

TABLE IX. – Basic Properties and Characteristics of Main Operational Liquid Injectants

Property or characteristic	Freon 114-B2	Injectant Strontium perchlorate (solution in water)	Nitrogen tetroxide
Side specific impulse, [1] lbf-sec/lbm	70 to 160	150 to 260	180 to 400
Density, lbm/ft^3	134.5	124.5, 62% solution 126.1, 72% solution	90.0
Freezing or crystallization point, °F	−31	32, 62% solution 50, 72% solution	12
Stability in storage	Very stable; nonflammable.	Solution is stable in sealed storage	Stable if dry and without impurities.
Reactivity with metals	Inert in absence of water.	Noncorrosive to stainless steels and aluminum.	Noncorrosive in absence of water to stainless steels and aluminum (ref. 110). Stress corrosion problem with titanium (ref. 111).
Reactivity with polymers	Penetrates and deteriorates polymers.	Almost no effect on elastomers and most other polymers (ref. 110).	Most elastomers are incompatible with N_2O_4 for long-term storage; some disintegrate in hours, others in days. Only nitroso compound AFE-110 and Parker compound B-591-8 are acceptable for 90-day storage (ref. 112).
Toxicity	Harmless on contact. Fumes harmless in moderate amounts.	Solution has low toxicity. No problem with good housekeeping. Dry perchlorate is moderately toxic and irritating to the skin.	Severely burns skin and eyes on contact. Inhalation of fumes can be fatal.
Vehicle on which injectant is used	Polaris A3 second stage; Minuteman II second stage; Sprint first stage.	Minuteman III third stage (66% solution)	Titan III

(1) Based on test data for which injection location in the nozzle and injector geometry were close to optimum.

Studies have been conducted to determine the compatibility of liquid injectants with various materials (refs. 111 through 119). The results of one such study are summarized in table X (ref. 120). As shown, Freon 114-B2 is almost completely inert with metals; however, it should not be stored in metallic materials subject to corrosion, since any water contamination causes hydrolysis and subsequent corrosion. Freon 114-B2 does not affect Teflon materials but does permeate various elastomers, thermosets, and thermoplastics; it leaches plasticizer from the plastics, making them hard and brittle. Both N_2O_4 and $Sr(ClO_4)_2$ are reactive. Strontium perchlorate must be contained in stainless steel or titanium storage tanks. It is stable and safe at 350° F (450 K), but at higher temperatures it decomposes and becomes a strong oxidizer. Within the range to 900 to 1000° F (755 K to 811 K), strontium perchlorate combines so readily with rubber that an almost explosive reaction occurs. This reaction has occurred near the end of the duty cycle in systems with gas-generator pressurization and is a potential problem for all reactive liquids. At normal storage temperatures, decomposition is not a problem for any of the liquids mentioned here.

Nitrogen tetroxide gives the highest side specific impulse of the injectants that are operational; its reactivity, however, makes it difficult to handle. It can be stored successfully only if strict requirements for purity and container inertness are met; otherwise, decomposition and degradation will occur. Elastomeric materials cannot be used for long-term seals. Handling precautions and storage requirements are well established in the industry and do not present significant problems. The current practical storability of N_2O_4 has been demonstrated in Titan III operational practice, where the LITVC system has been approved to remain loaded for up to 75 days and in readiness at operational pressure through a 30-day hold (refs. 47 and 114). Nitrogen tetroxide has been selected for use in the rocket engine for the Minuteman III post-boost control system.

The freezing or crystallizing temperature is the limiting low temperature for storage. Crystallization or separation does not occur either in Freon or nitrogen tetroxide. Freon 114-B2 freezes at -31° F (238 K) and N_2O_4 freezes at 12° F (262 K). Strontium percholorate in a 62% solution with water crystallizes out of the solution at 32° F (273 K).

Toxicity. — Nitrogen tetroxide burns on contact, and inhalation of fumes can be fatal, whereas Freon 114-B2 is harmless on contact and its fumes are harmless in moderate amounts. In comparison with Freon 114-B2, strontium perchlorate delivers 50% more specific impulse, costs half as much, and involves fewer compatibility and storage problems. However, strontium perchlorate is moderately toxic and irritating to the skin. Care must be exercised to prevent the perchlorate salt or solution from saturating clothing or wood, since these saturated materials would burn rapidly if ignited.

2.2.1.3 INJECTION PRESSURES AND INJECTION ORIFICES

In a typical LITVC system, the liquid is injected into the nozzle through an annular orifice formed by a convergent round outlet with a central pintle, as shown in the injector cross

TABLE X. — Compatibility of Selected Metals and Nonmetals with Freon 114-B2 and Aqueous Strontium Perchlorate (ref. 120)

Materials Tested	
Metals	Nonmetals
Ti-6A1-4V	Hypalon 20
4130 steel	Neoprenes CN and W
4340 steel	Polyvinyl alcohol
7505 aluminum	Thiokol ST (polysulfide)
2024 aluminum	Viton "A"
347 stainless steel	Tygon ST (polyvinyl chloride)
Molybdenum steel	Teflons 1, 6, and 100

Results after 3-week exposure at room temperature

Material	Freon 114-B2	Sr(ClO$_4$)$_2$
Metals	No visible effect on any metal.	4130 and 4340 steels showed some rust; other metals showed no visible effect.
Nonmetals	All specimens except the Teflons showed signs of permeation and deterioration. Significant pickup of liquid indicates permeability problems.	Polyvinyl alcohol and Thiokol ST showed signs of chemical reaction and deterioration; other specimens showed no visible effect. Pickup of liquid was negligible.

sections in figures 29, 30, and 31. The central pintle acts as the gate of the injector valve. Thus, the full system pressure is applied to the liquid up to the point of discharge through the orifice. The injection pressure, orifice size, and orifice spacing have a significant influence on side-thrust efficiency and system compexity.

Injection system pressure is important because it provides the force that drives the liquid through the orifice with the high momentum needed to obtain best side-thrust efficiency. System pressures in use range from 450 to 1500 psi (3.10 to 10.34 MN/m^2). Analysis of test data from small-scale motor firings with LITVC indicates that for maximum side-thrust efficiency the injection pressure should be set at about twice the chamber pressure of the rocket motor (ref. 121). Such high pressures may not be optimum for the entire system because these pressures also influence the weight of tanks, tubing, and injectors. If lower pressures are used, the probable loss in side-thrust efficiency can be estimated (refs. 108, 121, and 122).

Efficient development of side force by fluid injection depends mainly on rapid mixing and chemical reaction of the injectant with the hot exhaust gas close to the wall. This complex process involves droplet shattering, evaporation, and nonequilibrium chemistry. It should be noted that practically all injectants decompose and react chemically, including the so-called inert injectants, although for these liquids the energy released is small. Analytic models of this process and the effects that compose it are found in references 105, 106, 110, and 123.

For most efficient development of side force, the injectant should be thoroughly mixed and fully reacted with exhaust gas in the immediate neighborhood of the wall. For thorough mixing, the liquid jets should have the highest possible momentum and therefore velocity. However, to prevent the high-velocity jets from passing out of the immediate neighborhood of the wall and penetrating too far into the gas stream, where their effects would be lost, the individual jets must be made so small that in spite of their high momentum they will have broken up and become mixed with the gas while still close to the wall. At all flowrates, the momentum per unit mass of liquid discharged remains about the same, since it is dependent on the pressure of the injectant in the system. This momentum contributes to the LITVC effect by delivering a force against the supersonic stream that produces the initial shock and partially diverts the direction of flow. The balance of the LITVC effort results from the injectant and its reactions producing higher flow pressures acting against the wall.

For a well-designed pintle-type injector (figs. 29 and 30) having a given orifice size, the greatest side-thrust efficiency is obtained at low flowrates (ref. 108). This effect occurs because at low injector openings the jet maintains the usual high momentum per unit mass discharged but the annular jet stream has a thin section, so that it mixes efficiently and penetrates only into the gas that is closest to the wall. At high flowrates, however, the annular jet increases in thickness, so that it penetrates much more deeply into the nozzle gas stream, thereby carrying the injectant farther from the wall to which the pressure effects must be applied to be useful.
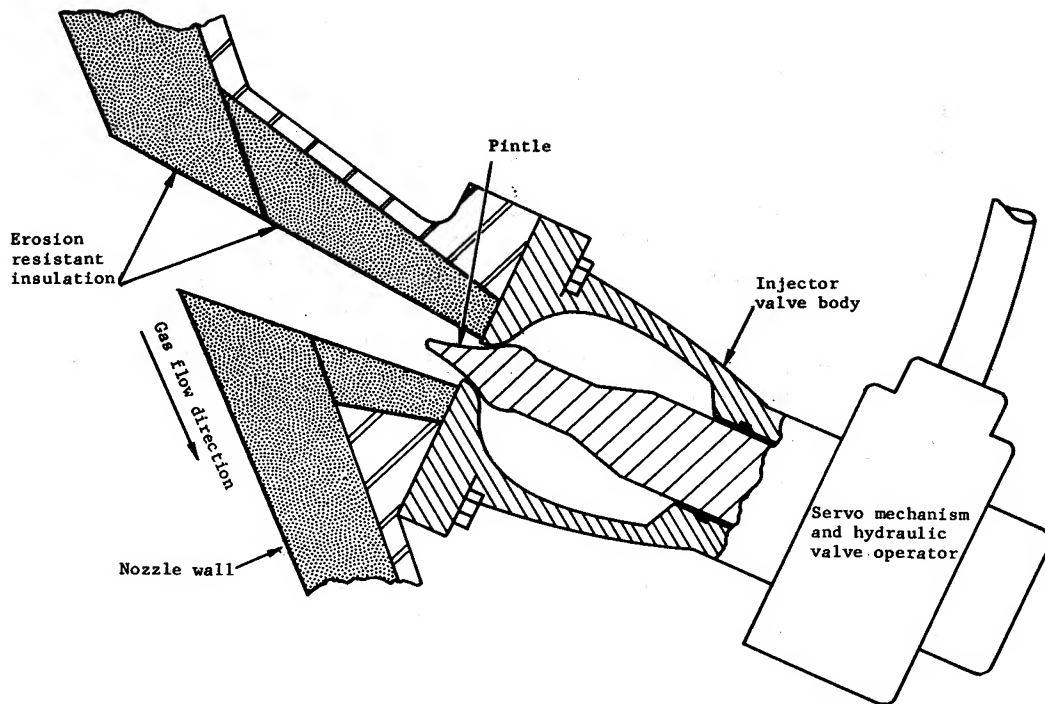
Figure 29. - Cross section drawing of typical single-orifice injector mounted on nozzle wall.
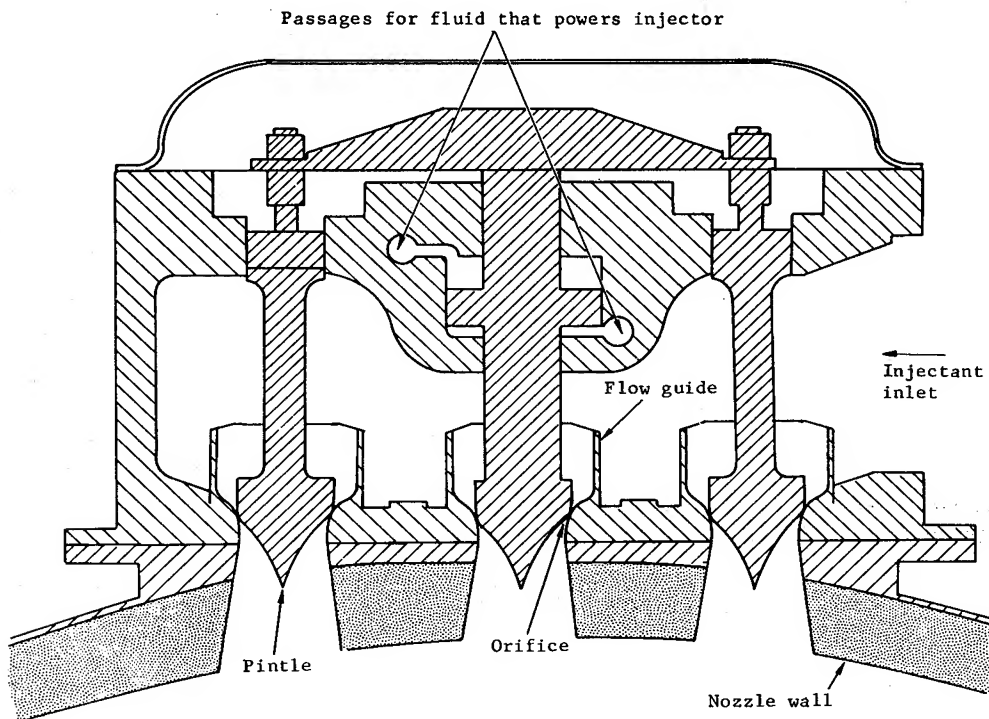
Figure 30. - Cross section drawing of three-orifice injector mounted on nozzle wall.
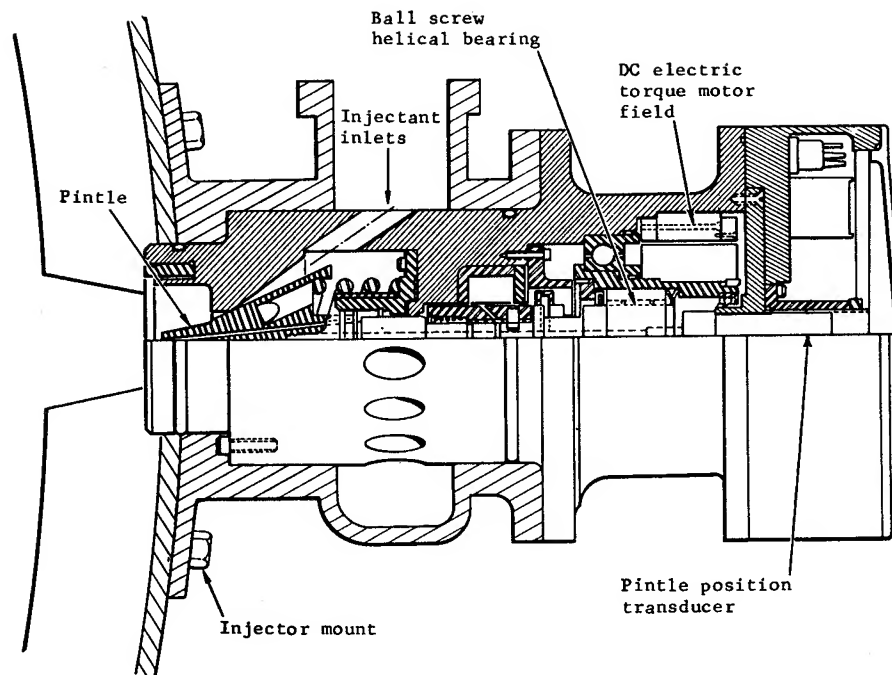
Figure 31. - Cross section drawing of an electromechanical injectant valve.

Side-specific-impulse efficiencies have an upper limit at very small orifice sizes and valve openings (ref. 108) because increasing orifice friction reduces jet momentum per unit mass. The drop in efficiency that occurs with large flow from a single orifice makes it advantageous to use a large number of small orifices. The flow is divided among individual jets, so that in spite of the great flow momentum the liquid does not penetrate deeply into the main stream; instead, the jets break up close to the wall, where the injectant mixes with the gas, vaporizes, and reacts to release energy that produces higher pressure on the wall. The large number of injectors, however, add to the complexity and the cost.

Increasing the number of injection ports increases the injection efficiency, provided that overlap losses and cosine losses are not excessive. Overlap losses result from the overlap of regions of shock pressure, mixing, and reacting. In these regions the local pressure increase is not the sum of influences from two separate orifices but a lesser amount, greater however than that for one orifice alone (refs. 108 and 124). Cosine losses result from the spreading of the LITVC wall pressures around the nozzle; this spreading causes a portion of the potential side force to be lost because opposing force components cancel. These losses are

called cosine losses because the local LITVC force is diminished, for TVC purposes, by the cosine of the angle between its direction and the desired side-force direction.

The basic liquid injection configuration has four or more injectors spaced equally around the rocket nozzle for positive and negative pitch and yaw control. Needed control forces acting between the pitch and yaw planes require that several adjacent injectors flow simultaneously, and the resultant force is obtained by vector addition of the control forces from these injectors. The use of more than four injectors (e.g., six, twelve, or twenty-four injectors equally spaced around the nozzle) decreases the amount of fluid required, because the injectors that must provide a given control force will more likely be located closer to the direction of the required force; with more injectors flowing simultaneously, each injector will deliver less flow and therefore will have higher side-thrust efficiency.

The predicted response of the system to changes in injection pressure or in orifice size, number, and spacing is reduced to curves and equations for use as inputs in the system optimization calculations (sec. 2.2.1.1). Examples of such curves and equations are contained in references 47, 121, 125, and 126.

2.2.1.4 INJECTOR LOCATION AND DISCHARGE ANGLE

The injector is positioned on the nozzle wall (fig. 23) at a location and a discharge angle that is optimum for the expected schedule of vectoring for a typical flight. The optimum location for injection is a compromise of two opposing tendencies that add to or subtract from the side force. If the injection point is as far upstream in the nozzle exit cone as possible, the nozzle wall area over which the pressures are augmented by injection is increased. However, as the injection point is moved upstream, the shock wave of the injectant-augmented portion of the flow spreads out around and across the nozzle until it produces a pressure on the opposite half of the nozzle that subtracts from the desired side force. This cross-interference tendency increases with rise in the ratio of injection flowrate to motor flowrate. For a very low injection flowrate, the optimum injector position on the nozzle wall is upstream and relatively close to the throat, but for larger injection flowrates the optimum position is downstream from the throat nearer the nozzle exit (refs. 107 and 126). The most favorable injection point for a particular motor is an intermediate location at which the total required program of thrust vectoring is accomplished with least expenditure of liquid.

The injector discharge (fig. 23) usually is directed upstream at angles ranging from 0° to 25°. The 25° angle has been found to be optimum in subscale tests (refs. 108 and 109). Pointing the liquid jets upstream produces several effects. The greater relative velocity between the exhaust gas and the liquid jet shatters the droplets to a smaller size, thus aiding evaporation and mixing. The injectant is delivered slightly upstream of the injection point, an effect equivalent to moving the injection upstream by that amount. Directing the fluid

jet upstream along the wall reduces the depth of penetration of the jet and keeps the injectant mixture and its higher pressures nearer the wall, where they will produce more side force. If the jet is directed too close to the wall, at angles appreciably greater than +25°, the beneficial effect of better mixing and improved positioning of the resulting higher pressure region is more than cancelled out by losses (ref. 125). These losses probably result from a reduction in the useful component of the injectant jet reaction force, loss in momentum of the main gas stream due to more direct opposition by the fluid jet, and greater loss of fluid momentum in the injector due to the larger diagonal passage through the nozzle wall.

The optimum injection location usually is closer to the throat than to the exit, with a value of optimum $X/L \approx 0.3$ being typical (X = distance from throat to the plane of the injector ports, and L = distance from throat to exit plane). Motors with submerged nozzles do not permit injection at the optimum location, and a performance penalty is thus imposed. For the Poseidon C3 motors, the penalty was so large that LITVC was eliminated from consideration as a TVC system, and the flexible-joint TVC system was adopted.

The injection location parameter X/L, while simple and convenient for specifying injection location, can be misleading when used in design, because it is only indirectly related to the phenomena that cause the side force. Other parameters including the expansion ratio, divergence angle, shock angle, and mixing-path dimensions are more directly related to the LITVC effect.

Since the location and angle of injection strongly influence the LITVC side-force efficiency, their effect is included in the system optimization calculations (sec. 2.2.1.1). Examples of curves presenting the effects of injector location and angle on side-force efficiency are contained in references 108, 122, and 125.

2.2.1.5 AMOUNT OF LIQUID INJECTANT REQUIRED

In the system optimization calculations, the amount of liquid required is the parameter that usually indicates the relative efficiency of each design concept considered. Not only is the amount of liquid the largest item of weight that must be carried, but it determines, through its equvalent volume, the size and weight of the tubing, injectors, and tankage. The latter is usually the heaviest item of inert weight. Thus, the system design concept that requires the smallest amount of injectant liquid usually is the one shown to be most desirable by the optimization calculations.

The amount of liquid required depends on the required vectoring program. A simple but very conservative method for calculating the amount of liquid uses the worst combination of maximum expected vectoring requirements. Statistically, such a combination is extremely unlikely, since it provides for the most unfavorable type of event at every stage of the flight including the most irregular launch or separation, the most severe weather and

wind shears at all altitudes, the most eccentric possible alignment of vehicle weights, and the greatest nozzle misalignment. The statistical odds for this worst combination usually is very small, typically less than 1 in 100 000. This "worst-on-worst" method generally has resulted in overestimates of the total side impulse required and in design of systems that carry grossly excessive amounts of liquid. Sometimes, after flight experience had revealed this fact as in the Polaris A3 program, the amount of liquid loaded in the tank has been reduced, but use of an oversized tank continued.

A better method of determining the amount of side impulse and therefore the amount of liquid required for vectoring employs statistical techniques such as the Monte Carlo method (refs. 47, 127, and 128). By this method, the amount of liquid required is determined as a function of the probability that the vehicle will not run out of liquid before the vehicle operation is completed. The calculation considers a random probable requirement for each separate part of the vectoring program and sums each part to obtain the total amount of injectant required. The calculation is repeated many times to develop a statistical basis for the amount of liquid to be carried. Preliminary estimates of total side impulse required for vectoring have been obtained by assuming a side force of 0.02 of total axial impulse for first-stage motors, 0.01 of total axial impulse for second-stage motors, and 0.006 of total axial impulse for third-stage motors.

In addition to the liquid that is needed for vectoring, liquid is carried for ullage, filling of pipes and valves, and valve operation; some injectant is lost when valves operate, because the valves cannot open and close instantaneously. This unusable liquid is minimized by designing the tank, bladder, piping, and valves to avoid trapping liquid and to have only the flow volume required. Also, some valves leak because of imperfect contact between the pintle and the valve seat. This leakage can be minimized and with good design should be too small to be included in establishing the amount of liquid.

The total required storage tank capacity thus includes the liquid for vectoring plus the "unusable" liquid required for ullage, system fill, valve operation, and possibly leakage. A typical procedure for determining the total amount of liquid is as follows:

(1) The vectoring requirement is determined. Preferably it is developed in itemized form by deflection angle and time; e.g., 3 deg for two seconds, 1.5 deg for one second, and 0.5 deg for the balance of the flight time. For each deflection angle the required side impulse is equal to the axial thrust times the sine of the deflection angle times the time required for this amount of deflection. Sometimes the total required side impulse and an average deflection angle are specified. In the latter case, the maximum deflection angle is also specified, since it is needed to estimate the injector size and location.

(2) Curves of estimated side specific impulse versus deflection angle are developed by scaling and replotting available data (refs. 46, 108, 109, 121, 124, 125, and 129).

(3) The liquid needed for vectoring each specified deflection angle is calculated by dividing the side impulse required by the side specific impulse indicated on the curve developed in (2). The amounts of liquid thus determined for the various required angles are then summed.

(4) The amount of additional liquid required for ullage, filling of piping, leakage, and similar needs is estimated and added to the above usable amount. For preliminary calculations, this amount is sometimes estimated at 10 percent of the total usable liquid.

2.2.1.6 AMOUNT OF PRESSURIZATION GAS REQUIRED

The liquid injectant in the system is kept under high pressures by gas that acts on the liquid in the tank either through a bladder (fig. 23) or piston or directly (fig. 27). The supply of compressed gas is made large enough so that when the liquid is expelled from the tank at the largest expected flowrate, its displaced volume is filled by fresh gas at a flowrate and pressure sufficient to ensure that the system pressure does not fall below its required level. The amount of gas that must be supplied to pressurize the LITVC system during its operation usually is determined in the final evaluation of a system concept, the pressure of the system and the amount of liquid to be injected having already been established.

If the LITVC system is to be pressurized by inert gas, only the exact amount of gas needed to expand into the volume occupied by the displaced injectant must be provided. The final pressure should, of course, not be less than the required injection pressure level (sec. 2.2.1.3). If pressurization gas is to be generated by burning solid propellant, more gas will be required than that needed for liquid displacement. The amount of gas required is the maximum expected gas demand rate integrated over the operating time. This demand rate is determined from the maximum expected injectant flowrate, which in turn is obtained from the "worst-on-worst" severe vectoring requirements taken at all times through the motor operating time.

If a vectoring program requires only occasional side forces of short duration but large magnitude and if these can occur over a wide time span, the required amount of generated gas can be very much greater than that required to displace the ejected injectant. In some cases, this excessive required amount has been reduced by taking advantage of excess tank volume to act as a gas accumulator. In other cases, it has been found to be better to use compressed inert gas.

2.2.2 Component Design

The design of the components of the LITVC system is begun after the optimum LITVC system concept has been developed; i.e., after the injectant has been selected; the injection

location, angle, maximum flowrate, orifice size and spacing, and system pressure have been determined; the amounts of injectant and pressurization gas have been calculated; and the approximate envelope available for the components has been checked and been found to be reasonably adequate. Component design, as considered in the following section, includes the detailed design of the LITVC system as well as adaptation of the rocket motor for LITVC.

The components of a typical LITVC system are the injectors, fittings and piping, tanks with or without bladders, gas supply for pressurization, meters to equalize tank drainage, and provisions for disposal of surplus injectant. The complete LITVC assembly usually is mounted around the nozzle on brackets that attach to the nozzle or the aft end of the motor. Erosion may be moderate or severe at the injectant holes in the nozzle wall, and this area may require special insulation and structure. Also, some form of heat barrier or insulation usually is required to protect the LITVC components from the heat of the exhaust plume.

2.2.2.1 INJECTORS

The injectors are automatically operated valves in which the valve closure is located in a streamlined discharge port, so that full injection system pressure is effective close to the point of release; thus high discharge velocity is imparted to the liquid injected into the hot-gas flow in the nozzle exit cone. The design of the injector critically affects LITVC efficiency. A good injector injects liquid in a linear, nondiverging jet at the highest possible velocity in order to impart high momentum to the fluid jet so that it interacts forcefully on the supersonic gas stream, thereby causing a shock wave and maximum droplet breakup, dispersion, and mixing (fig. 23).

A range of sizes and types of injectors is available from control-valve suppliers. These injectors have been designed for use on various rocket motors for which LITVC was chosen or considered as the means of vectoring.

Variable-orifice injectors. — The variable-orifice injector (figs. 29, 30, 31, 32, and 33) has become the most widely used because of its operating flexibility and consequent ease of adaptation to vehicle flight-control systems. Design features of this injector in various applications are summarized in table XI.

This injector has a pintle gate that moves axially in the port to throttle the flow. The pintle is approximately cone-shaped, so that when moved into the exit throat it reduces or closes the annular orifice. Injector discharge can be modulated from almost zero flow to full flow. Supply piping and passages usually are sized large enough to avoid pressure losses due to flow resistance, so that even at high flowrates full system pressure reaches the liquid in the injector valve and drives the jet through the orifice and into the nozzle. The orifice approach and pintle of the injector are designed with streamlined contours so that the flow is efficiently accelerated into a narrow, high-velocity stream. The injector pintle is controlled

90
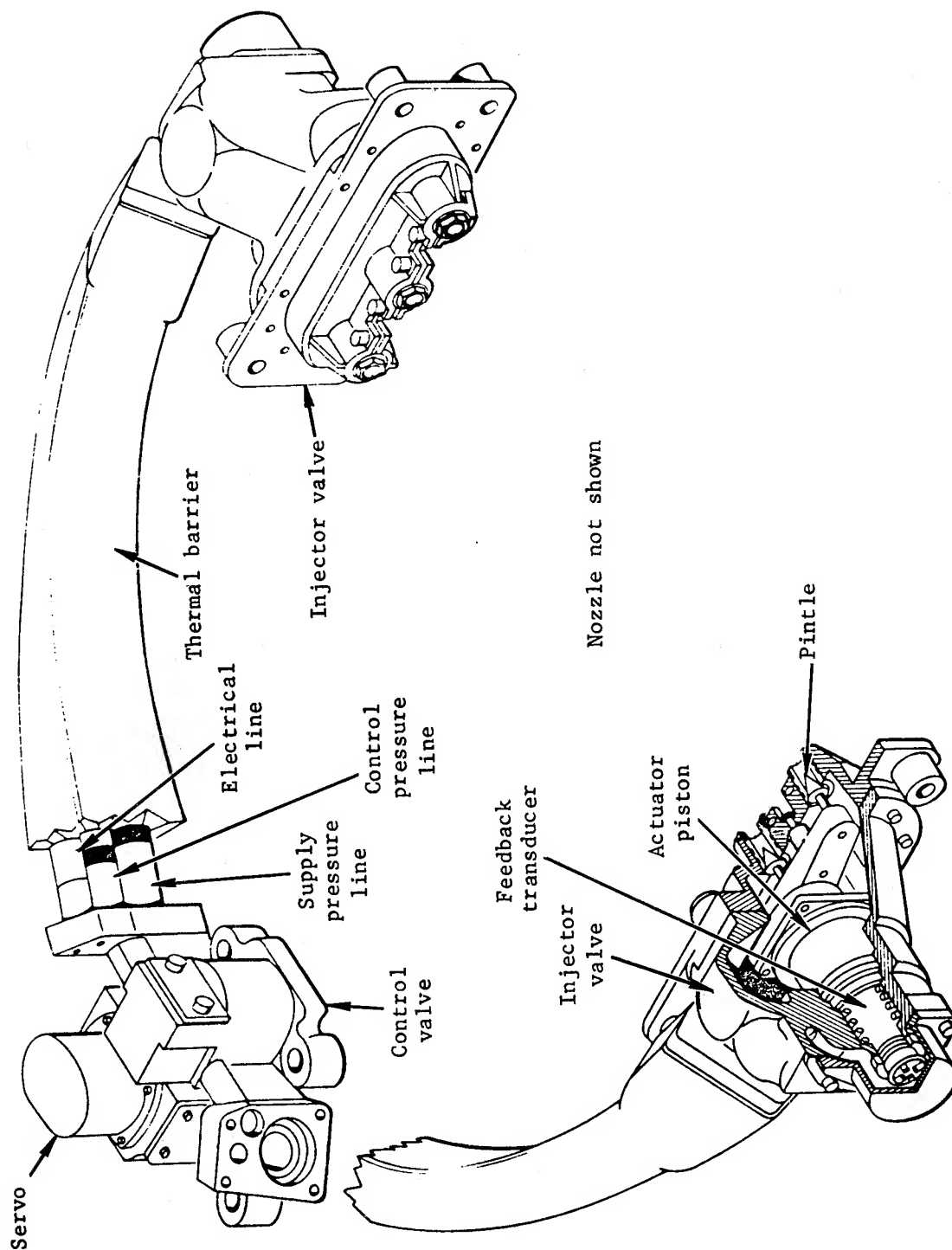
Figure 32. - Injector valve assembly with hydraulic-powered actuator.

91
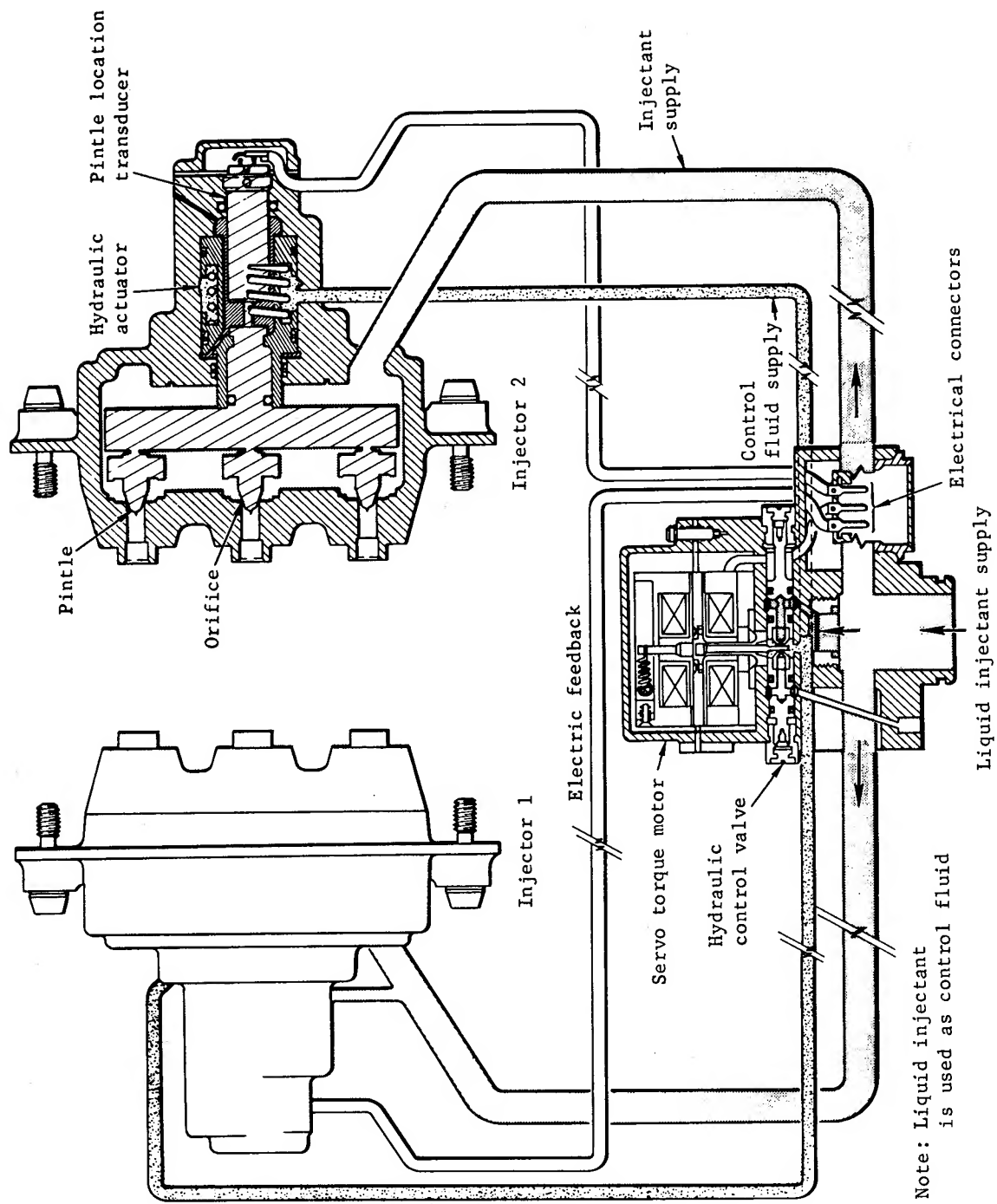
Figure 33. - Servo-controlled hydraulic power systems for variable-orifice injectors.

Pintle location transducer

Hydraulic actuator

Injectant supply

Electrical connectors

Control fluid supply

Injector 2

Pintle

Orifice

Liquid injectant supply

Injector 1

Electric feedback

Servo torque motor

Hydraulic control valve

Note: Liquid injectant is used as control fluid

TABLE XI. — Chief Design Features of Variable - Orifice Injectors on Operational LITVC Systems

Motor	Number of nozzles	Number of injectors	Number of orifices per injector	Angle of injection (fig. 23)	Injector weight, lbm	Type of actuation	Flowrate, lbm/sec	Operating pressure, psig	Response time, signal to full deflection, sec	References
Polaris A3 second stage	4	8 (2 per nozzle)	3	25°	4.4	Electro-hydraulic	12.	750	0.230	48
Minuteman II second stage	1	4	3	0°	5.2	Electro-hydraulic	60.	620	0.120	49, 113, 130
Minuteman III third stage	1	4	3	20°	4.0	Electro-mechanical	12.5	680	0.080	131
Sprint	1	4	3	0°	11.0	Electro-hydraulic	400.	800	0.022	50
Titan III	1	24	1	0°	24.0	Electro-mechanical	100.	750	0.190	46, 128, 132
156-Inch	1	24	1	0°	25.0	Electro-hydraulic	158.	750	0.400	133

Note: The first five systems listed are operational; the last was tested in a development program.

93

by a mechanism that provides variable control of the injector flow on command of electrical signals from the vehicle flight control. The control signals may be analog (variable voltage) or digital. The valve motor may be electric, hydraulic, or both. Usually it is electro-hydraulic (table XI). In this case, the valve operation is controlled by a servo mechanism in which an electrically operated pilot valve is used to admit pressurized hydraulic fluid to move the valve closure or pintle and thus to modulate the flow (figs. 29 and 30). The servo-operated injectors usually have three orifices and pintles (figs. 30, 32, and 33). Injectors with five orifices and pintles have been designed and presumably could be fabricated. In some electro-hydraulic systems, the pressurized injectant is used to provide hydraulic power to operate the injectors (figs. 32 and 33).

In the Titan III and NASA 260-in. (6.6 m) systems, the injectors are operated by electro-mechanical actuators (fig. 31). A dc electric motor moves the pintle axially. The pintle position is sensed by a linear potentiometer connected to an electronic controller that adjusts the dc current so that the pintle position matches the command from the flight control system (ref. 47).

Fixed-orifice injector. — On-off fixed-orifice injectors have been tested in various LITVC development programs and have been proposed for use, but to date no on-off system has been developed to operational status for any solid propellant motor and only one for a liquid propellant engine (Lance). The two potential advantages of the on-off injector are high efficiency and light weight. The high efficiency is obtained if the valve gate or pintle is withdrawn fully from a countoured orifice so that the flow of liquid is not obstructed by the pintle but is accelerated and interacts with the gas with maximum force. The size of the orifices must be made sufficiently small so that the jets break up and disperse close to the wall where mixing and reacting produces greatest wall pressure. The light weight results from the simple two-position actuation that requires no feedback for flowrate modulation. (The Lance injector weighs 1.1 lbm (0.50 kg) and has a flow rate of 5.7 lbm/sec (2.59 kg/sec) of hydrazine at 900 psi (6.21 MN/m²).

The disadvantage of on-off fixed-area actuators is that side-thrust modulation must be accomplished by varying the length of the flow pulses. The resulting force pulses produce a vibration effect that can cause structural or operating problems in the vehicle unless the LITVC frequency is set outside the ranges that can cause trouble.

Response time. — LITVC system response can be made very rapid. The four events included in response are the electric vector signal, the actuator pintle movement, the movement of liquid through the injector into the nozzle, and the mixing and reacting of injectant with gas in the nozzle. The electric signal is almost instantaneous. The time for the actuator drive to move the injector pintle takes the most time, typically 15 to 200 milliseconds. The liquid flow begins when the pintle first opens and accelerates as the pintle completes its motion. Time for the liquid to accelerate to full flow varies from 1 to 10 msec. The mixing and reacting of the injectant with the nozzle gas is very rapid, ranging from less than 1 msec for

average-size motors to 2.5 msec for large motors such as the Titan III. The total response time is the approximate sum of these times (note that injectant flow and pintle movement times overlap) and can be as little as 22 msec (ref. 139 and table XI). A shorter response time can be obtained by reducing the mass of the pintle, increasing the pintle drive force, and increasing the injectant pressure.

Supplemental injector hardware. — Screens usually are installed in the liquid-supply piping just upstream of the injector to catch any pieces of solid matter that might cause the valve to malfunction.

In some cases, closures are used at the injection orifices to prevent loss of liquid during storage or after system activation but before motor ignition. For example, the Titan III LITVC system is designed to be capable of being held at launch readiness for up to 75 days. The stored liquid is allowed to fill the entire system and is sealed from leakage loss at injector outlets by pyroseals (fig. 27). Pyroseals are fluid-tight plugs that burn off about 1/4 sec after ignition (ref. 47).

2.2.2.2 STORAGE TANK AND BLADDER

The chief design features of liquid storage systems for operational LITVC systems are summarized in table XII.

The liquid injectant is stored in one or more spherical, cylindrical, or toroidal tanks typically made of stainless steel, titanium, or aluminum. Each tank usually is connected to a system supplying compressed gas to pressurize the liquid. The gas may be cold and inert, usually nitrogen, or hot and reactive if generated by burning solid propellant.

A membrane or bladder usually is used in each tank to keep the gas separated from the liquid and prevent the gas from mixing with, exchanging heat with, reacting with, or bypassing the fluid. It is advantageous to eliminate the bladder if possible to reduce weight and eliminate a development problem. The bladder can be eliminated if the pressurizing gas and the liquid injectant are compatible and if the liquid is positively positioned over the tank outlet as in the LITVC system of the Minuteman III third stage. This system uses compressed helium to pressurize strontium perchlorate solution in a spherical tank. The gravity and acceleration forces apparently are sufficient to hold the liquid over the tank outlet. The bladder usually is a laminate of strong flexible plastic and fiber materials coated with an injectant-resistant material. Typically the internal fiber web has provided the needed mechanical strength and the facing plastic layers have provided thermal insulation on the gas side and an inert permeable seal on the liquid side. Much effort has been expended on bladder development, because the dependable separation of liquid and pressurizing gas has been critical to the success of most systems. A ruptured bladder may allow pressurizing gas to blow by the liquid and enter the piping to the injectors, thus causing loss of control

TABLE XII. – Chief Design Features of Liquid Storage Systems on Operational LITVC Systems

Motor	Liquid injectant	Injectant density, lbm/ft³	Amount of liquid stored, lbm	Liquid tank material	Tank shape	Separation between gas and liquid	Source of pressurization	Initial gas pressure, psia	Surplus liquid jettisoned into nozzle during flight	Dry weight of LITVC system, lbm
Polaris A3 second stage	Freon 114-B2	134.5	200	Aluminum	Toroidal	Bladder (Viton reinforced with Dacron)	Gas generator	NA	Yes	139
Minuteman II second stage	Freon 114-B2	134.5	259	Steel (17-7PH)	Toroidal	Bladder (Viton AVH reinforced with Dacron)	Gas generator	NA	Yes	228
Minuteman III third stage	$Sr(ClO_4)_2$ (62% solution in H_2O)	124.5	49.3	Ti-6Al4V	Spherical	None	Compressed helium gas	3320	No	42
Sprint	Freon 114-B2	134.5	160	Stainless steel	Cylindrical	Piston	Gas generator	NA	No	221
Titan III	N_2O_4	90.0	8424	Stainless steel (410)	Cylindrical	None	Compressed nitrogen gas	1100	Yes	7054
156-Inch	N_2O_4	90.0	8170	Stainless steel	Cylindrical	Bladder (stainless steel and chlorobutyl rubber)	Compressed nitrogen gas	5500	No	8808

Notes: Status of systems and references for data are indicated in Table XI.
NA = not applicable

effectiveness and system pressure. The consequence of bladder failure also may be sudden combustion of a reactive injectant. For example, in an LITVC test using lead perchlorate injectant in a system in which the bladder was eliminated, an explosion resulted. A less serious result has been the reduction of the pressurizing capacity of hot gas by loss of heat directly to the fluid and consequent contraction of the gas. In bladder development work, some of the best results have been obtained with laminated plastic and metal foil (refs. 115, 117, and 118).

A burst diaphragm at the tank outlet usually is used to seal the fluid in the tank during storage. On system activation, the rise of pressure in the fluid tank breaks the diaphragm, and fluid flows through the tubing and manifold and into the injectors.

A simpler alternate arrangement having neither a bladder nor a burst diaphragm stores the liquid and the pressurizing gas in the same tank and relies only on gravity and acceleration forces to position the fluid over the outlet. The Titan III system uses this system (fig. 27). The supply tubing, the injectors, and about 2/5ths of the tank are filled with nitrogen tetroxide fluid and then pressurized by addition of compressed nitrogen gas into the remaining tank volume. Leakage from the injectors is prevented by pyroseals (ref. 47).

2.2.2.3 PRESSURIZATION SYSTEM

High-pressure gas required to pressurize the fluid is provided either by a tank of compressed gas such as nitrogen or helium or by a solid-propellant gas generator (table XII). In some systems, the same gas generator is used as a source of gas for roll-control jets.

The compressed gas system, if independent of the liquid tank, consists of a metal gas tank or bottle of any convenient shape, a squib valve, and a pressure regulator valve. The initial pressure of the gas is from two to seven times the liquid system operating pressure (tables X and XI), so that after the gas tank has discharged the full amount needed, the tank pressure is still greater than the required minimum system operating pressure. During motor operation, the high gas pressure usually is reduced to the liquid system pressure by a pressure-reducing valve in order to obtain reproducible valve operation and to avoid an injection pressure so high that it will degrade side-thrust efficiency (ref. 116). If a common liquid/gas tank is used (fig. 27), the initial gas pressure is made high enough so that after the bulk of the liquid has been used, sufficient pressure still remains for effective operation. With this arrangement, the initial injectant pressure is the same as the initial gas supply pressure but becomes successively less during the TVC duty cycle. This reduced pressure will cause a certain amount of wasted injectant due to off-peak LITVC efficiency (ref. 133); also, in the case of electro-hydraulic valves operated by pressurized injectant, it will cause variation in injector response time.

Usually the high-pressure tank is left empty during storage and handling of the motor and is filled remotely just before launch. Otherwise, for the safety of personnel working near

pressure vessels, the tank must be made heavyweight with a factor of safety ranging from four to six. An advantage of pressurizing with compressed inert gas is that no bladder or other separation is needed, provided gravity or acceleration forces constantly hold the liquid over the tank outlets for positive expulsion. The mixing of injectant vapor into inert pressurization gas and the dissolving of pressurizing gas into injectant liquid are minor problems for which allowance can be made (ref. 47).

If a solid-propellant gas generator is used instead of compressed inert gas as a source of pressurization gas, the system may be designed with the typical low factors of safety used in rocketry and also may be storable indefinitely in readiness condition. The production of gas during motor operation depends on the burning rate of the solid propellant and the burning surface at the moment. The generator propellant grain is shaped to provide a changing burning surface area that approximately matches the expected program of maximum demand for pressurization gas. Accordingly, the gas generator provides a continuous flow of gas throughout the motor operation sufficient to displace the largest expected liquid flow that may occur in each period of the motor operating time. Large vectoring usually is needed only in the early part of the motor operation. Gas-generator propellant grains are designed to produce large initial gas flows and relatively low flows later in the firing.

Since adequate gas flow must occur at all times whether gas is used or not, significantly more gas must be produced than is needed to displace the total stored liquid. When excess tank volume is provided to act as an accumulator, the total amount of gas required can be reduced because gas produced at times of low liquid flow demand will be retained for a limited time for use at times of large demand.

The surplus gas generated that exceeds the liquid-displacement needs and the accumulator capacity is diverted by a pressure relief valve and released overboard, preferably through small nozzles pointed aft so that thrust is recovered from the unneeded gas. A screen is located upstream of the pressure relief valve to prevent any particles of propellant or residue from entering the valve or the remainder of the system.

The TVC pressurization system typically is activated either by firing a squib valve at the compressed gas tank outlet or, if a gas generator is used, by igniting the gas-generator propellant. In either case the released pressure acts to break the tank outlet membrane seals (if the tank is so sealed) to fill the lines and injectors rapidly and then provide high momentum to the fluid jets discharged into the nozzle exhaust flow.

An LITVC system is not activated until about a second before motor ignition; however, if the system is activated but not launched, then the fluid and pressurization devices must be replenished before another launch can be attempted. An exception is the Titan III LITVC system, which is filled with the fluid and pressurized in the standby state and requires only electrical activation and the burning off of seals at the injector port opening (ref. 114).

2.2.2.4 LIQUID STORAGE EQUALIZATION

When the system has two or more tanks, it is sometimes necessary to keep the weight of liquid distributed evenly between the tanks to prevent the vehicle center of gravity from shifting excessively. A device such as an interlocked flow-drive positive-displacement pump is used to equalize the discharge from the tanks.

2.2.2.5 DISPOSAL OF SURPLUS INJECTANT

LITVC systems almost always use liquid at a rate lower than that provided for in the design. This difference occurs because enough liquid must be carried for the worst possible flight control situation. Actual flight thrust vectoring requirements vary from vehicle to vehicle according to the mission requirements. Some flights needing little vectoring would be penalized by having to carry the excess weight of the liquid and not benefiting from the added thrust resulting from liquid injection. To prevent this unneeded liquid from penalizing the vehicle performance as additional inert weight, provision is made to jettision this liquid and obtain thrust from it during its disposal. Flow meters are installed in the liquid lines to measure the amount of liquid used and an integrator sums the total amount of liquid used. Flight control repeatedly compares the total used with the programmed use and signals the injectors to expend the excess liquid uniformly around the nozzle so that the motor thrust will be augmented without thrust deflection. The vehicle is lightened by expenditure of the excess liquid and axial thrust is gained as the liquid leaves through the injectors and the rocket exhaust.

2.2.2.6 ADAPTATION OF THE MOTOR FOR LITVC

Important advantages of LITVC are that it requires only light protection from the hot exhaust jet and usually does not complicate the structural design of the motor or the gas dynamic design of the nozzle. The design effort required to adapt the motor for LITVC is simple and is limited to providing for (1) erosion in the nozzle around the injection ports, (2) shielding of LITVC system components from exhaust plume heating, and (3) possible structural reinforcement of the nozzle and motor aft end to accommodate the fixed loads of the LITVC system and the dynamic loads due to vectoring. The non-axisymmetric pressure in the nozzle due to injection must be provided for in the nozzle design. This pressure creates circumferential bending of the nozzle in a direction in which the nozzle typically has low stiffness. The exit cone diameter will increase in the direction of injection and decrease in the direction at right angles to injection. In large nozzles of lightweight construction, the exit-cone structure may have to be increased.

Provisions for erosion. — The injection ports are the holes in the nozzle liner through which the liquid jets are injected into the exhaust-gas flow. The injector orifices are safely recessed within the injection ports in the wall of the nozzle (figs. 29, 30, and 31). The interface

between the injector and the nozzle structure usually contains a gas-tight seal such as an O-ring.

The wall of the nozzle around and downstream of the injection ports erodes abnormally to produce a characteristic pattern of grooves and ridges (fig. 34). Typically, there are two deep grooves that begin on each side of an injector port and extend aft (sometimes spreading out in a V-pattern), a crescent of moderate erosion around the leading edge of the port, and a ridge of almost uneroded surface extending directly aft from the port. The chemical and gas dynamic effects that produce these effects have been studied by analysis and test (ref. 119).

The amount of erosion depends on the reactivity of the injectant and the type of ablative material. If a reactive injectant such as strontium perchlorate is used, the entire wall area over which the exhaust-gas/injectant mixture passes usually has greater than normal erosion; typically, this erosion will be twice normal or more. Low-cost materials were considered for the 260-in. (6.6 m) motor, but subscale tests showed that these materials would be severely eroded (ref. 119).

An inert injectant such as Freon will produce a cooling effect, and erosion will be less than if there were no injection from the hole at all. However, at the outer edge of the mixture region where the shock wave contacts the wall, the erosion is increased slightly over normal.

The edges of holes through which the injectant enters the nozzle can be subject to very severe erosion by the hot exhaust gas; this erosion usually is concentrated on the downstream edges of the holes. If erosion is allowed to degrade the geometry of the injection port and the adjacent nozzle wall, LITVC performance may be reduced (ref. 47). The holes usually are tapered conically and are just large enough to accommodate the liquid jet so that gas circulation and consequent heating in the hole will be minimized. Holes that are relatively small, having diameters less than about six times the boundary layer thickness, erode only moderately, because the supersonic gas stream tends to skip over the hole. However, large holes erode severely and are subject to a high rate of heat transfer on their downstream edge, because the high-velocity gas impinges against the downstream edge as if against an obstacle (refs. 134 and 135). This hole-size effect has provided a reason for using a large number of small orifices in addition to that of obtaining greater side-specific-impulse efficiency. The problem of erosion in the immediate region of the injection ports has been overcome by making the holes as small as possible, and by use of inserts of erosion-resistant material such as graphite/phenolic. This method was used in the A3 Polaris second-stage and Minuteman III third-stage motors. Data on erosion of nozzle liners due to LITVC are given in reference 119.

Thermal protection of LITVC system. — The LITVC system must be protected from heating by radiation and sometimes by gas circulation from the rocket jet plume. In some instances, this heating has been sufficiently great that liquid in unprotected tanks and tubing boiled,
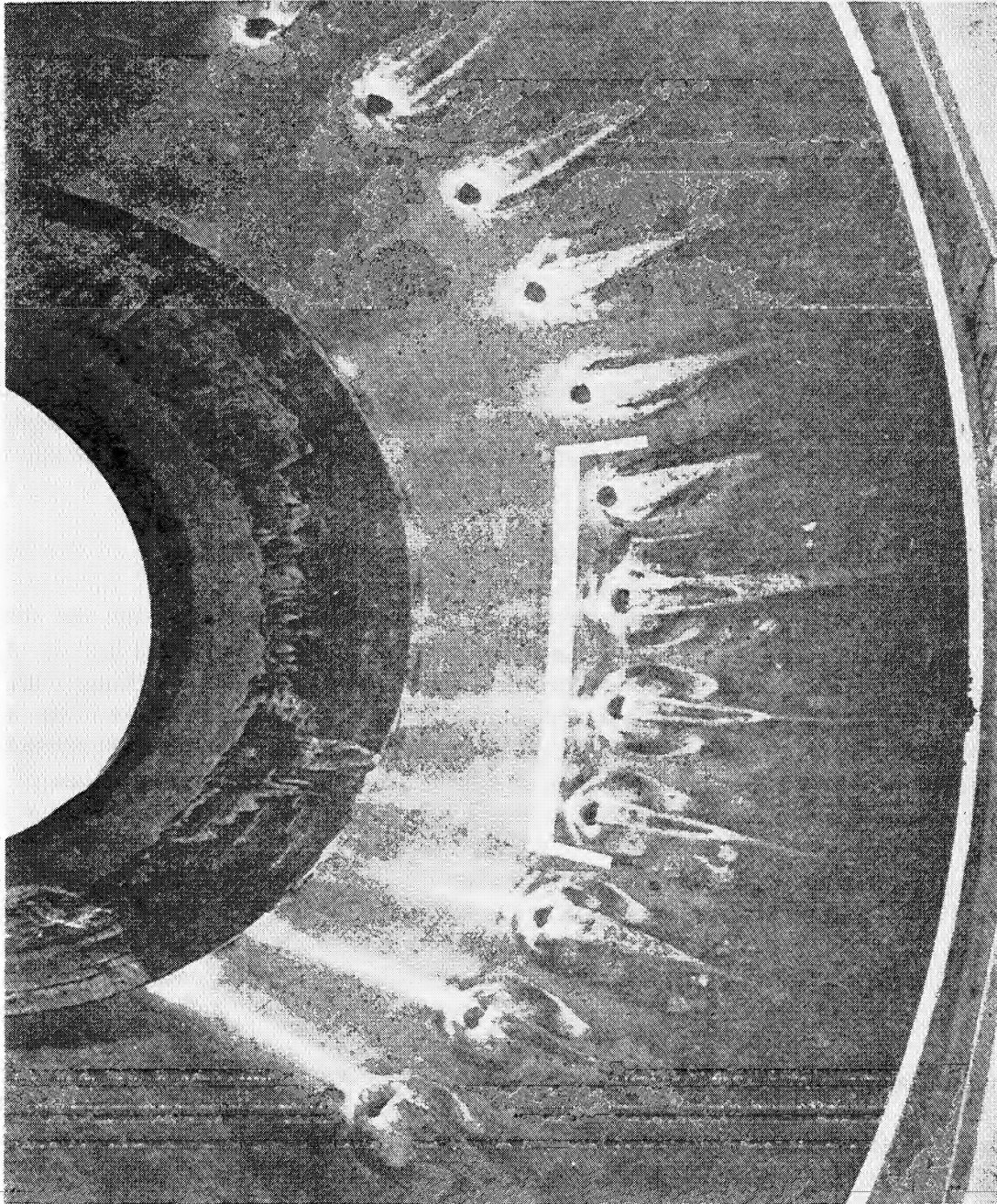
Figure 34. - Erosion around injector ports in the Titan III nozzle (ref. 119).

control circuitry burned and malfunctioned, and bracketry and pressure vessels failed. However, the problem is easily solved, since the heating is passive and accompanied by only weak or negligible gas flow. Adequate protection has been obtained by light insulation such as a thin layer of sheet cork or rubber. Sometimes a panel is installed between the exhaust plume and the LITVC components (fig. 28(b)).

Structural reinforcements. — The LITVC system is usually supported by brackets that transmit the load to the nozzle, the motor aft end, or both. Generally, it is advantageous to mount the entire LITVC system on the nozzle in order to avoid any problem of differential motion between the nozzle and the motor aft dome or skirt. Such movements have ranged from a fraction of an inch to several inches. When nozzle mounting is not possible, flexible lines or expansion joints are provided.

The dynamic loads caused by LITVC are the direct result of injection of liquid into the nozzle. The liquid jet produces a reaction thrust like a small rocket motor. This reaction amounts to a significant fraction of the total side force. It is withstood by the injector mounts to which the injectors are bolted and the adjacent nozzle structure. The emerging jet both blocks and mixes with the flow to produce a pattern of local loads on the nozzle wall (figs. 23, 24, and 25).

The character of this load can be best understood by considering the nature of the liquid injection effect in detail. Close to the hole, the jet acts like a solid object in blocking the main flow. A detached bow shock forms upstream of each jet and causes a large and abrupt increase in wall pressure upstream and along the sides of each injection port. Fluid dynamic shear breaks the drops of liquid into tiny droplets that rapidly evaporate and mix with the exhaust gas. This mass, thus added and mixed, increases the density and pressure in the local gas flow. If the liquid is chemically reactive, it adds thermal energy to the local portion of the main flow, which further increases its pressure. In either case, this portion of the exhaust flow that has been augmented by liquid injection expands and accelerates in a manner similar to, but more energetically than, the rest of the exhaust flow. It thus undergoes a greater change in local momentum than do normal (unaugmented) portions of the exhaust flow, and this change is transmitted to the nozzle wall as increased pressure. The increase of wall pressure due to addition of injectant mass and energy to the gas stream travels with the flow all the way to the nozzle exit, spreading out in a broad fan-shaped area (fig. 24).

The forces described combine to produce the total thrust vector control force caused by liquid injection. If the liquid is reactive, the total side force is 1½ to 3 times greater than that produced with an inert injectant. The increase is due to higher pressures resulting from reaction of the injectant with the gas. Comparative breakdowns of these effects are shown in table XIII.

A method that has been used for estimating these forces and their distribution on the nozzle wall is presented in reference 136. LITVC operation produces asymmetric pressure loads on

102

Table XIII. — Side Force Composition for Inert and Reactive Injectants (refs. 124 and 127)

Side force component	Percent of total side force	
	Inert liquid	Reactive liquid
Reaction thrust of the fluid jets	15 to 30	5 to 15
Pressure from shock waves	25 to 50	10 to 30
Pressure from addition of mass and energy to the exhaust flow	20 to 50	60 to 85

the nozzle equal to the vectoring side force. These loads usually are widely distributed and cause stresses that are not significant increases to the stresses due to symmetric gas flow. Other load conditions, including handling and assembly, ground level thrust, altitude thrust, vibration, and thermal loads, result in exit-cone designs that are more than adequate to withstand asymmetric LITVC loads. However, as mentioned previously, the asymmetric loads due to LITVC are usually the primary loads for large-expansion-ratio nozzles with thin-wall exit cones designed for minimum weight.

It is general practice to predict the heating, erosion, and load conditions by calculation. Pertinent test data are then used to check the accuracy of the calculated results, particularly those for erosion, and sometimes to evaluate the validity of empirical constants used in the calculations. The results of the analyses are used to modify the design, if necessary, to ensure operating integrity.

2.2.3 Performance Evaluation and Testing

Use of test data dominates all phases of LITVC performance analysis from the early conceptual design to full-scale operation, because the technology of the LITVC effect is still

basically empirical. Early in a development effort, data are obtained from the literature. These data are generalized by nondimensionalizing, cross-related by plotting, and then are transformed to the new operating conditions by use of relationships based on physical laws. This method results in some unavoidable errors. Later, subscale tests are conducted to provide data under conditions that are similar to those of the particular design problem. Finally, the full-scale rocket motor is tested with its LITVC system, and its vectoring capability is demonstrated. Operating-capability tests are routine procedures to ensure that the LITVC system operates as designed.

2.2.3.1 PERFORMANCE DATA FOR DESIGN

In the early stages of the development period when optimization and tradeoff studies are being made to determine the general configuration of the motor system, the only LITVC performance data usually available are those generated in previous LITVC development programs. Data from at least ten LITVC development efforts are available (refs. 46, 48, 50, 51, 107, 109, 121, 122, 124, through 127, 129, 133, and 137 through 142). These data usually are reduced to standard plots and correlations (sec. 2.2.3.2) for comparison with the particular motor being designed and for generating performance estimates for new systems.

The methods of plotting and correlating LITVC data generally involve converting the data and parameters to dimensionless ratios that eliminate factors of secondary importance for LITVC (e.g., the parameters of the main rocket motor). Thus, thrust vector capability is expressed as side-force specific impulse, the thrust vector deflection is the ratio F_s/F_a, and the injection rate becomes the ratio of injectant flowrate to nozzle exhaust flowrate. Similarly, the location of the injection port in the nozzle is expressed as the ratio of its distance from the throat to the distance from the throat to the exit (X/L). In the resulting plots (figs. 35 through 42), different sets of data appear as different curves and represent different basic efficiencies; the upper curve invariably indicates the more efficient injectant or condition.

The most popular and generally useful plot is that of side specific impulse versus the ratio of side force to axial force or deflection angle (figs. 35, 37, and 42). The data are presented in a form that is ready for use in estimating the fluid required and the maximum flowrates (sec. 2.2.1.5).

The next most common plot presents the ratio of side force to axial force (or deflection angle) versus the ratio of injectant flowrate to exhaust-gas flowrate (figs. 36 and 38). This plot is not as convenient for use by the designer of analyst, but has the redeeming feature that it reduces the scatter in data from motors that have varying chamber pressures and weight flowrates and, consequently, is useful for comparing data from diverse sources or conditions.
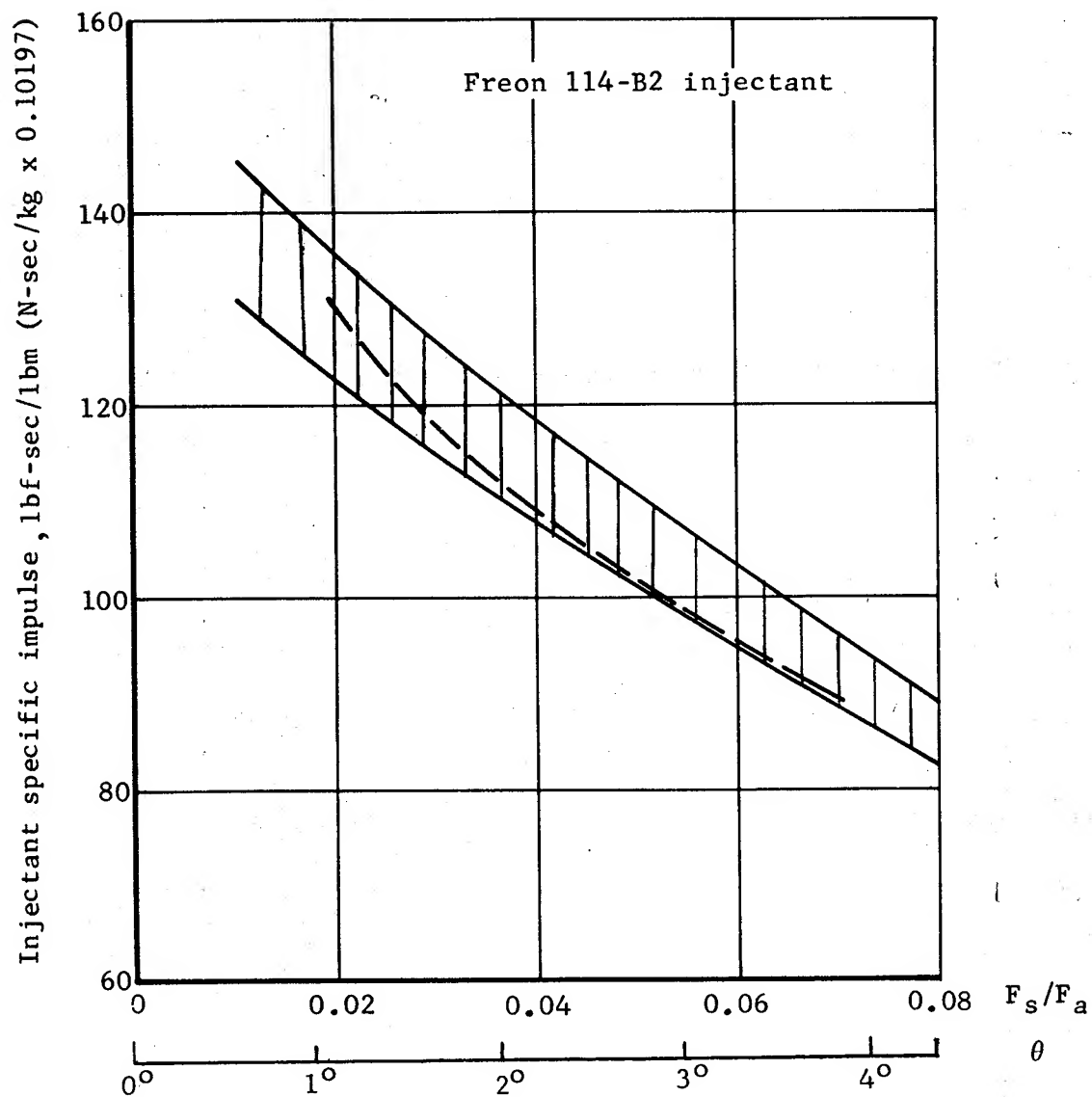
Figure 35. - Comparison of small-scale and full-scale data on injectant specific impulse vs deflection angle and side force (ref. 121).
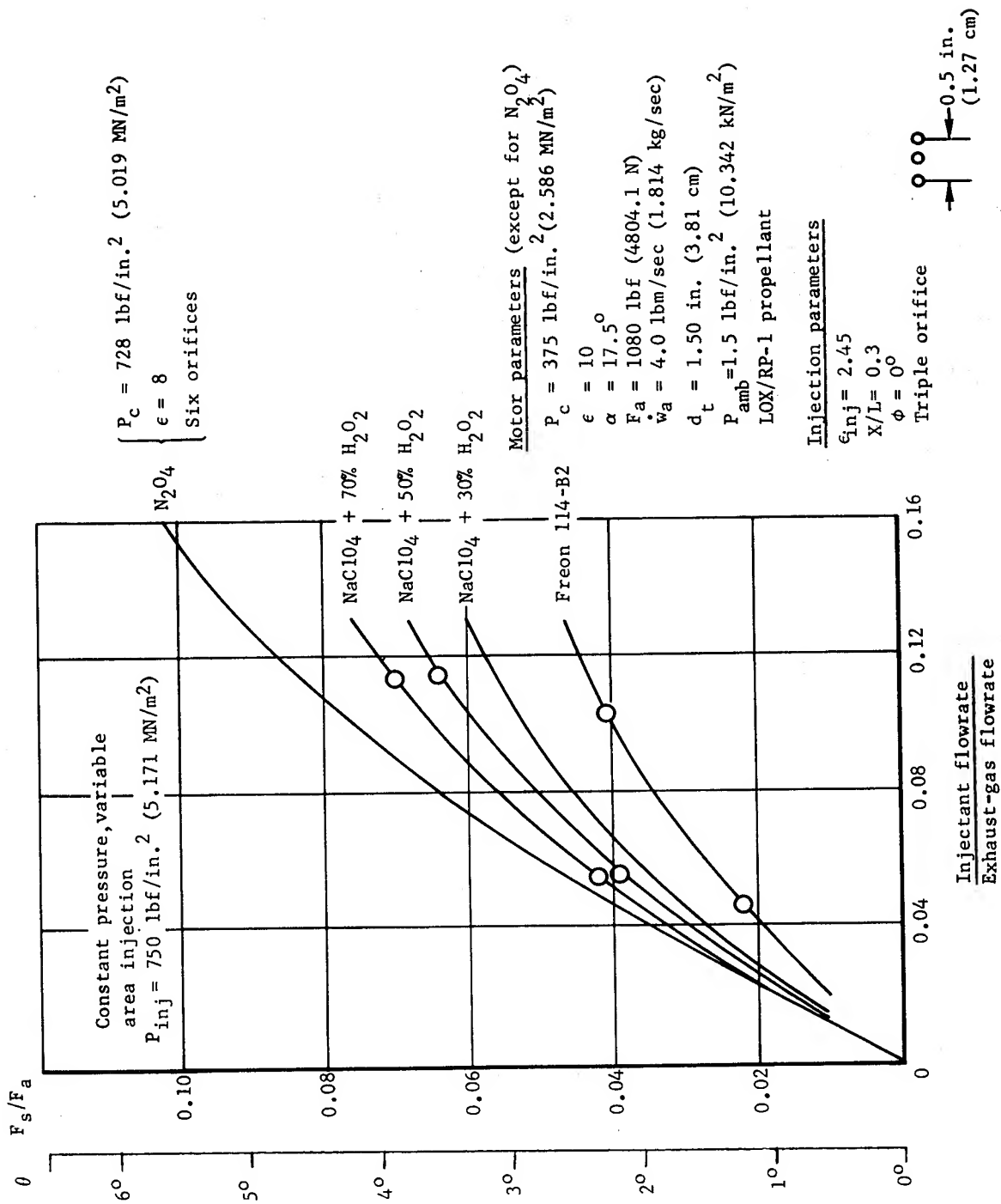
Figure 36. - Comparison of performance of inert and reactive injectants (data from refs. 121 and 142).
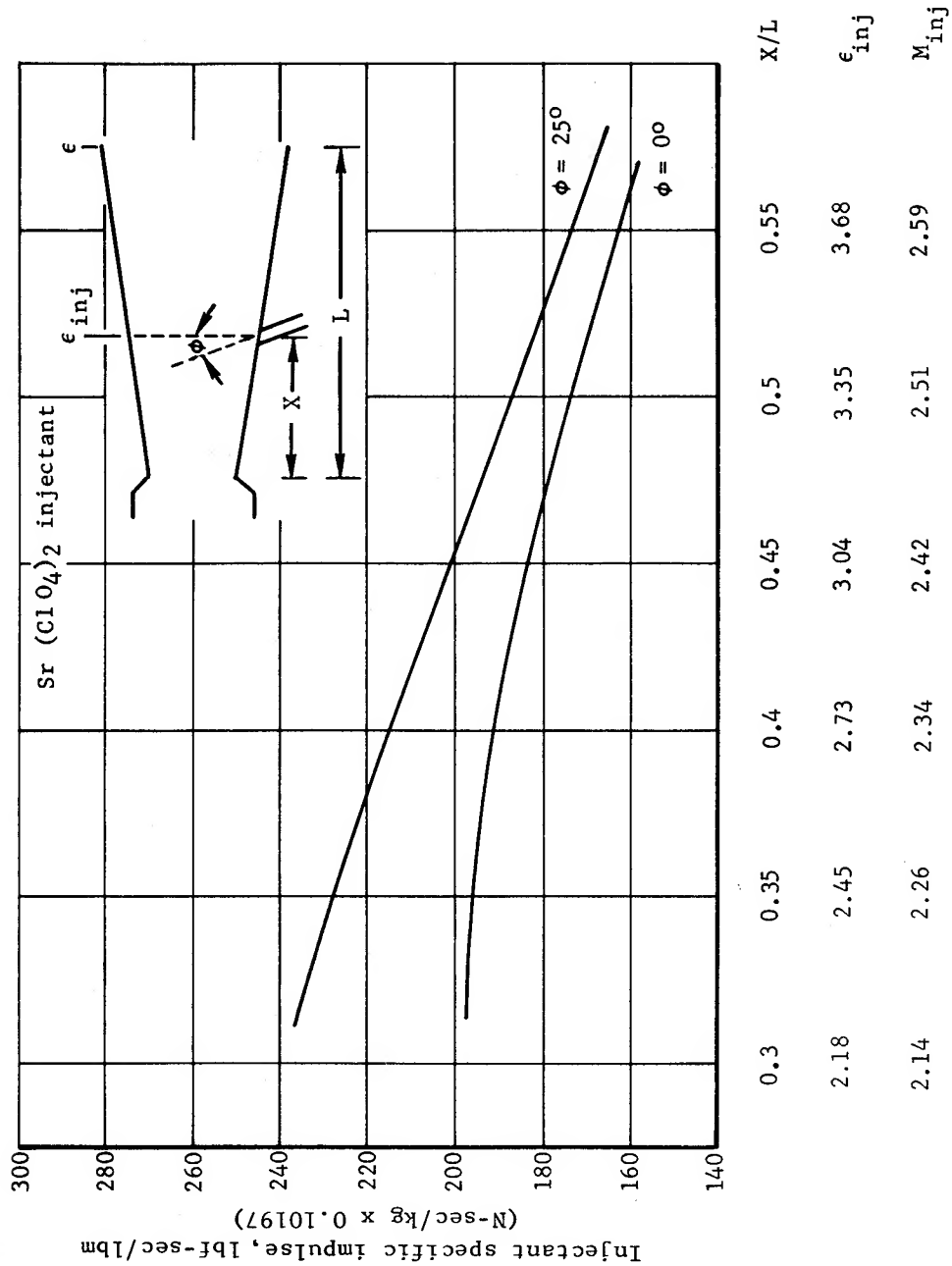
Data at a constant F_s/F_a value of 0.026, which corresponds to a jet deflection angle of 1.5°

Figure 37. - Effects of injection location and angle on injectant specific impulse (ref. 108).
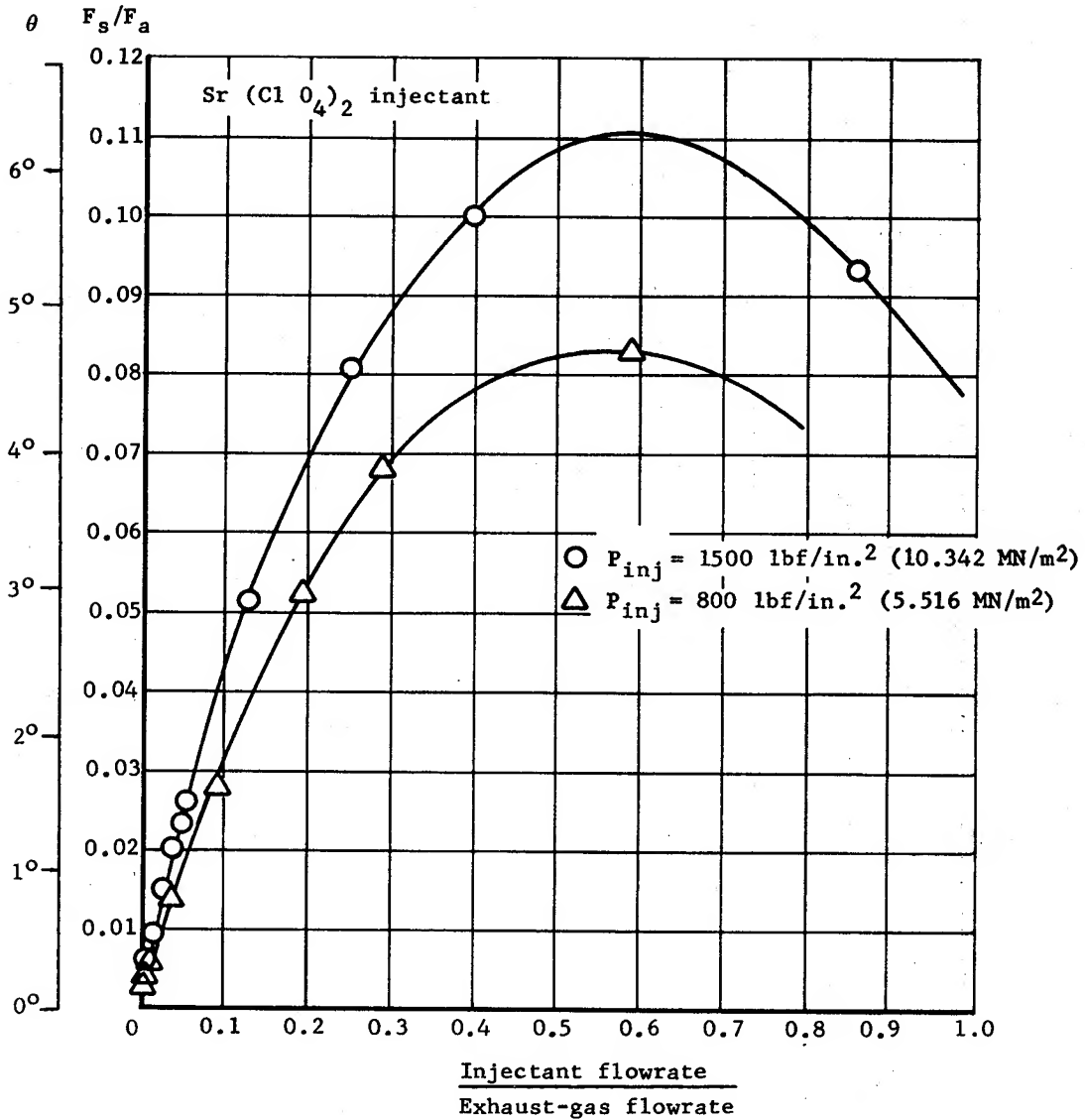
107

Figure 38. - Effect of injectant flowrate and injection pressure on side force (ref. 108).
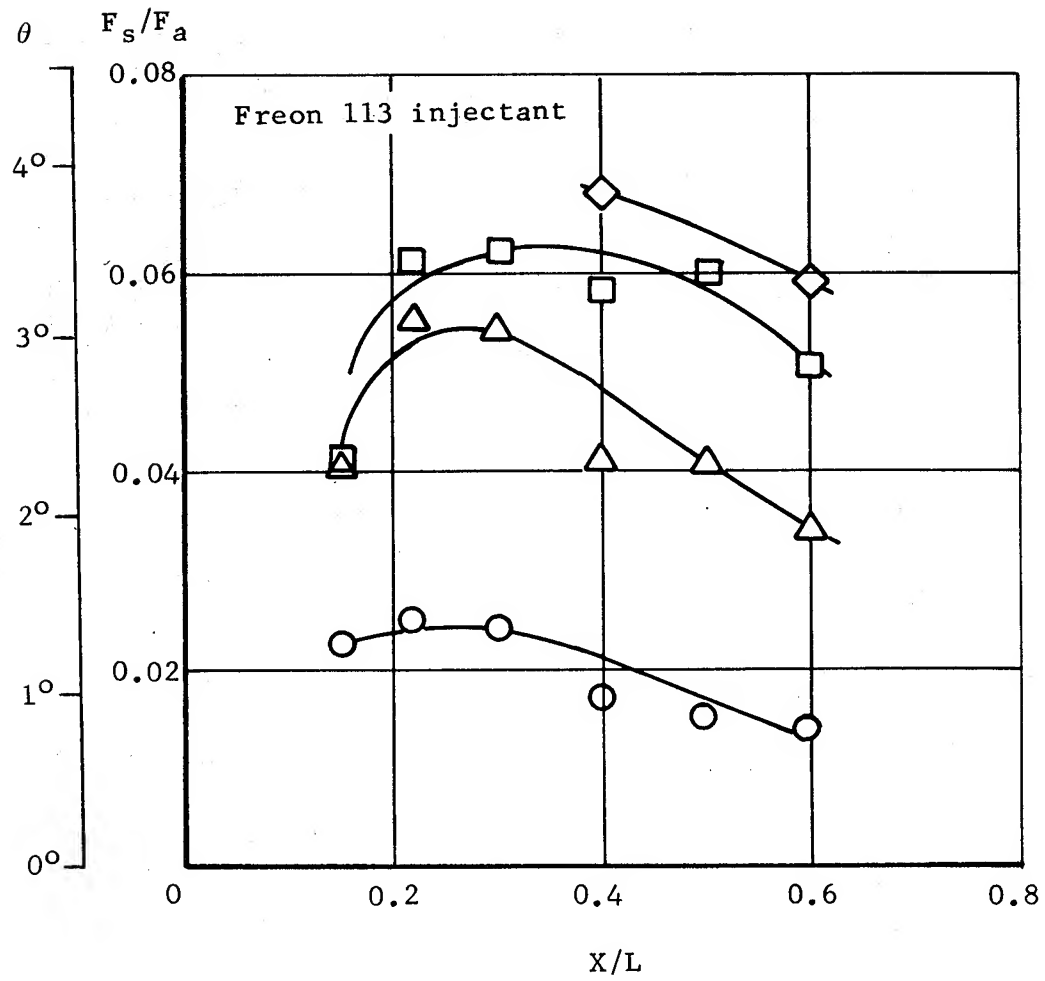
Figure 39. - Effect of injection location and orientation on side force for different injectant flowrates (adptd. from ref. 109).

Figure 40. - Transformation of data on injection pressure vs injectant specific impulse (adptd. from ref. 121).
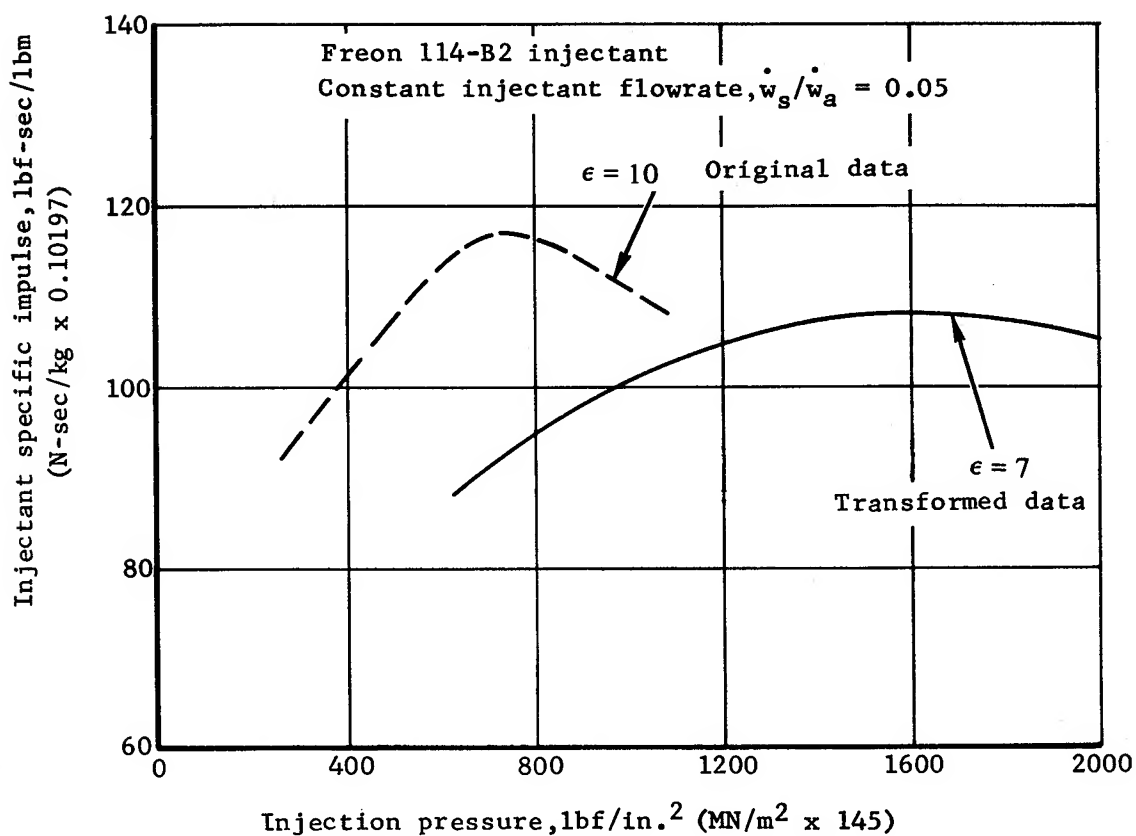
The ϵ = 10 data were used to calculate the values for ϵ = 7 by the relation

$$I_{sp(s)\ (\epsilon=7)} = \left(\frac{F_s}{F_a}\right)_{\epsilon=10} \times \left(F_a\right)_{\epsilon=7} \div \left[\left(\frac{\dot{w}_s}{\dot{w}_a}\right)_{\epsilon=10} \times \left(\dot{w}_a\right)_{\epsilon=7}\right]$$

The injection pressures were related by the expression

$$P_{inj\ (\epsilon=7)} = \left(P_{inj}/P_c\right)_{\epsilon=10} \times P_{c(\epsilon=7)}$$
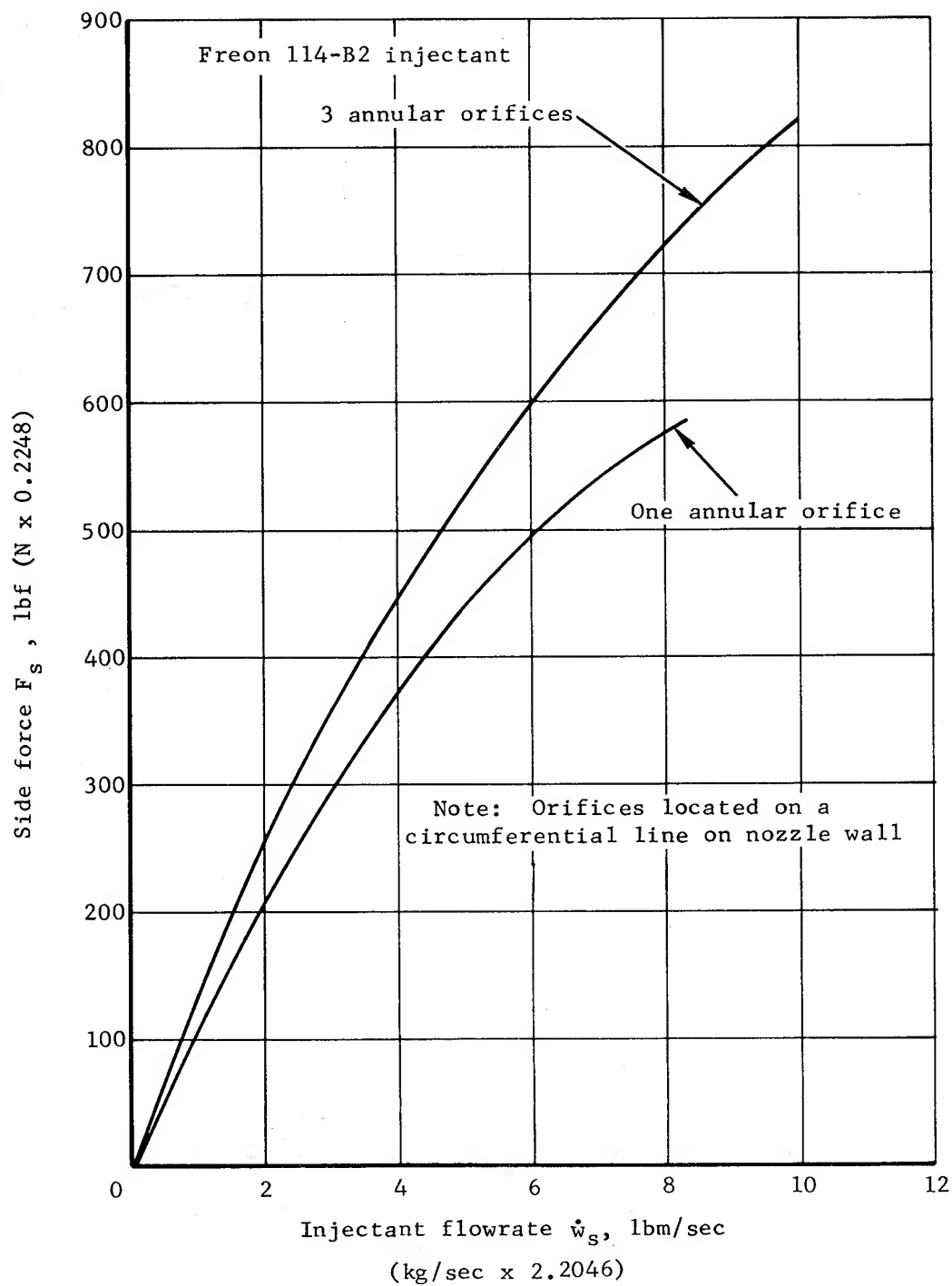
Figure 41. - Effect of number of annular orifices on side force as a function of injectant flowrate (ref. 124).
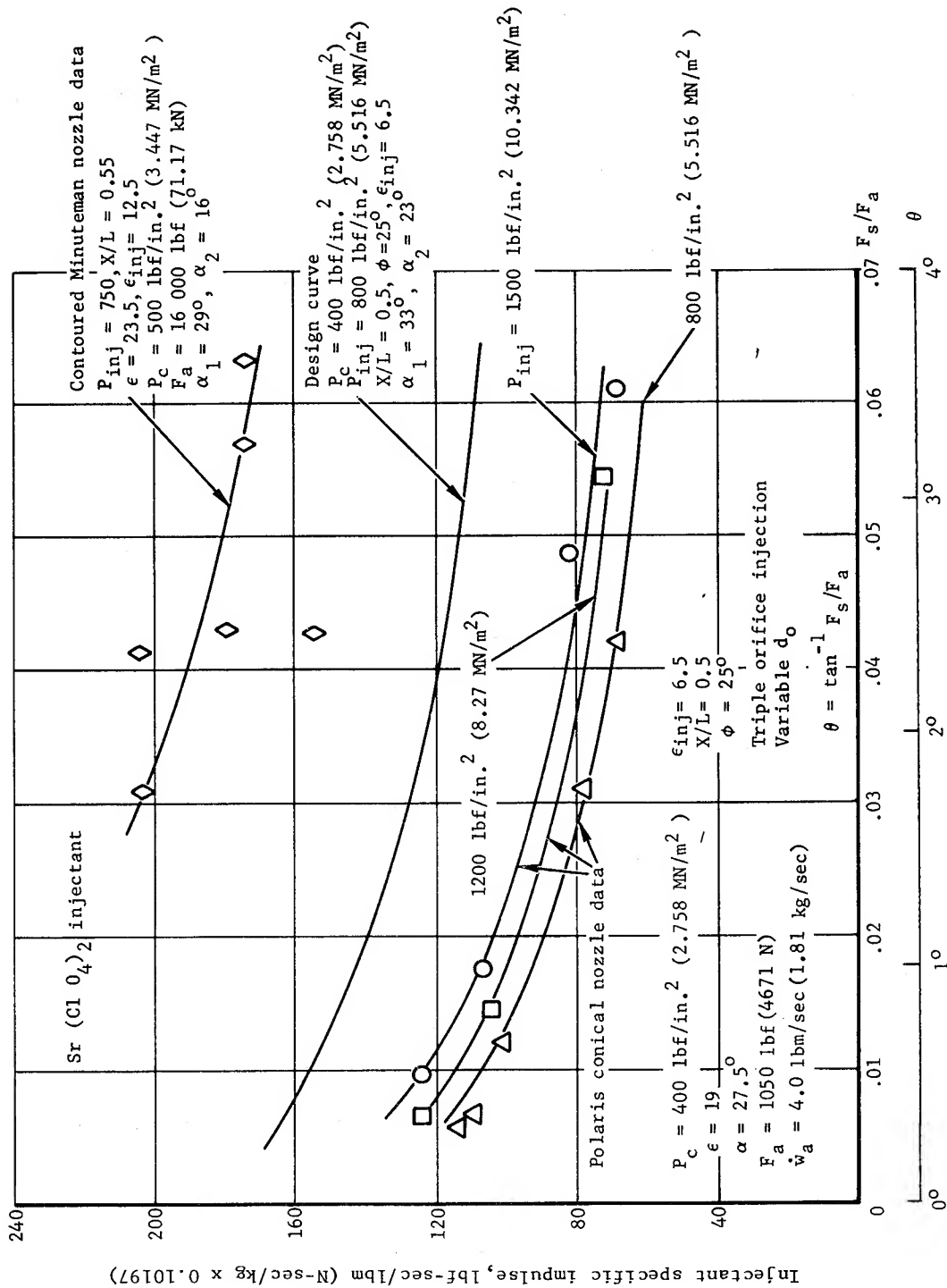
Figure 42. - Transformation of performance data for strontium perchlorate injectant (adptd. from ref. 108).

Other useful graphs are made to meet special design needs and generally show the effect of some LITVC design parameters on side specific impulse, force ratio, or thrust deflection (figs. 37 through 40).

The LITVC performance data accumulated from previous LITVC development programs represent motor configurations and operating conditions that are different from those of the motor and LITVC system being designed and, therefore, cannot be applied without modification. The data is transformed from the original test conditions to the new design conditions by applying one or more physical laws that appear to be dominant.

For inert liquids the momentum of the injected flow relative to the total nozzle gas flow has been shown to be the factor that could be used to predict the changes in side specific impulse due to changes in flowrate, pressure, or density (ref. 107). An example of the momentum principle used to transform data through a change in nozzle expansion ratio is shown in figure 40.

For reactive injectants, energy release is the dominant effect. Accordingly, the most successful data-transformation methods are based on the relative enthalpies and the fraction of the nozzle occupied by the energized flow (refs. 143 through 146). Figure 43 illustrates this method for transforming data collected for one reactive injectant. Side specific impulse is correlated with a parameter representing nozzle pressure and thermal energy and the residence time available for injectant mixing and reacting.

The effects of changes in nozzle geometry such as divergence angle, contour, and expansion ratio have been transformed by use of geometric, gas dynamic, and oblique shock wave relationships. Some of the changes in nozzle geometry and injection geometry and spacing can be transformed by simple geometric or vector summation methods (ref. 107).

For changes in injector location or nozzle length, the coefficient of thrust relationship, separated into portions that are in or out of the injection region, can be used. The injection effect can then be assumed to change in proportion to the fraction of the motor thrust that originates in the injection region. This approach tends to favor injection at upstream locations in the nozzle, making it necessary to include a calculation of the degrading effect on the side force of the shock wave caused by injection when the shock wave reaches the other side of the nozzle (refs. 107, 126, and 147).

A variety of computer programs for predicting the LITVC effect exist, but not one of them has adequately predicted the side force effect, because these programs are limited in the range of phenomena that they represent and the realism of their results. Some of the assumptions on which they are based are linearized supersonic flow with mass, bulk, or energy addition; displacement without mixing; boundary-layer separation and induced shock; droplet breakup, vaporization, and bulk formation; mixing, vaporization, and reaction with momentum interchange; and liquid breakup, mixing, vaporization, thermochemistry, and shock generation. Use of these computer programs has been inhibited

Figure 43. - Correlation of injectant specific impulse with key nozzle parameters (adptd. from ref. 122).

Plot axes:
- Y-axis: Injectant specific impulse, lbf-sec/lbm (N-sec/kg x 0.10197)
- X-axis: $\dfrac{(P_{s,inj}\, T_{s,inj}^{3}\, d)^{1/2}}{v_{inj}}$

$Sr(ClO_4)_2$ injectant
$P_{inj} = 1500$ lbf/in.^{2} (10.342 MN/m^2)
2° jet deflection angle
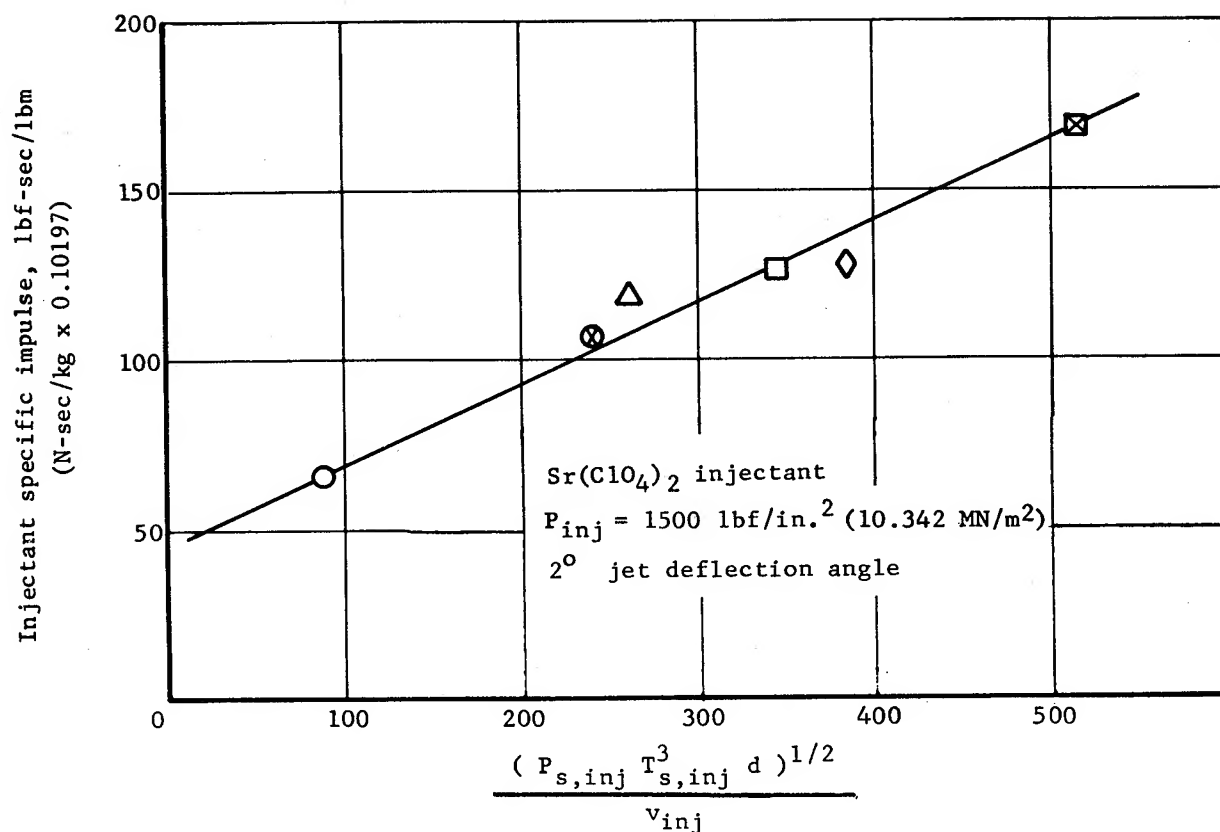
Nozzle parameters

Symbol	ϵ	ϵ_{inj}	M_{inj}	P_c lbf/in.^{2} (MN/m^2 x 145)	$P_{s,inj}$	$T_{s,inj}$ $^{\circ}R$ (K x 9/5)	d in. (m x 39.37)	v_{inj} ft/sec (m/sec x 3.281)
O	19	6.2	3.00	375	8.6	3010	2.66	8800
⊗	7	3.2	2.48	800	44.8	3550	1.83	7940
△	19	3.0	2.42	375	23.6	3620	3.74	7820
□	19	3.0	2.42	650	41.0	3620	3.74	7820
◇	19	3.0	2.42	800	50.4	3620	3.74	7820
⊠	7	2.1	2.12	800	85.5	3980	2.57	7200

Note: The correlation shown should be considered valid only within the range of the parameters listed in the above table.

by lack of correlation with test data. Therefore, the general practice has been to use empirical correlations for transforming data (ref. 51).

2.2.3.2 SMALL-SCALE TESTS

Early in the development period, the designer needs only approximate parametric information on which to define optimization studies and preliminary designs. Existing LITVC data are employed as far as possible, transformation-correlating methods being used to transform the data to the current design problem. The transformed data are approximate at best and contain errors that are in proportion to the differences between the motors from which the data came and the motor being designed. As the design proceeds, better data are needed; these data usually are obtained from tests of scale models of the motor nozzle with a variety of LITVC arrangements that are in the range of design interest. There is little scaling problem involved in translating small-scale model data to a full-scale counterpart. Figure 35 shows LITVC data obtained from small-scale tests compared with data from a full-scale motor.

A small-scale test series includes ranges of variation in the test conditions that will provide sufficient data for construction of the plots and correlations needed to establish the pertinent design parameters (sec. 2.2.3.1). Also, the small-scale motor is designed with features that represent its larger counterpart in propellant gas properties, nozzle geometry, injection geometry, and ambient pressures.

2.2.3.3 FULL-SCALE DEVELOPMENT TESTS

A full-scale test of a LITVC system is conducted at the first opportunity, usually the first static test of the full-scale rocket motor. In the full-scale tests, errors of data transformation and scaling are eliminated and possible LITVC design changes are detected and defined by high-confidence data at the earliest time. Static tests are usually conducted with the motor in the horizontal or vertical position. The orientation of the motor is considered in selecting the orientation of the LITVC tank and plumbing for the static test to allow for the change in direction of gravity force on the liquid.

2.2.3.4 OPERATING-CAPABILITY TESTS

The operating capability of the parts and components of the LITVC system are regularly determined at various stages of manufacture, assembly, storage, and launch preparation. The tank and bladder, tubing, fittings, flow meters, and check valves have been shown to be relatively insensitive to malfunction after they have been tested to demonstrate specified quality and operability.

115

The most critical components are the injector valves and the pressurization system because they are sensitive to malfunction. Surveillance tests to monitor the operating capability of these components have been developed (ref. 46). The injectors are evaluated in bench tests with an inert liquid (e.g., Freon) that evaporates and leaves the components clean. While this evaluation is not fully representative of actual conditions, it is sufficient because it provides an effective functional test of the components without degrading them. If a reactive or nonevaporating injectant is used in bench testing, thorough cleaning after testing is necessary. After assembly and installation of the injector valves and pressurization system on the motor, these components are tested by actuating the injector valves and checking the response through the electric feedback loop. These tests are repeated when desired during storage or launch readiness.

When a gas generator is used to pressurize the injectant, the igniter squib is checked at low voltage for continuity and resistance. If a tank of inert gas at high pressure is used, the gas pressure is monitored by pressure gages. The squib valve at the outlet of the inert-gas tank is checked for electrical continuity and resistance.

A complete check of injector valves sometimes is conducted while the system is on the rocket motor; this check is accomplished by connecting an auxiliary supply of pressurized liquid into the LITVC system, actuating the injectors, and noting the response. The liquid used is inert and evaporative to avoid contaminating the system.

By the means discussed above, it is possible to check the function of all critical LITVC components after the system has been installed and charged with injectant and gas but without activating it or disturbing its launch readiness.

3. DESIGN CRITERIA and Recommended Practices

3.1 FLEXIBLE JOINT

3.1.1 Configuration

3.1.1.1 DESIGN OPTIMIZATION

The flexible joint design shall be based on the movable-nozzle envelope constraints and joint, motor, vehicle, and mission design parameters that result in either maximum performance or maximum cost effectiveness, the choice depending on specific needs and characteristics of the program.

The basic motor and vehicle joint design parameters (motor pressure, vector angle, actuation rate, actuation acceleration, flight inertia loads, envelope constraints, mass properties, environmental conditions) should form the basis for the initial joint design. Whenever possible, the joint design parameters should be provided as explicit design points to the joint designer. Otherwise, these interdependent design points must be established on the basis of optimization analyses. The following procedure is recommended for establishing the optimum joint design (i.e., the least expensive joint that satisfies all mission objectives without violating any imposed restraints):

(1) Calculate the required nozzle vector angle that will produce a side force at some reference position consistent with the vehicle performance requirements.

(2) Prepare a preliminary layout drawing of a motor approximately the size anticipated for use in the vehicle. This motor is designed to a particular set of parameters: motor pressure, joint actuation torque, pivot-point location, and cone angle. The drawing for this motor should call for state-of-the-art materials, embody the design philosophy expected for the operational system, and be structurally adequate for all loading conditons. Calculate motor performance, joint performance, and weights for this motor design. This motor is the baseline design against which other designs will be compared to select an optimum design.

(3) Vary the independent design parameters — motor pressure, joint actuation torque, pivot point, and cone angle — and determine their influence on joint design, nozzle design, motor performance, and cost if considered. Continue to perform tradeoff and optimization analyses to obtain the near-optimum values of the independent parameters for use in the final design.

Since no parametric weight-scaling equations are available for flexible joints, the basic joint design should be varied geometrically for pivot position, joint diameter, and cone angle; and the effect of these parameters on weight at different motor pressures and spring torques should be calculated. Conduct structural analyses, using the empirical relationships of section 2.1.5 to establish joint component thicknesses. Layout drawings of the nozzle and joints should be prepared and compared with envelope constraints to establish limits for joint geometry as a function of pressure and spring torque. The joint weights as a function of motor pressure, spring torque, and geometric limits should be included in motor and vehicle optimization computer programs.

(4) Make new layout drawings based on the near-optimum values of the operating parameters and check to ensure that computer-predicted weights, lengths and volumes, and performances are valid. To ensure the validity of the design, perform necessary calculations external to the generalized computer program; e.g., structural analysis (sec. 2.1.5), detailed weight calculations, and grain design.

Steps 3 and 4 should be repeated as necessary. The joint design characteristics resulting from this procedure must be consistent with the required motor characteristics and with near-optimum system performance when all stages are considered.

The dependent design parameters considered in sections 3.1.2.3 and 3.1.2.4, the independent design parameters considered in section 3.1.2.5, the material properties (sec. 3.1.3), and other important parameters including internal pressure, axial load on the joint, flight loads, and loads resulting from the particular motor or vehicle configuration (sec. 3.1.4) should be included in the optimization analysis to the extent required by the particular application.

Specific recommended practices for component cost analysis cannot be made because of the many complexities involved. Cost-estimating techniques presented in reference 148 (ch. X) should be used as a guide. The general recommendation for cost analysis is to establish the joint design and then to continue to improve the design with cost effectiveness as the criterion. The mission performance of the vehicle should be maintained constant for each design alternative evaluated. The analysis must include the cost of all motor components redesigned as required to maintain constant vehicle performance.

3.1.1.2 ENVELOPE LIMITATIONS

The values for the inner and outer joint angles β_1 and β_2 shall ensure that the joint can operate as required.

It is recommended that the flexible joint be designed so that angle β_1 is not less than 40° nor greater than 45°, and angle β_2 is not less than 45° nor greater than 55°. (All successful

joints to date have operated between these limits, but joints with larger values for β_1 and β_2 may be possible). To reduce spring torque, the difference $(\beta_2 - \beta_1)$ should be a minimum consistent with the allowable stresses in the elastomer and reinforcements and any axial compression requirements.

3.1.2 Design Requirements

3.1.2.1 ACTUATION TORQUE

The total actuation torque — consisting of joint spring torque, frictional torque, offset torque, inertial and gravitational torques, and aerodynamic torques — shall be less than the torque available from the actuator.

The total actuation torque is the summation of all the contributing torques, each of which is dependent on the specific design of both nozzle and motor. It is recommended that each contributing torque, including the variability of the torque constituents, be calculated for the full range of motor service life. The service life consists of (1) vectoring for checkout at zero motor pressure and (2) vectoring over the entire range of motor operating pressures. Use the maximum actuation torques (nominal plus maximum variability) thus obtained to determine total required actuation torque, and compare this value with the capability of the actuation system. A valid statistical analysis is not possible at this point of design, since the necessary statistical data will not be available until a joint is designed, built, and tested.

3.1.2.1.1 Joint Spring Torque

The joint spring torque shall be the minimum required to fulfill motor operating requirements.

The joint spring torque should be calculated by the methods of section 2.1.2.1.1; use material properties obtained in a subscale test program (sec. 3.1.7.1). To establish the range of probable variability in spring torque, calculate the joint spring stiffness at zero motor pressure for the maximum and minimum elastomer shear modulus. This range should be assumed to exist at all motor operating pressures.

The spring torque at the maximum value of shear modulus is used in the design of the actuator. The spring torque at the minimum value of shear modulus affects design of the control system. If the joint is to be vectored to different angles during motor operation, take advantage of the reduction in spring torque due to motor pressure to reduce the actuation power requirements. Calculations using the average elastomer shear modulus must be made of the joint spring torque during motor firing. The expected variability calculated at zero motor pressure must be superimposed on the average values to establish the

119

maximum and minimum spring torques. It is desirable that the minimum spring torque be sufficiently large to prevent a negative joint spring stiffness due to pressure. If a joint designed to be vectored at pressure is to be vectored at zero pressure during motor preflight checkout, the vector angle at checkout must not result in a joint spring torque greater than that occurring during motor operation.

3.1.2.1.2 Friction Torque

The joint shall demonstrate coulomb and viscous friction consistent with the stability of the flight control system.

Neither the coulomb friction nor the viscous friction can be estimated for preliminary design. Both frictions should be measured during a static firing. It is recommended that a time of relatively constant motor pressure be selected and that the nozzle be actuated at three or four different rates. The wave form should be sinusoidal and run for at least 1½ cycles at each rate to avoid the force transients that occur at the start and stop points. Plot actuator force variation with either vector angle or actuator stroke for one cycle at each actuation rate, and determine the average actuator force at zero-degrees vector angle (fig. 14(a)). The test data should be smoothed and the actual instantaneous actuation rate at zero-degrees vector angle determined either by calculation or by use of a plot of vector angle variation with time. The variation of actuator force at zero vector angle with actuation rate should be plotted; record the zero intercept as the coulomb friction and the slope as viscous friction (fig. 14(b)).

3.1.2.1.3 Offset Torque

The flexible-joint and movable-nozzle offset torque shall be a minimum value consistent with reasonable manufacturing practice and cost.

A value for offset torque cannot be calculated unless air cold-flow tests are conducted to determine pressure distributions around the movable nozzle. For joints up to 22 in. (55.88 cm), the offset torque is small compared with the joint spring torque, and it is recommended that it be ignored in estimating actuation torque. For larger joints, an assessment should be made of the offset torque, pivot-point movement (sec. 2.1.2.3) being considered and worst-on-worst tolerances being assumed. The offset torque should also be measured during the bench test program. It is recommended that the offset torque be kept at a minimum by maintaining minimum tolerances consistent with design practice, cost requirements, and motor requirements.

3.1.2.1.4 Inertial Torque

The actuator torque shall provide for the maximum torque due to the inertia of the moving nozzle.

The inertial torque should be estimated from the mass of the movable nozzle assumed to be rotating about the geometric pivot point. It is recommended that half of the weight of the flexible joint be included with the movable section in calculating movable nozzle weight, center of gravity, and dynamic moment of inertia. It is recommended that the maximum inertial torque be included in the actuation torque.

3.1.2.1.5 Gravitational Torque

The actuator torque shall provide for the maximum torque due to vehicle accelerations.

Calculate the axial and lateral accelerations at the nozzle center of gravity that result from vehicle pitch and yaw. The torques acting at the geometric pivot point due to these accelerations should be calculated in the same manner as for inertial torque. It is recommended that the maximum gravitational torque be included in the actuation torque.

3.1.2.1.6 Insulating-Boot Torque

The insulating-boot torque shall be a minimum consistent with the insulating requirements and available motor envelope.

The insulating boot must be fabricated such that it has a minimum stiffness (product of modulus of elasticity and thickness) and yet is thick enough to satisfy insulation requirements. If a material such as silica-filled butadiene acrylonitrile rubber is used, the insulating boot must be the bellows type, whereas if a silicone rubber such as DC 1255 is used, a wrap-around insulating boot (fig. 7) will result in low boot torques. However, it is recommended that even with this material a bellows-type boot be used when the envelope allows.

It is difficult to estimate the insulating-boot torque. For joints up to 30 in. (76.2 cm) in diameter, with a bellows fabricated of silica-filled butadiene acrylonitrile rubber, it is recommended that the insulating-boot torque be assumed to be 35 percent of the joint spring torque. With the same insulating-boot material for joints approximately 90 in. (2.29 m) in diameter, it is recommended that the insulating-boot torque be assumed to be 15 percent of the joint spring torque. For designs using low modulus silicone rubber, it is recommended that the insulating-boot torque be assumed to be 25 percent of the joint spring torque.

3.1.2.1.7 Internal Aerodynamic Torque

Actuator torque shall include the effects of internal aerodynamic torque.

The aerodynamic torque must be estimated as a function of vector angle, motor pressure, and propellant grain/nozzle configuration for the maximum expected vector angles during

121

motor operation. The torque should be determined from a knowledge of the pressure distribution along the nozzle surfaces, using the methods outlined in section 2.1.2.1.2 (i.e., air cold-flow tests or two-dimensional method of characteristics).

When a joint has a forward pivot point, the total aerodynamic torque must be added to the actuation torque, so that the actuator can be sized properly. When a joint has an aft pivot point, the aerodynamic torque should be ignored.

3.1.2.1.8 External Aerodynamic Torque

The external aerodynamic torque shall not cause a negative actuation torque during flight.

For all motors in which the nozzle is not shrouded by a motor case skirt, the external aerodynamic torque in the high dynamic pressure region that occurs during flight must be estimated. This torque should be determined from a knowledge of the pressure distribution along the nozzle external surfaces and should be calculated in the same manner as the internal aerodynamic torque. The total aerodynamic torque stiffness in the high dynamic pressure region must be less than the joint spring stiffness to ensure positive actuation.

3.1.2.2 NOZZLE VECTOR ANGLE AND PIVOT POINT

The vector angle shall be large enough to cause sufficient side force for vehicle steering.

The vector angle required for steering either must be given in the motor requirements or calculated from a trajectory analysis that considers pitching requirements and worst-case winds. A method for calculating the required vector angle is given in reference 149.

If the vector angle is given in the motor requirements, the control-force moment arm (normal distance from the line of action of the motor thrust for a vectored nozzle to the vehicle center of gravity) or the required steering moment must be stated as a requirement. It is assumed that the side force causing a steering moment acts through the effective pivot point, and the effective pivot point should be calculated; from this location, the geometric pivot point should be determined. The geometric pivot point should be as far aft as possible consistent with optimum vehicle performance. However, envelope restrictions on actuators and exit cone movement must be considered. It is recommended that a forward pivot point be used for nozzles with little or no submergence, and an aft pivot point be used for submerged nozzles because the exit cone movement requires less envelope.

3.1.2.3 AXIAL DEFLECTION

Clearances between the movable and fixed nozzle components shall allow for the effects of axial deflection.

Joint axial deflection is the compressive response of the flexible joint that occurs when the motor is pressurized. The clearances between the movable and fixed nozzle components must be sized to allow for this movement as well as for rotational movement of the nozzle. The required clearances should be studied through the use of two layouts overlaid to show the nozzle as it deflects axially and in the vectored position.

The axial deflection should be calculated with a finite-element analysis (sec. 2.1.2.3) that considers the geometric changes of the joint during loading in at least four increments of loading. As soon as possible in the program, a joint should be bench tested to measure the axial-deflection characteristics and obtain the axial compressive spring stiffness. The axial spring stiffness must be known for the design of the guidance control system.

3.1.2.3.1 Nozzle Misalignment

The nozzle shall have a vectoring misalignment at zero pressure that results in alignment at a selected motor pressure.

The nozzle must be assembled in the motor at some vector angle such that the vectoring caused by motor pressure and fixed length actuators will result in alignment at a selected motor pressure. It is recommended that the pressure at which alignment occurs be the average pressure during which nozzle vectoring occurs.

Efforts should be made during the joint design to estimate the amount of misalignment that occurs in a nozzle, since the orientation of the actuator to the nozzle could result in excessive misalignment angles. A recommended procedure for estimating misalignment is as follows:

(1) Estimate the axial compression of the joint (sec. 2.1.2.3) and the approximate effective pivot point (sec. 2.1.2.3.1) during motor pressurization.

(2) Estimate the joint spring torque stiffness (sec. 2.1.2.1.1) during motor pressurization.

(3) Assuming that the nozzle is aligned at zero pressure, determine graphically the nozzle vectoring misalignment as the motor is pressurized to maximum expected operating pressure.

(4) Assume that the nozzle misalignment required at zero motor pressure is the same as the misalignment that occurs at the selected zero-misalignment pressure, and calculate the actuator null length.

The actuator null length must be checked during the static firing test program. The recommended procedure to determine the actuator null length is as follows:

(1) Estimate the effective pivot point at the motor pressure at which the nozzle and motor center lines are to be aligned (sec. 2.1.2.3).

(2) Align the nozzle to the motor at the pressure from item (1), and calculate the vector angle and actuator length at zero motor pressure, considering that the pivot point moves from the effective pivot to the geometric pivot point.

(3) Prior to the firing, actuate the nozzle in the motor and determine the vector angle per inch of actuator stroke.

(4) For the static firing, set the actuator length as determined in item (2) and measure the vector angle change of the nozzle at various motor pressures during the firing, the pressures being selected to give as wide a range as possible with the actuators held at the trial length from item (2) for at least one half-second.

(5) Compare the pre-firing and firing data to calculate the amount of zero-pressure misalignment.

3.1.2.4 FREQUENCY RESPONSE

The nozzle shall not be subject to excitation at its natural frequency of vibration.

The stiffnesses of all parts of the nozzle should be designed so that their natural frequencies are higher than the natural frequency of the hydraulic actuator system. If the nozzle natural frequency is almost equal to the natural frequency of the actuator system, coupling of the nozzle and the actuator system will occur and will produce instability. If the nozzle natural frequency is less than the natural frequency of the actuator, coupling with the guidance system will occur. Further, the nozzle natural frequency must be greater than the natural mechanical frequencies of the motor and vehicle to ensure that no coupling that could cause destructive failure of the nozzle results.

The natural frequency of the nozzle and motor assembly should be measured prior to static firing. The assembly should be subjected to a frequency range determined from consideration of the control system response, but if this is not known, it is recommended that a frequency range from 2 to 100 Hz be tested. If the motor is too large for practical frequency response tests, the natural frequency must be calculated. When the natural frequency is known, a notch filter should be incorporated into the control system to suppress vectoring commands at or near the natural frequency.

3.1.2.5 ENVIRONMENTAL PROTECTION

3.1.2.5.1 Thermal Protection

Thermal protection of the joint shall enable it to remain at or below allowable temperature limits for the full duration of the firing.

Protect the joint with an insulating boot or with sacrificial ablative protectors (fig. 7). The insulation material must be sufficiently thick to withstand the erosion by the flow of the hot motor gases and maintain the joint at allowable temperature. An insulating boot must be sufficiently thin to minimize the additional torque component due to the boot. If the motor envelope allows space, it is recommended that a radiation shield (fig. 7(a)) be used to shade the insulation boot from the hot motor gas. This practice allows use of thinner, more pliant boot materials that reduce the boot torque. Provide a clearance gap between the radiation shield and the fixed nozzle component to allow for joint axial deflection and vectoring. For the radiation shield to be effective, the gap must be located in a stagnant region in order to minimize circumferential flow of the motor gas as the joint is vectored.

The gap between sacrificial thermal protectors (fig. 7(b)) must be sufficient to prevent contact of adjacent protectors as a result of vectoring or motor pressure; otherwise, additional torque is generated. It is recommended that the joint protectors be located in a stagnant region in order to reduce the size of the protectors and to minimize circumferential flow of the motor gas as the joint is vectored.

3.1.2.5.2 Aging Protection

The joint elastomeric material shall not be subject to adverse effects of aging and oxidation during pre-fabrication and post-fabrication storage.

Polymerization of uncured elastomer should be minimized by storing the elastomer under conditions that maintain the elastomer within specifications. These conditions must be determined early in a program by the following steps: (1) Fabricate and test quadruple-lap shear specimens (sec. 2.1.7.1) from new elastomer stock to establish initial elastomer properties. (2) Store uncured elastomer at different conditions for the time period it is anticipated the elastomer will be stored during the program. (3) Fabricate and test quadruple-lap shear specimens from the stored elastomer stock to establish the change in elastomer properties. (4) Select storage conditions to be included in the elastomer processing specifications.

To minimize changes in joint performance, select elastomeric materials for which long-term aging data are available. To protect the joint against changes in the elastomer properties at surfaces exposed to ozone or oxygen, it is recommended that the joint be covered by an impervious coating such as chlorobutyl rubber or Hypalon.

125

3.1.2.6 PRESSURE SEALING

The joint shall not leak when subjected to either a pressure load or a combined pressure and vectoring load.

It is recommended that reliable joint sealing be accomplished by experimenting with the joint molding process until unbonded areas are at a minimum and then establishing controls to ensure that this process is continued on all subsequent manufacture. An inspection should be performed to determine unbonded areas. For joints fabricated by secondary bonding of the elastomer, inspect the elastomeric pads before joint molding and the bonds after joint molding by C-scan ultrasonic techniques (ref. 22). Joints fabricated by compression molding and injection molding can be inspected only by cutting apart a joint and inspecting the elastomer surface. It is recommended that joints fabricated by molding processes be inspected on a sampling basis to ensure that the molding process has not changed.

Quantitative criteria for the debonded area have not been established. It is recommended that the photographs presented in figures 44 and 45 be used as a guide. Figure 44(a) shows an acceptable joint, figure 44(b) shows a marginally acceptable joint, and figure 45 shows two examples of unacceptable joints.

3.1.3 Material Selection

3.1.3.1 ELASTOMERS

The elastomeric material shall possess at least the minimum mechanical properties needed for structural loading at the critical motor pressure, vector angle, actuation rate, and joint temperature, as imposed by design factors of safety.

The important mechanical properties to consider in the selection of the elastomeric material are secant shear modulus at 50 psi (0.345 MN/m^2), shear strength, and bonding to the metal reinforcements — all measured in a quadruple-lap shear specimen tested at the appropriate shear strain rate and operating temperature (sec. 2.1.7.1). The effect of compression on the shear properties should be determined if joint instability due to motor pressure is a potential problem (ref. 78 and sec. 2.1.2.1.1). The materials should be selected on the basis that the minimum values for these mechanical properties at the critical motor pressure, vector angle, actuation rate, and joint temperature are not less than those required to withstand the maximum joint loading as evaluated by appropriate structural analyses (sec. 2.1.5).

The specific material mechanical properties should be established from pre-existing test data on the selected elastomer material, or these properties should be established from specimen
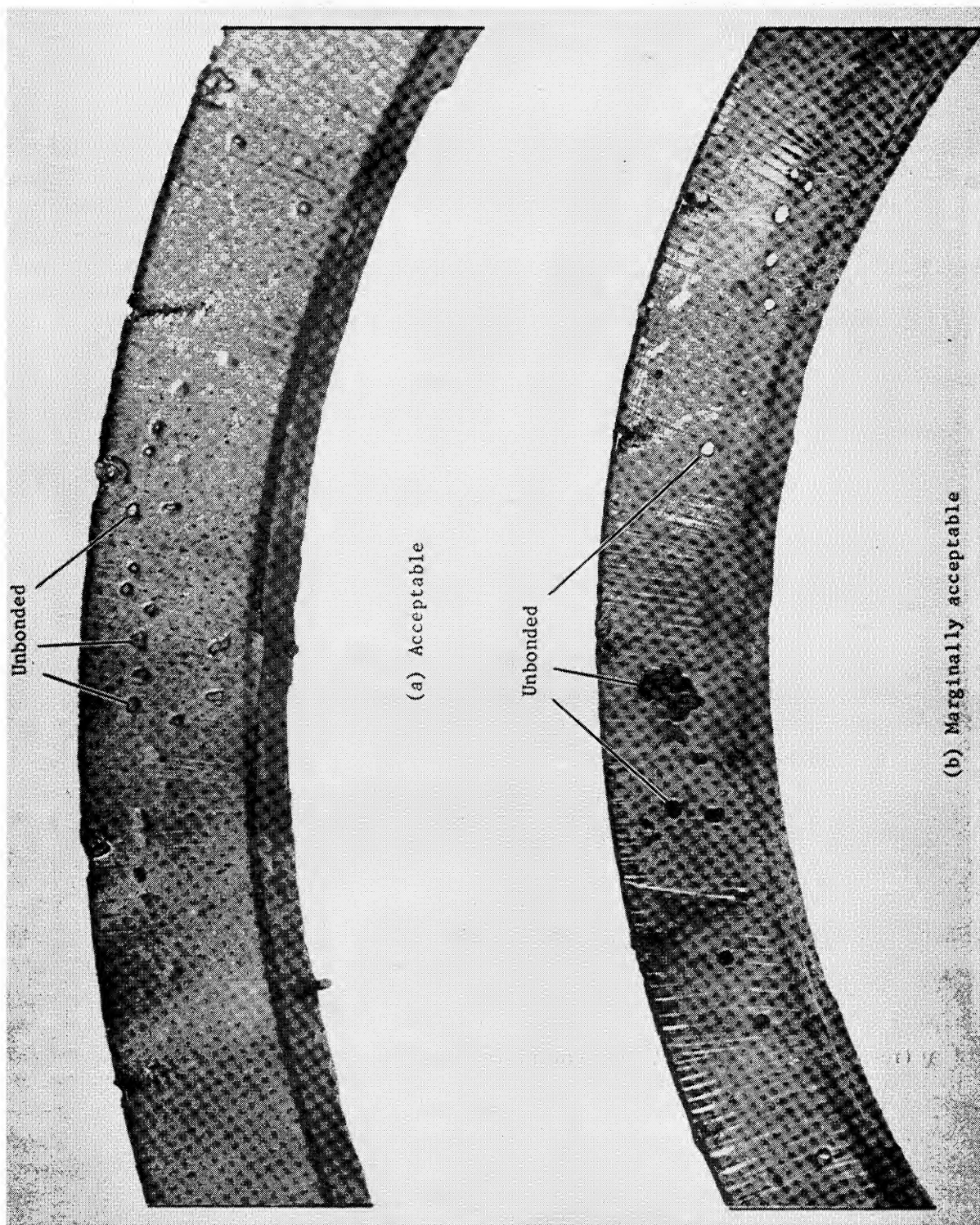
Figure 44. - Two examples of acceptable unbonded elastomer conditions.

127
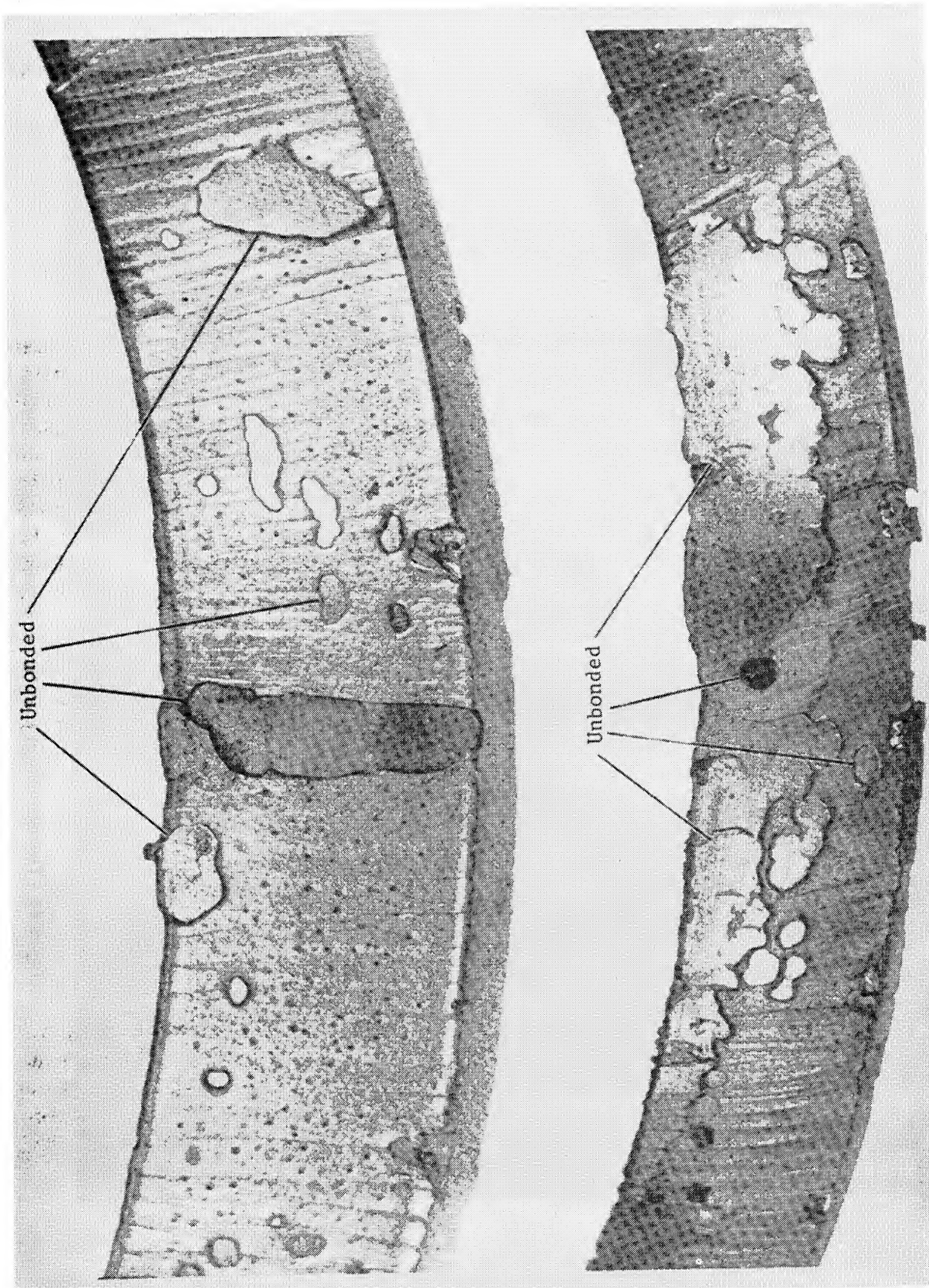
Figure 45. - Two examples of unacceptable unbonded elastomer conditions.

tests (sec. 2.1.7.1). Materials that have been used in successful joint programs are given in section 2.1.3.1.

3.1.3.2 REINFORCEMENTS

The reinforcement material shall possess at least the minimum mechanical properties needed for structural loading at the critical motor pressure and vector angle, as imposed by design factors of safety.

The important mechanical properties to consider in the reinforcement material to be used are the modulus of elasticity, the compressive yield strength, the ultimate tensile strength, and, for composite reinforcments, the interlaminar shear strength. For joints with metal reinforcements, the required buckling stress of the reinforcement can be calculated (sec. 2.1.5.2) from the modulus of elasticity and joint dimensions. For joints with composite reinforcements, the allowable compressive stress should be assumed to be 60 000 psi (414 MN/m²). The true allowable compressive stress for the laminate used must be determined from bench testing a joint to failure (sec. 2.1.4.1). The materials should be selected on the basis that the minimum values for the mechanical properties at the critical motor pressure and vector angle are not less than those required to withstand the maximum joint loading as evaluated by appropriate structural analyses (sec. 2.1.5).

The specific material mechanical properties should be established from existing data that are representative of the selected material, or these properties should be established by evaluation of specimen tests. Steel or composite materials are recommended as reinforcements. Aluminum alloys should also be considered for reinforcements but only if composite reinforcements are impractical.

3.1.3.3 ADHESIVE BOND SYSTEM

The adhesive bond system shall possess at least the minimum mechanical properties needed for structural loading at the critical motor pressure and vector angle, as imposed by design factors of safety.

To ensure that the adhesive bond system is stronger than the elastomer material, all failures in a specimen test program (sec. 2.1.7.1) must be cohesive. The processing of the specimen must be as nearly identical to that of the joint as possible. To maintain the quality of the adhesive bond system, controls on the system materials must be established. Systems recommended for use with injection-molded joints, compression-molded joints, and secondary-bonded joints are described in section 2.1.3.3.

3.1.3.4 JOINT THERMAL PROTECTION

The joint thermal-protection materials shall possess at least the minimum thermal properties needed to maintain joint temperatures at or below allowable limits.

The important thermal properties for the joint thermal-protection materials are low thermal diffusivity, high heat of ablation at strain levels anticipated in service, and mechanical flexibility with minimum char fracture at temperatures expected in service. Materials that have been used in previous programs are recommended; these are presented in section 2.1.3.4.

3.1.4 Mechanical Design

3.1.4.1 GENERAL CONSIDERATIONS

The flexible joint shall possess the combination of weight and structural strength that contributes most to optimum motor and vehicle performance.

The flexible joint should be designed to have the required structural capability while subjected to the critical design loads of motor pressure and vectoring and the effects of accompanying environmental conditions. Analytical verification of the joint structural integrity should be made; the recommended practices for structural analysis are given in section 3.1.5.

If axial compressive deflection is a requirement that cannot be met by a joint sufficient for structural strength, the thickness of the elastomer layers should be reduced, the result being an increased number of elastomer layers. The number of reinforcements will be increased, and these should be designed for structural capability according to practices recommended in section 3.1.5.2. Compliance with the axial compressive deflection requirement must be demonstrated by test.

Because the joint has little axial stiffness in tension, the design must incorporate limiters on the amount of tensile axial deflection that can occur as a result of ground handling. The limiters must also ensure that the nozzle cannot over-vector the joint during horizontal storage or transportation.

The joint design should be established to obtain positive margins of safety (sec. 2.1.4.1.1) as close to zero as possible. However, since the joint design is interdependent with design of the guidance control system and optimum motor performance, it is possible that less-than-optimum joint design will result in optimum motor design.

3.1.4.2 DESIGN FACTOR OF SAFETY

The joint shall have at least the minimum factor of safety required to obtain the specified joint reliability.

A design factor of safety should be used in the design of flexible joints to account for contingencies (e.g., approximation in estimation of joint stresses, undetected variations in material properties, and undetected manufacturing deviations). The factor of safety could be established from a statistical study of all variables contributing to joint performance correlated to the required reliability (ref. 150). Unfortunately, there is insufficient understanding of how these variables affect joint performance, and a single factor of safety is recommended. Usually design factors of safety are specified in a design for specific classes of loading conditions (i.e., operational or handling); these factors of safety have been developed through a history of successful designs and a knowledge and understanding of the variables involved. Since in the design of flexible joints this history is not available, it is recommended that a greater factor of safety be applied to the joint design than is applied to the overall motor design. For example, if the overall motor design factor of safety is 1.25, then a factor of 1.5 should be applied to the joint. The factor should be applied to the motor pressure and to the vector angle. It must not be applied redundantly to the parameters that define the joint structural capability (e.g., material mechanical properties, elastomer ring thickness, and joint geometric tolerances).

The joint reliability cannot be demonstrated explicitly because of the prohibitive number of tests and joints involved. It is recommended that the reliability be demonstrated by the convergence of the curves for upper and lower reliability levels. The upper reliability level is based upon the number of failures allowed during the development and production programs and must be greater than the required reliability; the lower reliability level is based upon the calculated reliability from test results during the development and production programs. After each test, the reliability from all test results is plotted and extrapolated to show the probability of achieving the required reliability. A test program to establish the upper and lower reliability levels should be set up before development program is begun.

3.1.4.3 FLEXIBLE-JOINT LOADS

The joint stress profile shall include all individual design loads or the worst combination of design loads.

All design loads (sec. 2.1.4.1) should be used to determine the critical design stresses. The critical joint loading condition, or worst critical combination loading, should be defined by summation of a load/time history of the joint. This profile should be prepared by tabulating all design loads, temperature exposure, and vectoring conditions encountered. The critical-loading condition for each structural element of the joint should be used in the joint

structural analysis (sec. 3.1.5) to determine that margins of safety for the joint are not less than zero.

3.1.5 Structural Analysis

The joint design stresses shall not exceed the allowable stresses.

The theories necessary to analyze a flexible joint have not been formulated. The joint should be analyzed with the use of empirical relationships (refs. 17 and 79) to obtain preliminary dimensions and reanalyzed with nonlinear finite-element methods (refs. 80, 81, and 82).

The following factors should be included in the requirements for the structural analysis:

- Loads used should be design loads (i.e., limit loads times appropriate factor of safety).

- Combined loading should be analyzed to determine the resultant stresses.

- The maximum permissible shear stress in the elastomer should be limited to the minimum 3-standard-deviation values of the failure shear stress measured from a quadruple-lap shear specimen (sec. 2.1.7.1) at the appropriate temperature and shear strain rate.

- The maximum permissible tensile stresses in metal reinforcements should be limited to the 0.2 percent yield stress at limit loads and to the ultimate stress at ultimate loads.

- The maximum permissible compressive stress in metal reinforcements at ultimate loads should be the lesser of the 0.2 percent yield stress and the buckling stress.

- The maximum permissible stresses in composite reinforcements should initially be assumed to be 60 000 psi (414 MN/m^2) and must subsequently be determined for the reinforcement laminate in bench tests to failure.

3.1.5.1 ELASTOMER THICKNESS

The elastomer thickness shall not be greater than the thickness that provides adequate shear strength.

The shear stress in the elastomer due to combined motor pressure and vectoring must be calculated at ultimate conditions. The empirical method and procedure given in section

132

2.1.5.1 are recommended. When calculating the shear stress due to vectoring, allow for the reduction in joint spring torque due to motor pressure (sec. 2.1.2.1.1).

Although the allowable shear stress at failure is increased when compression is superimposed, ignore this increase when establishing allowable shear stresses.

3.1.5.2 REINFORCEMENT THICKNESS

The reinforcement thickness shall be the minimum thickness that provides adequate compressive hoop and buckling strength.

The compressive stress on the inner surface of the reinforcement due to combined motor pressure and vectoring must be calculated at ultimate conditions. The empirical method and procedure given in section 2.1.5.2 are recommended. When calculating the compressive stress due to vectoring, allow for the reduction in joint spring torque due to motor pressure (sec. 2.1.2.1.1).

The allowable compressive stress at ultimate loads for metal reinforcements should be the lesser of the 0.2 percent compressive stress and the buckling stress calculated as shown in section 2.1.5.2. The allowable compressive stress for composite reinforcements must be determined from bench tests of joints to failure.

If a joint is to be used a number of times, the tensile stresses are important. The allowable tensile stresses must be based on the fatigue and fracture mechanics properties of the reinforcement material.

3.1.5.3 ADVANCED ANALYSIS

The design analyzed by empirical methods shall be confirmed by nonlinear finite-element methods.

The finite-element method of analysis must involve a sufficiently refined grid of nodes and panels to provide an accurate description of the internal stress distribution. It is recommended that each elastomer be divided into a minimum of four layers across the thickness, each reinforcement be divided into a minimum of three layers across the thickness, and both elastomer and reinforcements be divided into a minimum of 12 radial layers. It is recommended that the analysis include various nonlinear effects and that the methods outlined in section 2.1.5.3 be used.

The calculated stresses for combined motor pressure and vectoring should be compared with the allowable stresses as described in sections 3.1.5.1 and 3.1.5.2. The applied stresses in this comparison should be the average calculated stress at the centroid of each panel.

3.1.6 Manufacture

The joint fabrication process shall be the most cost effective for the particular joint and program needs.

An engineering study of fabrication processes should be accomplished to select the fabrication processes that afford the best compromise between fabrication schedule and costs. The engineering study should include detailed tradeoff evaluations of fabrication methods; past experience with and reliability of the various processes; status of the program: research, development, or production; effect of the processing on schedules; and fabrication, tooling, and facility costs versus the joint configuration.

The behavior of the material when it is exposed to various fabrication processes should be included as a tradeoff parameter when alternative structural materials are evaluated.

3.1.6.1 REINFORCEMENTS

The reinforcement fabrication processes shall be those most suitable for the particular joint needs.

Metal reinforcements are either thin or thick, the difference having an influence on the possible method of fabrication. Thin reinforcements are defined as reinforcements that can be fabricated by hydroforming or spinning (sec. 2.1.6.1) and will be used in joints with a limiting axial compression requirement (sec. 2.1.4.1). Hydroformed reinforcements are recommended for research or small development programs. Spun reinforcements are recommended for production programs. For both types, the forming should be made with the material in a normalized condition, and the material should be heat treated to the required properties prior to final machining.

Thick reinforcements should be machined from plates for research or small development programs. The plate should be normalized for rough machining and heat treated to the required properties prior to final machining. For production programs, thick reinforcements should be stamped to the required shape with the material in the normalized condition, and then heat treated to the required properties prior to final machining.

Heat treatment will cause some distortion of the reinforcements. This distortion should be considered in the assembly of a joint by inspecting the reinforcements for high and low spots and then assembling the reinforcements so that all the high spots are aligned and the elastomer thickness will be circumferentially uniform.

Although composite reinforcements have been fabricated by winding and molding, lay-up and molding, and molding with a mixture of chopped fiber and resin, it is recommended for

all production programs that composite reinforcements be fabricated by laying resin impregnated cloth cut into specific patterns into a matched metal mold and curing under pressure at a temperature and time suitable for the resin. However, in research or development programs, consideration should be given to compression molding with a compound of chopped fiber and resin. The sacrificial ablative protector (sec. 2.1.3.4) should be fabricated as an integral part of the reinforcement.

3.1.6.2 JOINT ADHESIVE SYSTEM

The joint adhesive system shall not fail before the elastomer material.

The joint adhesive system must be evaluated prior to joint fabrication by use of quadruple-lap shear specimens (sec. 2.1.7.1); an acceptable system must fail cohesively. The specimens must duplicate the thickness and cure condition of the elastomer and bond system in the joint. Fabricated joints should be bench tested at least to ultimate pressure and vectoring conditions to demonstrate the structural capability of the adhesive bond system.

Failures can occur when the bond system is either too thick or too thin. To control the thickness, the viscosity of the primer and the adhesive, the rate at which these materials are sprayed on the reinforcements, and the time for spraying should be monitored; limits on these items should be included in the joint fabrication specification.

Each lot of adhesive system materials should be tested prior to use in a joint by peel tests and quadruple-lap shear tests to ensure quality and to maintain a record of lot-to-lot variation.

3.1.6.3 FLEXIBLE JOINT

The joint fabrication process shall be consistent with the needs and characteristics of the particular joint.

The molding process selected must depend primarily upon the dimensions of the joint, the number of elastomer layers, and the thickness of the elastomer layers and reinforcements rather than on the scope of the joint program. Joints with thin elastomer layers (layers that cannot be fabricated by injection molding) should be fabricated by compression molding in order to improve the bond to the reinforcements. Compression molding has been successful on joints up to 60 in. (1.52 m) in diameter with thick and thin reinforcements, and this method is recommended for research and development programs as well as for production programs. Injection molding is a proven production technique and should be evaluated as a molding method. Secondary bonding is a proven process and should be evaluated as a

molding method, particularly for large joints where significant cost savings have been indicated.

Prior to molding by the injection or compression processes, the effect of the molding process on elastomer thickness and porosity should be evaluated (sec. 2.1.6.3). After molding, the first development joints should be cut open to show the joint cross section. This practice allows examination of the elastomer layer thicknesses, and if molding has been done by the injection process, determination of the effectiveness of the elastomer injection.

Advantages and disadvantages of the joint fabrication processes are listed in table VIII.

3.1.7 Testing

3.1.7.1 SUBSCALE TEST PROGRAM

The subscale specimen test program shall provide values for the elastomer mechanical properties used in design.

The important mechanical properties for the elastomer are the shear modulus, shear stress at failure, and the strength of the bond between the elastomer and the reinforcement material. QLS specimens should be tested at the strain rate and over the temperature range expected in the joint. The bond between the elastomer and reinforcement should be cohesive, and the QLS specimen should be used to develop a satisfactory adhesive and bonding system.

Joints have been designed and tested successfully without including the effects of superimposed compression and shear. However, if a joint is to be designed to operate at pressure to take advantage of the reduction in spring torque due to pressure, the change in shear modulus due to pressure must be measured. The reduced shear modulus is used to predict spring torque and the motor pressure at which the spring torque is unstable (sec. 2.1.2.1.1). A method that has been used to measure the changed shear modulus is given in reference 78.

If aging data are not available, a subscale test program to evaluate aging characteristics must be initiated as soon as possible in the motor program. This program should evaluate the aging characteristics of (1) several lots of the cured elastomer to enable prediction of service life and (2) several lots of the uncured elastomer in order to define uncured elastomer storage life. For the cured elastomer, the recommended test intervals are monthly up to six months and annually thereafter. For the uncured elastomer, the recommended test intervals are weekly until the shelf life has been established.

A subscale test program should be used to evaluate lot-to-lot variation of elastomer material and to establish acceptance criteria.

136

3.1.7.2 BENCH TEST PROGRAM

Bench tests of joint characteristics shall establish acceptance criteria for production joints and shall verify that the effective pivot point is compatible with the nozzle clearance envelope.

A joint bench test program must be set up during the motor development program to establish axial deflection characteristics, vectoring characteristics, and joint pressure sealing. The test for compressive axial deflection should be conducted in a test fixture with an unloading piston (fig. 21) so that the joint is subjected to the motor pressure and associated axial load. The vectoring test should be conducted in a test fixture that allows the joint to rotate freely about its effective pivot point while oriented as it would be in the motor. Prior to conducting the vectoring tests, a pressure test should be conducted in the same fixture to measure the actuator force and hence the offset torque necessary to maintain the joint in a null position. The vectoring tests should be conducted with and without the joint thermal protection to determine the effect of the protection on actuation torque. In addition to axial deflection, vector angle, and actuator force, the hoop strain on the inner surface of each reinforcement should be measured. To ensure that only reliable joints are used in a motor, a stringent tensile-pressure leak test (sec. 2.1.7.2) is recommended; this test should be conducted after the axial compression and vectoring tests.

The same tests should be conducted during the motor production program as acceptance criteria for the joints. If a joint fails an acceptance test in the elastomer, the elastomer should be removed, and the reinforcements used again.

It is necessary that the position of the effective pivot be determined for each joint. A test should be made at zero pressure, average motor operating pressure, and maximum expected operating pressure. The recommended procedure to find the effective pivot point is as follows:

(1) Mount a cross-hair-shaped target on a part of the test arrangement that is rigidly connected to the movable end ring and is near the theoretical pivot point. The axial target leg is to be aligned coincident with the center line of the fixed joint end ring.

(2) Pressurize the test arrangement and actuate the joint to an angle at least as large as the nozzle vectoring requirement. Illuminate the cross-hair target with a strobe light, and open the camera shutter for one complete actuation cycle.

(3) Interpret the photograph as indicated in the sketch in figure 46 to find the pivot point.

It is recommended that acceptable limits on pivot-point location be based on the clearances between fixed and movable nozzle components, rather than on clearances tailored to fit the

137
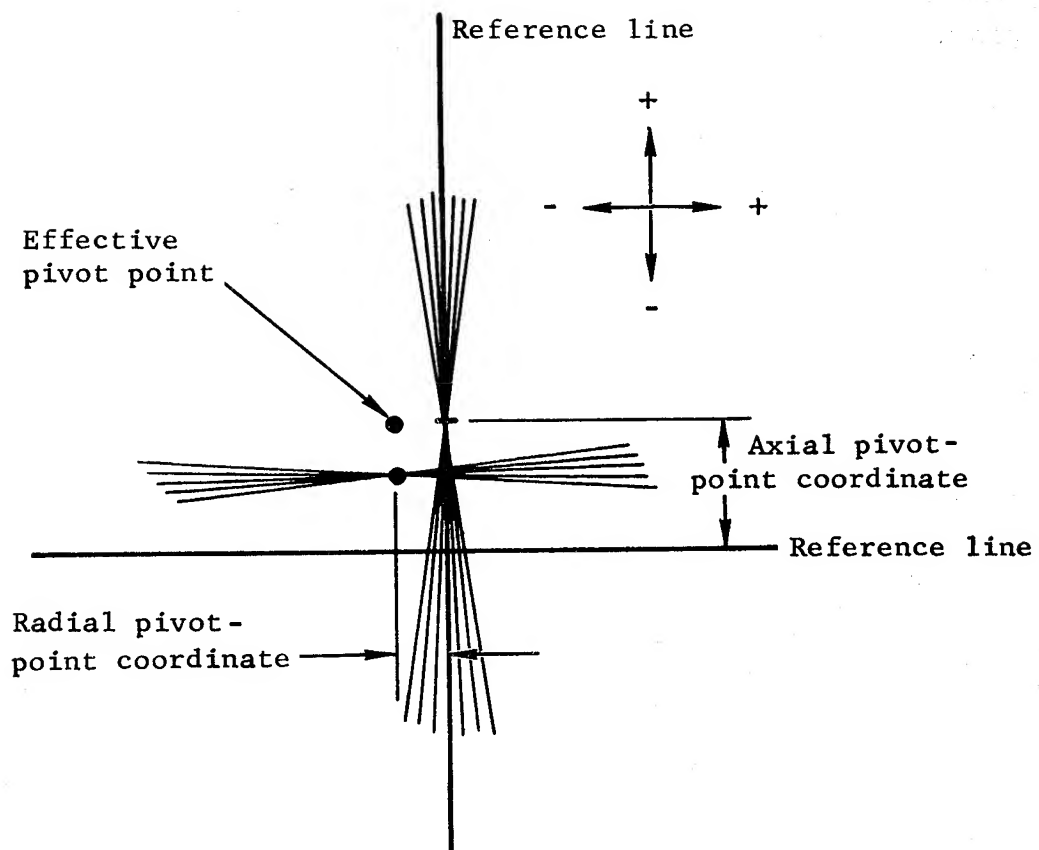
Figure 46. - Sketch illustrating factors involved in experimental determination of effective pivot point.

138

measured pivot point. The clearance past the radiation shield should be fixed in accordance with the purpose of providing radiation protection, and the pivot-point acceptance limits then should be established to be compatible with the required clearances.

The recommended design practice to study the effect of pivot-point location is to prepare a set of layouts of the nozzle. The movable components are drawn on one sheet and the fixed components on another sheet. Superimpose the two sheets with an axial deflection appropriate to the pressure being considered, and successively pin the two sheets together at a series of pivot points. The limiting pivot point should be one that just permits the movable component to rotate to the required nozzle vector angle.

3.1.7.3 STATIC-FIRING PROGRAM

The static-firing program shall demonstrate that the joint design fulfills the motor requirements and shall provide the data needed to design other components that interact with the nozzle.

Measurements should be made during the static firing program to determine nozzle misalignment requirements, friction characteristics, natural frequency, and damping coefficient of the nozzle, axial deflection, and vectoring capability. Sufficient data to develop a statistical variation should be obtained. Compare measured results and motor requirements. The final design of the guidance control system should be in accordance with the results of the static firing tests.

The actuation power requirements should be established during the static firing. Certain increments to the actuation torque — friction and insulating-boot torque — cannot be calculated. With a bellows-type design (fig. 7(a)), the boot torque has been as much as 50 percent of the spring torque for joints up to 30 in. (76.2 cm) diameter (ref. 13). Therefore, when a bellows-type insulating boot is exposed to the motor environment, it is recommended that the actuator be capable of developing 50 percent more torque than the sum of the calculated increments to the actuation torque (sec. 2.1.2.1). When an exposed wrap-around insulating boot is used with joints up to 30 in. (76.2 cm) diameter, the actuator should be capable of developing 75 percent more torque than calculated. For an insulating boot protected by a radiation shield (fig. 7(a)), the insulating material usually is a soft silicone rubber (e.g., DC 1255), and for joints up to 30-in. (76.2 cm) diameter the recommended actuator should be capable of developing 25 percent more torque than calculated.

3.1.7.4 DESTRUCTIVE TESTING

Destructive testing shall demonstrate joint failure characteristics.

The joint can fail in the elastomer layers or in the reinforcements (sec. 2.1.5). Each failure mode can be demonstrated in an actuation bench test. The joint without the insulating boot should be mounted in an actuation bench test fixture and actuated to the maximum vector angle at various pressures up to the maximum expected operating pressure MEOP. At pressures in excess of the MEOP, the vector angle should be increased in the ratio of the test pressure to the MEOP. Pressurization and vectoring should be increased at least up to the design ultimate pressure to demonstrate minimum compliance to motor requirements, and up to pressure producing joint failure if the failure characteristics are required. Failure is usually identified by failure of the joint to maintain a pressure seal.

3.1.7.5 AGING PROGRAM

The joint aging program shall demonstrate that joints possess acceptable storage life.

Bench tests should be conducted on joints that have been stored in the service environment, since changes in joint spring torque have been noted for joints using a natural-rubber formulation (sec. 2.1.2.5.2). It is recommended that stored joints be vectored at selected intervals and the spring torque measured. The changes in spring torque should be plotted versus time, and the results extrapolated to demonstrate that the joint will remain within motor specifications for the required joint life.

3.1.8 Inspection

3.1.8.1 INSPECTION PLAN

The inspection master plan shall incorporate inspection processes for use from initial material procurement through final joint acceptance to the extent necessary to assure conformance to design requirements.

Inspection processes should be used throughout the joint program beginning with material procurement and continuing through fabrication, process control, and final acceptance. Each phase can use different inspection techniques with different acceptance or rejection standards. For this reason, an overall master plan for the use and management of the quality-control program should be established prior to the start of fabrication. The scope of the master plan should be established on the basis of the required reliability level, the type and orientation of defects encountered, and the process sensitivity required. Also, the master plan should require the periodic evaluation of the equipment and of the skill and alertness of the operators; it should also provide for random checks on the execution of the planned requirements and procedures.

Particular caution should be used in planning the inspection requirements and in applying the inspection program so that material characteristics and fabrication processes that can affect the integrity of the inspection are identified. As an example, an inspection of elastomer thickness that is too infrequent could result in joints that were marginal because of elastomer layers that varied in thickness.

3.1.8.2 INSPECTION PROCESSES

The inspection processes shall have the capability of detecting all critical defects.

For the reinforcements, the following minimum inspection is recommended:

- Spherical radius at sufficient positions to establish expected thicknesses of elastomer rings in a joint.

- Concentricity.

- Thickness at various positions.

- Flatness.

- Inner and outer diameters.

For the elastomer, the minimum inspection should cover thickness and porosity. Mold a joint without adhesive on the reinforcement surfaces, then disassemble it. Measure elastomer thicknesses and evaluate porosity visually.

The recommended minimum dimensional inspection for the joint is overall length, the concentricity between the end attachment rings, and flange-to-flange parallelism. The minimum performance inspections recommended are the bench tests for compressive axial deflection, actuation, and tensile-pressure seal test (sec. 2.1.7.2). The data from the performance tests should be used to verify clearance envelopes. At intervals, production joints should be taken apart and the elastomer-to-reinforcement bond and elastomer porosity inspected to ensure that quality is being maintained.

141

3.2 LIQUID INJECTION THRUST VECTOR CONTROL

3.2.1 System Design

3.2.1.1 SYSTEM OPTIMIZATION

The design of the liquid injection system shall be based on a vehicle optimization study (including vehicle performance parameters, reliability, external envelope constraints, and cost) that results in optimum vehicle performance.

The recommended sequence of steps for determining the optimum LITVC system design is presented in chart form in figure 47.

The design requirement should be defined as the maximum required vectoring capability based on a statistical analysis of the operation of the vehicle on its various missions with allowance for the expected variation in the environments. This requirement should be determined correctly at an early date and the use of inflated initial estimates should be avoided, because the vectoring requirement strongly affects the design. The system weight increases almost linearly with the required side-thrust impulse.

The likely LITVC-system design options should be laid out without detail but should include basic design parameters such as type of injectant, injection pressure, source of pressurizing gas, number and spacing of orifices, injection location and angle, and tank type and shape.

General design information (including motor data, candidate injectant specific impulses, injector weight variation with flowrate, and tank weight variation with volume and pressure) should be assembled. Each possible design choice must be evaluated in terms of its effect on the desired vehicle performance (e.g., range, payload, final velocity), reliability, and cost. The results of these evaluations should be used as the basis for selecting the injectant, the injection configuration, the tank shape, and the pressurization method.

Initial design of a system should be based on performance data from previous programs. A large amount of data for LITVC systems is available (sec. 2.2.3.1) and should be used to provide an empirical basis for design analysis. The available data, however, will always represent motor geometry and operating conditions different from those of the motor for which the new LITVC system is to be developed. Therefore, those data must be transformed or scaled to the geometry and operating conditions of the present motor as described in section 3.2.3.

The thrust deflection angle can be as much as $10°$, but it is recommended that the thrust deflection angle be limited to $6°$, because the efficiency as measured by injectant specific

```
┌─────────────────────────────────────────┐
│ Define design requirements (required    │
│ vectoring capability, motor para-       │
│ meters, space envelope, and design      │
│ constraints).                           │
└─────────────────────────────────────────┘
                     │
                     ▼
┌─────────────────────────────────────────┐
│ Identify the LITVC design options       │
│ (each option will include one           │
│ combination of design parameters        │
│ including type of injectant,            │
│ injection pressure, injector loca-      │
│ tion, etc.).                            │
└─────────────────────────────────────────┘
                     │
                     ▼
┌─────────────────────────────────────────┐
│ Reduce available LITVC perform-         │
│ ance data and component weight          │
│ data to formulas and curves             │
│ adapted to the design problem.          │
└─────────────────────────────────────────┘
                     │
                     ▼
┌─────────────────────────────────────────┐
│ Determine weight and side-thrust        │
│ capability for each LITVC design        │
│ option, and establish the effects       │
│ of each option on the configura-        │
│ tion of the rocket motor.               │
└─────────────────────────────────────────┘
                     │
                     ▼
┌─────────────────────────────────────────┐
│ Calculate the vehicle performance       │
│ (range, payload, final velocity),       │
│ reliability, or cost as required        │
│ for each option to determine the        │
│ optimum LITVC system design.            │
└─────────────────────────────────────────┘
```

Figure 47. - Recommended sequence of steps for determining the optimum LITVC system design.

impulse drops to low values at the high injectant flowrates required for larger deflections (refs. 46, 108, and 122).

3.2.1.2 SELECTION OF INJECTANT

The injectant shall deliver maximum side specific impulse and have the highest density consistent with material compatibilities, storage requirements, and allowable toxicity.

Table IX summarizes the relevant data on the major operational injectants.

The selection of the injectant must consider the efficiency of the injectant in delivering side specific impulse. The relative efficiency of a candidate injectant may be known from existing data (secs. 2.2.1.2 and 2.2.3.1); if not, it should be checked by small-scale tests. Data on the relative efficiencies of various injectants are given in references 109, 121, and 141; figure 48 presents $I_{sp(s)}$ values for a number of inert and reactive liquids. The relative efficiency of a new injectant should be estimated from chemical-equilibrium calculations; various approaches and typical results are described in references 144, 145, and 146. Judgement must be used in interpreting the results of equilibrium calculations, since they make no allowance for the variation in evaporation rate and reaction time of different injectants. Excessive time delay in energy release reduces the potential effectiveness of an injectant. It is recommended that calculations be used only to screen injectant candidates and that the final evaluation be made by test firing.

The injectant should be selected for highest density, so that the fluid tanks, valves, and tubing can be made as small as possible to save both space and system weight. A preliminary estimate should be made of the volume required for the liquid injectant, and the storage tank that will contain this volume should be designed and fitted around the nozzle so that the envelope constraint can be evaluated.

The liquid selected must not chemically decompose, evaporate, or crystalize during long-term storage when kept within the temperature and pressure limits specified for storage of the vehicle. As examples of typical limiting conditions, a 62% solution of strontium perchlorate in water crystalizes at temperatures approaching 32° F (273 K), and hydrazine boils at 70° F (294 K) at a pressure of one atmosphere (ref. 115). The latter limitation should not be important with sealed systems under pressure.

The compatibility of the candidate injectants with the motor, propellant, and other neighboring systems should be checked, because certain reactive injectants ignite some solid propellants on contact. Danger to personnel may be important, especially in confined places. If positive safeguards against inadvertent spillage of an effective but highly reactive injectant cannot be provided, then the injectant will have to be eliminated from

144

The $I_{sp(s)}$ listed is for typical booster stages ($P_c \approx 800$ psia, $\epsilon \approx 12$) for the following conditions: single orifice injection; $P_{inj} = 1800$ psia; $\phi = 25°$; $\epsilon_{inj} = 2.5$; $F_s/F_a = 0.02$.

320 —— UDMH + N_2H_4 (EXOTHERMIC DECOMPOSITION)

Decomposition occurs only under certain conditions. These I_{sp} values are difficult to achieve.

280

—— MHF-3 (EXOTHERMIC DECOMPOSITION)

240

NITROGEN TETROXIDE ——

200

—— HYDROGEN PEROXIDE

68% STRONTIUM PERCHLORATE + —160—— STRONTIUM PERCHLORATE + METHANOL
WATER
—— LEAD PERCHLORATE + WATER
—— MHF-3

120—— FREON 12, FREON 113 (INERT)
FREON 114-B2 (INERT) —— —— BROMINE
—— UDMH + N_2H_4
—— NITROMETHANE
UDMH —— —— FREON 114-I2 (INERT)
—— PERCHLOROETHYLENE
80 —— BENZENE

—— ISOPROPYL ALCOHOL
—— IRFNA (ENDOTHERMIC DECOMPOSITION)
—— ZINC BROMIDE OR IODIDE (INERT)
40 —— WATER (INERT)

$I_{sp(s)}$, lbf-sec/lbm

Injectants for which TVC performance is well defined

Injectants for which TVC performance is not well defined

Figure 48. - Values of side specific impulse for reactive and inert liquid injectants (data from refs. 121, 125, and 129).

145

consideration. For example, a toxic fluid such as nitrogen tetroxide or bromine should not be selected unless it is practical to provide protection to personnel and the environment during loading, checkout, ground testing, launch, and possible other release due to mishap.

The liquid must be compatible with every tank or bladder material with which it comes in contact. The tank or bladder materials must neither react with the liquid nor catalyze the liquid's decomposition. The materials should resist decomposition by the liquid and remain impermeable, because liquid that has permeated a material is not available for injection. Results of investigations of the permeability of various bladder materials given in references 115 through 118 should be consulted.

3.2.1.3 INJECTION PRESSURES AND INJECTION ORIFICES

The injection pressure, the orifice size, and the number, spacing, and grouping of the orifices shall maximize the side thrust efficiency.

The most efficient pattern for injection is obtained from many circular orifices located in a circumferential line on the nozzle wall (figs. 29 and 31 and refs. 109, 121, 124, and 125). For greatest efficiency, these orifices should have omniaxis control rather than pitch-yaw control (ref. 142). Minimum spacing to avoid overlap losses should be 7 to 14 times the orifice diameter, but the available data should be studied and transformed to the system being designed (sec. 3.3.3.1). If this is not possible, the spacing effect should be evaluated in tests. It is recommended that cosine losses due to spreading the orifices around the circumference be estimated by vector addition of the estimated side-force effects.

The injection pressure should be about twice the rocket chamber pressure to achieve highest side-thrust specific impulse (figs. 38 and 40 and refs. 108 and 121). However, hardware system weight should be compared with loss in side-thrust efficiency for lower injection pressures, and the overall optimum pressure should be used.

The three-orifice injector is recommended, since it provides excellent side-thrust efficiency for minimum weight and simple plumbing, but this effectiveness must be confirmed by an optimization study.

The simplest LITVC injector arrangement has four injectors 90° apart. However, thrust deflection may be required in any plane, not just the pitch and yaw planes. In this event, the side force is the vector sum of the forces produced by the two injectors. Two such injectors operating simultaneously will use injector liquid at a rate approximately $\sqrt{2}$ times that of a single injector to produce the same side thrust.

As noted previously, injection is more efficient at low flowrates per orifice. If, for a given flowrate or side-force level, the number of injectors is increased, then the side-thrust

efficiency is increased. The efficiency of a number of injectors used to produce a single side force is estimated by vector addition of their side-force contributions. Each injector is considered to produce a side force at its location independent of the adjacent injectors. Therefore, the efficiency of multiple-injector LITVC can be estimated from the equation

$$\text{Cosine efficiency} = \frac{\sum_{i=1}^{n} \cos \psi_i}{n_{inj}} \tag{12}$$

where

n_{inj} = number of injectors operating

ψ_i = angle between total side force and the side force produced by the ith injector

Equation (12) does not include the efficiency increase due to reduced flowrate per injector or efficiency decrease due to overlapping of adjacent mixing and shock areas.

3.2.1.4 INJECTOR LOCATION AND DISCHARGE ANGLE

The injector location and discharge angle shall maximize side-thrust efficiency.

For highest side-thrust efficiency, locate the injection orifices as far upstream in the rocket nozzle as is possible without incurring significant corss-nozzle effects at maximum thrust vector deflection. (Cross-nozzle effects are pressure increases on the wall of the opposite side of the nozzle caused by shocks and injectant that cross over.) One or more of the following three methods should be used to estimate the optimum location of the injector on the nozzle exit-cone wall:

(1) Use the empirical ratios for X/L listed below (refs. 108 and 125):

Nozzle divergence half-angle	Optimum X/L	
	Small thrust deflection (about $1°$)	Large thrust deflection (about $6°$)
$17.5°$	0.3	0.4
$27.5°$	0.2	0.3

X = distance (along nozzle axis) from throat to point of injection

L = distance from throat to nozzle exit plane

147

(2) Estimate the optimum injector location by use of empirical curves (fig. 49). Generate a straight line from the nozzle rim opposite the proposed injection point such that the line crosses the nozzle centerline at the angle λ obtained from the curves for ϕ in figure 49. The point at which the line reaches the nozzle wall is the probable optimum injection site (refs. 107 and 147).

(3) Use the methods of fluid mechanics and gas dynamics to estimate the path of the shock and injectant-mixture disturbance in the nozzle from various possible injection points; however, check the method selected against known test results before it is applied to the design problem. One such method utilizes the Boeing computer program (ref. 151); however, in its present form the program is formulated only for inert injectants.

The optimum discharge angle (figs. 23 and 37) results in the greatest collision effect and mixing of the motor gas and injectant. From various studies (refs. 107, 108, and 125), the discharge angle should be 25°. However, as the discharge angle influences the location of the injectors and their plumbing, envelope considerations should be a factor in the selection of the discharge angle. For systems that must be an optimum, the discharge angle should be evaluated by test.

3.2.1.5 AMOUNT OF LIQUID INJECTANT REQUIRED

The amount of liquid injectant shall be the minimum amount necessary for the maximum vehicle flight duty cycle.

The weight of liquid injectant required must be calculated from the maximum required vectoring capability of the motor, the injectors and their location having been selected as described in section 3.2.1.4. The vectoring requirements will be given explicitly as thrust deflection angle θ for pitch and yaw and required side thrust F_s, each as a function of time. The following procedure is recommended for calculating the weight of injectant required:

(1) For each candidate liquid injectant, determine the side specific impulse $I_{sp(s)}$ as a function of deflection angle, and plot the results. Examples of such plots are given in figure 42.

(2) Noting the motor vectoring requirements of deflection angle θ as a function of time t, use the results of item (1) to obtain the estimated side specific impulse as a function of time.

(3) Noting the motor side force requirements F_s as a function of time, calculate the injectant weight flowrate $\dot{w}_s$ as a function of time.
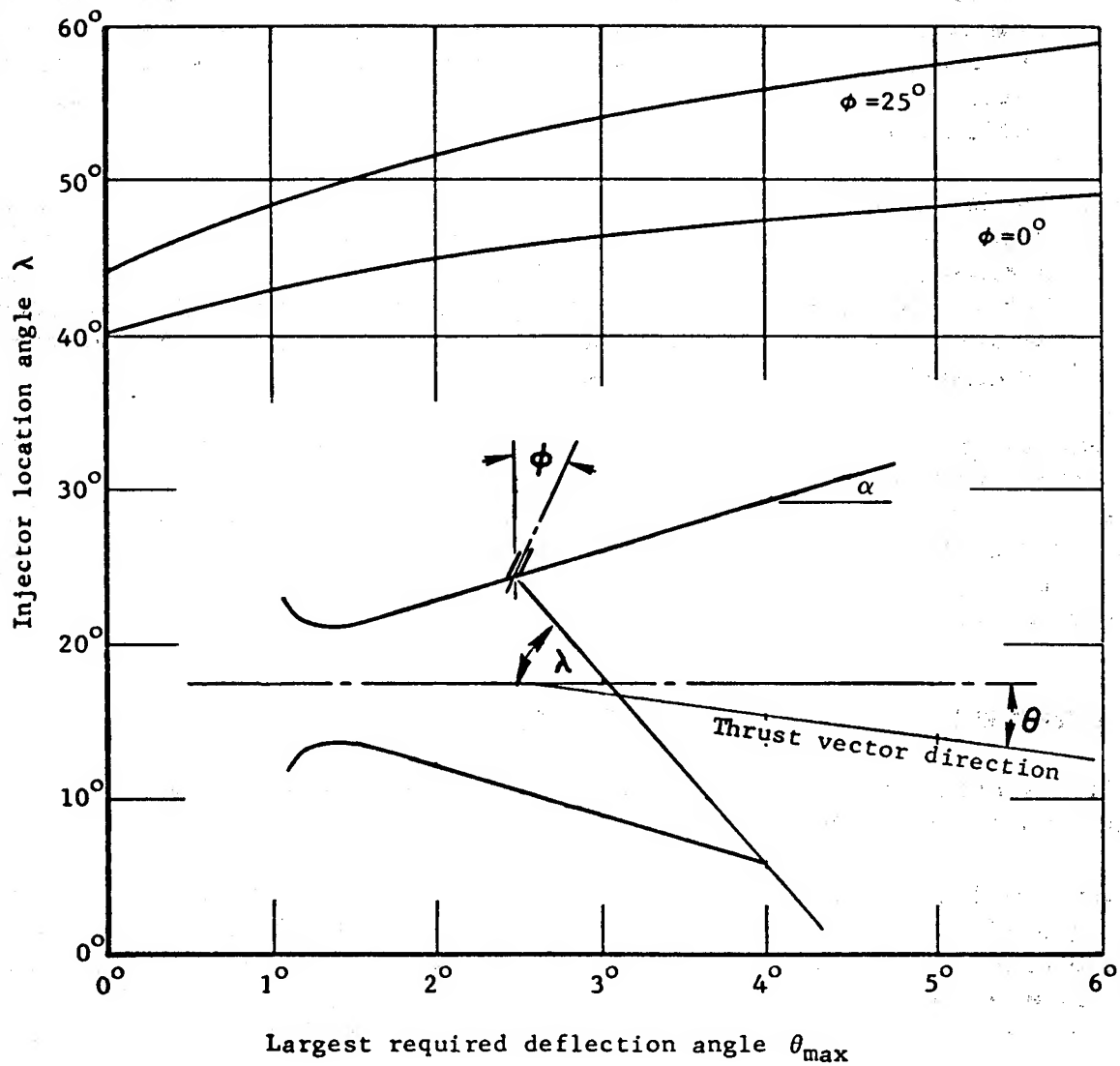
Notes: The diagonal from the injection port to the nozzle
rim is not the location of the shock wave (cf. fig. 23).

Figure is based on data from conical and contoured
nozzles having $\epsilon = 7$ to 20, $\alpha = 18$ to $28°$, and
both inert and reactive injectants.

Figure 49. - Relation of thrust deflection angle to injector location (refs. 107 and 147).

149

(4) Integrate the injectant flowrate $\dot{w}_s$ from motor ignition to the end of firing to estimate the amount of liquid injectant required, or use statistical methods to determine the amount of side impulse for the various deflection angles required to achieve the specified probability of flight success.

(5) The amount of injectant not available for vectoring, including that for tank ullage, for filling piping and valves, and for valve operation and valve leakage, must be calculated and added to the amount needed for vectoring. For preliminary estimates, add 10% for these purposes.

The side specific impulse of the injectant should be carefully estimated for the motor being designed and, for the injector configuration and location selected by use of available test data, correlated and transformed for application to the current design problem (sec. 3.2.3).

3.2.1.6 AMOUNT OF PRESSURIZATION GAS REQUIRED

The gas flow into the liquid tank shall expel the liquid at a rate that will produce the required side impulse within the specified response time.

The gas flow into the tank of liquid should be from a tank of compressed inert gas or from a solid-propellant warm-gas generator, or the gas can be contained with the liquid in a common tank.

If a tank of cold gas under high pressure is the source of the gas used to pressurize the liquid, the gas should have a volume at LITVC operating pressure equal to the total of its own stored volume, the volume of the piping and the manifold, and volume of liquid to be expelled. Because the specified injectant pressure must be delivered to the fluid at the injection point and be sustained during sudden demands for large flows, the effects of liquid acceleration and flow friction should be evaluated. The pressure applied to the liquid injectant in the tank may have to be significantly higher than the minimum required injectant pressure at the injector valve. The piping sizes, the gas supply rate, and pressure should be sufficient to respond to the worst conditions.

The pressure of the gas delivered to the liquid tank should be reduced by a pressure regulator so that liquid is not injected at pressures excessively above the pressure level set by the design.

The weight of gas so required should be calculated from one of the equations of state of a real gas, such as the Beattie-Bridgeman equation or the equation of state with compressibility factor (ref. 152). An example of such a calculation for a LITVC system is contained in reference 153. An estimate of the weight of the gas required, usually with an error $< 10\%$, can be obtained from the ideal-gas equation of state:

$$\rho = \frac{CPM}{RT} \tag{13}$$

where

ρ = density, lbm/ft^3 (kg/m^3)

P = pressure, psia (N/m^2)

M = molecular weight of the gas, lbm/lbm-mole (kg/kg-mole)

R = universal gas constant, 1545.3 lbf-ft/lbm-mole-°R (8314.3 J/kg-mole-K)

T = absolute temperature, °R (K)

C = conversion factor, 144 in.^{2}/ft^2 (1 J/N-m)

If a warm-gas generator is used in place of cold compressed inert gas, a larger total quantity of gas will be required than that calculated above. This condition arises because the supply of gas must be maintained at the maximum expected demand level through all periods of firing time, even though the actual demand for pressurization gas usually will be much lower than the maximum. The propellant grain in the warm-gas generator must be designed to produce sufficient pressurizing gas to cause the injectant to comply with the motor vectoring requirements (ref. 154). The gas that is produced, but not used, should be released overboard through a pressure relief valve.

If a common liquid/gas tank with no separation between the liquid and the gas is used, allowance should be made for the dissolving of part of the gas in the liquid and for evaporation of some of the liquid into the gas. The latter phenomenon usually is negligible; for example, in the Titan III system at 70° F (294 K), the pressurizing N_2 contains 1.5% N_2O_4 vapor (ref. 47). These effects of dissolving and evaporating should be calculated by the methods of the thermodynamics of mixtures (ref. 152). Care should be taken to use the real and not the ideal properties of the gases in order to avoid substantial errors at high pressures.

3.2.2 Component Design

The size of LITVC components shall be based on verified empirical curves that represent the LITVC system to be designed.

The empirical curves must provide adequate data of sufficient accuracy for selection of type of injectant fluid, injector location, number of orifices, injection angle, and injection pressure. Any additional data required must be generated from subscale tests (sec. 3.2.3.2). These curves must be based on test data, because available analytical methods do not reliably predict LITVC performance.

Data for these curves should be obtained from earlier development programs and subscale tests. These data should be plotted and correlated, then transformed for use in the current design (sec. 3.2.3.1).

After the first complete set of LITVC components has been designed, it should be fabricated, assembled, and evaluated in a full-scale test (sec. 3.2.3.3) at the earliest opportunity to confirm the design and to verify performance data for use in further design improvement or performance prediction.

3.2.2.1 INJECTORS

Injectors shall deliver injectant to the exhaust flow in columnar jets at maximum velocity within the required response time.

The injector valves should be sized no larger than necessary for the maximum required flowrate as determined by methods described in sections 3.2.1.3 and 3.2.1.4; use data of satisfactory accuracy for design. The injectors must contain flow passages and orifices that are specially contoured and streamlined to accelerate the fluid to the maximum possible velocity on discharge. The pintles or gates must likewise be contoured and streamlined to achieve maximum acceleration of the fluid, so that on discharge the fluid is travelling at the highest obtainable speed in jets that diverge as little as possible. In this way, the system pressure will be most efficiently converted to injection momentum.

The use of center-pintle type injectors with servo or electro-mechanical control for variable-flowrate capability is recommended, because these injectors can provide high side-thrust efficiency and versatile control with minimal shock loading.

Off-on injectors may be preferred in certain cases because of their low weight and simplicity. These injectors should be of the center-pintle type designed for maximum flow momentum when fully open. To avoid vibration problems, their operating frequency should be set in a range different from the natural frequencies of the structures of the vehicle.

The method of actuating the injector valves must be determined from the required speed of vectoring response, the inert weight penalty, cost constraints, and flight control limitations (ref. 76).

Screens should be installed in the liquid supply entrance to each injector valve to catch and hold any debris that might cause trouble in the injector valve. Measures for the control of contamination of fluid, components, and system may suffice in lieu of active screens or filters.

3.2.2.2 STORAGE TANK AND BLADDER

The liquid injectant tank shall preserve the liquid without degradation or loss during vehicle storage and provide positive expulsion of the liquid during motor operation.

The shape of the tank should be selected to result in minimum weight. The required amount of injectant to be carried should be determined as described in section 3.2.1.5. It is recommended that, if the amount of liquid required is relatively small, one or more spherical tanks be used, because the sphere is the most efficient shape; but, if a large amount of liquid must be carried, the tank should be toroidal, since this is the shape with the largest volume that fits around a nozzle. In intermediate cases, cylindrical tanks are suitable. The tank should be designed according to the recommended practices of reference 155, fabricated from a lightweight or high-strength alloy such as aluminum or stainless steel, and be compatible with the liquid. If the tank is to be left pressurized during storage or standby conditions when personnel may be near, the tank must be designed to meet the prevailing pressure-vessel safety code. To avoid this requirement so that a low factor of safety can be used, provision should be made to pressurize the tank when the vehicle is prepared for launch and after personnel have been cleared from the vicinity.

If a cool inert gas is used for pressurizing and if gravity or acceleration forces can be depended upon to keep the liquid puddled over the outlet, it is recommended that the gas be allowed to contact the liquid directly.

A bladder to separate the gas from the liquid is recommended if the liquid is pressurized by warm gas, because the gas loses heat to the liquid rapidly, contracts, and must be replenished by more warm gas. With reactive injectants and warm gas, the bladder must provide a positive seal because contact between liquid and gas could result in failure through combustion or explosion in the tank. The bladder should be fabricated from laminated fiber and plastic.

Special means should be provided to completely seal the injectant liquid in the tank. The filling and trapped-gas vent fittings should be designed with provision for positive closure (e.g., crimped or soldered metal closures). The tank outlet should be sealed with a metal diaphragm scored to break open without loose fragments when the liquid is pressurized (ref. 156).

3.2.2.3 PRESSURIZATION SYSTEM

The pressurization system shall, within the prescribed time, pressurize the injectant to a level within the design pressure range for injection into the nozzle.

When the LITVC system is activated, the injectant must be brought up to operating pressure in time for the first vector-control signal. The pressurization system can be either a high-pressure inert-gas system or a warm-gas generator. The choice should be based on an optimization study that considers pressurization system performance and weight and LITVC performance. The capacity of the pressurized-gas storage volume should be determined according to practices given in section 3.2.1.6.

If a high-pressure tank system is used, the tank outlet should be sealed by a squib valve that is opened by an electric signal or system activation. The gas flow from the high-pressure tank should be stepped down to the design injectant pressure level by a pressure-control valve. If there is any possibility that harmful debris might come from the tank, valve, or line, screens should be installed ahead of the controller. An inert gas such as nitrogen should be used in a high-pressure tank system to minimize corrosion and compatibility problems. If weight is important, helium should be used, but special attention should be given to the unusual ability of helium to diffuse through materials (ref. 118).

If a common liquid/gas tank is to be used, the range of pressures provided should be optimum for the system. Also, the minimum pressure remaining when almost all of the liquid is used should be sufficient for effective injector-valve operation and thrust vector deflection.

Warm-gas generator systems usually employ solid propellants and are designed like miniature solid rocket motors. The warm-gas generator should be designed to deliver the gas-flowrate/time profile that is calculated as described in section 3.2.1.6 and reference 157. The propellant grain shape should be adjusted to cause the flowrate to vary to fit the desired curve (ref. 154). Usually a high rate is needed initially to provide for launch or staging pertubrations; this condition is followed by a period of low demand during the rest of flight when only vector trim and course corrections are needed. The propellant for the warm-gas generator should be a clean-burning low-flame-temperature (2000° F to 3000° F (1367 K to 1922 K)) propellant that does not produce deposits and that is not too hot to use with alloy-steel tubing and valves. Propellants that burn at temperatures above 2500° F (1644 K) will be usable only if the operating period is short enough to limit heating of steel parts to safe levels. Otherwise insulation or high-temperature metals will have to be used.

The gas flow from the generator should pass through a screen to catch debris and into a pressure regulator designed to step down the pressure to the design injection pressure level (ref. 156). Since the production of gas by the generator is predetermined and independent of actual gas demand, the surplus gas must be diverted through a pressure relief valve for

disposal to the environment. If possible, this unneeded gas should be released from a small nozzle pointed aft, so that a small increment of thrust can be recovered through its release. However, if the vehicle has a coast period and if the gas generator burns after the rocket motor has burned out, the small exhaust jet could cause unwanted changes in vehicle attitude. This condition should be prevented by exhausting the unneeded gas through two equal orifices that are oriented in opposite directions.

If the main vehicle system requires a supply of gas for roll control, the possibility of using the same gas generator for this purpose and for LITVC pressurization should be considered.

3.2.2.4 LIQUID STORAGE EQUALIZATION

Flow from and sloshing in multiple tanks and large lateral tanks shall not change vehicle inertial properties.

If there is more than one tank, provision must be made to drain the tanks at equal rates to prevent offsetting the vehicle center of gravity. Uniform expulsion of liquid from a toroidal tank is dependent on the ability of the bladder to deflect and fold uniformly around the circumference of the toroid during expulsion. The bladder should not be allowed to buckle so that one sector freely collapses on the liquid while other sectors are restrained. If vehicle movement could generate undesirable sloshing, the sloshing should be inhibited by baffles.

3.2.2.5 DISPOSAL OF SURPLUS INJECTANT

Injection system design shall provide for disposal of surplus injectant to reduce flight weight and to obtain additional thrust.

The injectant flow rate should be measured and integrated over time, so that at any instant of flight time the total amount of liquid actually used will be known. A computer or control device should continuously compare the amount of liquid used with the maximum that could be used up to that time without jeopardizing the completion of the mission. Flight control should then signal the injectors to expend the excess liquid equally around the nozzle so that the motor thrust will be augmented but there will be no thrust deflection.

The axial thrust added by jettisoning the surplus liquid can be estimated with the following expression:

$$\Delta F_a = I_{sp(s)\,(\theta\,=\,0°)}\,\dot{w}_s\,\tan\alpha_{inj} \tag{14}$$

where

ΔF_a = axial thrust added by surplus injectant, lbf (N)

$I_{sp(s)\,(\theta\,=\,0°)}$ = specific impulse of the liquid injectant in the side direction at $0°$ deflection, estimated from a plot of $I_{sp(s)}$ versus θ (e.g., figs. 35 and 42), lbf-sec/lbm (N-sec/kg)

$\dot{w}_s$ = flowrate of liquid injectant, lbm/sec (kg/sec)

α_{inj} = the equivalent half angle of the nozzle from the injection point to the exit, determined as the angle between the nozzle centerline and a line from the injection point to the exit rim, deg

This equation is applicable to both conical and contoured nozzles (ref. 126). The $I_{sp(s)}$ extrapolated to $0°$ deflection angle is used because it best represents the LITVC effects that augment axial thrust. These effects are the increased pressures on the exit cone caused by injectant energy and mass and by injection shocks. $I_{sp(s)}$ values obtained at larger deflection angles should not be used in equation (14) because these $I_{sp(s)}$ values have been reduced by losses in measured side forces due to the circumferential spreading of the side forces around the nozzle. Such losses detract from side thrust but not from axial thrust. Correlation with the data in reference 121 shows an accuracy within $\pm\,10\%$ for nozzles with expansion ratios up to 10.

Equation (14) may underestimate the added thrust when applied to long contoured nozzles having expansion ratios greater than 20 with injection far upstream from the exit. This result occurs because the wall angle at the center of this region of added pressure usually is significantly larger than the equivalent half-angle α_{inj}. The center of the region of added pressure generally is located a short distance downstream of the injection orifices. For such nozzles, then, the value for the half-angle used in equation (14) will be less than the local wall angle at the injection point but greater than α_{inj} as defined above; this effective half-angle is estimated from experience. The added thrust due to expending injectant in the nozzle is more accurately estimated by the use of data from subscale tests or, if an adequate mathematical model exists (sec. 2.2.3), by integrating the product of the added pressure and the tangent of the wall angle over the nozzle wall area affected.

A detailed performance analysis of a liquid-injectant dump system is presented in reference 47.

3.2.2.6 ADAPTATION OF THE MOTOR FOR LITVC

The motor design shall provide injector mounts and ports and external brackets for system support.

The nozzle design should make provision for holes and mounts for the injectors. The metal orifice ends of the injectors should be recessed sufficiently inside the injection port (fig. 29) that they will not be damaged by heat flux. The heat flux at the inside end of the injection port should be estimated (refs. 134 and 135). The port hole should be made conical to fit the shape of the liquid jet and only large enough to permit the jet to be discharged without momentum losses due to wall friction. Small port hole size will minimize heat transfer into the hole and will minimize the erosion at the hole edges that results from impingement of the exhaust-gas flow.

Provide a gas-tight seal such as an O-ring at the interface between the injector and the nozzle liner.

The injector mount, to which the injector will be bolted, and its attachment to the nozzle wall should have sufficient strength to withstand the full injector reaction thrust in addition to other loads. If possible, the entire LITVC system should be mounted on the nozzle to avoid any problems of differential motion between the nozzle and the motor aft dome or skirt. If this mounting is not possible, provide flexible lines or expansion joints.

Mechanical and thermal analyses (i.e., stress, gas flow, heat transfer, and erosion) should be made of the nozzle and related portions of the motor. Loads due to the weight of the LITVC system and to the intermittent TVC pressures on the exit cone walls that produce the major part of the vectoring force must be included in these analyses. The distribution of these vectoring pressures on the exit-cone wall can be estimated (ref. 136).

The only thermal problem of consequence due to LITVC is the severe heating and erosion that occurs around and immediately downstream of the injection port holes (fig. 34). The amount of erosion depends on the exhaust flow properties, the reactivity of the injectant, and the type of ablative material used. To predict this erosion, use methods for predicting erosion that include the capability for treating the effects of chemically reactive injectant and exhaust-gas mixtures (refs. 158 and 159). The analysis should be cross checked by scaling known LITVC hole erosion to the design condition, appropriate heat-transfer relationships being used as the scaling factors. A design of an injector mounting pad with typical heating and erosion patterns is shown in figure 50.
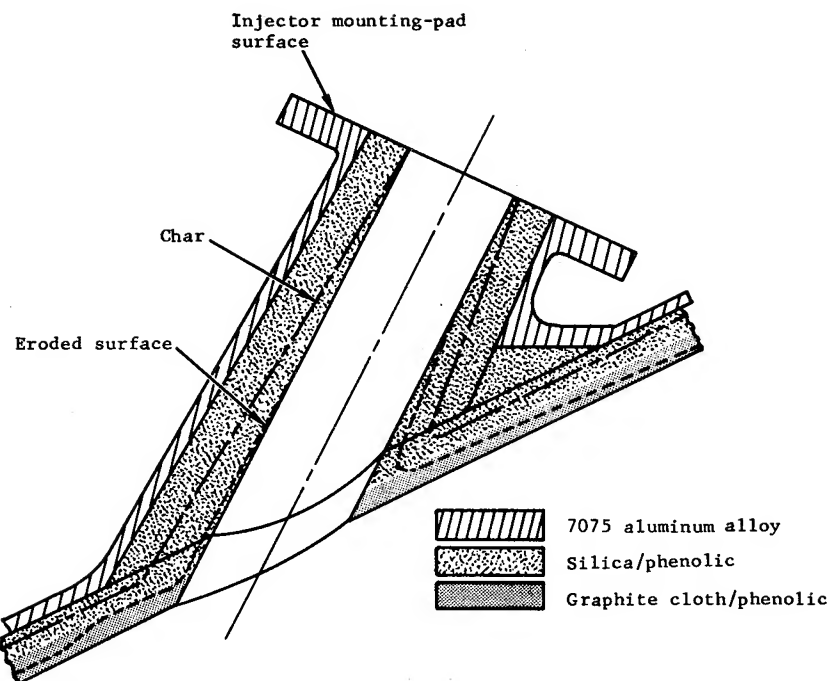
Figure 50. - Typical LITVC port configuration showing erosion and char patterns.

3.2.3 Performance Evaluation and Testing

Test data shall support the LITVC system development and demonstrate operational capability.

Test data from other LITVC systems transformed and correlated by analysis to the LITVC being designed should be used for conceptual design and motor tradeoff studies to determine the general configuration of the motor system. As soon as possible, these data should be supported by data from subscale tests conducted under test conditions that simulate actual motor conditions. The full-scale motor operating capability must be demonstrated at test conditions simulating actual flight conditions.

3.2.3.1 PERFORMANCE DATA FOR DESIGN

Performance data from other LITVC programs shall be demonstrably applicable to the LITVC system required..

Existing LITVC data that can be transformed to the required LITVC system should be used for motor optimization studies, tradeoff studies, and preliminary conceptual design. These studies must be conducted early in the program to determine the adequacy of the data and to define needed additional data so that a test program can be commenced.

The data obtained from various sources must represent the variation of side-force specific impulse with injectant flowrate, injector location, injection angle, injection pressure, orifice size, and orifice spacing. The available test data should be transformed to dimensionless form except for the side-force specific impulse, which is retained in units of lbf-sec/lbm (N-sec/kg). Each of the design variables should be presented as a family of curves, wherein all other parameters are constant at one or more arbitrary configurations. These configurations should be selected to represent a range that includes the optimum design. An example of this practice is shown in figure 42 for an evaluation of injection pressure. Other plotting formats as illustrated in figures 36 through 40 should be used if they are more convenient. Data that have originated from rocket motors that were significantly different from the design motor should be transformed; use the dominant physical laws as described in section 2.2.3.1 to make them applicable.

The suitability of the transformed data to the design motor must be evaluated for consistency and agreement by using data from different sources plotted on the same graph. If the results form a continuous plot with little scatter, the results can be used with confidence. If the scatter is larger than can be tolerated within design specifications, a test program must be initiated to generate data in the expected design range. Awaiting test data could result in a delay in a program, and in such a period the transformed data will be the only available data. These data must be used for initial optimization studies and preliminary design; use engineering judgement to allow for an amount of error defined by data scatter. The results obtained with such data must be reevaluated when test data in the expected design range become available.

3.2.3.2 SMALL-SCALE TESTS

Small-scale tests using system parameters in the expected design range shall provide design data not otherwise available.

Small-scale tests should be conducted to obtain data that are not available from transformation of other test data. The test motors should use rocket nozzles and LITVC injection geometries that are scale models of the expected full-scale design configuration; the test motor chamber pressure should be the same as that of the design motor; and the test propellant exhaust gas should be similar to that of the full size motor in temperature and in oxidizing species that are free to react. To obtain valid data, the test motor need not be a solid-propellant motor but can be a liquid propellant motor, a change that usually results in cost savings and test convenience (ref. 121).

3.2.3.3 FULL-SCALE DEVELOPMENT TESTS

A full-scale firing test shall evaluate the LITVC system design.

An evaluation of the full-scale LITVC system should be conducted on the first static test firing of the motor, so that design changes can be incorporated without causing significant program delays or increased costs. Measurements must be made of all parameters affecting design of the LITVC system and the results used to reevaluate the injector valves, injectant requirements, and injectant tank size. If the motor is to operate at high altitude, the test should be conducted at the corresponding ambient pressure. The final LITVC design must be evaluated in static test firings, so that its actual performance and characteristics can be known for flight-control use. Vertical orientation of the motor or at least of the liquid tanks may be necessary for such tests.

3.2.3.4 OPERATING-CAPABILITY TESTS

Procedures for the component testing, assembly installation, checkout and operation of the LITVC system shall be developed and documented.

The functional capability of all components of the LITVC system should be determined by test before assembly. These tests should employ pressurized gas and liquid supplies and control connections as necessary to simulate operating conditions. The bench testing should be performed with an inert liquid (e.g., Freon) that will evaporate and leave the components clean. If a reactive or nonevaporating injectant is used in bench testing, components must be thoroughly cleaned after testing.

After the system has been assembled and installed on the motor, the critical components should be checked during storage or launch readiness as often as necessary to ensure satisfactory operating capability. Procedures for these check operations should be documented. The critical components are the gas pressurization subsystem and the injectors. The other components including the meters, check valves, injectant tank and bladder, piping, and fittings are important but they are not nearly as sensitive to malfunction. Also, procedures for correct installation, filling, operation, and unloading of the LITVC system on the rocket motor should be documented.

If a gas generator is used, the igniter squib should be checked at low voltage for continuity and resistance. If a tank of inert gas under high pressure is used, its pressure, sensed by pressure gage, should be monitored, and the squib valve at its outlet should be electrically checked for continuity and resistance.

The more sensitive electric portions of the injectors should be actuated and their movements monitored by feedback signals.

APPENDIX A

Conversion of U. S. Customary Units to SI Units

Physical quantity	U.S. customary unit	SI unit	Conversion factor[a]
Angle	degree	radian	1.745×10^{-2}
Density	lbm/ft^3	kg/m^3	16.02
Force	lbf	N	4.448
Length	in.	cm	2.54
	ft	m	0.3048
Mass	lbm	kg	0.4536
Molecular weight	lbm/lbm-mole	kg/kg-mole	1.00
Peel strength	lbf/in.	N/cm	1.75
Pressure	atm	N/m^2	1.013×10^5
	psi	N/m^2	6.895×10^3
	psi	N/cm^2	0.6895
Specific impulse	lbf-sec/lbm	N-sec/kg	9.80665
Stress	psi	N/m^2	6.895×10^3
Temperature	°F	K	$K = \frac{5}{9}(°F + 459.67)$
	°R	K	$K = \frac{5}{9}(°R)$
Temperature difference	°F	K	$K = \frac{5}{9}(°F)$
	°R	K	$K = \frac{5}{9}(°R)$
Torque	in.-lbf	m-N	0.1130

[a]Multiply value given in U. S. customary unit by conversion factor to obtain equivalent value in SI unit. For a complete listing of conversion factors, see Mechtly, E. A.: The International System of Units. Physical Constants and Conversion Factors. Second Revision, NASA SP-7012, 1973.

APPENDIX B

GLOSSARY[*]

Symbol	Definition	Appears In
A	reinforcement material constant affecting value of elastomer shear modulus with superimposed pressure	eq. (3)
C	conversion factor, 144 in.^{2}/ft^2	eq. (13)
d	distance from point of liquid injection to nozzle exit, in. (cm)	fig. 43
d_o	diameter of the discharge orifice of the injector, in. (cm)	figs. 39 and 42
d_t	nozzle throat diameter, in. (cm)	fig. 36
E	hoop modulus of elasticity of reinforcement, psi (N/m^2)	fig. 19
F_a	axial component of the rocket motor thrust, lbf (N)	figs. 35, 36, 37, 38, 39, 40, and 42 and eq. (14)
F_s	side force due to liquid injectant, i.e., component of the total rocket motor thrust perpendicular to the motor axis, lbf (N)	figs. 35 - 42
G	effective elastomer shear modulus when subjected to external pressure, psi (N/m^2)	eqs. (2) and (3)
G_o	elastomer secant shear modulus at 50 psi (3.45 x 10^5 N/m^2) shear stress and no externally applied pressure, at the temperatures expected in operation, psi (N/m^2)	eqs. (1), (3), and (6)

[*]Divided into three sections: Symbols, Material Designations, and Organization Abbreviations

163

Symbol	Definition	Appears In
$I_{sp(s)}$	side specific impulse, ratio of side force produced by injectant to injectant flowrate causing side force, lbf-sec/lbm (N-sec/kg)	table VIII, figs. 40 and 48, and eq. (14)
$I(\beta)$	integral values for calculation of flexible-joint spring torque	table V
$I(\beta_1)$ and $I(\beta_2)$	integral values at angles β_1 and β_2, respectively	eq. (1)
K_e	correction factor to elastomer stresses, a function of cone angle	fig. 18 and eq. (7) .
K_r	correction factor to reinforcement stresses, a function of cone angle	fig. 18 and eqs. (9) and (10)
L	distance from nozzle throat to nozzle exit plane, in. (cm)	figs. 35, 36, 37, 38, 39, and 42
M	molecular weight of pressurization gas, lbm/lbm-mole (kg/kg-mole)	eq. (13)
M_{inj}	Mach number of the rocket exhaust gas at the point of secondary injection	fig. 43
MEOP	maximum expected operating pressure	text
MS	Margin of Safety: fraction by which the allowable load or stress exceeds the design load or stress, $$MS = \frac{1}{R} - 1$$	eq. (5)
n	number of elastomer rings in a flexible joint	eqs. (6), (9), and (10)
n_{inj}	number of injectors operating	eq. (12)
P	pressure, psi (N/m^2)	eq. (13)
P_{amb}	ambient air pressure	fig. 36
P_c	motor pressure: pressure in the combustion chamber of the rocket motor	eqs. (4), (7), and (9), figs. 25, 36, 38, 39, 40, 42, 43, and 48

164

Symbol	Definition	Appears In
P_{inj}	liquid injectant pressure delivered to the injector valves	figs. 35, 36, 38, 39, 40, 42, and 43
P_s	static pressure of gas flow in the nozzle	fig. 25
$P_{s, inj}$	static pressure of gas flow in the nozzle at the injection location	fig. 43
QLS	quadruple - lap shear	various places in text
R	(1) ratio of design load or stress to the allowable load or stress	eq. (5)
	(2) universal gas constant, lbf-ft/lbm-mole $^{\circ}$R (J/kg-mole-K)	eq. (13)
R_i	inner joint radius	fig. 12
R_o	outer joint radius	fig. 12
R_p	pivot radius of joint measured from geometric pivot point, in. (cm) $$R_p = \frac{R_o + R_i}{2}$$	fig. 12 and eqs. (6), (7), (9), and (10)
r_i	$R_p - nt_e/2$	eqs. (1) and (2)
r_o	$R_p + nt_e/2$	eqs. (1) and (2)
T	absolute temperature, $^{\circ}$R (K)	eq. (13)
T_q	flexible-joint spring torque, in. - lbf (m-N)	eqs. (1) and (2)
$T_{s, inj}$	static temperature of the gas flow in the nozzle at the point of injection, $^{\circ}$R (K)	fig. 43
t	time from start of motor operation, sec	calculation procedure in sec. 3.2.1.5
t_e	thickness of elastomer ring in flexible joint, in. (cm)	figs. 12 and 19, eqs. (6) and (7)
t_r	thickness of reinforcement in flexible joint, in. (cm)	figs. 12 and 19, eqs. (6), (7), and (10)

Symbol	Definition	Appears In
v_{inj}	velocity of gas flow in the nozzle at the point of injection, ft/sec (m/sec)	fig. 43
$\dot{w}_a$	weight flowrate of the exhaust gas from the rocket motor, 1bm/sec (kg/sec)	figs. 36, 38, 39, 40, and 42
$\dot{w}_s$	weight flowrate of the injectant from the injector into the rocket nozzle, 1bm/sec (kg/sec)	figs. 39, 40, and 41 and eq. (14)
X	distance measured along the nozzle center-line from the nozzle throat to a plane containing the centers of the injection ports, in. (cm)	figs. 35 - 39 and 42
α	divergence half-angle of nozzle exit cone, deg	figs. 36, 38, and 49
α_1	divergence half-angle of a contoured exit cone measured near the nozzle throat, deg	fig. 42
α_2	divergence half-angle of a contoured exit cone measured near the exit cone lip, deg	fig. 42
α_{inj}	equivalent nozzle half-angle from the injection point to the exit plane, determined as the angle between nozzle centerline and a line from the injection point to the exit rim, deg; for a conical nozzle, $\alpha_{inj} = \alpha$	eq. (14)
β	joint angle, the angle between the nozzle centerline and a line from the geometric pivot point to the middle of the flexible joint, deg	fig. 12 eqs. (9) and (10)
β_1, β_2	inner and outer joint angles defining flexible joint geometry, deg	fig. 12 and eqs. (1), (2), (4), (9), and (10)
γ	shear strain in elastomer measured in quadruple-lap shear test	sec. 2.1.7
$\triangle$	incremental change in a quantity	eq. (14)

Symbol	Definition	Appears In
λ	angle between the nozzle centerline and a line from an injection port to the opposite-side exit-plane rim, deg	fig. 49
ϵ	nozzle expansion ratio, defined as ratio of exit plane area to throat area	figs. 25, 35, 38, 39, 40, 42, 43, and 48
ϵ_{inj}	expansion ratio of the nozzle exit cone at the plane of the injection ports, defined as the ratio of the area at this plane to the throat area	figs. 36, 40, 43, and 48
θ	(1) angle between motor centerline and centerline of nozzle when nozzle is rotated about the effective pivot point, deg	fig. 13; eqs. (1), (2), (6), and (10)
	(2) angle between motor centerline and deflected thrust vector	figs. 35, 36, 38, 39, 42, and 49; eq. (14)
ρ	density, lbm/ft^3 (kg/m^3)	eq. (13)
σ	parameter relating applied motor pressure and flexible-joint configuration	eqs. (3) and (4)
σ_P	compressive hoop stress in reinforcements due to motor pressure, psi (N/m^2)	eqs. (9) and (10)
σ_r	resultant compressive hoop stress in reinforcements due to motor pressure and nozzle vectoring, psi (N/m^2)	eq. (11)
σ_v	compressive hoop stress in reinforcements due to nozzle vectoring, psi (N/m^2)	eqs. (10) and (11)
τ	shear stress in elastomer as measured in quadruple-lap shear test, psi (N/m^2)	sec. 2.1.7
τ_P	shear stress in elastomer due to motor pressure, psi (N/m^2)	eqs. (7) and (8)
τ_r	resultant shear stress in elastomer due to motor pressure and nozzle vectoring, psi (N/m^2)	eq. (8)
τ_v	shear stress in elastomer due to nozzle vectoring, psi (N/m^2)	eqs. (6) and (8)

Symbol	Definition	Appears In
ϕ	(1) flexible-joint cone angle, deg (2) discharge angle of the injectant jet relative to the nozzle centerline, deg	fig. 12 and eq. (4) figs. 23, 35, 36, 37, 38, 39, 40, 42, 48, and 49
ψ_i	angle between side force resultant and the side force vector of the ith injector	eq. (12)
Ω	$$\frac{R_p^{2.4} \cos \beta}{3283\, t_r^3 + t_r \cos^2 \beta \left\{ R_p^2\, (\beta_2 - \beta_1)^2 - 3283\, t_r^2 \right\}}$$	eqs. (9) and (10)

Material	Identification
Chemlok 205, 305, 220, 231, and 608	trade names of Hughson Chemical Co. for primer and adhesive epoxy systems
Dacron	trade name of E. I. du Pont de Nemours & Co., Inc. for a polyester fiber (polyethylene terephthalate)
DC 1255	trade designation of Dow Corning Corp. for silicone rubber
elastomer	polymeric material that at room temperature can be stretched to twice its length and on release return quickly to its original length
EPDM	abbreviation for ethylene propylene diene terpolymer
ERL 2256	trade designation of Union Carbide Corp. for bisphenol-A epoxy resin with viscosity modifier
ERR 4205	trade designation of Union Carbide Corp. for epoxy resin viscosity modifier
FM 4030-190	trade designation of Fiberite Corp. for phenolic impregnated chopped S-glass compression molding material
FMC 47	trade designation of FMC Corp. for epoxy resin system
Freon	trade name of E. I. du Pont de Nemours & Co., Inc. for a series of fluorocarbons
GTR 44125	trade designation of General Tire and Rubber Co. for natural rubber compound (now available only from B. F. Goodrich Co. as BFG 20-WS-45).

168

Material	Identification
GTR V-45	trade designation of General Tire and Rubber Co. for silica-filled butadiene/acrylonitrile compound (now produced by Hill-Gard Rubber Co.)
Hypalon	trade name of E. I. du Pont de Nemours & Co., Inc. for chlorosulphonated polyethylene synthetic rubber
IRFNA	inhibited red fuming nitric acid, propellant grade per MIL-P-7254
K1255	trade designation of Union Carbide Corp. for silicone rubber
LOX	liquid oxygen, propellant grade per MIL-P-25508
MHF-3	mixed hydrazine fuel
Neoprene CN and Neoprene W	trade name of E. I. du Pont de Nemours & Co., Inc. for general purpose synthetic rubber (polychloroprene)
nitroso rubber	1:1 copolymer of trifluoronitrosomethane and tetrafluoroethylene
nitroso AFE-110	carboxy-nitroso polymer developed by the Air Force Materials Laboratory (WPAFB, OH)
Parker B-591-8	now Parker B-591-80; a butyl rubber compound used for O-rings; manufactured by Parker-Hannifin Corporation
RP-1	kerosene-base high-energy hydrocarbon fuel, propellant grade per MIL-P-25576
rubber	an elastomer, either a synthetic or a natural compound obtained from the hevea brasiliensis tree
S-glass	high-strength $MgO-Al_2O_3-SiO_2$ glass developed by Owens-Corning Fiberglas Corp.
S-901	trade designation of Owens-Corning Fiberglas Corp. for S-glass fiber with aging surface finish
S-904	trade designation of Owens-Corning Fiberglas Corp. for S-glass fiber non-aging surface finish
S34/901	trade designation of Owens-Corning Fiberglas Corp. for woven S-901 glass fiber cloth

169

Material	Identification
TCC TR 3005	trade designation of Thiokol Corp. for natural rubber formulation
Teflon	trade name of E. I. du Pont de Nemours & Co., Inc. for a series of tetrafluoroethylene polymers
Thiokol ST	trade name of Thiokol Corp. for polysulfide elastomer
Tonox 6040	trade name of Uniroyal, Inc. for a blend of aromatic amines used as a curing agent for epoxy and urethane resins
Tygon ST	trade name of U. S. Stoneware Co. for polyvinyl chloride
UDMH	unsymmetrical dimethylhydrazine, propellant grade per MIL-P-25604
Viton A	trade name of E. I. du Pont de Nemours & Co., Inc. for a copolymer of vinylidene fluoride and hexafluoropropylene
17-7PH	semi-austenitic precipitation-hardening stainless steel
301 304 347	designations for austenitic nickel-chromium steels
410	martensitic chromium steel
2024	wrought aluminum alloy with Cu as principal alloying element
4130 4340	high-strength martensite-hardening low-alloy steels
6061-T6	wrought aluminum alloy with Mg and Si as principal alloying elements, temper T-6
7075-T6	wrought aluminum alloy with Zn as principal alloying element, temper T-6

ABBREVIATIONS

Organization	Identification
ABL	Allegany Ballistics Laboratory
ABMA	Army Ballistic Missile Agency
AEDC	Arnold Engineering Development Center
AFRPL	Air Force Rocket Propulsion Laboratory
AIAA	American Institute of Aeronautics and Astronautics
BOWACA	Bureau of Weapons Advisory Committee for Aeroballistics
CPIA	Chemical Propulsion Information Agency
DAC	Douglas Aircraft Company
ICRPG	Interagency Chemical Rocket Propulsion Group
JANAF	Joint Army-Navy-Air Force
JANNAF	Joint Army-Navy-NASA-Air Force
JANAF-ARPA-NASA	Joint Army-Navy-Air Force-Advanced Research Project Agency-National Aeronautics and Space Administration
LMSC	Lockheed Missiles and Space Company
LMSD	Lockheed Missiles and Space Division
LPC	Lockheed Propulsion Company
NAVORD	Naval Ordnance Command
NOTS	Naval Ordnance Test Station
SAE	Society of Automotive Engineers
UTC	United Technology Center
WPAFB	Wright-Patterson Air Force Base

REFERENCES

1. Anon.: Pintle Thrust Vector Control. NASA CR-87450, June 1967.

2. Schaefer, R. L.; and Wilson, K. C.: The Isentropic Spike Nozzle for Trajectory Control of Solid Propellant Rockets. Bulletin of 16th JANAF Solid Propellant Group, Vol. 2 (AD-317113), CPIA, June 1960, pp. 203-225.

3. Amick, J. L.; Stubbleium, W.; and Chan, P. C. Y.: Experimental Interaction Effects of Forward Located Side Jets on a Body of Revolution. WTM 276, University of Michigan, March 1963.

4. Strike, W. T.; Schuelez, C. J.; and Deitering, J. S.: Interactions Produced by Sonic Lateral Jets Located on Surfaces in a Supersonic Stream. AEDC TDR-63-22 (AD-401911), Von Karman Gas Dynamics Facility, ARO Inc., April 1963.

5. Kardon, S.; Lippert, T. E.; Lease, P. F.; and Drewry, D. G.: A Unique Unitized Thrust Vector Control System. ABL/Z-66 (AD-349158L), Hercules Inc., December 1963.

6. Podell, H. L.: The Shillelagh Missile Propulsion Subsystem (U). CPIA Publ. 18, Vol. 1, CPIA, June 1963, pp. 113-134. (CONFIDENTIAL)

7. Anon.: Rocket Velocity and Attitude Control System. LMSC A120083, Lockheed Missiles and Space Co., May 1962.

8. Fuller, G. M.: Phase II Study of Head-End Steering for a Simplified Manned Space Vehicle. NASA CR-66173, March 1966.

9. Fuller, G. M.: A Feasibility Study of Head-End Steering for a Simplified Manned Space Vehicle. DAC SM-48152 (N66-16017), McDonnell-Douglas Aircraft Co., December 1964.

10. Mitchell, C. M.; and Jones, A. T.: Pershing Propulsion System. Bulletin of 16th JANAF Solid Propellant Group, Vol. 1 (AD-317112), CPIA, June 1960, pp. 85-109.

11. Graves, W. F.: The Nike-Zeus Propulsion System. Bulletin of 16th JANAF Solid Propellant Group, Vol. 1 (AD-317112), CPIA, June 1960, pp. 111-127.

12. Hickey, D. P.: Correlation of Certain Thrust Vector Control Systems. DAC SM-27957, Douglas Aircraft Co., October 1961.

13. McNeer, J. E.; Miltenberger, L. E.; Murray, J. A.; Vicario, A. A.; and Tulpinski, J. E.: Thrust Magnitude, Thrust Vector Control for Advanced Systems (U). ABL-TR-69-26 (AD-507149), Annual Supporting Research Report — 1969, Vol. 2, Hercules Inc., December 1969. (CONFIDENTIAL)

14. McNeer, J. E.; and Murray, J. A.: Thrust Magnitude, Thrust Vector Control for Advanced Systems (U). DCN-N-5-14 (AD-513921), Annual Exploratory Development Report — 1970, Vol. 2, Hercules Inc./ABL, December 1970, pp. 1-59. (CONFIDENTIAL)

15. Anon.: Propulsion Development Department Review. NOTS TP 4100-6 Part 1 (AD-382851L), Naval Ordnance Test Station, June 1967.

16. Wu, Jain-Ming; and Lee, Shen Ching: Electric Air Discharge in Supersonic Flow for Thrust Vector Control. AFRPL TR-67-202 (AD-822593), University of Tennessee, September 1967.

*17. Wilson, J. W.: Final Report, Poseidon C3 Joint Venture Joint. Rep. TWR-2486, Thiokol Chemical Corp./Hercules Inc. (A Joint Venture), July 1967.

18. Nance, B.: Advanced Dual Chamber Propulsion System Component Design Report (U). AFRPL TR-70-52 (AD-509374), Thiokol Chemical Corp./Wasatch Div., May 1970. (CONFIDENTIAL)

19. Marugg, H. C.; and Bratton, C. R.: 100-Inch Motor Demonstration Program, Book 1 (U). TMC-68-4-9-Bk1 (AD-502026L), Thiokol Chemical Corp./Wasatch Div., May 1969. (CONFIDENTIAL)

20. Marugg, H. C.; and Bratton, C. R.: 100-Inch Motor Demonstration Program, Book 2 (U). TMC-68-4-9-Bk2 (AD-502027L), Thiokol Chemical Corp./Wasatch Div., May 1969. (CONFIDENTIAL)

21. Anon.: Development of an Elastomeric Seal for Omniaxial Movable Nozzles (Lockseal). AFRPL TR-66-112 (AD-373032), Lockheed Propulsion Co., April 1966.

22. Wong, E. O.: Design, Fabrication and Test of Omnidirectional Flexible Seals for Thrust Vector Control of Large Solid Rocket Motors. NASA CR-72889, June 1971.

23. Anon.: Final Report — Development and Demonstration of an Omniaxial Flexible Seal Movable Nozzle for Thrust Vector Control. AFRPL TR-67-196, (AD-385084), Thiokol Chemical Corp./Wasatch Div., October 1967.

24. Miltenberger, L. E.; McNeer, J. E.; and Murray, J. A.: Integral Rocket Ramjet Booster Thrust Vector Control and Nozzle Eject System Demonstration (U). DCN-N-37-23, Annual Research and Exploratory Development Report — 1973, Hercules Inc./ABL, January 1974, pp. 115-199. (CONFIDENTIAL)

25. Sherard, H.: Development of Advanced Flex Joint Technology. AIAA Paper 73-1262, AIAA/SAE 9th Propulsion Conference (Las Vegas, NV), Nov. 5-7, 1973.

26. Anon.: Poseidon Propulsion TES Technical Review Report — 1 July through 30 September 1973. SE083-A2AC3HTJ-2, Hercules Inc./Thiokol Chemical Corp. (A Joint Venture), October 1973.

27. Wilson, W. G.: Poseidon Second Stage Elastocomposite Joint, Final Report Task II A-5. Poseidon Investigation Mill Order 74475, Hercules Inc./ABL, February 1971.

---

*Dossier for design criteria monograph "Solid Rocket Thrust Vector Control." Unpublished. Collected source material available for inspection at NASA Lewis Research Center, Cleveland, Ohio.

28. White, T. C.: Thrust Vector Control — Elastocomposite Joint (U). DCN-N-17-6, Annual Exploratory Research Report — 1971, Vol. 2, Hercules Inc./ABL, February 1972, pp. 1-68. (CONFIDENTIAL)

29. Miltenberger, L. E.: Elastocomposite Joint — Thrust Vector Control (U). DCN-N-26-2, Annual Research and Exploratory Development Report — 1972, Vol. 2. Hercules Inc./ABL, December 1972, pp. 119-202. (CONFIDENTIAL)

30. Hurley, L. H.; and Kimmel, N. A.: Application of Controllable Solids in Reentry Measurements Program (U). Rep. TR-0059 (S6816-89)-1, Aerospace Corp., Aug. 31, 1970. (CONFIDENTIAL)

31. Bertocci, R. P.: The Nike-Zeus Propulsion and Jethead Control Systems (U). Bulletin of 18th JANAF-ARPA-NASA Solid Propellant Group, Vol. 1 (AD-330129), CPIA, June 1962, pp. 161-179. (CONFIDENTIAL)

32. Kirchner, W. R.: Development of Advanced Polaris First Stage Propulsion System (U). Bulletin of 18th JANAF-ARPA-NASA Solid Propellant Group, Vol. 1 (AD-330129), CPIA, June 1962, pp. 3-27. (CONFIDENTIAL)

33. Ellis, R. A.: Development of a Carbon-Carbon Nozzle for the Trident I (C4) Third Stage Motor (U). CPIA Publ. 242, Vol. I, CPIA, November 1973, pp. 89-115.

34. Sinclair, C. A.: Development of a High Performance Third Stage Motor for the Trident I (C4) (U). CPIA Publ. 242, Vol. I, CPIA, November 1973, pp. 117-145. (CONFIDENTIAL)

35. Goddard, S. G.: Demonstration of Advanced ICBM Components Program, Phase I. AFRPL-TR-73-37, Vol. I, Thiokol Chemical Corp./Wasatch Div., January 1974.

36. Schoen, L. L.; Bahnsen, E. B.; Conner, G. E.; and Grimsley, J. L.: Exploratory Development for the Techroll® Seal Movable Nozzle System. AFRPL-TR-73-47, Vol. I, United Technology Center, June 1973.

37. Crooks, J. R.: Skybolt Propulsion System. Bulletin of 18th JANAF-ARPA-NASA Solid Propellant Group, Vol. I (AD-330129), CPIA, June 1962, pp. 113-122. (CONFIDENTIAL)

38. Anon.: 156 Inch Diameter Motor Movable Nozzle Program. AFRPL-TR-65-4 (5 vols: AD-365660, AD-365661, AD-365662, AD-365663, and AD-470452), Thiokol Chemical Corp./Wasatch Div., August 1965.

39. Nance, P. D.: Final Report, Submerged Gimbal Nozzle Development, Appendix D. BSD-TR-66-31/C (AD-376999), Thiokol Chemical Corp./Wasatch Div., June 1966.

40. Hirsch, N. A.; Slegers, L.; and Thrasher, D. I.: Gimballed Integral Nozzle. AFRPL-TR-64-172 (AD-371800), Air Force Systems Command, (Edwards Air Force Base, CA), December 1965.

41. Waldeck, G. H.; Hensley, R. V.; Deslauriers, E. J.; and McVey, F. D.: Flexible Skirt Nozzle Program. Rep. 6602-1, Pneumodynamics Corp., (Washington, D.C.), September 1959. (CONFIDENTIAL)

42. Waldeck, G. H.: Flexible Skirt Nozzle Program (U). Rep. 6602-i, Pneumodynamics Corp., July 1960. (CONFIDENTIAL)

43. Waldeck, G. H.: Flexible Skirt Nozzle Program (U). Rep. 6602-k, Pneumodynamics Corp., November 1960. (CONFIDENTIAL)

44. Spann, R. E.: Reinforced Grain Advanced Development Program. AFRPL-TR-66-239 (AD-377073), Rocketdyne Div., North American Aviation, Inc., October 1966.

45. Hoover, G. H.: An Omnivector Nozzle for Thrust Vector Control (U). CPIA Publ. 111, Vol. 2 (AD-373908), CPIA, June 1966, pp. 813-842. (CONFIDENTIAL)

46. Rains, D. A.: Solid Propellant Motor Thrust Vector Control System for Titan III (U). Bulletin of 20th Interagency Solid Propulsion Meeting, Vol. 1 (AD-352176), CPIA, May 1964, pp. 225-262. (CONFIDENTIAL)

47. Anon.: TVC Systems Analysis, Parts I and II. UTC 4404-70-330, United Technology Center (Sunnyvale, CA), April 1971.

*48. Huff, W. G.: Theoretical Analysis and Functional Description of the Polaris A3 Thrust Vector Control System (U). LMSC 806591, Lockheed Missiles and Space Corp., May 1967. (CONFIDENTIAL)

49. Collis, D. R.; and Rimington, D. A.: Thrust Vector Control of the Minuteman Stage II Motor by Liquid Injection (U). Bulletin of 20th Interagency Solid Propulsion Meeting, CPIA, Vol. 1 (AD-352176), May 1964, pp. 263-281. (CONFIDENTIAL)

50. Conklin, C. L.: The Sprint Thrust Vector Control System (U). CPIA Publ. 167, Vol. 1, (AD-389918), CPIA, June 1968, pp. 219-232. (CONFIDENTIAL)

51. Anon.: Thrust Vector Control System Study Program, Final Report and Final Report Summary. NASA CR-72727, Thiokol Chemical Corp., June 1 1970.

52. Kennedy, C. G.: Development and Demonstration of a Chamber Bleed Hot Gas Thrust Vector Control System for LSRM — Final Report (U). AFRPL-TR-68-166, Vols. I, II, and III (AD-395219, AD-847113, and AD-847114), Thiokol Chemical Corp./Wasatch Div., October 1967. (VOL. I CONFIDENTIAL)

53. Benjock, G. F.: Design of Propellant Gas Secondary Injection Thrust Vector Control (U). ABL X102 (AD-350933), Hercules Inc., February 1964. (CONFIDENTIAL)

54. Anon.: Development of a Hot Gas Valve for Secondary Injection Thrust Vector Control. AFRPL-TDR-64-33 (AD-348778), Lockheed Propulsion Co., March 1964.

---

*Dossier for design criteria monograph "Solid Rocket Thrust Vector Control." Unpublished. Collected source material available for inspection at NASA Lewis Research Center, Cleveland, Ohio.

55. Brownson, H.: Feasibility Demonstration for Direct Chamber Bleed Hot Gas Secondary Injection Thrust Vector Control — Final Report. AFRPL-66-224 (Vol. 1, Bk 1: AD-800937; Vol. 1, Bk 2: AD-800938; Vol. 2: AD-800939), Lockheed Propulsion Co., September 1966.

56. Anon.: Proportional Solid Propellant Secondary Injection Thrust Vector Control Study. NASA CR-637, November 1966.

57. Bonin, J.; Fitzgerald, J. E.; and Miller, E.: Hybrid Thrust Vector Control Systems (U). Rep. LPC 572-F (AD-330226), Lockheed Propulsion Co., June 1962. (CONFIDENTIAL)

58. Drewry, D. G.; and Newman, R. M.: Methods for Thrust Vector Control of Solid Propellant Rockets. Bulletin of 16th JANAF Solid Propellant Group, Vol. 2 (AD-317113), CPIA, June 1960, pp. 227-248.

59. Anon.: Stage I Minuteman (M55A1) Production Support — Final Report, Appendix C, Submerged Hot Gas Valve Development. BSD-TR-66-31 (AD-373063L), Thiokol Chemical Corp./Wasatch Div., May 1966.

60. Anon.: Development and Demonstration of Flightweight Thrust Vector Control Hardware, Interim Progress Report No. 2 (U). AFRPL-TR-67-92 (AD-380241), Thiokol Chemical Corp./Wasatch Div., March 1967. (CONFIDENTIAL)

61. Anon.: NASA Propellant Gas Valve Scale-Up Program Final Report. NASA CR-78004, March 1966.

62. Shipley, J. D.; and Drewry, D. G.: Application of Propellant Gas Valves for Thrust Vector Control of High Pressure, High Acceleration Solid Propellant Rocket Motors. Rep. ABL/Z-72 (AD-353317), Hercules Inc., May 1964.

63. Robinson, D. J.; and Montgomery, L. C.: Sergeant Motor Jet Vanes (U). Rep. JPL 20-136 (AD-321938), Jet Propulsion Lab., Calif. Inst. Tech., June 1960. (CONFIDENTIAL)

64. Skirmer, E. H.; 504, and Werner, C. T.: X SAM-N-66 Talos Weapon Jet Vane Aerodynamic Report, X230-A5 Booster Unit. Rep. BPD 4330, Bendix Corp., February 1955.

65. Davis, R. E.; O'Callaghan, T.; and Selbert, J. R.: The Jetevator as a Vector Control Device, Development of the Polaris Jetevator. CPIA Publ. 18A, Vol. 4 (AD-346945), CPIA July 1963, pp. 391-412.

66. Gowen, L. F.: Subroc Propulsion System. Bulletin of 16th JANAF Solid Propellant Group, Vol. 1, CPIA, June 1960, pp. 63-83.

67. Edwards, S. S.; and Parker, G. H.: An Investigation of the Jetevator as a Means of Thrust Vector Control. Rep. LMSD-2630, Lockheed Missiles and Space Co., February 1958.

68. Huizinga, J.: Jetevator Effectiveness and Base Pressure Measurements for FTV-1 and AX Polaris Missiles Tested at NASA — Lewis Laboratory. Rep. LMSC 462055, Lockheed Missiles and Space Co., November 1958.

69. Anon.: XM-38 Solid Propellant Rocket Motor, Vol. I (U). Rep. TU-68-5-59, Thiokol Chemical Corp./Wasatch Div., June 1959. (CONFIDENTIAL)

70. Anon.: Jet Tab Thrust Vector Control. Rep. LMSC 800917, Lockheed Missiles and Space Co., December 1961.

71. Hollstein, H. J.: Jet Tab Thrust Vector Control. J. Spacecraft Rockets, vol. 2, no. 6, Nov.-Dec. 1965, pp. 927-930.

72. Anon.: Cooled Probe TVC Systems for Full Scale Rocket Motor Firing Evaluation (U). Rep. BPAD-863-14544, Bendix Corp., September 1962. (CONFIDENTIAL)

73. Auble, C. M.; and Spielberger, L. J.: Jet Tab Thrust Vector Control for Large Solid Rocket Motors. CPIA Publ. 18, Vol. 3 (AD-338667L), CPIA, June 1963. pp. 241-286.

74. Anon.: 156-Inch Diameter Motor Jet Tab Program — Final Report. AFRPL-TR-64-167 (Vol. 1: AD-357024, Vol. 2: AD-357025, Vol. 3: AD-357026, Vol. 4: AD-357027, Vol. 5: AD-357028), Lockheed Propulsion Co., January 1965.

75. Anon.: Solid Rocket Motor Nozzles. NASA Space Vehicle Design Criteria Monograph, NASA SP-8115 (to be published).

76. Anon.: Liquid Rocket Actuators and Operators. NASA Space Vehicle Design Criteria Monograph, NASA SP-8090, May 1973.

77. Harrison, T.; Colbert, L.; Dykstra, H.; Sullivan, P.; and McCorkle, J.: Design Study and Cost Estimate for Application of Lockseal to 260-Inch Solid Rocket Motor — Final Report. NASA CR-83073, December 1966.

*78. Galford, J. E.: Unstable Joint Analysis — Poseidon Investigation Task II-A. Hercules Inc./Magna, February 1971.

*79. Woodberry, R. F. H.: Rapid Design Equations for Elastometallic Joints. Memo to J. E. McNeer, Ref. No. Misc/6/50-1113, Hercules Inc./Bacchus, Nov. 30, 1973.

80. Matthews, F. W.: Application of Large Deformation Theory to Chamber Analysis and Design. Chemical Propulsion Structural Integrity Survey 1972, CPIA Publ. 229, CPIA, September 1972.

81. Wilson, E. L.: Structural Analysis of Axisymmetric Solids. AIAA J., vol. 3, no. 12, December 1965, pp. 2269-2274.

82. Dunham, R. S.; and Nickell, R. E.: Finite Element Analysis of Axisymmetric Solids with Arbitrary Loadings. Rep. SEL-67-6 (AD-655253), University of California (Berkeley, CA), June 1967.

---

*Dossier for design criteria monograph "Solid Rocket Thrust Vector Control." Unpublished. Collected source material available for inspection at NASA Lewis Research Center, Cleveland, Ohio.

83. Eringen, A. C.: Small Twist Superimposed on a Finite Compression of a Thick Anisotropic Spherical Shell. Tech. Rep. 12-3, General Technology Corp. (Lawrenceville, N. J.), December 1970.

84. Kafadar, C. B.; and Eringen, A. C.: An Anisotropic, Elastic, Solid Spherical Annular Ring Subject to Hydrostatic Pressure and Prescribed Bending. Tech. Rep. 12-2, General Technology Corp. (Lawrenceville, N. J.), December 1970.

85. Danninger, G. A.; Pignoli, C. R.; and White, A. R.: Project Quick Turn Movalbe Nozzle Thrust Vector Control Demonstration Program (U). Rep. NWC-TP-4794, Lockheed Propulsion Co. for the Propulsion Development Department, Naval Weapons Center, August 1971. (CONFIDENTIAL)

*86. Cronkrite, W. R.: Analysis of Second Stage Poseidon Machined Flexible Joint Axial Deflection and Actuation Torque Tests. Rep. 17-10203/6/40-475 (HA-05960), Hercules Inc./Magna, October 1967.

*87. Cronkrite, W. R.: Analysis of First Stage Poseidon Flexible Joint Axial Deflection and Actuation Torque Tests. Rep. 17-10203/6/40-455 (HA-04006), Hercules Inc./Magna, October 1967.

88. Allen, M. J.: Poseidon C3 Second Stage Phase II Design Compliance Report (U). Data Item SE048-A2A01HTJ, Rep. 9, Hercules Inc., March 1971. (CONFIDENTIAL)

89. Lund, R. K.: Final Report — Cold Flow Tests Poseidon C3 First and Second Stage. Rep. TWR-2320, Thiokol Chemical Corp./Hercules Inc. (A Joint Venture), February 1967.

90. Shapiro, A. H.: The Dynamics and Thermodynamics of Compressible Fluid Flow. Vol. 1, Ch. 15. The Ronald Press Co., 1953.

*91. Anon.: Nozzle Joint, Method for Actuation, Axial Deflection, and Leak Tests. OD 43336C, Department of the Navy, Naval Ordnance Systems Command, March 1971.

*92. Briggs, W.; and Greenleaf, G.: Lockseal Subscale Test Report Results of Test Series No. 4, 8, and 15. Rep. LPC 754-STR-3, Lockheed Propulsion Co., Feb. 1968.

93. Anon.: Silicone Rubber for Design Engineers. General Electric Technical Data Book S-1D, General Electric Co. (Waterford, N.Y.), no date.

*94. Wells, R. D.: Final Report Task I and II — Synthetic Elastomer Development Program. Rep. LPC 893-F, Lockheed Propulsion Co., February 1969.

95. Anon.: Poseidon C3 First Stage Phase II Design Compliance Report, Fleet Ballistic Missile Weapon System (U). Hercules Inc./Thiokol Chemical Corp., Mar. 16, 1971. (CONFIDENTIAL)

96. Anon.: Poseidon C3 Second Stage Phase II Design Compliance Report, Fleet Ballistic Missile Weapon System (U). Hercules Inc./Thiokol Chemical Corp., Mar. 24, 1971. (CONFIDENTIAL)

---

*Dossier for design criteria monograph "Solid Rocket Thrust Vector Control." Unpublished. Collected source material available for inspection at NASA Lewis Research Center, Cleveland, Ohio.

*97. Peterson, M. R.: Poseidon Phase II — Quarterly Reliability Status Report (U). Data Item No. SF002-A2A01HTJ, Submittal No. 20A, Hercules Inc./Thiokol Chemical Corp. (A Joint Venture), March 1971. (CONFIDENTIAL)

*98. Anon.: Natural Rubber Compound, Weapons Specification. WS 8008E, Department of Navy, Naval Ordnance Systems Command, August 1970.

*99. Anon.: Natural Rubber Compound, Weapons Specification. WS 12006B, Department of the Navy, Naval Ordnance Systems Command, September 1969.

*100. Anon.: Memorandum — Elastomer Material 44125, Lots 14, 15, and 16. Ref. No. GA 15729, General Tire and Rubber Co., November 1968.

*101. Anon.: Special Test Report, First Stage Buckle Test Unit D008 (D010). Ref. No. OML 77223, Lockheed Propulsion Co., Aug. 4, 1967.

*102. Anon.: Special Test Report, Second Stage Buckle Test Unit D005/D008. Ref. No. OML 77222, Lockheed Propulsion Co., Aug. 4, 1967.

103. Isakson, G.; Armen, H.; and Pipko, A.: Discrete Element Methods for the Plastic Analysis of Structures. NASA CR-803, October 1967.

104. Newton, J. F.; and Spaid, F. W.: Interaction of Secondary Injectants and Rocket Exhaust for Thrust Vector Control. ARS J., vol. 32, August 1962, pp. 1203-1211.

105. Povinelli, F. P.: Displacement of Disintegrating Liquid Jets in Crossflow. NASA TN D-4334, February 1968.

106. Kurzins, S. C.; and Raab, F. H.: Measurement of Droplet Sizes in Liquid Jets Atomized in Low Density Supersonic Streams (U). NASA CR-1242, December 1968. (CONFIDENTIAL)

*107. Zeamer, R. J.: Principles of Rocket Thrust Vector Control by Fluid Injection. Memorandum, Hercules Inc./ABL, July 1961.

*108. Grunwald, G. J.: Polaris B3 First and Second Stage Secondary Injection Thrust Vector Control Data Report (U). LMSC 804506, Lockheed Missiles and Space Co., October 1964. (CONFIDENTIAL)

*109. Huizinga, J.: Liquid Injection Thrust Vector Control Effectiveness (U). Rep. LMSC 800877, Lockheed Missiles and Space Co., August 1961. (CONFIDENTIAL)

*110. Anon.: Chemical Aspects of Fluid Injection (U). Rep. Nos. R-1, R-2, and R-3 of P-27, Dynamic Science Corp. (Sunnyvale, CA), May 1961, July 1961, and August 1961. (CONFIDENTIAL)

111. Anon.: Stress Corrosion Test Evaluation, Final Report (Titan III). UTC-4802-67-181, United Technology Center (Sunnyvale, CA), July 10, 1969.

---

*Dossier for design criteria monograph "Solid Rocket Thrust Vector Control." Unpublished. Collected source material available for inspection at NASA Lewis Research Center, Cleveland, Ohio.

112. Anon.: Titan III-M TVC System Seal Material Compatibility and Pyroseal Development Test Report. UTC-4802-68-104, United Technology Center (Sunnyvale, CA), April 22, 1968.

113. Childress, H. E.; and Mastrolia, E. J.: System Support Studies Under Production Support Program. Rep. 0162-06 TDR-9, Vol. 2 (Part 1, AD-479227; Part 2, AD-479205), Aerojet General Corp., September 1965.

114. Anon.: Static Test Report TVC 50-Cycle/75-Day Hold and Recycle. UTC 4404-70-230. United Technology Center (Sunnyvale, CA), September 1970.

115. Honma, J.: Research Study, Strontium Perchlorate Water Solutions. Rep. IDC 52-30, Lockheed Missiles and Space Co., September 1963.

116. Hess, F. D.: Diffusion of Perchlorate Solutions Through Elastomer Membranes. BSD-TR-66-93, TOR-669(6855-20)-1 (AD-482982), Aerospace Corp., February 1966.

117. Anon.: Freon Compatibility Studies. Monthly Progress Reports 1-10, LMSC Subcontract 18-10703, Atlantic Research Corp., 1961-1962.

118. Anon.: An Evaluation of Composite Teflon-Aluminum Foil Bladders for the Surveyor Vernier Propulsion System. NASA CR-84663, March 1967.

119. Ross, L. G.; and LeFebvre, C. A.: Determination of the Effects of Liquid Injectants on Nozzle Ablative Performance. NASA CR-72792, December 1970.

*120. Hirsch, R. L.: Physical Properties and Compatibility of Strontium Perchlorate. Interoffice Memo, Aerojet-General Corp., June 24, 1963.

*121. LeCount, R. L.: Fluid Injection TVC Research (U). Report to Rocket and Nozzles Jet Effects Panel (BOWACA), Lockheed Missiles and Space Co., July 1963. (CONFIDENTIAL)

*122. Grunwald, G. J.; and LeCount, R. L.: Fluid Injection TVC Research (U). TM 53-42-4, LMSC 803311, Lockheed Missiles and Space Co., October 1963. (CONFIDENTIAL)

123. Wu, Jain-Ming; Chapkis, R. L.; Ai, D. K.; and Rao, G. V. R.: Liquid Injection Thrust Vector Control. National Engineering Science Co. (Pasadena, CA), July 1961.

*124. Grunwald, G. J.; and Anderson, R. G.: Preliminary Results of P-29 Fluid Injection Thrust Vector Control Tests. Rep. IDC-57-11-356, Lockheed Missiles and Space Co., November 1961.

*125. LeCount, R. L.; et al.: Preliminary Data Release of Fluid Injection Thrust Vector Control Tests. LMSC DP/M-431, DP/M-557, and DP/M-722, Lockheed Missiles and Space Co., 1960.

*126. Zeamer, R. J.: The Effect of Some Nozzle and TVC Parameters on TVC Effectiveness and Motor Thrust. Memorandum, Hercules Inc./Magna, September 1965.

*Dossier for design criteria monograph "Solid Rocket Thrust Vector Control." Unpublished. Collected source material available for inspection at NASA Lewis Research Center, Cleveland, Ohio.

*127. Anon.: Polaris B3 Fluid Injection TVC (U). LMSC 804632, Lockheed Missiles and Space Co., October 1964. (CONFIDENTIAL)

*128. Anon.: Titan III Thrust Vector Control Fluid Requirement Utilizing UBS. Tech. Memo. 5141/31-68-02, Martin-Marietta Corp. (Denver, CO) January 1968.

*129. LeCount, R. L.: Fluid Injection Thrust Vector Control Test P-10. Rep. IDC-57-11-59, Lockheed Missiles and Space Co., May 1961.

130. Anon.: Weapons System 133B, Second Stage Minuteman Wing VI Motor Data Book (U). GM-TR-0165-00478, Aerojet-General Corp., Revised March 21, 1969. (CONFIDENTIAL)

131. Anon.: Item Detailed Specification No. S-133-1003-0-4, Motor, Solid Propellant Model SR-73-AJ-1 (U). Figure A6658, Thiokol Corp., Jan. 6, 1972. (CONFIDENTIAL)

132. Anon.: TVC System Analysis (Titan III C/D). UTC 4404-70-330, United Technology Center, December 1970.

133. Anon.: 156-Inch Diameter Motor Liquid Injection TVC Program Final Report, Test Results, Motor 156-5. AFRPL-TR-66-109, Vol. 2, Lockheed Propulsion Co., July 1966.

134. Charwat, A. F.; Roos, J. N.; Dewey, F. C.; and Hitz, J. A.: An Investigation of Separated Flows — Part I — The Pressure Field. J. Aerospace Sci., vol. 28, no. 6, June 1961, pp. 457-470.

135. Charwat, A. F.; Roos, J. N.; Dewey, F. C.; and Hitz, J. A.: An Investigation of Separated Flows — Part II — Flow in the Cavity and Heat Transfer. J. Aerospace Sci., vol. 28, no. 7, July 1961, pp. 513-527.

*136. Zeamer, R. J.: Fluid Injection Thrust Vector Control, Distribution of Loads Due to Vectoring. Memorandum, Hercules Inc./ABL, August 1963.

137. Anon.: 156-Inch Fiberglass LITVC Motor Program. AFRPL-TR-65-192, Thiokol Chemical Corp., October 1965.

138. Anon.: Hibex. Rep. D2-99600-1 (AD-371266L), The Boeing Co., March 1966.

*139. McQueen, J. E.: Thrust Vector Control System Operation Report (U). Rep. ZM-656-401D, Hercules Inc./ABL, October 1965. (CONFIDENTIAL)

140. Starrett, D.: Final Report — Sprint Missile Control Study (U). Rep. LMSC 665480, Lockheed Missiles and Space Co., October 1964. (CONFIDENTIAL)

141. Anon.: Polaris Fluid Injection Thrust Vector Control. Rep. LMSC 800550, Lockheed Missiles and Space Co., March 1961.

142. Speisman, C.; and Kallis, J.: Preliminary Results, Quadrant Interaction Analytical Study Effort. Rep. 63-1942.27-28, Aerospace Corp., (San Bernadino, CA), June 3, 1963.

---

*Dossier for design criteria monograph "Solid Rocket Thrust Vector Control." Unpublished. Collected source material available for inspection at NASA Lewis Research Center, Cleveland, Ohio.

143. Hair, L. M.; and Baumgartner, A. T.: An Empirical Performance Model of Secondary Injection for Thrust Vector Control (U). Rep. LMSC 4-64-014, Lockheed Missiles and Space Co., October 1964. (CONFIDENTIAL)

*144. Green, C. J.: Desired Properties of the Injectant. Rep. 4511-196, U. S. Naval Ordnance Test Station, August 1960.

145. Green, C. J.: Effects of Additives on Propellant Performance and Motor Operating Conditions. Preliminary Summary Report 1DP1210, U. S. Naval Ordnance Test Station, December 1960.

146. Walker, R. E.; and Shandor, M.: Influence of Injectant Properties for Fluid Injection Thrust Vector Control. Preprint No. 64-112, AIAA Solid Propellant Rocket Conference (Palo Alto, CA), Jan. 29-31, 1964.

147. Anon.: Secondary Injection Scaling Effects. Rep. 4511-195, U. S. Naval Ordnance Test Station, August 1960.

148. Large, J. P.: Concepts and Procedures of Cost Analysis. Rep. RM-3589-PR (AD 411554), RAND Corp., June 1963.

149. Daniels, C. J.; et al.: Thrust Vector Control Requirements for Launch Vehicles Using a 260-Inch Solid Rocket First Stage. NASA TM X-1906, December 1969.

150. Lloyd, D. K.; and Lipow, M.: Reliability: Management, Methods and Mathematics. Prentice-Hall, Inc., 1962.

151. Lee, R. S. N.: A Computer Program for Conducting Parametric Studies of Liquid Injection Thrust Vector Control Systems. Rep. BOAC D2-30873 (AD-812413L), The Boeing Company, 1964.

152. Obert, E. F.: Concepts of Thermodynamics. McGraw-Hill Book Co. (New York), 1960.

153. Anon.: Ullage Blowdown System Fluid Expulsion Performance. UTC 440A-70-310, Rev. A., United Technology Center, March 11, 1971.

154. Anon.: Solid Propellant Grain Design and Internal Ballistics. NASA Space Vehicle Design Criteria Monograph, NASA SP-8076, March 1972.

155. Anon.: Liquid Rocket Metal Tanks and Tank Components. NASA Space Vehicle Design Criteria Monograph, NASA SP-8088, May 1974.

156. Anon.: Liquid Rocket Pressure Regulator, Relief Valves, Check Valves, Burst Disks, and Explosive Valves. NASA Space Vehicle Design Criteria Monograph, NASA SP-8080, March 1973.

157. Anon.: Solid Rocket Motor Performance Analysis and Prediction. NASA Space Vehicle Design Criteria Monograph, NASA SP-8039, May 1971.

---

*Dossier for design criteria monograph "Solid Rocket Thrust Vector Control." Unpublished. Collected source material available for inspection at NASA Lewis Research Center, Cleveland, Ohio.

*158. Anon.: Structural and Thermal Analysis Final Report, Poseidon First Stage Motor. Vol. III — Nozzle. Data Item No. SE025-A2A00HTJ, Rep. 1, Hercules Inc./Thiokol Chemical Corp. (A Joint Venture), October 1970.

159. Heaton, H. S.; and Daines, W. L.: Flow Field Analysis of Rocket Motors (U). AFRPL-TR-70-98 (AD-510749), Hercules Inc./Magna, September 1970. (CONFIDENTIAL)

---

*Dossier for design criteria monograph "Solid Rocket Thrust Vector Control." Unpublished. Collected source material available for inspection at NASA Lewis Research Center, Cleveland, Ohio.

NASA SPACE VEHICLE DESIGN CRITERIA
MONOGRAPHS ISSUED TO DATE

ENVIRONMENT

SP-8005	Solar Electromagnetic Radiation, Revised May 1971
SP-8010	Models of Mars Atmosphere (1967), May 1968
SP-8011	Models of Venus Atmosphere (1972), Revised September 1972
SP-8013	Meteoroid Environment Model—1969 (Near Earth to Lunar Surface), March 1969
SP-8017	Magnetic Fields—Earth and Extraterrestrial, March 1969
SP-8020	Mars Surface Models (1968), May 1969
SP-8021	Models of Earth's Atmosphere (90 to 2500 km), Revised March 1973
SP-8023	Lunar Surface Models, May 1969
SP-8037	Assessment and Control of Spacecraft Magnetic Fields, September 1970
SP-8038	Meteoroid Environment Model—1970 (Interplanetary and Planetary), October 1970
SP-8049	The Earth's Ionosphere, March 1971
SP-8067	Earth Albedo and Emitted Radiation, July 1971
SP-8069	The Planet Jupiter (1970), December 1971
SP-8084	Surface Atmospheric Extremes (Launch and Transportation Areas), Revised June 1974
SP-8085	The Planet Mercury (1971), March 1972
SP-8091	The Planet Saturn (1970), June 1972
SP-8092	Assessment and Control of Spacecraft Electromagnetic Interference, June 1972

SP-8103	The Planets Uranus, Neptune, and Pluto (1971), November 1972
SP-8105	Spacecraft Thermal Control, May 1973
SP-8111	Assessment and Control of Electrostatic Charges, May 1974

STRUCTURES

SP-8001	Buffeting During Atmospheric Ascent, Revised November 1970
SP-8002	Flight-Loads Measurements During Launch and Exit, December 1964
SP-8003	Flutter, Buzz, and Divergence, July 1964
SP-8004	Panel Flutter, Revised June 1972
SP-8006	Local Steady Aerodynamic Loads During Launch and Exit, May 1965
SP-8007	Buckling of Thin-Walled Circular Cylinders, Revised August 1968
SP-8008	Prelaunch Ground Wind Loads, November 1965
SP-8009	Propellant Slosh Loads, August 1968
SP-8012	Natural Vibration Modal Analysis, September 1968
SP-8014	Entry Thermal Protection, August 1968
SP-8019	Buckling of Thin-Walled Truncated Cones, September 1968
SP-8022	Staging Loads, February 1969
SP-8029	Aerodynamic and Rocket-Exhaust Heating During Launch and Ascent May 1969
SP-8030	Transient Loads From Thrust Excitation, February 1969
SP-8031	Slosh Suppression, May 1969
SP-8032	Buckling of Thin-Walled Doubly Curved Shells, August 1969
SP-8035	Wind Loads During Ascent, June 1970
SP-8040	Fracture Control of Metallic Pressure Vessels, May 1970
SP-8042	Meteoroid Damage Assessment, May 1970

SP-8043	Design-Development Testing, May 1970
SP-8044	Qualification Testing, May 1970
SP-8045	Acceptance Testing, April 1970
SP-8046	Landing Impact Attenuation for Non-Surface-Planing Landers, April 1970
SP-8050	Structural Vibration Prediction, June 1970
SP-8053	Nuclear and Space Radiation Effects on Materials, June 1970
SP-8054	Space Radiation Protection, June 1970
SP-8055	Prevention of Coupled Structure-Propulsion Instability (Pogo), October 1970
SP-8056	Flight Separation Mechanisms, October 1970
SP-8057	Structural Design Criteria Applicable to a Space Shuttle, Revised March 1972
SP-8060	Compartment Venting, November 1970
SP-8061	Interaction with Umbilicals and Launch Stand, August 1970
SP-8062	Entry Gasdynamic Heating, January 1971
SP-8063	Lubrication, Friction, and Wear, June 1971
SP-8066	Deployable Aerodynamic Deceleration Systems, June 1971
SP-8068	Buckling Strength of Structural Plates, June 1971
SP-8072	Acoustic Loads Generated by the Propulsion System, June 1971
SP-8077	Transportation and Handling Loads, September 1971
SP-8079	Structural Interaction with Control Systems, November 1971
SP-8082	Stress-Corrosion Cracking in Metals, August 1971
SP-8083	Discontinuity Stresses in Metallic Pressure Vessels, November 1971
SP-8095	Preliminary Criteria for the Fracture Control of Space Shuttle Structures, June 1971

| SP-8099 | Combining Ascent Loads, May 1972 |
| SP-8104 | Structural Interaction With Transportation and Handling Systems, January 1973 |

GUIDANCE AND CONTROL

SP-8015	Guidance and Navigation for Entry Vehicles, November 1968
SP-8016	Effects of Structural Flexibility on Spacecraft Control Systems, April 1969
SP-8018	Spacecraft Magnetic Torques, March 1969
SP-8024	Spacecraft Gravitational Torques, May 1969
SP-8026	Spacecraft Star Trackers, July 1970
SP-8027	Spacecraft Radiation Torques, October 1969
SP-8028	Entry Vehicle Control, November 1969
SP-8033	Spacecraft Earth Horizon Sensors, December 1969
SP-8034	Spacecraft Mass Expulsion Torques, December 1969
SP-8036	Effects of Structural Flexibility on Launch Vehicle Control Systems, February 1970
SP-8047	Spacecraft Sun Sensors, June 1970
SP-8058	Spacecraft Aerodynamic Torques, January 1971
SP-8059	Spacecraft Attitude Control During Thrusting Maneuvers, February 1971
SP-8065	Tubular Spacecraft Booms (Extendible, Reel Stored), February 1971
SP-8070	Spaceborne Digital Computer Systems, March 1971
SP-8071	Passive Gravity-Gradient Libration Dampers, February 1971
SP-8074	Spacecraft Solar Cell Arrays, May 1971
SP-8078	Spaceborne Electronic Imaging Systems, June 1971

SP-8086	Space Vehicle Displays Design Criteria, March 1972
SP-8096	Space Vehicle Gyroscope Sensor Applications, October 1972
SP-8098	Effects of Structural Flexibility on Entry Vehicle Control Systems, June 1972
SP-8102	Space Vehicle Accelerometer Applications, December 1972

CHEMICAL PROPULSION

SP-8087	Liquid Rocket Engine Fluid-Cooled Combustion Chambers, April 1972
SP-8113	Liquid Rocket Engine Combustion Stabilization Devices, November 1974
SP-8107	Turbopump Systems for Liquid Rocket Engines, August 1974
SP-8109	Liquid Rocket Engine Centrifugal Flow Turbopumps, December 1973
SP-8052	Liquid Rocket Engine Turbopump Inducers, May 1971
SP-8110	Liquid Rocket Engine Turbines, January 1974
SP-8081	Liquid Propellant Gas Generators, March 1972
SP-8048	Liquid Rocket Engine Turbopump Bearings, March 1971
SP-8101	Liquid Rocket Engine Turbopump Shafts and Couplings, September 1972
SP-8100	Liquid Rocket Engine Turbopump Gears, March 1974
SP-8088	Liquid Rocket Metal Tanks and Tank Components, May 1974
SP-8094	Liquid Rocket Valve Components, August 1973
SP-8097	Liquid Rocket Valve Assemblies, November 1973
SP-8090	Liquid Rocket Actuators and Operators, May 1973
SP-8080	Liquid Rocket Pressure Regulators, Relief Valves, Check Valves, Burst Disks, and Explosive Valves, March 1973

SP-8064	Solid Propellant Selection and Characterization, June 1971
SP-8075	Solid Propellant Processing Factors in Rocket Motor Design, October 1971
SP-8076	Solid Propellant Grain Design and Internal Ballistics, March 1972
SP-8073	Solid Propellant Grain Structural Integrity Analysis, June 1973
SP-8039	Solid Rocket Motor Performance Analysis and Prediction, May 1971
SP-8051	Solid Rocket Motor Igniters, March 1971
SP-8025	Solid Rocket Motor Metal Cases, April 1970
SP-8041	Captive-Fired Testing of Solid Rocket Motors, March 1971